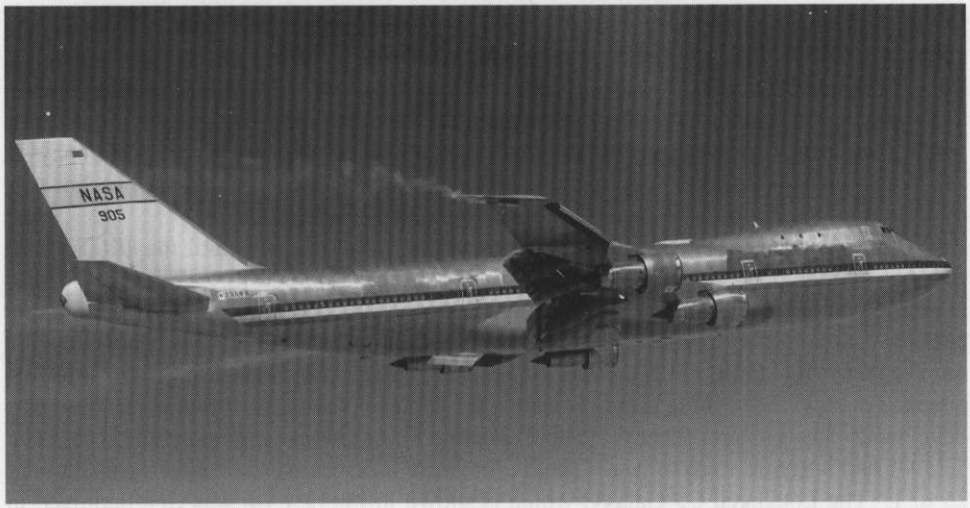


Figure 2.1.15. The Boeing 747-100 entered service on January 22, 1970 powered by four Pratt and Whitney JT9D-7A turbofan engines that each provided a thrust of 46,500 pounds. (NASA Photograph)

engines that provided a total thrust of 186,000 pounds. The later 400-series, which went into service in 1988, develops more than 253,000 pounds of thrust when powered by four Pratt and Whitney PW4062 turbofan engines. The PW4062 has a maximum thrust-to-weight ratio of more than 6.0 and a minimum thrust-specific fuel consumption of less than 0.45 lb-fuel/hr/lb-thrust. Even at 40,000 feet with a Mach number of 0.8, the PW4062 has a thrust-specific fuel consumption of less than 0.6 lb-fuel/hr/lb-thrust. With four of these engines and a 57,285-gallon fuel capacity, the 747-400 has a maximum takeoff weight of 875,000 pounds and a range of more than 8,000 miles.

During the last three decades of the twentieth century, the continuous improvement of turbomachinery components led to the evolution of turbojet and turbofan engines with greater thrust-to-weight ratio and higher overall efficiency. This evolution produced higher compressor pressure ratios, higher turbine inlet temperatures, and higher bypass ratios. During this period, the small to medium-sized aircraft market also benefited tremendously from improvements in turbomachinery technology. Today, the turboshaft or turboprop engine is commonly used to power short-range commuter aircraft like the de Havilland Dash 8 shown in Fig. 2.1.16.

A turboprop engine can be designed to turn at constant rotational speed during most phases of aircraft operation. The design is typified by the Allison T56-A-15 engines that power the C-130 Hercules shown in Fig 2.1.17. The T56-A-15 turns continuously at 13,820 rpm, which allows the turbine to maintain its most efficient operating speed. Since this speed is too fast for the efficient operation of any propeller, in the C-130 installation, each engine turns a 162-inch propeller through a gear reduction assembly having a total reduction ratio of 13.54 to 1. To maintain the constant rotational speed, changes in power requirements are met by changing the fuel flow and propeller pitch.



Figure 2.1.16. Two Pratt and Whitney PW121, 2000-horsepower turboprop engines power the de Havilland Dash 8-100 regional airliner. (Photograph by John Martin)



Figure 2.1.17. Four Allison T56-A-15 constant-speed turboprop engines turning at 13,820 rpm power the C-130H Hercules. With a power-to-weight ratio of 2.65 hp/lb, the T56-A-15 is capable of developing 4,910 horsepower and weighs only 1,850 pounds. (U.S. Air Force)

From the pilot's point of view, controlling a constant-speed turboprop engine is remarkably simple. A single throttle lever controls the engine's propeller, electrical, and fuel systems. This is accomplished through an electromechanical control system. The throttle is linked to the fuel control system, which meters the fuel flow to maintain constant engine power. A power setting is established by the position of the throttle, and a fuel-trimming system maintains the power at a constant level by monitoring the turbine inlet temperature and changing the fuel flow accordingly. As the fuel flow is changed, the automatic control system very precisely adjusts the propeller pitch to maintain constant engine rpm.

The constant-speed turboprop engine offers excellent fuel efficiency at a relatively high power-to-weight ratio. At low subsonic Mach numbers, a thrust-specific fuel consumption on the order of 0.2 lb-fuel/hr/lb-thrust is attainable and the power-to-weight ratio for these engines can be in excess of 2.5 hp/lb. In addition, the constant-speed turboprop engine provides another important operational feature. Since the engine is always turning at full speed, response to a change in power demand is almost instantaneous. This provides excellent performance characteristics during takeoff, landing, and emergency situations.

In effect, a turboprop engine is an extension of the turbofan engine to higher bypass ratios. At low subsonic airspeeds, the modern turboprop provides excellent overall efficiency. However, conventional propellers operating at high subsonic Mach numbers suffer a substantial loss in efficiency, due to compressibility effects. Turboprops have been designed to provide high propulsive efficiency at Mach numbers as high as 0.8, but no such design has yet been placed in commercial service. Improvements in the power-to-weight ratio and thermodynamic efficiency of turboshaft engines also played a major role in the development of modern helicopters.

In the first 100 years since the maiden flight of the 1903 Wright Flyer, great strides have been made in the development of aircraft propulsion systems. A 12-horsepower piston engine with a power-to-weight ratio of approximately 0.06 hp/lb powered the 1903 Wright Flyer. Today, modern gas turbine engines have a power-to-weight ratio in excess of 2.5 hp/lb, and the largest gas turbines develop close to 100,000 horsepower. The 1903 Wright Flyer first lifted from the Earth with a gross weight of 750 pounds and covered a total distance of 120 feet. Today, transport aircraft powered by modern turbofan engines have a maximum takeoff weight approaching 1,000,000 pounds and a maximum range of more than 8,000 miles. Based on these astounding advancements, it is indeed difficult to imagine what the next century holds in store.

2.2. The Propeller

An airplane propeller has much in common with a finite wing. In fact, each blade of the propeller can be viewed as a rotating wing. Like a wing, the cross-section of a propeller blade is an airfoil section, as shown in Fig. 2.2.1. Both the wing and the propeller blade are designed to produce lift. The lift developed by a wing is usually directed to support the weight of the airplane and keep it aloft. The lift developed by a propeller is typically aligned more or less with the direction of flight and is intended to support the airplane drag and accelerate the airplane in the direction of motion. To a person not familiar with the terminology of aeronautics, it might seem strange to say that we can direct lift to produce a horizontal force in the direction of motion. However, recall that the aerodynamic definition of lift is not a force opposing gravity but a force normal to the relative airflow. It is primarily the motion of the airplane through the air that provides the relative airflow over an airplane wing. Thus, the lift on a wing is normal to the direction of flight. The relative airflow over a propeller blade is provided primarily by the rotation of the propeller. Thus, the lift on a propeller blade is directed approximately along the axis of rotation. The component of the aerodynamic force that is parallel to the axis of rotation is the *thrust*.

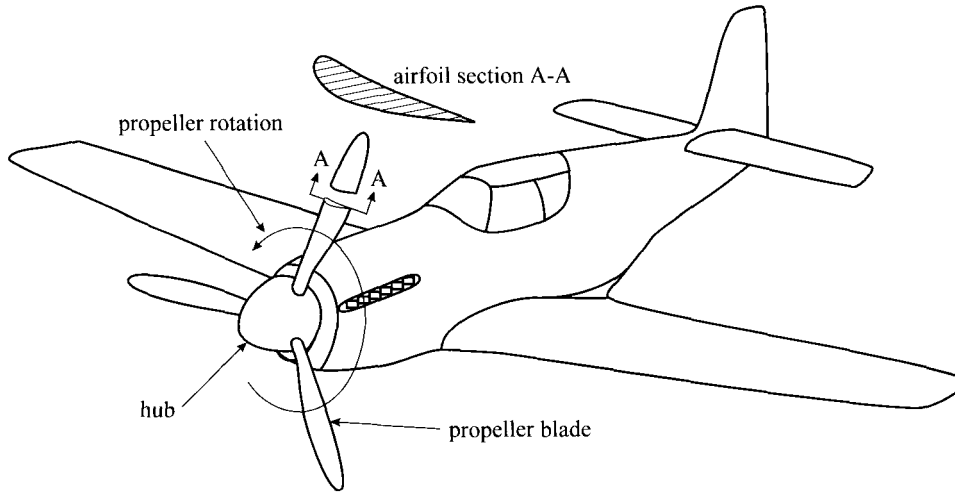


Figure 2.2.1. Airfoil cross-section of an airplane propeller blade.

Because the velocity of each section of a rotating propeller blade depends on the distance of the section from the axis of rotation, a propeller blade usually has much more twist or geometric washout than a typical wing. As shown in Fig. 2.2.2, the sections close to the axis are moving more slowly and form a larger angle with the plane of rotation, while the sections close to the tip are moving faster and form a smaller angle with the plane of rotation. The angle that the section zero-lift line makes with the plane of rotation will be called the *aerodynamic pitch angle*. This pitch angle varies with the radial distance, r, and will be denoted as $\beta(r)$.

The reader should be cautioned that pitch angles are often tabulated relative to the section chord line or to a flat lower surface of the airfoil section. However, the aerodynamic pitch angle, which is used in this text, is more convenient for aerodynamic analysis. If the airfoil section geometry is known and a pitch angle is given in terms of some other definition, the aerodynamic pitch angle can be determined. For example,

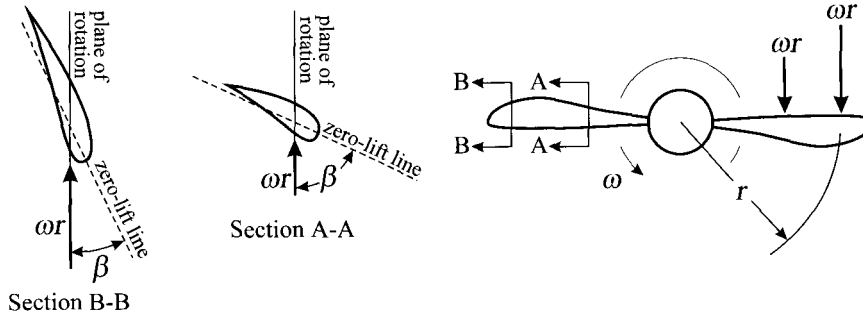


Figure 2.2.2. Radial variation in aerodynamic pitch angle along a propeller blade.

if β_c is the pitch angle relative to the chord line, the aerodynamic pitch angle, β, can be written simply as

$$\beta(r) = \beta_c(r) - \alpha_{L0}(r) \tag{2.2.1}$$

where α_{L0} is the zero-lift angle of attack for the airfoil section of the blade that is located at radius, r.

The pitch of a propeller is not commonly specified in terms of a pitch angle, but rather in terms of a pitch length, which is usually referred to simply as the *pitch*. The pitch length for a propeller is similar to that for a common screw. In fact, propellers were originally called *airscrews*. If the propeller were turned through the air without slipping, the distance that the propeller would move forward in each revolution is the pitch length. In this text, the aerodynamic pitch length is given the symbol λ and is defined relative to the section zero-lift line as

$$\lambda(r) = 2\pi r \tan\beta \tag{2.2.2}$$

This geometric relation is shown schematically in Fig. 2.2.3. Here again the reader is cautioned that propeller pitch is normally tabulated relative to the section chord line or to a flat lower surface of the airfoil section. The aerodynamic pitch, λ, is determined from the chord-line pitch, λ_c, according to the relation

$$\lambda(r) = 2\pi r \frac{\lambda_c - 2\pi r \tan\alpha_{L0}}{2\pi r + \lambda_c \tan\alpha_{L0}} \tag{2.2.3}$$

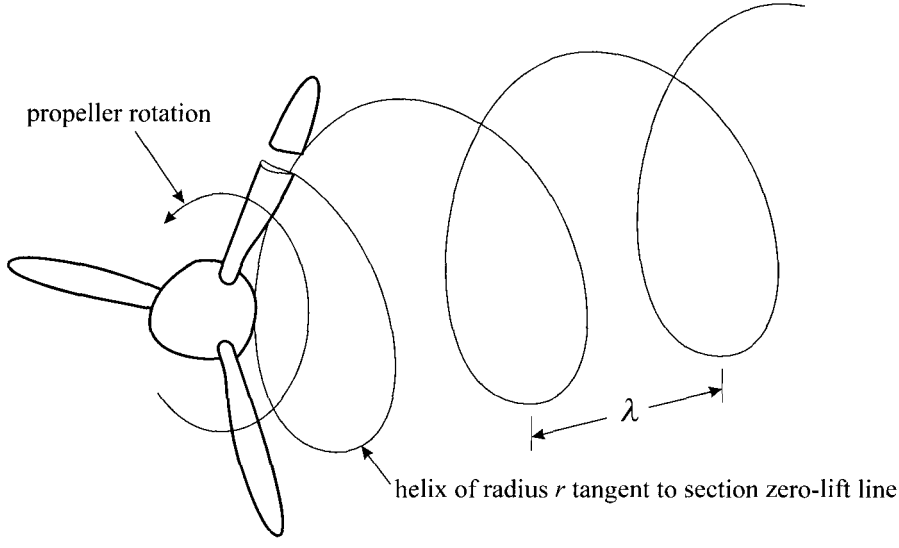


Figure 2.2.3. The helix that defines aerodynamic pitch length.

For the special case of a *constant-pitch propeller*, the pitch length does not vary with the radial coordinate, r. Thus, in a constant-pitch propeller, the tangent of the pitch angle decreases with increasing radius in proportion to $1/r$. The term *constant-pitch* should not be confused with the term *fixed-pitch*, which is related to the term *variable-pitch*. In a *variable-pitch propeller* the propeller pitch can be changed by rotating each blade about an axis that runs along the length of the blade. A *fixed-pitch propeller* is one in which the pitch cannot be varied. As previously stated, a *constant-pitch propeller* is one in which the pitch length does not vary with r.

Like a wing, each blade of the propeller will be subject to a drag force as well as a lift force. Since the propeller blade length is finite, there will be both parasitic drag and induced drag. Because drag is defined as the component of the aerodynamic force that is parallel to the relative airflow, the drag on a rotating propeller blade produces a moment about the propeller axis that opposes the propeller rotation. The torque necessary to counter this moment and the power required to sustain the rotation must be provided by the airplane's engine. Since the axis of propeller rotation is typically aligned closely with the direction of motion, this propeller-induced moment is felt by the airplane as a rolling moment, which must be countered with an aerodynamic moment produced by the airframe or by another propeller rotating in the opposite direction.

Maximizing thrust while minimizing the torque necessary to turn a propeller is obviously one important aspect of good propeller design. The ratio of the thrust developed to the torque required for a propeller is analogous with the lift-to-drag ratio for a wing. The torque required to turn the propeller multiplied by the angular velocity is called the propeller *brake power*. It is this power that must be supplied by the engine. The thrust developed by the propeller multiplied by the airspeed of the airplane is called the *propulsive power*. This is the useful power that is provided to propel the airplane forward against the airframe drag. The ratio of the propulsive power to the brake power for a propeller is called the *propulsive efficiency*. This is one important measure of propeller performance. However, it is not the only important measure. The thrust that is developed by a propeller when the airplane is not moving is called the *static thrust*. It is important for a propeller to produce high static thrust when accelerating an airplane from brake release on takeoff. Since the airspeed is zero for the case of static thrust, the propulsive power and the propulsive efficiency are both zero. Thus, propulsive efficiency is not a particularly good measure of a propeller's ability to accelerate an airplane from a standing start.

The thrust force and the rolling moment are not the only aerodynamic force and moment produced by a rotating propeller. Additional aerodynamic reactions are produced if the propeller rotation axis is not aligned perfectly with the direction of flight. The angle that the propeller axis makes with the freestream airflow is called the *thrust angle* or the *propeller angle of attack*. Since the engine and propeller are typically mounted directly to the airframe, the propeller angle of attack will change with the airplane angle of attack. Because the airplane angle of attack can change during flight, the propeller angle of attack can also change.

When a rotating propeller is at some positive angle of attack relative to the freestream flow, there is a component of the freestream in the plane of propeller rotation, as seen in Fig. 2.2.4. This component of the freestream changes the relative airflow over

each blade of the propeller. It increases the relative airspeed for the downward-moving blades and decreases the relative airspeed for the upward-moving blades. Thus, both the lift and drag are increased on the downward-moving side of the propeller and decreased on the upward-moving side. The difference in thrust generated by the two sides of the propeller produces a yawing moment and the difference in circumferential force produces a net normal force in the plane of rotation, as seen in Fig. 2.2.4.

The axial component of the airplane's airspeed will also affect the aerodynamic forces and moments acting on a rotating propeller. Since this component of the airspeed is normal to the plane of propeller rotation, it changes the angle of attack for the individual blades. This acts very much like the downwash on a finite wing, and like downwash on a wing, this normal component of airflow changes the aerodynamic forces generated on each blade of the propeller.

Even in the static case, when the airplane is not moving, there is airflow normal to the plane of propeller rotation. As is the case with any finite wing, the vorticity shed from each blade of the propeller produces downwash along its own length. However, in addition to being subjected to its own downwash, each blade of a propeller is "flying directly behind" the blade that precedes it in the rotation sequence. The blades of a rotating propeller act very much like an infinite series of finite wings, flying in a row one behind the other. The downwash on any one such wing would be increased by the vorticity shed from every other wing that proceeds it in the flight line. Similarly, the downwash on each blade of a rotating propeller is amplified by its proximity to the other blades. In the case of a rotating propeller, the total downwash generated by all of the propeller blades combined is usually called the propeller's *induced velocity*.

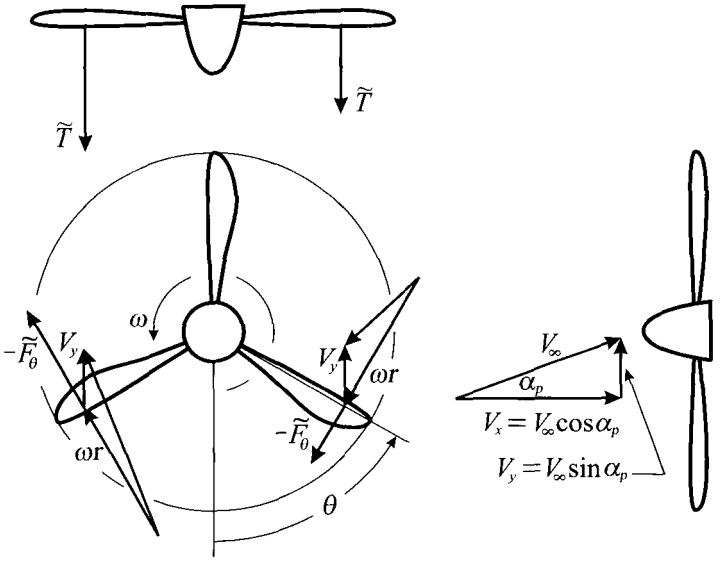


Figure 2.2.4. Effect of propeller angle of attack on the aerodynamic forces acting on a rotating propeller.

A propeller, or even a common house fan, provides a good means for the student to get a feel for the downwash produced by a lifting surface. The downwash produced by a rotating propeller or a common house fan is concentrated in a much smaller area than is that produced by a moving wing. Because the blades are passing repeatedly through the same small section of the fluid, the downwash is amplified with each successive pass. This concentrated downwash is readily detected by the human senses. Although the downwash induced by a rotating propeller is much stronger than the downwash induced by the lifting wing of an airplane, it is conceptually no different in physical origin.

Similar to the lift on a wing, the thrust developed by a propeller is imparted to the individual blades directly through a pressure difference between the upstream and downstream sides of the blade. However, also like a wing, the same pressure difference is imposed on the fluid as well. The pressure difference acting on the fluid generates fluid momentum in a direction opposite to the aerodynamic force exerted on the propeller. The velocity increase induced at the plane of the propeller disk is the downwash that is usually referred to as the propeller's induced velocity.

Optimizing the performance of an airplane powered by an engine-propeller combination depends on properly matching the propeller with the engine, as well as matching the engine-propeller combination with the airframe. Understanding propeller performance is critical to this optimization process. For this purpose, it is useful to be able to predict the aerodynamic forces and moments acting on a rotating propeller as a function of the operating conditions.

2.3. Propeller Blade Theory

In order to quantitatively understand and predict the performance of a rotating propeller, it is necessary to analyze the aerodynamics of the blade in detail. To this end, consider the cross-section of the propeller blade that is shown in Fig. 2.3.1. The blade is rotating with an angular velocity of ω and is advancing through the air with a relative airspeed of V_∞. Initially we shall assume that the forward velocity vector is aligned with the axis of propeller rotation so that there is no component of the forward airspeed in the plane of rotation. The angle that the zero-lift line for the blade section makes with the plane of rotation is what we have called the *aerodynamic pitch angle*, β. In general, this pitch angle varies with the radial distance, r.

The total downwash angle, ε_b, for the blade cross-section located at radius r is the sum of two parts, the downwash angle that results from the propeller's forward motion, ε_∞, and the induced downwash angle, ε_i,

$$\varepsilon_b(r) = \varepsilon_\infty(r) + \varepsilon_i(r) \tag{2.3.1}$$

In this text, ε_∞ is named the *advance angle*, ε_i is called the *induced angle*, and ε_b is simply referred to as the *downwash angle*. This downwash angle reduces the angle of attack for the airfoil section and tilts the lift vector back, as is shown in Fig. 2.3.1. This tilting of the lift vector through the angle ε_b increases the torque required to turn the propeller in much the same way that downwash adds induced drag to a lifting wing. From the geometry shown in Fig. 2.3.1, the section thrust and circumferential force are

related to the section lift and drag forces through this local downwash angle according to the relations

$$\widetilde{T} = \widetilde{L}\cos\varepsilon_b - \widetilde{D}\sin\varepsilon_b \tag{2.3.2}$$

$$\widetilde{F}_\theta = -\widetilde{D}\cos\varepsilon_b - \widetilde{L}\sin\varepsilon_b \tag{2.3.3}$$

From the axial and circumferential components of induced velocity, V_{xi} and $V_{\theta i}$, the downwash angle, ε_b, is determined from the geometry shown in Fig. 2.3.1,

$$\varepsilon_b(r) = \tan^{-1}\left(\frac{V_\infty + V_{xi}}{\omega r - V_{\theta i}}\right) \tag{2.3.4}$$

From the known rotational speed and forward airspeed, the advance angle, ε_∞, is determined directly from this same geometry as

$$\varepsilon_\infty(r) = \tan^{-1}\left(\frac{V_\infty}{\omega r}\right) \tag{2.3.5}$$

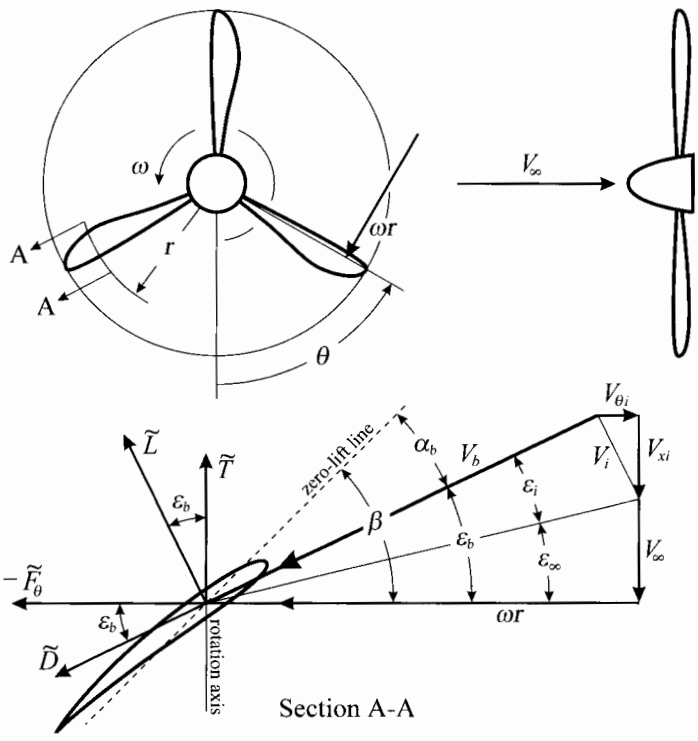


Figure 2.3.1. Section forces and velocities acting on a rotating propeller blade.

Thus, using Eq. (2.3.1), the induced angle, ε_i, is

$$\varepsilon_i(r) = \tan^{-1}\left(\frac{V_\infty + V_{xi}}{\omega r - V_{\theta i}}\right) - \tan^{-1}\left(\frac{V_\infty}{\omega r}\right) \tag{2.3.6}$$

The aerodynamic angle of attack for the blade section, α_b, measured relative to the section zero-lift line is simply the aerodynamic pitch angle, β, less the downwash angle, ε_b. From Eq. (2.3.1), this can be written as

$$\alpha_b(r) = \beta(r) - \varepsilon_b(r) = \beta(r) - \varepsilon_\infty(r) - \varepsilon_i(r) \tag{2.3.7}$$

The fluid velocity relative to the blade cross-section located at radius r is designated as V_b. This is the vector sum of the velocity created by the rotation of the blade, the forward velocity of the propeller, and the propeller induced velocity. The largest component of V_b is usually the circumferential component, ωr, which results from the blade rotation. In addition, there is an axial component of the airspeed, relative to the blade section, which results from the propeller's forward airspeed, V_∞. There is also a component of velocity relative to the blade section that results from the propeller's induced velocity. The induced velocity results from the same aerodynamic pressure difference that produces the lift on the propeller blades. In general, the propeller's induced velocity will have both an axial component, V_{xi}, and a circumferential component, $V_{\theta i}$. The induced velocity will vary with the radial coordinate, r. From the geometry shown in Fig. 2.3.1, the total relative airspeed, V_b, at the plane of the blade section is given by

$$V_b^2 = (\omega r - V_{\theta i})^2 + (V_\infty + V_{xi})^2 = \omega^2 r^2 \left[\left(1 - \frac{V_{\theta i}}{\omega r}\right)^2 + \left(\frac{V_\infty}{\omega r} + \frac{V_{xi}}{\omega r}\right)^2\right] \tag{2.3.8}$$

Using Eqs. (2.3.8), the section lift for the blade section located at radius r is expressed as

$$\widetilde{L} = \tfrac{1}{2}\rho V_b^2 c_b \widetilde{C}_L = \tfrac{1}{2}\rho\omega^2 r^2 c_b \widetilde{C}_L \left[\left(1 - \frac{V_{\theta i}}{\omega r}\right)^2 + \left(\frac{V_\infty}{\omega r} + \frac{V_{xi}}{\omega r}\right)^2\right] \tag{2.3.9}$$

where c_b is the local section chord length and $\widetilde{C}_L$ is the local section lift coefficient, which is a function of the local section aerodynamic angle of attack given by Eq. (2.3.7). Also using Eqs. (2.3.8), the local section drag can be written

$$\widetilde{D} = \tfrac{1}{2}\rho V_b^2 c_b \widetilde{C}_D = \tfrac{1}{2}\rho\omega^2 r^2 c_b \widetilde{C}_D \left[\left(1 - \frac{V_{\theta i}}{\omega r}\right)^2 + \left(\frac{V_\infty}{\omega r} + \frac{V_{xi}}{\omega r}\right)^2\right] \tag{2.3.10}$$

where $\widetilde{C}_D$ is the local 2-D section drag coefficient, which includes only parasitic drag. The induced drag is included as part of the lift vector. In general, the section drag coefficient is also a function of the local section angle of attack.

Applying Eqs. (2.3.9) and (2.3.10) to Eq. (2.3.2), the axial component of section force is written

$$\widetilde{T} = \tfrac{1}{2}\rho\omega^2 r^2 c_b \left[\left(1-\frac{V_{\theta i}}{\omega r}\right)^2 + \left(\frac{V_\infty}{\omega r}+\frac{V_{xi}}{\omega r}\right)^2\right]\left(\widetilde{C}_L\cos\varepsilon_b - \widetilde{C}_D\sin\varepsilon_b\right) \tag{2.3.11}$$

Similarly, from Eq. (2.3.3), the circumferential component of section force is

$$\widetilde{F}_\theta = -\tfrac{1}{2}\rho\omega^2 r^2 c_b \left[\left(1-\frac{V_{\theta i}}{\omega r}\right)^2 + \left(\frac{V_\infty}{\omega r}+\frac{V_{xi}}{\omega r}\right)^2\right]\left(\widetilde{C}_D\cos\varepsilon_b + \widetilde{C}_L\sin\varepsilon_b\right) \tag{2.3.12}$$

The thrust per unit radial distance for the full prop-circle is the axial section force per blade multiplied by the number of blades, k. Thus, from Eq. (2.3.11),

$$\begin{aligned}\frac{dT}{dr} &= k\widetilde{T} \\ &= \frac{k}{2}\rho\omega^2 r^2 c_b \left[\left(1-\frac{V_{\theta i}}{\omega r}\right)^2 + \left(\frac{V_\infty}{\omega r}+\frac{V_{xi}}{\omega r}\right)^2\right]\left(\widetilde{C}_L\cos\varepsilon_b - \widetilde{C}_D\sin\varepsilon_b\right)\end{aligned} \tag{2.3.13}$$

The torque required to turn the propeller is simply the aerodynamic rolling moment, ℓ, that is produced about the axis of propeller rotation. Thus, the torque per unit radial distance, for the full prop-circle, is the circumferential section force per blade multiplied by the radius and the number of blades. From Eq. (2.3.12), this results in

$$\begin{aligned}\frac{d\ell}{dr} &= -kr\widetilde{F}_\theta \\ &= \frac{k}{2}\rho\omega^2 r^3 c_b \left[\left(1-\frac{V_{\theta i}}{\omega r}\right)^2 + \left(\frac{V_\infty}{\omega r}+\frac{V_{xi}}{\omega r}\right)^2\right]\left(\widetilde{C}_D\cos\varepsilon_b + \widetilde{C}_L\sin\varepsilon_b\right)\end{aligned} \tag{2.3.14}$$

If the propeller geometry were completely defined, the section chord length and section pitch angle would be known functions of the radial coordinate, r. The section lift and drag coefficients would be known functions of the radial coordinate, r, and the local section angle of attack, α_b. If the rotational speed and the forward airspeed are known, the advance angle, ε_∞, is known from Eq. (2.3.5). Even so, the two differential equations expressed in Eqs. (2.3.13) and (2.3.14) contain four unknowns: the thrust, T, the torque, ℓ, and the two components of the propeller induced velocity, V_{xi}, and $V_{\theta i}$. If these two components were known, the downwash angle, ε_b, could be determined from Eq. (2.3.4). With only two equations and four unknowns, obviously, additional information is needed

before Eqs. (2.3.13) and (2.3.14) can be solved. For this additional information we will now consider the vortex lifting law and the vorticity that is shed from the rotating propeller blades.

Just as is the case for a lifting wing, lift cannot be generated on a rotating propeller blade without the simultaneous generation of vorticity. Furthermore, as was previously done for a finite wing, the lift on a finite propeller blade can be related to the bound vorticity through the vortex lifting law. This requires that for any cross-section of a propeller blade, the section lift, $\widetilde{L}$, is related to the fluid density, ρ, the relative airspeed, V_b, and the total section circulation, Γ, according to

$$\widetilde{L} = \rho V_b \Gamma \tag{2.3.15}$$

Thus, using Eqs. (2.3.8) and (2.3.9) with Eq. (2.3.15), the local section circulation for any cross-section of a propeller blade can be related to previously defined variables,

$$\Gamma = \tfrac{1}{2} V_b c_b \widetilde{C}_L = \tfrac{1}{2} \omega r c_b \widetilde{C}_L \sqrt{\left(1 - \frac{V_{\theta i}}{\omega r}\right)^2 + \left(\frac{V_\infty}{\omega r} + \frac{V_{xi}}{\omega r}\right)^2} \tag{2.3.16}$$

Since the lift on a propeller blade is generated directly from a pressure difference between the two sides of the blade, the lift must go to zero at the blade tip, where such a pressure difference cannot be supported. This fact, combined with Eq. (2.3.16), requires that vorticity must be shed from the blade tips of a rotating propeller, just as it is from a lifting wing. It is this shed vorticity that produces the induced downwash on the propeller blades. The bound vorticity does not influence the induced downwash. Because of the symmetry of the blades in the prop-circle, each blade receives as much upwash from the bound vorticity on other blades as it does downwash.

The primary difference between the vorticity shed from a propeller blade and that shed from a lifting wing is the path that the vorticity takes as it moves downstream. Whereas the wingtip vortices shed from a lifting wing move downstream in a fairly linear fashion, the blade-tip vortices shed from a rotating propeller follow a helical path, as is seen in Fig. 2.3.2. In this photograph, the path of each blade-tip vortex can be visualized as a result of contrails, which are caused by moisture condensing in the low-pressure region near the core of each vortex. Since the blade-tip vortices all rotate in the same direction, the region inside the propeller's helical trailing vortex system is a region of very strong downwash. This downwash is the air movement that can be felt directly behind a rotating propeller or in front of a common house fan. This cylindrical region of strong downwash is called the *slipstream*. In the region just outside the slipstream, there is upwash. It should be remembered that in aerodynamics terms, "downwash" and "upwash" have nothing to do with "up" and "down" in the conventional sense. *Downwash* is airflow in a direction opposite to the lift vector, and *upwash* is airflow in the same direction as the lift vector. Thus, the induced upwash in the region outside the slipstream is an upstream flow that replaces the air, which has been removed from the region forward of the propelled disk by the induced downwash. This flow pattern is shown schematically in Fig. 2.3.3.

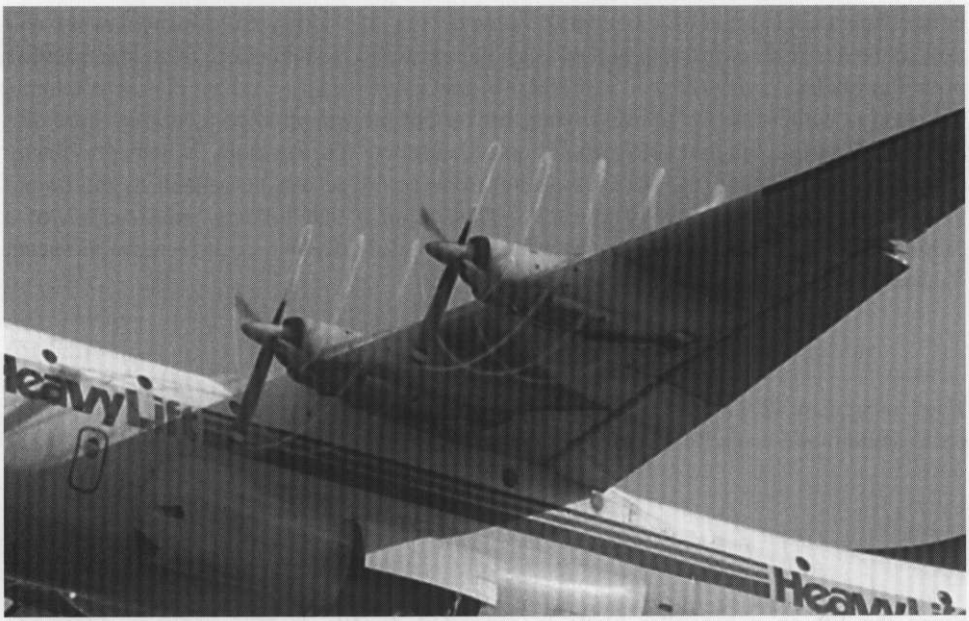


Figure 2.3.2. Contrails showing the helical path of the blade-tip vortices shed from a rotating propeller. (Photograph by Miguel Snoep)

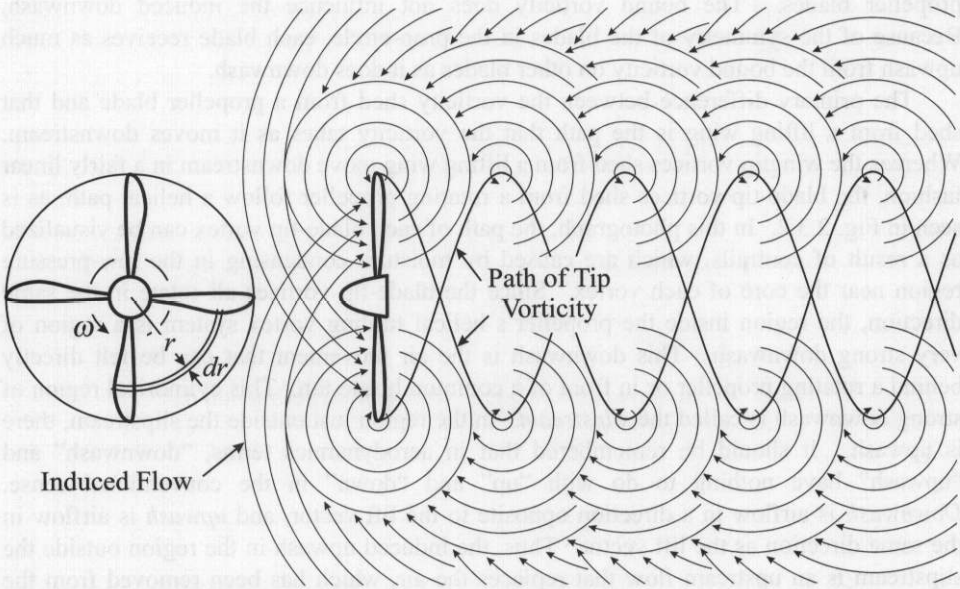


Figure 2.3.3. Schematic cross-section of the vortex-induced flow in the vicinity of a rotating propeller.

Because the vortex lines follow a helical path rather than a circular path, the velocity induced by each vortex, which is normal to the vorticity vector, has a component in the circumferential direction. Thus, the air in the slipstream rotates as it moves downstream. This rotation is not obvious from the feel of the air in the slipstream of a propeller or a common house fan. However, by holding a piece of light yarn in the slipstream of a fan, this rotation is easily seen.

In Fig. 2.3.3, an attempt has been made to show separately the velocity induced by each section of each blade-tip vortex. At any point in space, the resultant induced velocity is the vector sum of the velocity induced by the entire length of all vortex filaments in the slipstream. Since the velocity induced by a vortex filament at any point in space decreases with the distance from the filament, the closest filaments have the greatest influence on the velocity induced at a particular point. However, the induced velocity at any point is influenced by the entire helical vortex system. In the slipstream downstream from the propeller, the upstream portion of the vortex system as well as the downstream portion produces downwash. As a result, downstream from the propeller, the induced velocity is greater than it is in the plane of the propeller, where the only vorticity is downstream. Far downstream from the propeller, the helical vortex system extends essentially from negative infinity to positive infinity, while at the plane of the propeller itself, the vortex system extends only from zero to infinity. Thus, far downstream from the propeller, the induced velocity is about twice what it is in the plane of the propeller disk.

As one might imagine, computing the velocity induced by the helical vortex system trailing downstream from a rotating propeller is considerably more complex than computing the velocity induced by the vortex sheet trailing from a finite lifting wing. One method for predicting this induced velocity is known as *Goldstein's vortex theory*. To predict the velocity induced in the plane of the propeller disk, Goldstein (1929) made two simplifying hypotheses. First, **the vortex sheet trailing from a rotating propeller blade was assumed to lie along a helical surface of constant pitch.** Second, **the induced velocity was assumed to be normal to the resultant velocity, which is the vector sum of the rotation velocity, the forward velocity, and the induced velocity itself.** These assumptions were not made arbitrarily. It can be shown that these conditions are both satisfied in the ultimate slipstream of an optimum propeller. This is the so-called *Betz condition* (see Betz 1919). However, Goldstein's assumptions are difficult to justify in the plane of a propeller having blades of arbitrary pitch and planform shape. Nevertheless, McCormick (1995) states that "studies have been performed that support normality at the plane of the propeller" and he has shown that this theory gives results that are in reasonable agreement with experimental data.

From the normality hypothesis, shown in Fig. 2.3.4, the total relative airspeed, V_b, is given by

$$V_b = \sqrt{\omega^2 r^2 + V_\infty^2}\cos\varepsilon_i = \frac{\omega r}{\cos\varepsilon_\infty}\cos\varepsilon_i \tag{2.3.17}$$

Similarly, from Fig. 2.3.4, the induced velocity and its axial and circumferential components can be written as

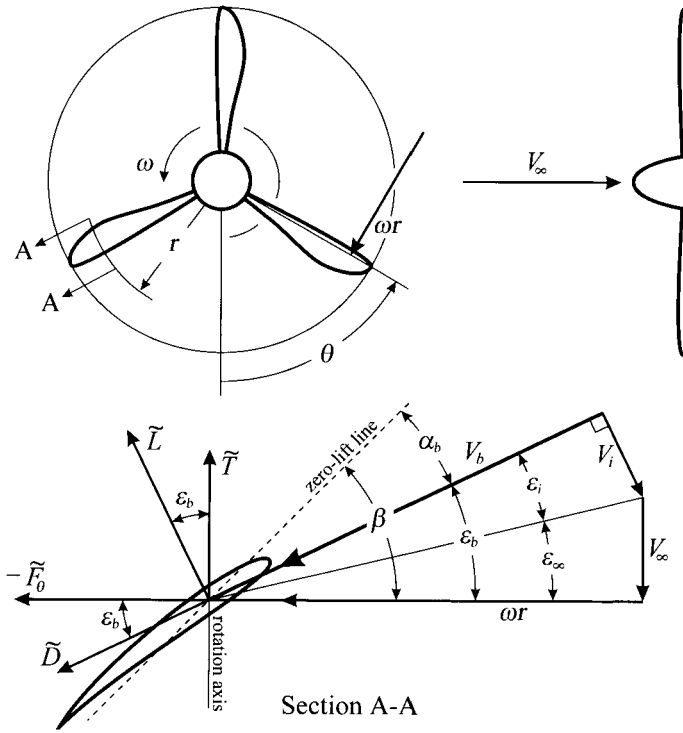


Figure 2.3.4. Section forces and velocities acting on a rotating propeller blade under Goldstein's hypothesis.

$$V_i = \sqrt{\omega^2 r^2 + V_\infty^2} \sin \varepsilon_i = \frac{\omega r}{\cos \varepsilon_\infty} \sin \varepsilon_i \tag{2.3.18}$$

$$V_{xi} = V_i \cos \varepsilon_b = \frac{\omega r}{\cos \varepsilon_\infty} \sin \varepsilon_i \cos(\varepsilon_i + \varepsilon_\infty) \tag{2.3.19}$$

$$V_{\theta i} = V_i \sin \varepsilon_b = \frac{\omega r}{\cos \varepsilon_\infty} \sin \varepsilon_i \sin(\varepsilon_i + \varepsilon_\infty) \tag{2.3.20}$$

From the hypothesis of constant pitch in the trailing helical vortex sheet, Goldstein's vortex theory predicts that the local circumferential component of induced velocity, $V_{\theta i}$, in the plane of the propeller disk is related to the local section circulation, Γ, by

$$k\Gamma = 4\pi\kappa r V_{\theta i} \tag{2.3.21}$$

The proportionality constant, κ, known as *Goldstein's kappa factor*, is available in graphical form but has never been presented in closed form.

A close approximation to Goldstein's result can be obtained from the relation

$$k\Gamma \cong 4\pi f r V_{\theta i} \tag{2.3.22}$$

The parameter f is known as *Prandtl's tip loss factor* (see Prandtl and Betz 1927), which can be expressed as

$$f = \frac{2}{\pi}\cos^{-1}\left\{\exp\left[-\frac{k(1-2r/d_p)}{2\sin\beta_t}\right]\right\} \tag{2.3.23}$$

where β_t is the aerodynamic pitch angle at the propeller blade tip. Using Eq. (2.3.17) in Eq. (2.3.16), the section circulation can also be written as

$$\Gamma = \tfrac{1}{2}V_b c_b \widetilde{C}_L = \tfrac{1}{2}\omega r c_b \widetilde{C}_L \frac{\cos\varepsilon_i}{\cos\varepsilon_\infty} \tag{2.3.24}$$

After applying Eqs. (2.3.20) and (2.3.24) to Eq. (2.3.22), we obtain the relation

$$\frac{kc_b}{16r}\widetilde{C}_L - \cos^{-1}\left\{\exp\left[-\frac{k(1-2r/d_p)}{2\sin\beta_t}\right]\right\}\tan\varepsilon_i \sin(\varepsilon_\infty + \varepsilon_i) = 0 \tag{2.3.25}$$

With knowledge of the propeller geometry, the rotational speed, and the forward speed, Eq. (2.3.25) contains only a single unknown, the induced angle, ε_i. This equation is easily solved numerically to determine the induced angle as a function of the radial coordinate, r.

Once the induced angle is known as a function of radius, the total thrust developed by the propeller is determined by using Eq. (2.3.13) with Eq. (2.3.17) and integrating from the hub radius, r_h, to the tip radius, r_o,

$$\begin{aligned} T &= \int_{r=r_h}^{r_o} \frac{dT}{dr}dr \\ &= \frac{k\rho\omega^2}{2}\int_{r=r_h}^{r_o} r^2 c_b \frac{\cos^2\varepsilon_i}{\cos^2\varepsilon_\infty}\left[\widetilde{C}_L\cos(\varepsilon_\infty+\varepsilon_i) - \widetilde{C}_D\sin(\varepsilon_\infty+\varepsilon_i)\right]dr \end{aligned} \tag{2.3.26}$$

In a similar manner, the total torque required to turn the propeller is found by integrating Eq. (2.3.14) with Eq. (2.3.17),

$$\begin{aligned} \ell &= \int_{r=r_h}^{r_o} \frac{d\ell}{dr}dr \\ &= \frac{k\rho\omega^2}{2}\int_{r=r_h}^{r_o} r^3 c_b \frac{\cos^2\varepsilon_i}{\cos^2\varepsilon_\infty}\left[\widetilde{C}_D\cos(\varepsilon_\infty+\varepsilon_i) + \widetilde{C}_L\sin(\varepsilon_\infty+\varepsilon_i)\right]dr \end{aligned} \tag{2.3.27}$$

Equations (2.3.26) and (2.3.27) can be integrated numerically to determine the propeller thrust and torque. The brake power required to turn the propeller is just the torque multiplied by the angular velocity,

$$P_b \equiv \ell\omega \tag{2.3.28}$$

As is the case with lift and drag, the aerodynamic forces and moments for a propeller are normally expressed in terms of dimensionless coefficients. Whereas the freestream velocity was used as the characteristic velocity in defining the lift and drag coefficients for a wing, the freestream velocity is not the most important velocity associated with the production of thrust by a rotating propeller. The velocity that has the greatest influence on propeller thrust is the rotational velocity of the blades. While there are several characteristic dimensions associated with a propeller, the one most commonly used in the definition of dimensionless propeller coefficients is the propeller diameter, d_p. Although other definitions have occasionally been used, by far the most common definitions for the propeller coefficients are:

Thrust coefficient

$$C_T \equiv \frac{T}{\rho(\omega/2\pi)^2 d_p^4} \tag{2.3.29}$$

Torque coefficient

$$C_\ell \equiv \frac{\ell}{\rho(\omega/2\pi)^2 d_p^5} \tag{2.3.30}$$

Power coefficient

$$C_P \equiv \frac{\ell\omega}{\rho(\omega/2\pi)^3 d_p^5} \tag{2.3.31}$$

With these definitions, Eqs. (2.3.25) through (2.3.28) are readily nondimensionalized to yield

$$\frac{\hat{c}_b}{8\zeta}\widetilde{C}_L(\alpha_b,\zeta) - \cos^{-1}\left\{\exp\left[-\frac{k(1-\zeta)}{2\sin\beta_t}\right]\right\}\tan\varepsilon_i\sin(\varepsilon_\infty+\varepsilon_i) = 0 \tag{2.3.32}$$

$$C_T = \frac{\pi^2}{4}\int_{\zeta=\zeta_h}^{1}\zeta^2\hat{c}_b\frac{\cos^2\varepsilon_i}{\cos^2\varepsilon_\infty}\left[\widetilde{C}_L\cos(\varepsilon_\infty+\varepsilon_i)-\widetilde{C}_D\sin(\varepsilon_\infty+\varepsilon_i)\right]d\zeta \tag{2.3.33}$$

$$C_\ell = \frac{\pi^2}{8}\int_{\zeta=\zeta_h}^{1}\zeta^3\hat{c}_b\frac{\cos^2\varepsilon_i}{\cos^2\varepsilon_\infty}\left[\widetilde{C}_D\cos(\varepsilon_\infty+\varepsilon_i)+\widetilde{C}_L\sin(\varepsilon_\infty+\varepsilon_i)\right]d\zeta \tag{2.3.34}$$

$$C_P = 2\pi C_\ell \tag{2.3.35}$$

where β_t is the aerodynamic pitch angle at the blade tip. The local section lift and drag coefficients are evaluated at the local section angle of attack,

$$\alpha_b(\zeta) = \beta - \varepsilon_\infty - \varepsilon_i \tag{2.3.36}$$

and

$$\zeta \equiv \frac{r}{d_p/2} \tag{2.3.37}$$

$$\hat{c}_b \equiv \frac{kc_b}{d_p} \tag{2.3.38}$$

$$\beta \equiv \tan^{-1}\left(\frac{K}{\pi\zeta}\right) \tag{2.3.39}$$

$$\varepsilon_\infty \equiv \tan^{-1}\left(\frac{J}{\pi\zeta}\right) \tag{2.3.40}$$

$$K \equiv \frac{\lambda}{d_p} \tag{2.3.41}$$

$$J \equiv \frac{2\pi V_\infty}{\omega d_p} \tag{2.3.42}$$

The local *chord length ratio*, $\hat{c}_b$, is the total chord length for all blades combined divided by the propeller diameter. The dimensionless quantity, K, is the local *pitch-to-diameter ratio*. The dimensionless quantity, J, is called the *advance ratio* and is the distance that the propeller is advanced in one revolution divided by the propeller diameter. In general, both $\hat{c}_b$ and K will vary with ζ. However, for a propeller with constant aerodynamic pitch, the aerodynamic pitch length does not vary with radius and thus K is constant.

Knowing the propeller diameter and the planform shape of the blade, we can determine the dimensionless chord length ratio, $\hat{c}_b$, as a function of ζ from Eq. (2.3.38). From the known variation in pitch length and propeller diameter, the pitch-to-diameter ratio, K, is also determined as a function of ζ using Eq. (2.3.41). With knowledge of the forward speed and rotational speed, the advance ratio, J, is found from Eq. (2.3.42). Knowing the variation in pitch-to-diameter ratio and advance ratio we can now compute both $\beta(\zeta)$ and $\varepsilon_\infty(\zeta)$ from Eqs. (2.3.39) and (2.3.40). From the known section properties of the propeller blade, the section lift and drag coefficients are known functions of α_p and ζ. With this knowledge, the induced angle, $\varepsilon_i(\zeta)$, is determined by solving Eq. (2.3.32) numerically. With the induced angle known, the aerodynamic coefficients are determined numerically from Eqs. (2.3.33) through (2.3.35).

Having determined the advance ratio, the thrust coefficient, and the power coefficient, the propulsive efficiency for the propeller can be determined. The propulsive efficiency is defined as the propulsive power divided by the brake power,

$$\eta_p \equiv \frac{TV_\infty}{\ell\omega} = \left[\frac{T}{\rho(\omega/2\pi)^2 d_p^4}\right]\left[\frac{V_\infty}{(\omega/2\pi)d_p}\right]\left[\frac{\rho(\omega/2\pi)^3 d_p^5}{\ell\omega}\right] \tag{2.3.43}$$

Thus, the propulsive efficiency is

$$\eta_p = \frac{C_T J}{C_P} \tag{2.3.44}$$

Notice that the propeller thrust coefficient, C_T, the torque coefficient, C_ℓ, the power coefficient, C_P, and the propulsive efficiency, η_p, are all functions of the chord length ratio, $\hat{c}_b(\zeta)$, the pitch-to-diameter ratio, $K(\zeta)$, and advance ratio, J. These coefficients also depend on the blade cross-section through the section lift and drag coefficients. Since results must be determined numerically, to examine the nature of propeller performance we must turn to a specific example using some particular geometry.

EXAMPLE 2.3.1. To examine how propeller performance depends on pitch-to-diameter ratio and advance ratio, we shall consider a family of fixed-pitch propellers having two blades with an elliptic planform shape. The blade chord length varies with radial position according to the relation

$$\frac{c_b}{d_p} = 0.075\sqrt{1-\zeta^2}$$

The airfoil section as well as the chord-line pitch length, λ_c, for this family of propellers is constant along the blade. The hub diameter is 10 percent of the propeller diameter. The zero-lift angle of attack for the airfoil section is -2.1 degrees and the section lift and drag coefficients can be approximated as

$$\widetilde{C}_L = \begin{cases} 2\pi\alpha_b, & \alpha_b \le 0.25 \\ \dfrac{\pi}{2}\dfrac{\cos\alpha_b}{\cos(0.25)}, & \alpha_b > 0.25 \end{cases}$$

$$\widetilde{C}_D = \begin{cases} 0.224\alpha_b^2 + 0.006, & \alpha_b \le 0.25 \\ 16.6944\alpha_b^2 - 1.0234, & 0.25 \le \alpha_b \le 0.30 \\ \dfrac{\pi}{2}\dfrac{\sin\alpha_b}{\cos(0.25)}, & \alpha_b \ge 0.30 \end{cases}$$

where α_b is the aerodynamic angle of attack, measured relative to the zero-lift line. We wish to study the performance of this family of propellers, over a range of operating conditions, based on the propeller blade theory presented in this section.

Solution. For this propeller, the chord-line pitch length, λ_c, is said to be constant. However, this does not mean that the aerodynamic pitch length is constant. The aerodynamic pitch length is related to the chord-line pitch length according to Eq. (2.2.3),

$$\lambda = 2\pi r \frac{\lambda_c - 2\pi r \tan\alpha_{L0}}{2\pi r + \lambda_c \tan\alpha_{L0}}$$

or

$$K = \pi\zeta \frac{K_c - \pi\zeta \tan\alpha_{L0}}{\pi\zeta + K_c \tan\alpha_{L0}}$$

For this airfoil the zero-lift angle of attack is -2.1 degrees ($\tan\alpha_{L0} = -0.0367$).

The geometry, the aerodynamic angles, and thrust and power distribution, as predicted by Goldstein's theory, are presented in Figs. 2.3.5 and 2.3.6 for one of these propellers at two different operating conditions. There are two things that should be observed from these figures. First, notice that even though this propeller would typically be called a constant-pitch propeller, the aerodynamic pitch varies considerably over the length of the blade. Also notice that at an advance ratio of 0.25, despite an aerodynamic pitch angle as high as 60 degrees, the forward motion and induced velocity keep the angle of attack low and the propeller blades do not stall. However, at an advance ratio of zero, the blades are stalled in the region near the hub, with angles of attack approaching 40 degrees.

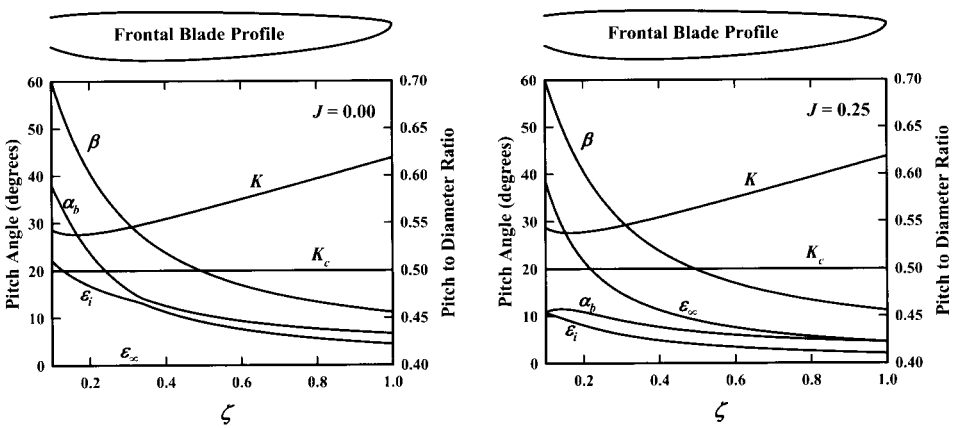


Figure 2.3.5. Pitch and aerodynamic angles for the propeller in Example 2.3.1.

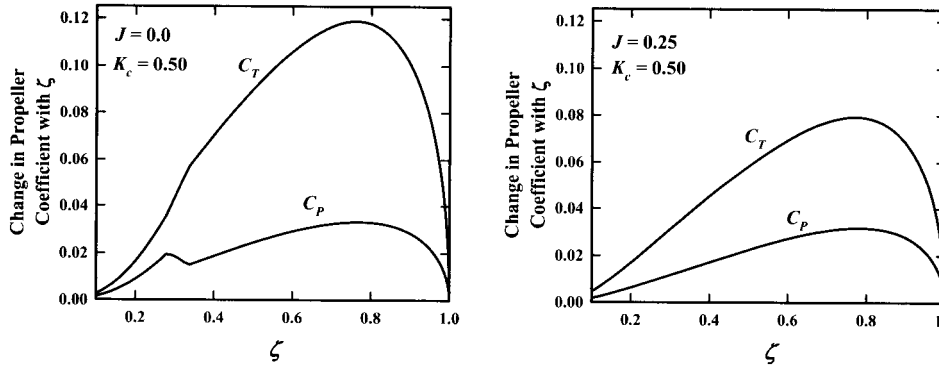


Figure 2.3.6. Thrust and power distribution for the propeller in Example 2.3.1.

As an example calculation, consider the 75 percent radius section of one of these propellers with a chord-line pitch-to-diameter ratio of 0.5 operating at an advance ratio of 0.25. The aerodynamic pitch-to-diameter ratio for this cross-section is

$$K = \pi\zeta\frac{K_c - \pi\zeta\tan\alpha_{L0}}{\pi\zeta + K_c\tan\alpha_{L0}} = \pi(0.75)\frac{0.5 - \pi(0.75)(-0.0367)}{\pi(0.75) + 0.5(-0.0367)} = 0.591$$

From Eq. (2.3.39), the aerodynamic pitch angle for this cross-section is

$$\beta \equiv \tan^{-1}\left(\frac{K}{\pi\zeta}\right) = \tan^{-1}\left(\frac{0.591}{\pi 0.75}\right) = 0.2458 = 14.08°$$

From Eq. (2.3.40), the advance angle for this cross-section is

$$\varepsilon_\infty \equiv \tan^{-1}\left(\frac{J}{\pi\zeta}\right) = \tan^{-1}\left(\frac{0.25}{\pi 0.75}\right) = 0.1057 = 6.06°$$

From Eq. (2.3.38), the chord length ratio for this cross-section is

$$\hat{c}_b \equiv \frac{kc_b}{d_p} = k\,0.075\sqrt{1-\zeta^2} = (2)0.075\sqrt{1-0.75^2} = 0.09922$$

Using these values, Eq. (2.3.32) is solved numerically to give

$$\varepsilon_i = 0.04815 = 2.76°$$

With these results, the integrands in Eqs. (2.3.33) and (2.3.34) are

$$\frac{dC_T}{d\zeta} = 0.0791 \text{ and } \frac{dC_P}{d\zeta} = 0.0315$$

Integrating similar results from $\zeta = 0.1$ to 1.0, we obtain

$$C_T = \underline{0.0465},\ C_P = \underline{0.0182},\ \text{and } \eta_p = \frac{C_T J}{C_P} = \underline{0.637}$$

Based on Goldstein's theory and this particular propeller geometry, the results of a parametric study showing how the thrust coefficient, power coefficient, and propulsive efficiency depend on the advance ratio and pitch-to-diameter ratio are presented in Figs. 2.3.7 through 2.3.9. These figures are for a family of propellers with similar geometry. Because these are fixed-pitch propellers, each curve shown in each of these figures is for a different propeller. The pitch-to-diameter ratio for one of these propellers is fixed by the design and manufacture of the blades. It does not vary with operating conditions. The advance ratio, on the other hand, depends primarily on the operating conditions and is directly proportional to the forward airspeed. Notice that for any given propeller, the thrust and power both decrease with increasing advance ratio, going to zero at some particular advance ratio. However, the propulsive efficiency increases with advance ratio to some point of maximum efficiency and then rapidly decreases to zero as the advance ratio is further increased.

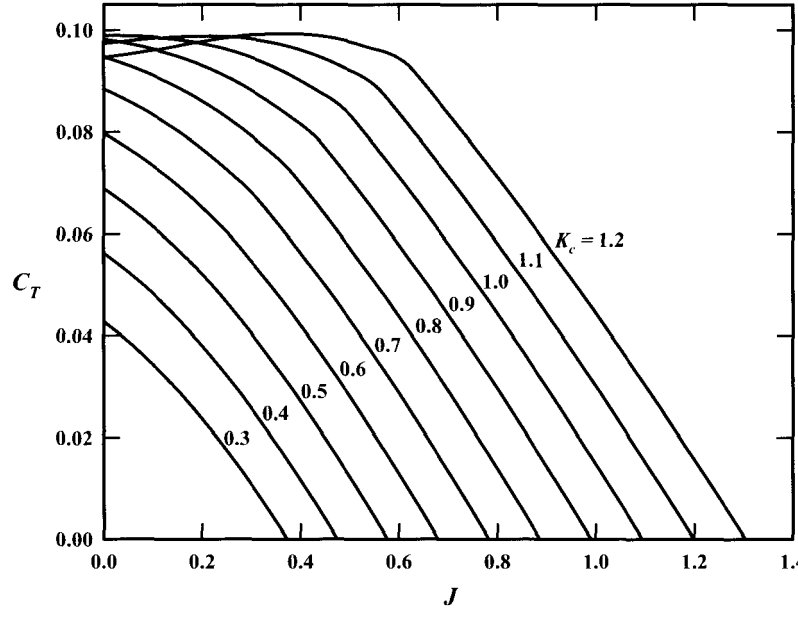


Figure 2.3.7. Thrust coefficient for the family of propellers in Example 2.3.1.

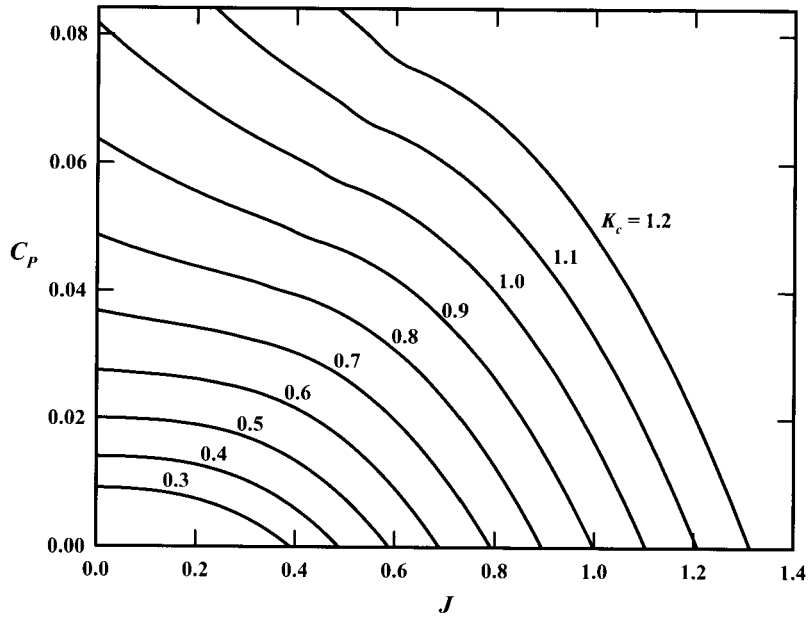


Figure 2.3.8. Power coefficient for the family of propellers in Example 2.3.1.

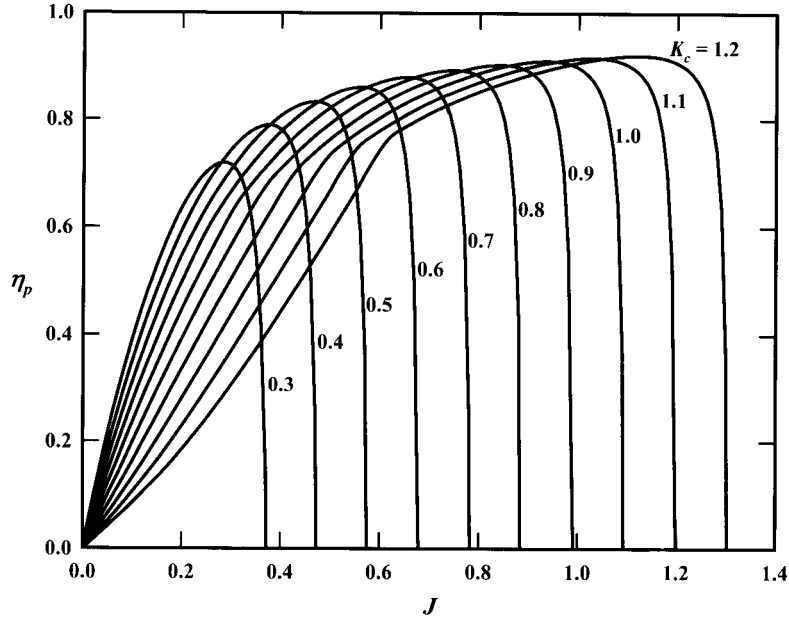


Figure 2.3.9. Propulsive efficiency for the family of propellers in Example 2.3.1.

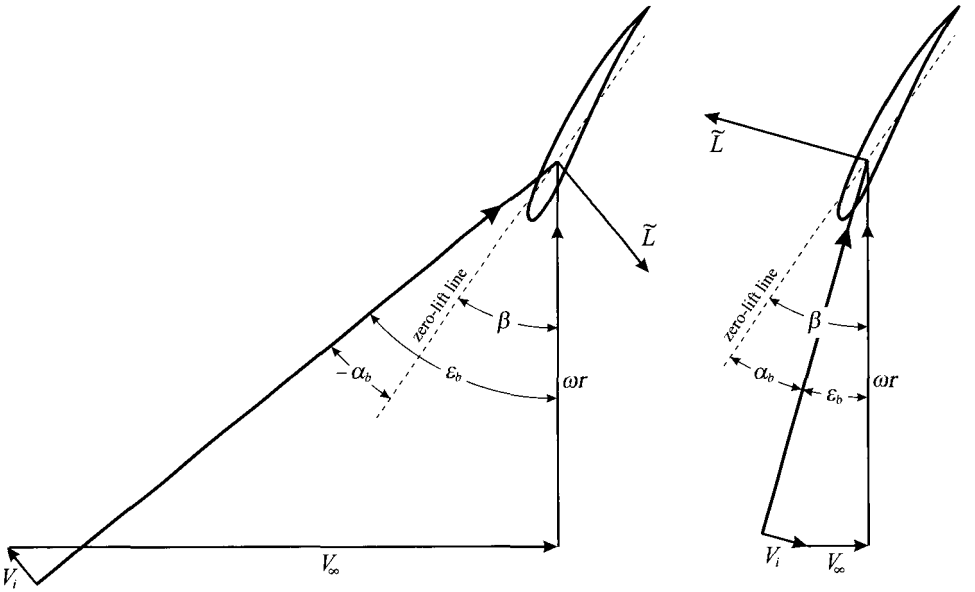


Figure 2.3.10. Variation of blade angle of attack and section lift with advance ratio.

Several important points can be observed from Example 2.3.1. First of all, notice from Fig. 2.3.7 that in the range of advance ratio where the blades are not stalled, the thrust coefficient decreases in a nearly linear fashion with increasing advance ratio. This is because for small angles, the angle of attack for each blade section is nearly a linear function of advance ratio. This can be seen in Fig. 2.3.10. When the advance ratio becomes large enough, the aerodynamic angle of attack becomes negative and both the thrust and the brake power required to turn the propeller become negative as well. Under such conditions the propeller is operating as a wind turbine. A wind turbine produces power that can be used to do work but it also produces a negative thrust (i.e., drag). When the engine of an airplane is not running, a fixed-pitch propeller will operate as a wind turbine. When an airplane propeller is turning in this fashion it is said to be *windmilling*. The negative thrust produced by a windmilling propeller can greatly increase the drag on an airplane when one engine or more is inoperative. When a variable-pitch propeller is used, the pitch can be adjusted to minimize this added drag. This is called *feathering the prop*.

The power produced by the windmilling propeller of an airplane has sometimes been put to good use. In the early days of aviation, airplane engines were hand started by turning the engine over with the prop. The pilot or an assistant would stand behind the propeller and slowly turn the engine to the beginning of a compression stroke. One blade of the propeller would then be pulled down rapidly to turn over and hopefully start the engine. Although it is not common, the engines of some small single-engine airplanes are sometimes still started in this manner today. Years ago, when hand starting was the only means of starting an airplane engine, these engines were much less reliable than

aircraft engines are today. If an engine stalled in flight, putting the airplane into a dive would sometimes restart the engine. With the added airspeed attained in the dive, the power generated by the windmilling propeller would turn the engine over more rapidly and the engine would sometimes restart. This was a risky tactic, however, because should the engine fail to restart, much precious altitude was lost.

Understanding the relationship between advance ratio and blade angle of attack that is shown in Fig. 2.3.10 makes it easy to understand the relationship between advance ratio and propeller efficiency, which is presented in Fig. 2.3.9. Once we realize that very large advance ratios will produce negative angles of attack on the propeller blades, we realize that the thrust developed by a propeller must go to zero for some particular value of the advance ratio. Since the propulsive power is just the thrust multiplied by the airspeed, when the thrust goes to zero the propulsive power must go to zero as well. At the advance ratio that results in exactly zero thrust, some power is still required to turn the propeller against the blade drag. Thus, the point of zero thrust is a point of zero propulsive efficiency. The point of zero advance ratio corresponds to the condition of zero forward airspeed. Thus, this is also a point of zero propulsive power and zero propulsive efficiency. Regardless of how much static thrust is developed by the propeller, the thrust multiplied by the airspeed is always zero at the static condition. This explains the two points of zero propulsive efficiency for the curves shown in Fig. 2.3.9. The point on the right corresponds to zero thrust, and the point on the left corresponds to zero airspeed.

A very important observation should be made from Fig. 2.3.9. Since each curve in this figure is for a different fixed-pitch propeller, we see that maximum efficiency is attained with a fixed-pitch propeller only at one specific value of advance ratio. Furthermore, the advance ratio that results in maximum efficiency is a function of the pitch-to-diameter ratio. Propellers with low pitch-to-diameter ratio perform best at low advance ratio while propellers with high pitch-to-diameter ratio perform best at high advance ratio. Considering conditions during takeoff as well as cruise, an airplane must operate over a wide range of airspeeds. Thus, in the early days of aviation when only fixed-pitch propellers were available, the performance of airplanes was severely limited by this propeller characteristic. This problem was remedied in 1924 when H. S. Hele-Shaw and T. E. Beacham patented the first variable-pitch propeller in England. The blades of a variable-pitch propeller are attached to a mechanism in the hub that rotates the entire blade about an axis that runs along the length of the blade, as shown in Fig. 2.3.11. This allows the blade pitch to be varied continuously by the pilot to maintain optimum efficiency at any airspeed. By the early 1930s such propellers were in production in the United States.

A further improvement along these same lines was the introduction of the *constant-speed propeller* in 1935. A constant-speed propeller is simply a variable-pitch propeller that is controlled by a governor mechanism, which continuously and automatically varies the propeller pitch to maintain the torque on the engine so that the rotational speed of the engine is held constant. This is advantageous because the brake power output from a piston engine is optimized at some particular rotational speed. By controlling the engine speed with a constant-speed propeller, the engine can be made to operate at either maximum efficiency or maximum power, depending on how the governor is adjusted by

the pilot. On takeoff the pilot will typically adjust the governor for maximum power. In cruise, the governor can be adjusted for maximum efficiency or for some compromise between airspeed and efficiency.

The introduction of the variable-pitch and constant-speed propellers was one of the most important developments in aviation history. With such mechanisms, the propulsive efficiency for modern propellers can be maintained in the range from approximately 80 to 90 percent over a wide range of airspeed.

Example 2.3.1 shows how propeller efficiency is related to propeller pitch and forward speed. However, efficiency is not always the primary concern in aircraft propulsion. Sometimes it is more important to maximize thrust. From the results shown

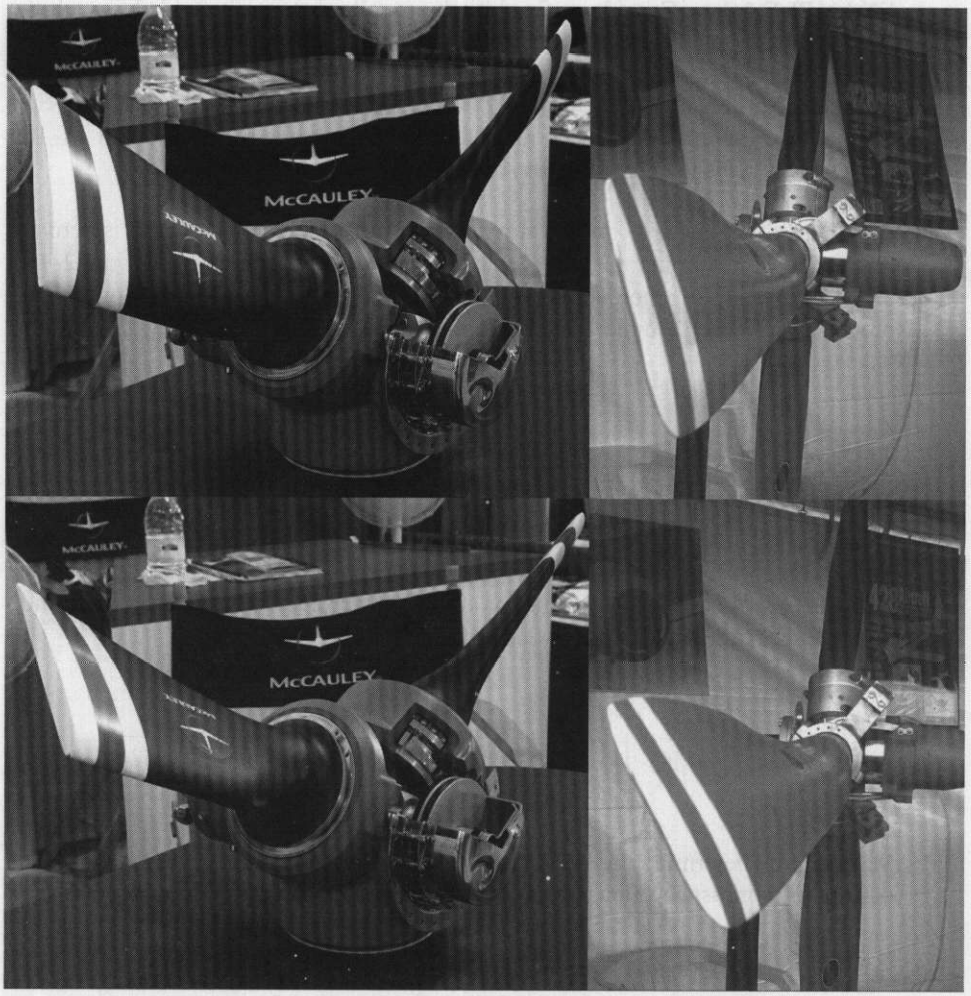


Figure 2.3.11. Variable-pitch propeller. (Photographs by Barry Santana)

in Fig. 2.3.7 we have seen that for a given advance ratio, the thrust coefficient for a propeller is always increased by increasing the pitch-to-diameter ratio, provided that the propeller blades do not stall. From this figure, a student might reach the erroneous conclusion that a pitch-to-diameter ratio of about 1.0 would result in the greatest static thrust. Figure 2.3.7 can be somewhat misleading in this regard, because the thrust coefficient is nondimensionalized with respect to the rotational speed of the propeller. Both the thrust and rotational speed depend on the brake power that is applied to the propeller shaft. For a given brake power input, as pitch-to-diameter ratio is increased, the rotational speed of the propeller will decrease. Thus, it is not clear from Fig. 2.3.7 how the static thrust will vary with pitch-to-diameter ratio for a given brake power input. This is examined in the following example.

EXAMPLE 2.3.2. Consider a fixed-pitch propeller having three blades, with the same blade geometry as that described in Example 2.3.1. We wish to examine how the static thrust developed by such a propeller depends on propeller pitch and diameter. For this purpose, we wish to plot the static thrust at standard sea level as a function of pitch-to-diameter ratio for a constant brake power input of 180 horsepower. This is to be done for several different propeller diameters.

Solution. Since we are concerned with static thrust, the advance ratio is zero for any value of rotational speed. As an example calculation, consider a 72-inch propeller having a chord-line pitch-to-diameter ratio of 0.6. Following the procedure used in Example 2.3.1, for $J = 0.0$ and $K_c = 0.6$, we obtain

$$C_T = 0.11004$$

and

$$C_P = 0.03952$$

Since we know that the brake power is 180 horsepower, the rotational speed of the propeller can be determined from the known power coefficient and the definition of power coefficient, which is given by Eq. (2.3.31). This gives

$$\frac{\omega}{2\pi} = \left(\frac{\ell\omega}{\rho d_p^5 C_P}\right)^{\frac{1}{3}} = \left[\frac{(180\times 550)\ \text{ft}\cdot\text{lbf/sec}}{0.0023769\ \text{slug/ft}^3 (72/12)^5\ \text{ft}^5 (0.03952)}\right]^{\frac{1}{3}}$$

$$= 51.37\ \text{rps} = 3{,}082\ \text{rpm}$$

We can now determine the static thrust from the known thrust coefficient and the definition of thrust coefficient, which is given by Eq. (2.3.29). Thus we have

$$T = \rho(\omega/2\pi)^2 d_p^4 C_T$$

$$= 0.0023769\ \text{slug/ft}^3 (51.37\,\text{sec}^{-1})^2 (72/12)^4\ \text{ft}^4 (0.11004) = \underline{894\ \text{lbf}}$$

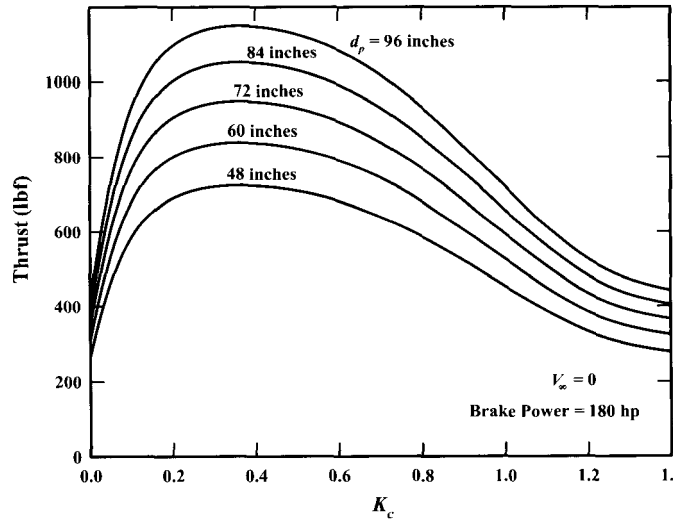


Figure 2.3.12. Variation in static thrust with pitch-to-diameter ratio for the propellers in Example 2.3.2, with a brake power input of 180 horsepower.

Repeating these calculations for different values of pitch-to-diameter ratio and different propeller diameters, we obtain the results that are shown in Fig. 2.3.12. Notice that for this blade geometry, maximum static thrust is realized for a chord-line pitch-to-diameter ratio of about 0.36. The existence of this maximum is not obvious from direct examination of the dimensionless results that are plotted in Fig. 2.3.7.

Similar results are shown in Fig. 2.3.13, for the same propellers with a 300-horsepower input. Notice that while the increased power increases the magnitude of the static thrust, it does not change the shape of the curves. For incompressible flow and this particular blade geometry, a chord-line pitch-to-diameter ratio of about 0.36 will produce the greatest static thrust for any fixed power input and any propeller diameter.

A very important point is demonstrated in Example 2.3.2. Notice from Figs. 2.3.12 and 2.3.13 that for incompressible flow with fixed power input and fixed pitch-to-diameter ratio, the static thrust is always greatest for the propeller with the largest diameter. With the brake power and pitch-to-diameter ratio held constant, increasing propeller diameter requires decreasing the rotational speed. When the diameter is increased and the rotational speed is decreased to maintain constant power input, the mass flow rate of the air drawn through the propeller disk is increased, but the slip-stream velocity that is imparted to that air is decreased. As was pointed out in Sec. 2.1, thrust is produced with the greatest efficiency when the mass flow rate is large and the velocity increment is small. Thus, large-diameter propellers with correspondingly lower rotational speeds result in the most efficient production of thrust. Similar results are

shown in Figs. 2.3.14 and 2.3.15 for forward speeds of 50 and 100 mph. In all cases, **for incompressible flow with fixed power input, maximum thrust is attained with the largest propeller diameter.**

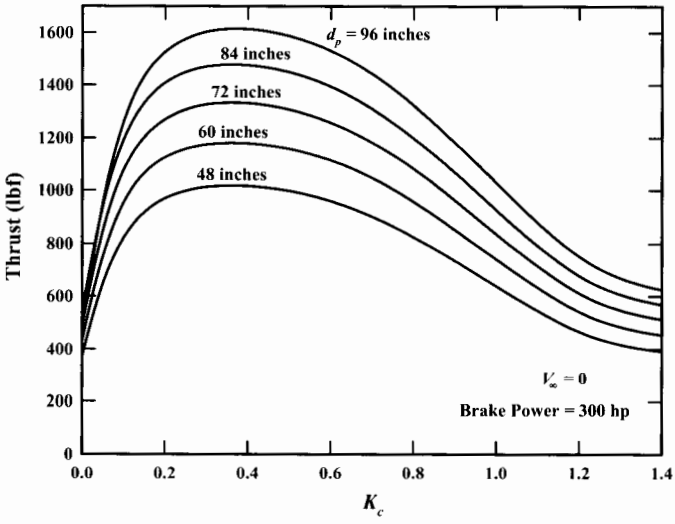


Figure 2.3.13. Variation in static thrust with pitch-to-diameter ratio for the propellers in Example 2.3.2 with a brake power input of 300 horsepower.

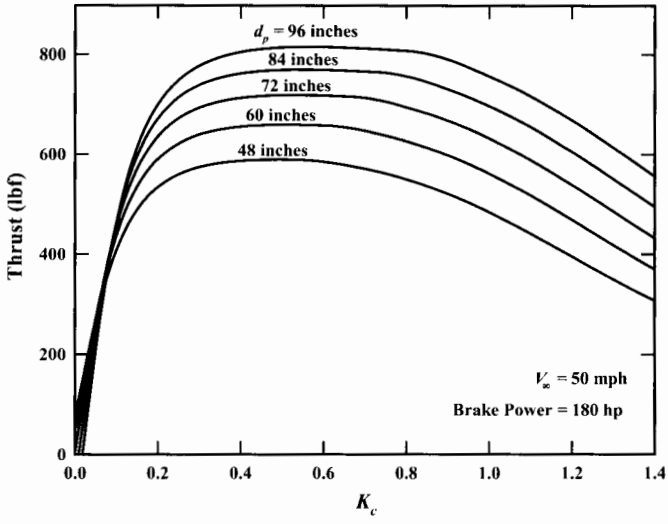


Figure 2.3.14. Thrust variation for the propellers in Example 2.3.2 with a forward speed of 50 miles per hour.

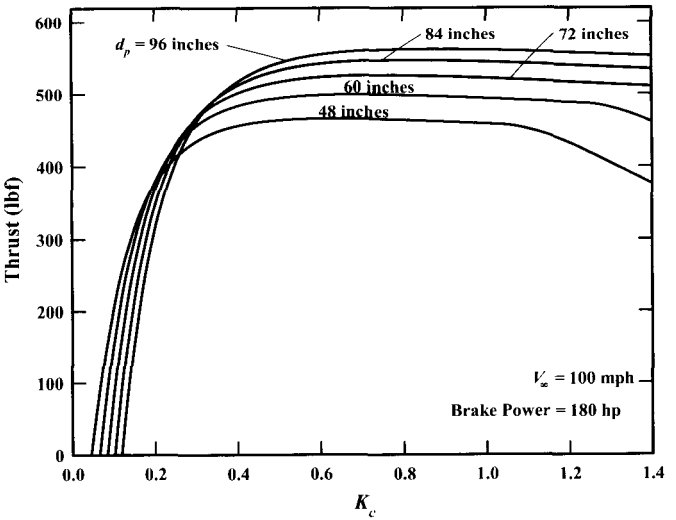


Figure 2.3.15. Thrust variation for the propellers in Example 2.3.2 with a forward speed of 100 miles per hour.

In Example 2.3.2, propeller diameter was held constant and the rotational speed necessary to give a specified brake power was computed. However, a piston engine produces maximum power only at one particular rotational speed. When selecting a propeller for a particular piston engine, both the diameter and the pitch can be varied to match the propeller to the engine and the application. This is demonstrated in the following two examples.

EXAMPLE 2.3.3. At sea level, a particular piston engine develops maximum brake power of 180 horsepower at 2900 rpm. For this example, we wish to select a fixed-pitch propeller for this engine that will maximize the static thrust at sea level. We assume a three-blade configuration with the same blade geometry as that described in Example 2.3.1.

Solution. As an example calculation, we again consider a propeller having a chord-line pitch-to-diameter ratio of 0.6. From Example 2.3.2, for $J = 0.0$ and $K_c = 0.6$, we obtain

$$C_T = 0.11004$$

and

$$C_P = 0.03952$$

Since we require a brake power of 180 horsepower and a rotational speed of 2900 rpm, Eq. (2.3.31) can be used to fix the propeller diameter. This gives

$$d_p = \left(\frac{\ell\omega}{\rho(\omega/2\pi)^3 C_P}\right)^{\frac{1}{5}} = \left[\frac{(180\times550)\text{ ft}\cdot\text{lbf/sec}}{0.0023769\text{ slug/ft}^3(2{,}900/60)^3\text{ sec}^{-3}(0.03952)}\right]^{\frac{1}{5}}$$

$$= 6.223\text{ ft} = 74.68\text{ inches}$$

From Eq. (2.3.29) and the known thrust coefficient, the sea-level static thrust developed by this engine-propeller combination would be

$$T = \rho(\omega/2\pi)^2 d_p^4 C_T$$

$$= 0.0023769\text{ slug/ft}^3(2{,}900/60)^2\text{ sec}^{-2}(6.223\text{ ft})^4(0.11004) = \underline{916\text{ lbf}}$$

Repeating these calculations for different values of pitch-to-diameter ratio, we obtain the results that are plotted in Fig. 2.3.16. Thus, Goldstein's vortex theory for incompressible flow predicts that maximum static thrust for this engine and propeller geometry is realized at a chord-line pitch-to-diameter ratio of about 0.19 with a 105-inch propeller. However, this propeller and operating condition would produce a tip speed of 1,329 ft/sec, which corresponds to a tip Mach number of nearly 1.2. **This incompressible flow theory is not valid for a tip Mach number this large, so the solution is not realistic.** When the tip Mach number is greater than unity, the brake power required to turn the propeller at a certain speed goes up dramatically. Thus, for fixed power input, the speed or the diameter would need to be decreased and the thrust would decrease accordingly.

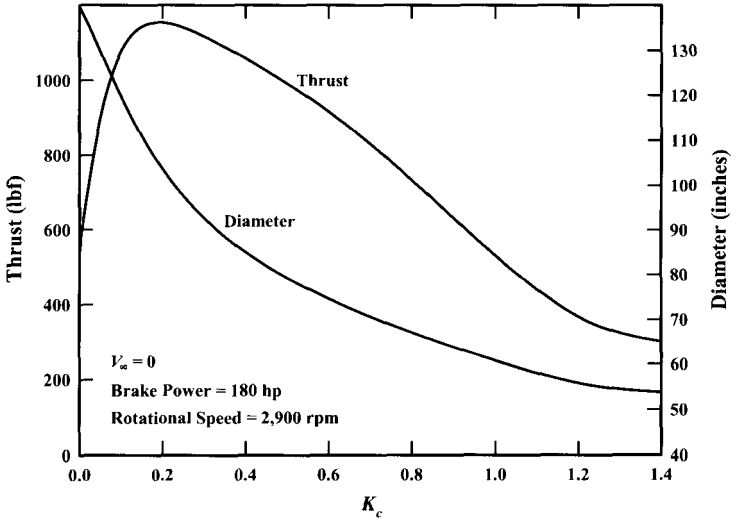


Figure 2.3.16. Variation in thrust with pitch-to-diameter ratio for the engine-propeller combination in Example 2.3.3.

If compressibility effects were accounted for, maximum static thrust would be realized with a smaller propeller having a larger pitch-to-diameter ratio. Partly to avoid supersonic tip speeds, aircraft engines are typically designed to develop maximum power at a rotational speed that is considerably less than that for comparable automobile engines. Considerations other than aerodynamic performance, such as noise level, ground clearance, and structural considerations, can also limit the maximum propeller diameter.

Although high static thrust is important for good takeoff performance, an airplane propeller is not typically optimized for maximum static thrust. A similar procedure can be used to select a propeller that will optimize some other performance criterion. However, when the forward speed associated with the performance criterion is non-zero, an additional iterative procedure is usually required. This is demonstrated in the following example.

EXAMPLE 2.3.4. For best efficiency and engine life, the manufacturer of the piston engine in Example 2.3.3 recommends that for continuous operation, the engine should be operated at 65 percent of maximum power and 2350 rpm. In this example we wish to select a fixed-pitch propeller for this engine and operating condition that will maximize the propulsive efficiency at standard sea level with an airspeed of 120 mph. Again, we will assume a three-blade propeller configuration with the same blade geometry as that described in Example 2.3.1.

Solution. As an example calculation, we again consider a propeller having a chord-line pitch-to-diameter ratio of 0.6. For this case we cannot compute the advance ratio directly, because the propeller diameter is unknown. We must start with an assumed propeller diameter: for example, 100 inches. For this assumed diameter the advance ratio would be

$$J = \frac{V_\infty}{(\omega/2\pi)d_p} = \frac{(120\times 5{,}280/3{,}600)\,\text{ft/sec}}{(2{,}350/60)\,\text{sec}^{-1}(100/12)\,\text{ft}} = 0.539234$$

Following the procedure used in Example 2.3.1, with this value of J and $K_c = 0.6$ the power coefficient for this propeller and operating condition is found to be

$$C_P = 0.019498$$

and

$$\ell\omega = \rho(\omega/2\pi)^3 d_p^5 C_P = (0.0023769)(2{,}350/60)^3(100/12)^5(0.019498)$$
$$= 111{,}852\ \text{ft·lbf/sec} = 203.4\ \text{hp}$$

Since we require a brake power of 117 horsepower, the assumed diameter is too large. As a second estimate we will use

$$d_p = 90 \text{ inches} = 7.5 \text{ ft}$$

$$J = \frac{V_\infty}{(\omega/2\pi)d_p} = \frac{(120\times 5{,}280/3{,}600)\text{ ft/sec}}{(2{,}350/60)\text{ sec}^{-1}(7.5)\text{ ft}} = 0.599149$$

$$C_P = 0.012830$$

$$\ell\omega = \rho(\omega/2\pi)^3 d_p^5 C_P = (0.0023769)(2{,}350/60)^3(7.5)^5(0.012830)$$
$$= 43{,}480 \text{ ft·lbf/sec} = 79.1 \text{ hp}$$

Continuing with this iteration, using the secant method, we rapidly converge on

$$d_p = 93.6416 \text{ inches} = 7.80347 \text{ ft}$$

$$J = \frac{V_\infty}{(\omega/2\pi)d_p} = \frac{(120\times 5{,}280/3{,}600)\text{ ft/sec}}{(2{,}350/60)\text{ sec}^{-1}(7.80347)\text{ ft}} = 0.575849$$

$$C_P = 0.015572$$

$$\ell\omega = \rho(\omega/2\pi)^3 d_p^5 C_P = (0.0023769)(2{,}350/60)^3(7.80347)^5(0.015572)$$
$$= 64{,}350 \text{ ft·lbf/sec} = 117.0 \text{ hp}$$

$$C_T = 0.022818$$

From Eq. (2.3.29) and the known thrust coefficient, the sea-level thrust developed by this engine-propeller combination at 120 mph would be

$$T = \rho(\omega/2\pi)^2 d_p^4 C_T = (0.0023769)(2{,}350/60)^2(7.80347\text{ ft})^4(0.022818)$$
$$= 308.5 \text{ lbf}$$

The propulsive efficiency for this propeller and operating condition is then computed as the propulsive power divided by the brake power,

$$\eta_p = \frac{TV_\infty}{\ell\omega} = \frac{308.5 \text{ lbf}\,(120\times 5{,}280/3{,}600)\text{ ft/sec}}{64{,}350 \text{ ft·lbf/sec}} = \underline{0.844}$$

Repeating these calculations for other pitch-to-diameter ratios, we obtain the results plotted in Fig. 2.3.17. These results predict that a maximum propulsive efficiency of 0.867 is achieved with an 80-inch propeller having a chord-line pitch-to-diameter ratio of about 0.79.

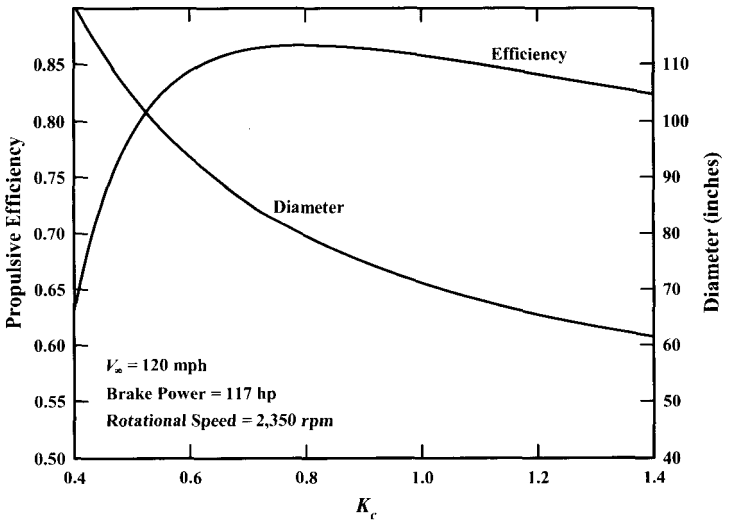


Figure 2.3.17. Variation in propeller diameter and propulsive efficiency with pitch-to-diameter ratio for the propeller in Example 2.3.4.

It should be noted that the penalty for slightly decreasing the diameter and increasing the pitch is not too great. A 72-inch propeller having a chord-line pitch-to-diameter ratio of about 0.97 would provide the same load at 2,350 rpm and would decrease the efficiency by less than 1 percent. The propeller actually selected for this engine and some particular airframe would probably be a compromise between cruise and takeoff performance, plus other considerations, such as noise level, ground clearance, and structural considerations.

A few comments are in order concerning the accuracy of the propeller theory presented in this section. First of all, we should not expect the theory to be accurate in the region of advance ratio where the propeller blades are stalled. The basis for this propeller analysis is potential flow theory, which is an inviscid theory. When the blades are not stalled, the effects of viscosity are confined to the boundary layers at the blade surfaces. These effects were added to the basic potential flow model by including parasitic drag as an additional aerodynamic force. This technique works quite well when the blades are not stalled, because the viscous forces are small. However, when the blades are stalled, the viscous effects in the blade wakes dominate the flow. Under these conditions, the flow pattern is significantly altered by the presence of the viscous wakes, and the method used to predict the induced velocity is not expected to be accurate.

As already stated, another source of error in this propeller model is Goldstein's original hypothesis. The model used for predicting the velocity induced on the propeller blades by the trailing vortex sheet is based on the Betz condition, which is only valid in the ultimate wake of an optimum propeller. In the plane of the prop-circle of a propeller having blades of arbitrary planform shape, this will clearly introduce some error.

Another source of error in this model is the assumption of incompressible flow. The highest relative airspeeds are encountered at the blade tips. For many high-performance aircraft engines, propeller tip speeds approach or exceed the speed of sound. Obviously, as local Mach numbers approach 1.0 at the blade tips, the assumption of incompressible flow is not reasonable. As the blade tip speed approaches the speed of sound, shock waves develop on the blades and the blade drag goes up considerably. This increases the power required to turn the propeller at a given speed and reduces the propeller efficiency. When the propeller blade-tip speed exceeds the speed of sound, the propeller efficiency begins to drop dramatically. This is the primary reason why propellers were never successfully used for supersonic flight. The effects of compressibility can be reasonably accounted for in Goldstein's model by including Mach number dependence in the relations for the section lift and drag coefficients. This is left as a programming exercise for the student.

In spite of some sources of error, if the blade geometry and aerodynamic section lift and drag coefficients are accurately described as a function of radial position, angle of attack, and Mach number, Goldstein's theory gives results that are in reasonable agreement with experimental data. Furthermore, the trends and insight into propeller performance, which are shown by this model, are valid even when the actual performance deviates somewhat from that predicted by the model.

Perhaps the greatest source of error encountered when using Goldstein's model to predict the performance of a commercial propeller is a lack of knowledge of the blade geometry. Propeller manufacturers guard such information closely and are very reluctant to share information on blade geometry with customers. The propeller and hub diameters as well as the section chord length as a function of radial position are easily measured. However, the variations in chord-line pitch and airfoil section geometry with radial position are not so readily determined.

Manufacturers typically provide propeller pitch as a single number specified in inches. This could lead the user to believe that the propeller has a pitch length that is constant along the axis of the blade. This is seldom actually the case. Figure 2.3.18 shows how chord-line and aerodynamic pitch vary with radial position for one particular commercial propeller. The geometry shown in this figure was obtained from a commercially purchased propeller using a laser coordinate measuring machine. For comparison, the pitch specified by the manufacturer is also shown in this figure as a flat line. Notice that the measured chord-line pitch is in close agreement with the pitch specified by the manufacturer only at one location along the axis of the blade. Such variation in pitch with radial position is not unusual in commercial propellers. The pitch length specified by the manufacturer for any particular propeller should be viewed only as a manufacturer's naming convention. This specified pitch length is, at best, only a relative measure of propeller pitch and is typically quite useless as input to Goldstein's analytical model. Determining the actual variation in chord-line pitch and airfoil section geometry with radial position may be the most difficult part of predicting the performance of a commercial propeller.

Once the propeller blade geometry has been accurately determined, the section lift and drag coefficients for any airfoil cross-section of the blade can be determined numerically as a function of angle of attack and Mach number. With such input,

Goldstein's model provides a reasonable means for predicting propeller performance. This is demonstrated in Figs. 2.3.19 and 2.3.20. The data shown in this figure are from Phillips, Anderson, and Kelly (2003) and were taken using the same propeller for which the geometry is shown in Fig. 2.3.18. The data shown in these figures were taken at propeller angles of attack of –6, 0, and +6 degrees. Notice that within the accuracy of the experimental measurements, the propeller thrust and power coefficients are independent of the propeller angle of attack.

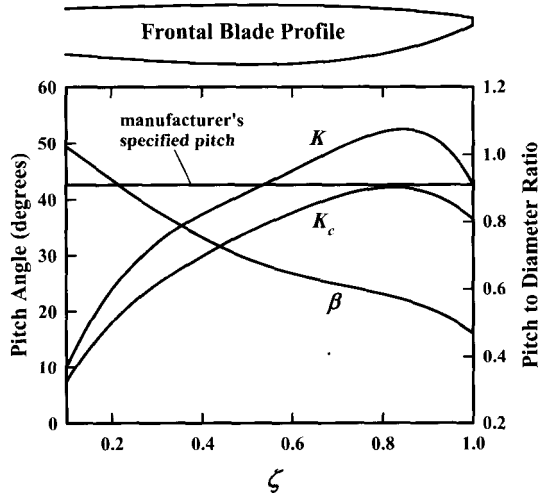


Figure 2.3.18. Variation in propeller pitch with radial position for a commercial propeller.

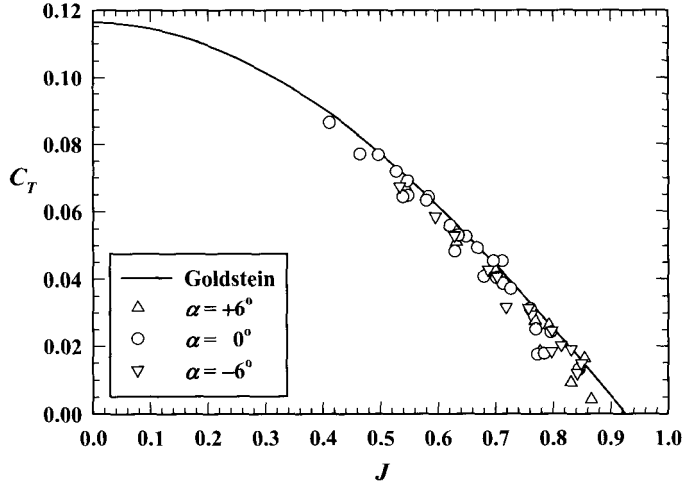


Figure 2.3.19. Comparison between the thrust coefficient predictions from Goldstein's theory and experimental data for the propeller geometry shown in Fig. 2.3.18.

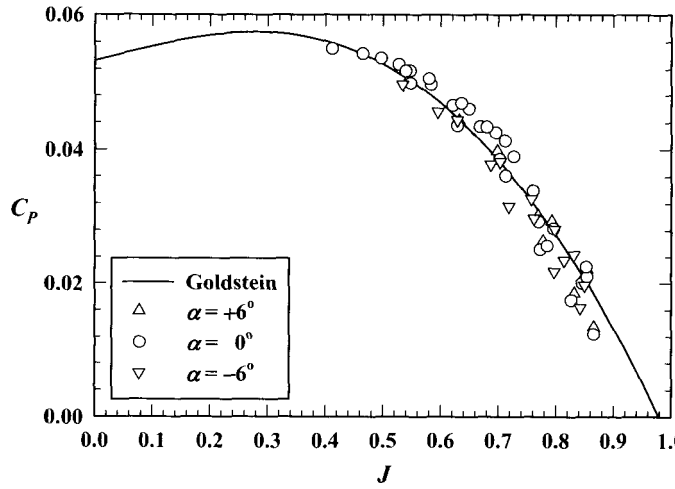


Figure 2.3.20. Comparison between the power coefficient predictions from Goldstein's theory and experimental data for the propeller geometry shown in Fig. 2.3.18.

2.4. Propeller Momentum Theory

Another method that has been used for predicting propeller induced velocity is known as *propeller momentum theory*. Like Goldstein's vortex theory, momentum theory is based on inviscid, incompressible flow. However, this flow model is very different from that hypothesized by Goldstein. Momentum theory is based on the hypothesis of a streamtube, which exactly encloses the propeller disk as shown in Fig. 2.4.1. This streamtube is assumed to extend from a plane infinitely far upstream from the propeller disk to a plane infinitely far downstream. Both far planes are assumed parallel with the plane of the propeller disk, and the static pressure in both far planes is assumed constant and equal to the freestream static pressure. All of the fluid that enters this streamtube on the far upstream side must pass through the propeller disk and exit on the far downstream side.

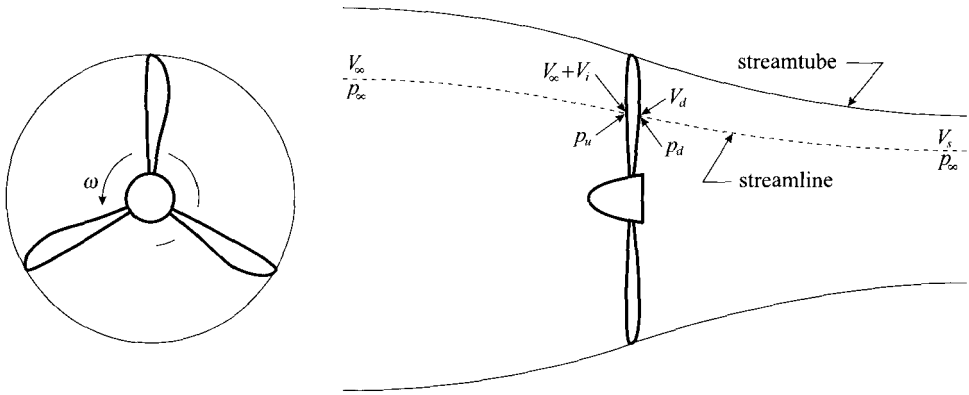


Figure 2.4.1. Classical momentum theory model for the fluid flows about a rotating propeller.

In addition to the foundation hypothesis of streamtube flow as shown in Fig. 2.4.1, classical propeller momentum theory imposes four simplifying approximations, i.e.,

1. The flow is assumed to be inviscid and incompressible.
2. All rotation of the fluid within the streamtube is neglected.
3. The flow velocity is assumed uniform over each cross-section of the streamtube.
4. The pressure is assumed uniform over each cross-section of the streamtube.

These assumptions result in an idealized one-dimensional solution that is normally considered to represent an upper limit for propeller performance.

To evaluate the induced velocity from classical propeller momentum theory, we consider the flow along the streamline shown in Fig. 2.4.1. The fluid far upstream from the propeller disk has pressure p_∞ and velocity V_∞. If the propeller is developing positive thrust, the pressure just upstream from the propeller disk is below ambient, while the pressure just downstream from the propeller disk is above ambient. The near upstream pressure is denoted as p_u and the near downstream pressure is represented as p_d. By definition, the velocity on the near upstream side of the propeller disk is the freestream velocity plus the induced velocity, $V_\infty + V_i$, and the velocity on the near downstream side is designated as V_d.

Since we are neglecting all rotation of the fluid within the streamtube, the fluid velocity on the downstream side of the propeller disk is readily determined as a direct result of continuity combined with the assumption of incompressible flow. If we apply conservation of mass to the propeller disk area, A_p, we have

$$\rho V_d A_p = \rho(V_\infty + V_i) A_p$$

For the assumed incompressible flow, this reduces to the rather obvious result that the fluid velocity cannot change in passing through the propeller disk,

$$V_d = V_\infty + V_i \tag{2.4.1}$$

The velocity does change, however, as the fluid approaches and leaves the propeller disk.

Applying Bernoulli's equation along the streamline shown in Fig. 2.4.1, upstream from the propeller disk we obtain

$$\frac{p_\infty}{\rho} + \frac{V_\infty^2}{2} = \frac{p_u}{\rho} + \frac{(V_\infty + V_i)^2}{2} \tag{2.4.2}$$

Likewise, for the streamline on the aft side of the propeller disk, from a point just behind the propeller to a point in the far slipstream, using Eq. (2.4.1), we can write

$$\frac{p_\infty}{\rho} + \frac{V_s^2}{2} = \frac{p_d}{\rho} + \frac{(V_\infty + V_i)^2}{2} \tag{2.4.3}$$

where V_s is the ultimate slipstream velocity at a downstream point where the pressure has returned to ambient. Subtracting Eq. (2.4.2) from Eq. (2.4.3) results in

$$\frac{V_s^2}{2} - \frac{V_\infty^2}{2} = \frac{p_d}{\rho} - \frac{p_u}{\rho} \tag{2.4.4}$$

The axial force on the propeller disk is expressed in terms of the pressure difference across the disk and in terms of the momentum imparted to the fluid. The thrust acting on the prop-circle is expressed as the downstream pressure, p_d, minus the upstream pressure, p_u, multiplied by the area, A_p,

$$T = A_p(p_d - p_u) \tag{2.4.5}$$

Since this force is applied directly to the fluid, it will result in a fluid momentum increase, which must satisfy

$$T = \dot{m}(V_s - V_\infty) \tag{2.4.6}$$

where $\dot{m}$ is the mass flow rate through the area, A_p, which is given by

$$\dot{m} = A_p\rho(V_\infty + V_i) \tag{2.4.7}$$

Using Eq. (2.4.7) in Eq. (2.4.6), the thrust can be written as

$$T = A_p\rho(V_\infty + V_i)(V_s - V_\infty) \tag{2.4.8}$$

Combining Eqs. (2.4.5) and (2.4.8) to eliminate the thrust, we obtain

$$A_p(p_d - p_u) = A_p\rho(V_\infty + V_i)(V_s - V_\infty)$$

or

$$\frac{p_d}{\rho} - \frac{p_u}{\rho} = (V_\infty + V_i)(V_s - V_\infty) \tag{2.4.9}$$

Using Eq. (2.4.4) to eliminate the pressure from Eq. (2.4.9), the ultimate slipstream velocity can be related to the freestream velocity and the propeller induced velocity,

$$\frac{V_s^2}{2} - \frac{V_\infty^2}{2} = \frac{(V_s - V_\infty)(V_s + V_\infty)}{2} = (V_\infty + V_i)(V_s - V_\infty)$$

Solving this for V_s gives

$$V_s = V_\infty + 2V_i \tag{2.4.10}$$

Thus, we see that classical momentum theory predicts that the difference between the ultimate slipstream velocity and the freestream velocity is twice the induced velocity.

Similarly, from the energy equation, the brake power, P, that is required to turn the propeller must satisfy the relation

$$P = \dot{m}\left(h_s - h_\infty + \frac{V_s^2}{2} - \frac{V_\infty^2}{2}\right)$$

where h_s and h_∞ are, respectively, the ultimate slipstream and freestream enthalpy. Since the fluid is assumed incompressible and the ultimate slipstream pressure is assumed equal to the freestream pressure, the enthalpy in the ultimate slipstream is equal to that in the freestream. Thus, after applying Eq. (2.4.7), the energy equation becomes

$$P = A_p\rho(V_\infty + V_i)\left(\frac{V_s^2}{2} - \frac{V_\infty^2}{2}\right) \tag{2.4.11}$$

Using Eq. (2.4.10) in Eqs. (2.4.8) and (2.4.11), the thrust can be written as

$$T = 2A_p\rho(V_\infty + V_i)V_i \tag{2.4.12}$$

and brake power required to turn the propeller is

$$P = 2A_p\rho(V_\infty + V_i)^2 V_i \tag{2.4.13}$$

Equation (2.4.12) is quadratic in V_i and can be solved for the induced velocity to give

$$V_i = \sqrt{\frac{V_\infty^2}{4} + \frac{T}{2A_p\rho}} - \frac{V_\infty}{2} \tag{2.4.14}$$

Using Eq. (2.4.14) in Eq. (2.4.13), the brake power required to turn the propeller can be expressed as a function of the thrust and the freestream airspeed,

$$P = T\left(\frac{V_\infty}{2} + \sqrt{\frac{V_\infty^2}{4} + \frac{T}{2A_p\rho}}\right) \tag{2.4.15}$$

The propulsive efficiency for the propeller is the propulsive power output, TV_∞, divided by the brake power input, P. Since this is an inviscid, incompressible flow model, the propulsive efficiency obtained from classical propeller momentum theory is usually called the *ideal efficiency*, η_i. From Eqs. (2.4.12) and (2.4.13) we obtain

$$\eta_i \equiv \frac{TV_\infty}{P} = \frac{2A_p\rho(V_\infty + V_i)V_iV_\infty}{2A_p\rho(V_\infty + V_i)^2 V_i} = \frac{V_\infty}{V_\infty + V_i} = \frac{1}{1 + V_i/V_\infty}$$

or with Eq. (2.4.14),

$$\eta_i = \left(\frac{1}{2} + \sqrt{\frac{1}{4} + \frac{T}{2A_p \rho V_\infty^2}} \right)^{-1} \tag{2.4.16}$$

For convenience, we can express Eq. (2.4.14) in terms of the usual dimensionless propeller variables. This gives

$$\frac{V_i}{(\omega/2\pi)d_p} = \sqrt{\frac{J^2}{4} + \frac{2C_T}{\pi}} - \frac{J}{2} \tag{2.4.17}$$

where $C_T \equiv T/[\rho(\omega/2\pi)^2 d_p^4]$ and $J \equiv V_\infty/[(\omega/2\pi)d_p]$. Similarly, Eq. (2.4.15) can be written in dimensionless form as

$$C_P = C_T \left(\frac{J}{2} + \sqrt{\frac{J^2}{4} + \frac{2C_T}{\pi}} \right) \tag{2.4.18}$$

where $C_P \equiv P/[\rho(\omega/2\pi)^3 d_p^5]$. From Eq. (2.4.16), the ideal propulsive efficiency predicted by classical propeller momentum theory can be written in terms of these same dimensionless variables,

$$\eta_i = \frac{C_T J}{C_P} = \left(\frac{1}{2} + \sqrt{\frac{1}{4} + \frac{2C_T}{\pi J^2}} \right)^{-1} \tag{2.4.19}$$

Classical propeller momentum theory is relatively simple and quite appealing. As a result, this theory has been commonly applied in the literature. The major objection to the theory has been its failure to account for rotation of the fluid within the slipstream. There is no physical basis for neglecting slipstream rotation. Clearly, torque must be applied to turn the propeller and that torque must result in rotation of the fluid within the slipstream. Since some of the power supplied to the propeller must go to support this rotation, the thrust and propulsive efficiency are reduced as a result of slipstream rotation. In the following analysis, we examine the magnitude of this effect.

The exclusion of slipstream rotation is not the only objection that can be raised against classical propeller momentum theory. The assumptions of uniform flow and uniform pressure result in a one-dimensional solution that is not consistent with results predicted from propeller vortex theory. However, here we wish to concentrate on examining the effects of slipstream rotation on the results predicted by propeller momentum theory. Thus, we shall now consider the incorporation of the angular momentum equation into this propeller model. To isolate the effects of slipstream rotation, we continue with the assumptions of inviscid, incompressible, uniform flow but we now allow for rotation of the fluid within the streamtube.

Accordingly, we continue to assume the existence of a streamtube, which encloses the complete propeller disk as shown in Fig. 2.4.2. This streamtube is still assumed to

extend infinitely far upstream from the propeller disk, to a plane where the static pressure is constant and equal to the freestream static pressure, p_∞. In this plane, the axial velocity is the freestream velocity, V_∞, and there is no circumferential velocity. Likewise, the streamtube is assumed to extend infinitely far downstream from the propeller disk, to a plane where the velocity in the slipstream is no longer changing in the axial direction. Consistent with the uniform flow assumption used in classical propeller momentum theory, we continue to assume uniform axial velocity but now allow for a uniform angular velocity as well. Since we wish to examine the effect of slipstream rotation on the results predicted by propeller momentum theory, at first thought one might be tempted to continue with the assumption of uniform pressure, which is also imposed in classical propeller momentum theory. However, this assumption is not consistent with rotation in the ultimate slipstream.

The solution from classical propeller momentum theory does not satisfy the angular momentum equation. If we continue with the uniform pressure assumption from classical momentum theory while allowing fluid rotation, we find that there is only one possible case for which the angular momentum equation together with the other laws of Newtonian mechanics can all be satisfied with a finite propeller rotational speed. That is the case of zero thrust. Since we are now allowing for fluid rotation in the streamtube and considering a propeller developing finite thrust, we can no longer assume uniform pressure over each cross-section of the streamtube. We must instead allow the pressure in the streamtube to be a function of the radial position, r, as well as the axial position, x.

On the near upstream side of the propeller disk, the axial fluid velocity is equal to the sum of the forward airspeed and the axial component of induced velocity, $V_\infty + V_{xi}$. On the near downstream side of the propeller disk the axial fluid velocity is designated V_{xd}. The circumferential velocity on the near upstream side of the propeller disk is just the circumferential component of the propeller induced velocity, $V_{\theta i}$, and the circumferential velocity on the near downstream side of the propeller disk is denoted as $V_{\theta d}$.

The circumferential component of fluid velocity just upstream from the propeller disk can be deduced by applying the angular momentum equation to the section of

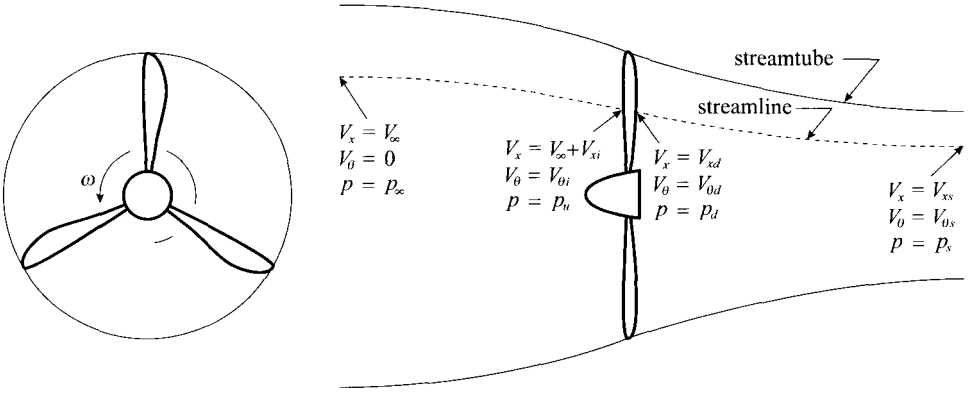


Figure 2.4.2. Momentum theory model for the pressures and velocities of the fluid that flows through the disk of a rotating propeller, including the effects of fluid rotation.

streamtube that is upstream from the propeller. Because there is no torque acting on this section of the streamtube, there can be no change in the angular momentum of the air as it passes through this section. Since the air has no angular momentum far upstream from the propeller disk, it cannot have angular momentum when it reaches the upstream side of the propeller disk. This requires that

$$V_{\theta i} = 0 \tag{2.4.20}$$

and thus

$$V_{xi} = V_i \tag{2.4.21}$$

There is angular momentum imparted to the air as it flows through the propeller disk. This results from the torque applied to the propeller. In the section of streamtube that is downstream from the propeller disk the angular momentum flux must again remain constant, since there is no torque applied to this section of the streamtube. At first thought, one might be led to conclude that the angular velocity remains constant in the downstream section of the streamtube, just as it did in the upstream section. However, this is not the case. The angular velocity remains constant in the upstream section of the streamtube only because the angular velocity is zero at the inlet. As air flows from the region far upstream toward the low-pressure side of the propeller disk, the axial velocity is increased due to the pressure decrease. Likewise, as air flows away from the high-pressure side of the propeller disk, the axial velocity continues to increase as a result of the pressure difference between the downstream side of the propeller disk and the far slipstream. This acceleration causes the streamtube enclosing the slipstream to contract in diameter with increasing distance downstream from the propeller disk. This is shown in Fig. 2.4.2. Since the diameter of the streamtube decreases and the angular momentum flux for the air remains constant, the angular velocity of the air in the slipstream must increase along with the axial velocity as it moves away from the downstream side of the propeller disk.

The axial component of fluid velocity just downstream from the propeller disk is related to the axial component on the upstream side through the continuity equation. If we use the notation shown in Fig. 2.4.2 and apply conservation of mass across any segment of the propeller disk, we have

$$\rho V_{xd} = \rho(V_\infty + V_{xi})$$

Since the fluid density is assumed constant, this fixes the axial component of fluid velocity just downstream from the propeller disk. In view of Eq. (2.4.21), this gives

$$V_{xd} = V_\infty + V_i \tag{2.4.22}$$

The pressure and velocity just upstream from the propeller disk are related to the freestream pressure and velocity through Bernoulli's equation. Applying Bernoulli's

equation along the streamline shown in Fig. 2.4.2 and using Eqs. (2.4.20) and (2.4.21), upstream from the propeller disk we obtain

$$\frac{p_\infty}{\rho}+\frac{V_\infty^2}{2} = \frac{p_u}{\rho}+\frac{(V_\infty+V_i)^2}{2} \tag{2.4.23}$$

Here we see that since there is no rotation of the fluid in the upstream section of the streamtube, the uniform flow approximation requires uniform pressure upstream from the propeller disk. For the streamline on the aft side of the propeller disk, from a point just behind the propeller to a point in the far slipstream, using Eq. (2.4.22) we can write

$$\frac{p_s}{\rho}+\frac{V_{xs}^2+V_{\theta s}^2}{2} = \frac{p_d}{\rho}+\frac{(V_\infty+V_i)^2+V_{\theta d}^2}{2} \tag{2.4.24}$$

where V_{xs} and $V_{\theta s}$ are the axial and circumferential components of the ultimate slipstream velocity far downstream from the propeller disk. Subtracting Eq. (2.4.23) from Eq. (2.4.24) results in

$$\frac{p_s}{\rho}-\frac{p_\infty}{\rho}+\frac{V_{xs}^2+V_{\theta s}^2}{2}-\frac{V_\infty^2}{2} = \frac{p_d}{\rho}-\frac{p_u}{\rho}+\frac{V_{\theta d}^2}{2} \tag{2.4.25}$$

From the uniform flow approximation, the circumferential velocity in the ultimate slipstream can be written as the product of the local angular velocity and the local radius. Thus, Eq. (2.4.25) can be written as

$$\frac{p_s}{\rho}-\frac{p_\infty}{\rho}+\frac{V_{xs}^2+\omega_s^2 r_s^2}{2}-\frac{V_\infty^2}{2} = \frac{p_d}{\rho}-\frac{p_u}{\rho}+\frac{V_{\theta d}^2}{2} \tag{2.4.26}$$

where ω_s and r_s are the angular velocity and radial coordinate at the location of the streamline far downstream from the propeller.

In the ultimate slipstream this axisymmetric flow becomes independent of the axial position, x. Thus, the continuity equation in the ultimate slipstream requires that

$$\frac{d(r_s V_{rs})}{dr_s} = 0 \tag{2.4.27}$$

where r_s is the radial position and V_{rs} is the radial velocity at a point in the ultimate slipstream. Similarly, the three components of the momentum equation in the ultimate slipstream reduce to

$$\rho\left(V_{rs}\frac{dV_{rs}}{dr_s}-\frac{V_{\theta s}^2}{r_s}\right) = -\frac{\partial p_s}{\partial r_s} \tag{2.4.28}$$

$$\rho\left(V_{rs}\frac{\partial V_{\theta s}}{\partial r_s}+\frac{V_{rs}V_{\theta s}}{r_s}\right) = 0 \tag{2.4.29}$$

$$\rho V_{rs}\frac{\partial V_{xs}}{\partial r_s} = 0 \tag{2.4.30}$$

Equation (2.4.27) combined with the boundary condition, which specifies no radial velocity at the outer edge of the ultimate slipstream, gives

$$V_{rs} = 0 \tag{2.4.31}$$

As a result of Eq. (2.4.31), Eqs. (2.4.29) and (2.4.30) are identically satisfied, whereas Eq. (2.4.28) reduces to

$$\frac{\partial p_s}{\partial r_s} = \rho\frac{V_{\theta s}^2}{r_s} = \rho\omega_s^2 r_s \tag{2.4.32}$$

The solution to Eq. (2.4.32), subject to the boundary condition of freestream static pressure at the outer edge of the slipstream, $r_s = R_s$, is

$$p_s(r_s) = p_\infty - \frac{\rho\omega_s^2}{2}(R_s^2 - r_s^2) \tag{2.4.33}$$

Using Eq. (2.4.33) in Eq. (2.4.26) gives

$$\omega_s^2\left(r_s^2 - \frac{R_s^2}{2}\right)+\frac{V_{xs}^2}{2}-\frac{V_\infty^2}{2} = \frac{p_d}{\rho}-\frac{p_u}{\rho}+\frac{V_{\theta d}^2}{2} \tag{2.4.34}$$

Applying the continuity equation to the flow inside the stream surface that contains the streamline under consideration, we have

$$\pi r_p^2\rho(V_\infty + V_i) = \pi r_s^2\rho V_{xs}$$

where r_p is the radial position of the streamline at the propeller. After rearranging, this results in

$$r_s^2 = \frac{V_\infty + V_i}{V_{xs}}r_p^2 \tag{2.4.35}$$

Using Eq. (2.4.35) in Eq. (2.4.34) results in

$$\omega_s^2\left(r_p^2 - \frac{R_p^2}{2}\right)\frac{V_\infty + V_i}{V_{xs}}+\frac{V_{xs}^2}{2}-\frac{V_\infty^2}{2} = \frac{p_d}{\rho}-\frac{p_u}{\rho}+\frac{V_{\theta d}^2}{2} \tag{2.4.36}$$

where R_p is the propeller's outside radius. Since angular momentum remains constant downstream from the propeller, we have

$$r_p V_{\theta d} = r_s V_{\theta s} = r_s^2 \omega_s$$

or in view of Eq. (2.4.35),

$$V_{\theta d} = \frac{V_\infty + V_i}{V_{xs}} r_p \omega_s \tag{2.4.37}$$

After applying Eq. (2.4.37), Eq. (2.4.36) becomes

$$\omega_s^2 \left(r_p^2 - \frac{R_p^2}{2} \right) \frac{V_\infty + V_i}{V_{xs}} + \frac{V_{xs}^2}{2} - \frac{V_\infty^2}{2} = \frac{p_d}{\rho} - \frac{p_u}{\rho} + \left(\frac{V_\infty + V_i}{V_{xs}} \right)^2 \frac{r_p^2 \omega_s^2}{2}$$

or

$$\frac{p_d}{\rho} - \frac{p_u}{\rho} = \omega_s^2 \left[\left(1 - \frac{V_\infty + V_i}{2V_{xs}} \right) r_p^2 - \frac{R_p^2}{2} \right] \frac{V_\infty + V_i}{V_{xs}} + \frac{V_{xs}^2}{2} - \frac{V_\infty^2}{2} \tag{2.4.38}$$

The axial velocity in the ultimate slipstream is related to the thrust through the axial momentum equation,

$$T + \int_{A_s} (p_\infty - p_s) dA_s = \int_{A_s} (V_{xs} - V_\infty) d\dot{m}$$

In view of Eq. (2.4.33), this gives

$$T + \int_{r_s=0}^{R_s} \frac{\rho \omega_s^2}{2} (R_s^2 - r_s^2)(2\pi r_s dr_s) = \int_{r_s=0}^{R_s} (V_{xs} - V_\infty)(\rho V_{xs} 2\pi r_s dr_s)$$

which is easily integrated to yield

$$T = \pi R_s^2 \rho V_{xs} (V_{xs} - V_\infty) - \frac{\pi R_s^4 \rho \omega_s^2}{4}$$

or with Eq. (2.4.35),

$$T = \pi R_p^2 \rho \left[(V_\infty + V_i)(V_{xs} - V_\infty) - \left(\frac{V_\infty + V_i}{2V_{xs}} \right)^2 \omega_s^2 R_p^2 \right] \tag{2.4.39}$$

Since there is no change in axial velocity across the propeller disk, the thrust acting on the prop-circle can also be expressed as

$$T = \int_{A_p} (p_d - p_u) dA_p = \int_{r_p=0}^{R_p} (p_d - p_u) 2\pi r_p dr_p$$

With Eq. (2.4.38), this is readily integrated to yield

$$T = \pi R_p^2 \rho \left[\frac{V_{xs}^2}{2} - \frac{V_\infty^2}{2} - \left(\frac{V_\infty + V_i}{2V_{xs}} \right)^2 \omega_s^2 R_p^2 \right] \tag{2.4.40}$$

Combining Eqs. (2.4.39) and (2.4.40) to eliminate the thrust we have

$$\frac{V_{xs}^2}{2} - \frac{V_\infty^2}{2} = (V_\infty + V_i)(V_{xs} - V_\infty)$$

This is solved for the axial component of the ultimate slipstream velocity to give

$$V_{xs} = V_\infty + 2V_i \tag{2.4.41}$$

Thus we see that the relation given by Eq. (2.4.10), which was developed from classical momentum theory neglecting rotation of the slipstream, is valid with slipstream rotation, provided that only the axial component of the ultimate slipstream velocity is used.

The rotation in the ultimate slipstream is related to the propeller torque through the angular momentum equation

$$\ell = \int_{A_s} r_s V_{\theta s} d\dot{m} = \int_{r_s=0}^{R_s} r_s^2 \omega_s (\rho V_{xs} 2\pi r_s dr_s) = \frac{\pi}{2} \rho V_{xs} \omega_s R_s^4$$

Again, applying Eq. (2.4.35), this becomes

$$\ell = \pi \rho \frac{(V_\infty + V_i)^2}{2V_{xs}} \omega_s R_p^4 \tag{2.4.42}$$

The brake power required to turn the propeller must satisfy the energy equation,

$$\omega \ell = \int_{A_s} \left(h_s - h_\infty + \frac{V_{xs}^2 + V_{\theta s}^2}{2} - \frac{V_\infty^2}{2} \right) d\dot{m}$$

For the assumed uniform, incompressible flow this reduces to

$$\omega \ell = \int_{r_s=0}^{R_s} \left(\frac{p_s}{\rho} - \frac{p_\infty}{\rho} + \frac{V_{xs}^2 + \omega_s^2 r_s^2}{2} - \frac{V_\infty^2}{2} \right) \rho V_{xs} (2\pi r_s dr_s)$$

Applying Eq. (2.4.33) and integrating, this gives

$$\omega \ell = \pi R_s^2 \rho V_{xs} \left(\frac{V_{xs}^2}{2} - \frac{V_\infty^2}{2} \right)$$

or after using Eq. (2.4.35),

$$\omega \ell = \pi R_p^2 \rho (V_\infty + V_i) \left(\frac{V_{xs}^2}{2} - \frac{V_\infty^2}{2} \right) \tag{2.4.43}$$

Combining Eqs. (2.4.42) and (2.4.43) to eliminate the torque, we can solve for the angular velocity in the ultimate slipstream. This gives

$$\omega_s = \frac{V_{xs}(V_{xs}^2 - V_\infty^2)}{\omega R_p^2 (V_\infty + V_i)}$$

Using Eq. (2.4.41) to eliminate the axial component of the ultimate slipstream velocity, we have

$$\omega_s = \frac{4(V_\infty + 2V_i)V_i}{\omega R_p^2} \tag{2.4.44}$$

Applying Eqs. (2.4.41) and (2.4.44) to either Eq. (2.4.39) or (2.4.40), the thrust developed by the propeller can be expressed as

$$T = 2\pi R_p^2 \rho (V_\infty + V_i) V_i \left[1 - \frac{2(V_\infty + V_i)V_i}{\omega^2 R_p^2} \right] \tag{2.4.45}$$

Likewise, applying Eqs. (2.4.41) and (2.4.44) to either Eq. (2.4.42) or (2.4.43), the brake power required to turn the propeller can be expressed as

$$P = \omega \ell = 2\pi R_p^2 \rho (V_\infty + V_i)^2 V_i \tag{2.4.46}$$

From Eqs. (2.4.45) and (2.4.46), the ideal propulsive efficiency predicted by propeller momentum theory, including the effects of slipstream rotation, is given by

$$\eta_i \equiv \frac{TV_\infty}{P} = \frac{V_\infty}{V_\infty + V_i} - \frac{2V_\infty V_i}{\omega^2 R_p^2} \tag{2.4.47}$$

Equation (2.4.45) is quadratic in $(V_\infty + V_i)V_i$. Thus, we have

$$(V_\infty + V_i)V_i = \frac{\omega^2 R_p^2}{4} \left(1 \pm \sqrt{1 - \frac{4T}{\pi \rho \omega^2 R_p^4}} \right)$$

This result is quadratic in V_i and can be solved for the induced velocity,

$$V_i = -\frac{V_\infty}{2} \pm \sqrt{\frac{V_\infty^2}{4} + \frac{\omega^2 R_p^2}{4}\left(1 \pm \sqrt{1 - \frac{4T}{\pi\rho\omega^2 R_p^4}}\right)}$$

In the limit as the rotational speed of the propeller becomes large, the induced velocity must be positive and finite. This specifies the signs in the previous relation to give

$$V_i = \sqrt{\frac{V_\infty^2}{4} + \frac{\omega^2 R_p^2}{4}\left(1 - \sqrt{1 - \frac{4T}{A_p\rho\omega^2 R_p^2}}\right)} - \frac{V_\infty}{2} \tag{2.4.48}$$

Notice that in the limit as the angular velocity of the propeller approaches infinity, the result predicted by Eq. (2.4.48) reduces to that predicted by Eq. (2.4.14).

In terms of the usual dimensionless propeller variables, Eq. (2.4.48) becomes

$$\frac{V_i}{(\omega/2\pi)d_p} = \sqrt{\frac{J^2}{4} + \frac{\pi^2}{4}\left(1 - \sqrt{1 - \frac{16C_T}{\pi^3}}\right)} - \frac{J}{2} \tag{2.4.49}$$

and from Eq. (2.4.47), the ideal propulsive efficiency can be written as

$$\eta_i = \left[\frac{1}{2} + \sqrt{\frac{1}{4} + \frac{\pi^2}{4J^2}\left(1 - \sqrt{1 - \frac{16C_T}{\pi^3}}\right)}\right]^{-1} - \frac{J^2}{\pi^2}\left[\sqrt{1 + \frac{\pi^2}{J^2}\left(1 - \sqrt{1 - \frac{16C_T}{\pi^3}}\right)} - 1\right] \tag{2.4.50}$$

By comparing Eqs. (2.4.49) and (2.4.50) with Eqs. (2.4.17) and (2.4.19) it can be shown that slipstream rotation increases induced velocity and decreases propulsive efficiency. However, it is not clear from examination of these equations what the magnitudes of these effects are. To display the effect of slipstream rotation on propeller induced velocity, Fig. 2.4.3a shows the percent error in Eq. (2.4.17) as compared with results predicted from Eq. (2.4.49). The effect of slipstream rotation on propulsive efficiency is shown in Fig. 2.4.3b through a similar comparison of results predicted from Eqs. (2.4.19) and (2.4.50). From these two figures we see that the effect of slipstream rotation on the induced velocity and propulsive efficiency, as predicted by propeller momentum theory, is on the order of 5 percent or less for the range of thrust coefficient and advance ratio that is normally encountered in airplane propellers.

The induced velocity predicted by either Eq. (2.4.17) or Eq. (2.4.49) can be used with propeller blade theory to replace the relation for induced velocity obtained from Goldstein's vortex theory. However, this method is not being recommended and will not be discussed in detail. The major difference between the induced velocity predicted from momentum theory, and that predicted from vortex theory is that momentum theory predicts a zero circumferential component of induced velocity on the upstream side of the propeller. This is a direct result of the hypothesized streamtube flow.

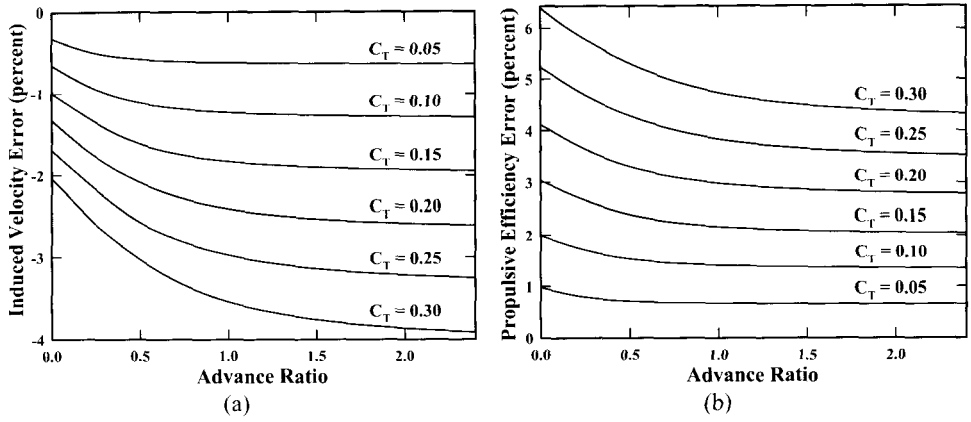


Figure 2.4.3. Errors in Eqs. (2.4.17) and (2.4.19) that result from neglecting slipstream rotation, as predicted by Eqs. (2.4.49) and (2.4.50).

The airflow that is induced by a rotating propeller results directly from the lift developed on the blades. The work done by the rotating blades moves air from the forward side of the propeller disk to the aft side. This creates a region of low pressure in front of the propeller disk. Clearly, air must flow into this low-pressure region, to replace the air that is evacuated by the propeller. The foundation of propeller momentum theory is the assumption that this induced airflow comes from a region far upstream from the propeller disk. This assumption is simply not valid. In reality, the induced airflow entering the low-pressure region forward of the propeller disk comes from the downstream side of the propeller, not from the upstream side.

A more realistic description of the flow induced by a rotating propeller was shown schematically in Fig. 2.3.3. The induced airflow on the aft side of the propeller disk is divided into two regions by the helical blade-tip vortices. In the slipstream, which is enclosed by this helix, the induced flow is moving in the downstream direction, away from the propeller disk. In the region outside the slipstream, the induced flow is moving back upstream. This upstream flow continues into the region slightly ahead of the propeller disk. In this region the induced flow becomes radial, moving inward to replace the air that is being evacuated from this region by the propeller. Near the blade tips the streamlines for this induced flow become almost circular, going from the aft side of the propeller out around the blade tips and back into the upstream side of the propeller disk. In the region upstream from the propeller disk, the induced flow rapidly goes to zero with increasing distance from the propeller. Because the downstream velocity of the induced flow within the slipstream is much greater than the upstream velocity outside the slipstream, there is a net momentum flux, which is balanced by the thrust.

This flow pattern is easily verified by interrogating the flow around a common house fan with a piece of light yarn. The fan should be placed in the center of a large room. If the yarn is held in the slipstream, both the axial velocity and the rotation of the air within the slipstream can be observed. If the yarn is held slightly downstream and slightly outboard from the blade tips, it will be drawn back upstream, around the blade tips, and

into the fan. If the yarn is held upstream at various distances from the fan, it will be observed that the air a short distance upstream from the fan is essentially undisturbed.

Even though propeller momentum theory does not provide a particularly accurate description of flow in the vicinity of a rotating propeller, the effects of circumferential induced velocity are fairly small for lightly loaded propellers, and momentum theory provides some valuable insight into propeller performance with comparatively little effort. Furthermore, because propeller momentum theory is widely presented in the literature, the student should be aware of its existence and its shortcomings.

2.5. Off-Axis Forces and Moments Developed by a Propeller

In the propeller analysis that we have considered to this point, we have assumed that the direction of forward motion is perfectly aligned with the axis of propeller rotation. For this case, a thrust force and a rolling moment are produced, which are both aligned with the axis of rotation. No other aerodynamic forces or moments are produced when the propeller axis is aligned in this manner. Additional aerodynamic reactions are produced if the propeller rotation axis is not aligned perfectly with the direction of flight. The angle that the propeller axis makes with the freestream airflow is the propeller angle of attack. Since the engine and propeller are typically mounted directly to the airframe, the propeller angle of attack will change with the airplane angle of attack, which can change during flight.

When a rotating propeller is at a positive angle of attack relative to the freestream flow, there is a component of the freestream in the plane of propeller rotation, as seen in Fig. 2.5.1. This component of the freestream changes the relative airflow over each blade of the propeller. It increases the relative airspeed for the downward-moving blades and decreases the relative airspeed for the upward-moving blades. Thus, both the lift and drag are increased on the downward-moving side of the propeller and decreased on the upward-moving side. The difference in thrust generated by the two sides of the propeller produces a yawing moment and the difference in circumferential force produces a net normal force in the plane of propeller rotation, as shown in Fig. 2.2.4. Similarly, sideslip will cause a pitching moment and a side force. These off-axis forces and moments can have a significant effect on airplane trim and stability.

To see how propeller angle of attack affects the propeller forces and moments, consider the cross-section of the propeller blade that is shown in Fig. 2.5.1. The blade is rotating counterclockwise with an angular velocity of ω and is advancing through the air with a relative airspeed of V_∞. The angle of attack that the forward velocity vector makes with the axis of propeller rotation is denoted as α_p. When this angle is nonzero, the velocity of the air relative to the blade cross-section depends on the angular coordinate, θ, as well as the radial coordinate, r.

The airspeed relative to the blade cross-section, located at radius, r, and angular position, θ, is designated as V_b. This is the vector sum of the velocity created by the rotation of the blade, the forward velocity of the propeller, and the propeller induced velocity. The circumferential component of this relative airspeed varies slightly with the angle, θ, because of the component of forward airspeed that is in the plane of propeller rotation. For convenience, we shall define V_e to be the magnitude of that portion of this

vector sum that includes only the velocity created by the rotation of the blade and that resulting from the forward motion. This definition is shown graphically in Fig. 2.5.1. From the geometry shown in this figure, we can write

$$V_e^2(r,\theta) = (\omega r - V_\infty \sin\alpha_p \sin\theta)^2 + (V_\infty \cos\alpha_p)^2 \tag{2.5.1}$$

Because the propeller angle of attack, α_p, is typically small, we apply the small-angle approximation to this angle only and Eq. (2.5.1) is closely approximated as

$$V_e^2(r,\theta) \cong \omega^2 r^2 + V_\infty^2 - 2\omega r V_\infty \alpha_p \sin\theta \tag{2.5.2}$$

If we now apply the Betz condition according to Goldstein's vortex theory, the total airspeed relative to the blade cross-section is

$$V_b(r,\theta) = V_e \cos\varepsilon_i = \sqrt{\omega^2 r^2 + V_\infty^2 - 2\omega r V_\infty \alpha_p \sin\theta}\,\cos\varepsilon_i \tag{2.5.3}$$

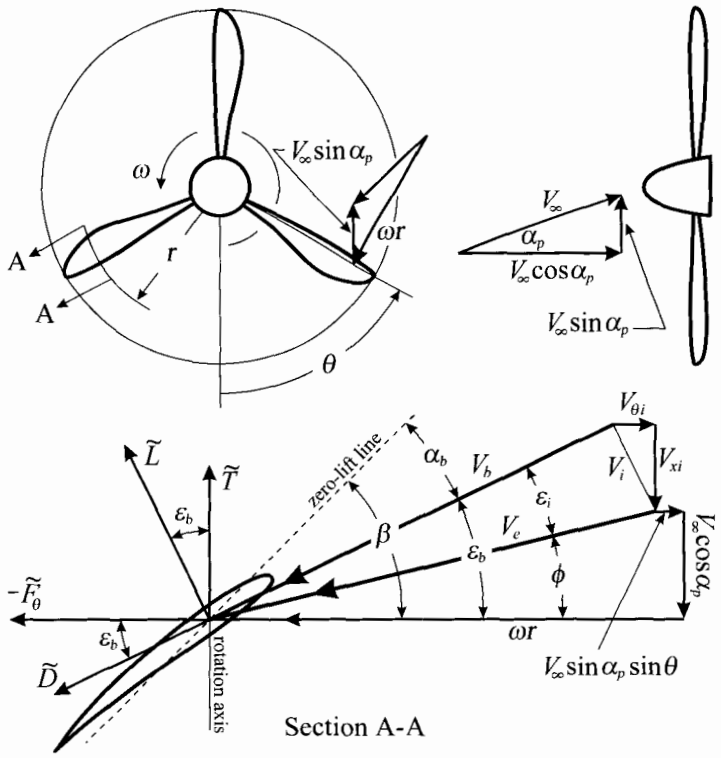


Figure 2.5.1. Effect of propeller angle of attack on the section forces and velocities acting on a rotating propeller blade.

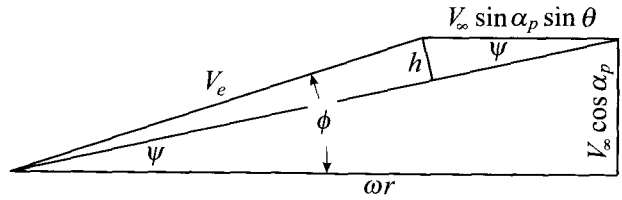


Figure 2.5.2. Trigonometric details for the angle, ϕ, that results from the propeller's total forward motion and is shown in Fig. 2.5.1.

The blade section angle of attack, α_b, measured relative to the section zero-lift line, is equal to the aerodynamic pitch angle, β, less the downwash angle, ε_b. In Fig. 2.5.1 the downwash angle for the blade section is shown to be the sum of two parts, the induced angle, ε_i, and the angle that results from the propeller's total forward motion, ϕ. From the geometry shown in Fig. 2.5.2, we can write

$$\begin{aligned}\phi &= \psi + \sin^{-1}\left(\frac{h}{V_e}\right) = \psi + \sin^{-1}\left[\frac{(V_\infty \sin\alpha_p \sin\theta)\sin\psi}{V_e}\right] \\ &= \psi + \sin^{-1}\left[\left(\frac{V_\infty \sin\alpha_p \sin\theta}{V_e}\right)\frac{V_\infty \cos\alpha_p}{\sqrt{(\omega r)^2 + (V_\infty \cos\alpha_p)^2}}\right]\end{aligned} \tag{2.5.4}$$

After applying Eq. (2.5.1), the result in Eq. (2.5.4) can be written as

$$\begin{aligned}\phi &= \tan^{-1}\left(\frac{V_\infty \cos\alpha_p}{\omega r}\right) \\ &\quad + \sin^{-1}\left[\frac{(V_\infty \sin\alpha_p \sin\theta)(V_\infty \cos\alpha_p)}{\sqrt{(\omega r - V_\infty \sin\alpha_p \sin\theta)^2 + (V_\infty \cos\alpha_p)^2}\sqrt{(\omega r)^2 + (V_\infty \cos\alpha_p)^2}}\right]\end{aligned} \tag{2.5.5}$$

Again assuming that the propeller angle of attack is small, Eq. (2.5.5) is very closely approximated as

$$\phi \cong \tan^{-1}\left(\frac{V_\infty}{\omega r}\right) + \frac{V_\infty^2}{(\omega r)^2 + V_\infty^2}\alpha_p \sin\theta \tag{2.5.6}$$

The total downwash angle, ε_b, for the blade cross-section, located at radius, r, and angular position, θ, is the sum of the angle, ϕ, and the induced angle, ε_i. Thus, we can write

$$\varepsilon_b(r,\theta) = \varepsilon_\infty + \varepsilon_i + \alpha_p \sin^2\varepsilon_\infty \sin\theta \tag{2.5.7}$$

where ε_∞ is the previously defined advance angle,

$$\varepsilon_\infty \equiv \tan^{-1}\left(\frac{V_\infty}{\omega r}\right) \tag{2.5.8}$$

The aerodynamic angle of attack is simply the aerodynamic pitch angle less the total downwash angle. Thus, from Eq. (2.5.7), this can be written as

$$\alpha_b(r,\theta) = \beta - \varepsilon_b = \beta - \varepsilon_\infty - \varepsilon_i - \alpha_p \sin^2\varepsilon_\infty \sin\theta \tag{2.5.9}$$

From Eqs. (2.5.3) and (2.5.9) we see that a positive propeller angle of attack will decrease both the relative airspeed and the section angle of attack for $0 < \theta < \pi$ and will increase both of these values in the range $\pi < \theta < 2\pi$. This will clearly result in a difference in both the lift and drag between the propeller blades on the right and left sides of the propeller disk.

From this point we follow a development similar to that presented in Sec. 2.3. The section thrust and circumferential forces are related to the section lift and drag forces through the local downwash angle according to the relations

$$\widetilde{T} = \widetilde{L}\cos\varepsilon_b - \widetilde{D}\sin\varepsilon_b \tag{2.5.10}$$

and

$$\widetilde{F}_\theta = -\widetilde{D}\cos\varepsilon_b - \widetilde{L}\sin\varepsilon_b \tag{2.5.11}$$

Using the result given by Eq. (2.5.7) along with the small-angle approximation for α_p, the cosine of the total downwash angle, ε_b, can be written as

$$\begin{aligned}\cos\varepsilon_b &= \cos(\varepsilon_\infty + \varepsilon_i)\cos(\alpha_p \sin^2\varepsilon_\infty \sin\theta) \\ &\quad - \sin(\varepsilon_\infty + \varepsilon_i)\sin(\alpha_p \sin^2\varepsilon_\infty \sin\theta)\end{aligned}$$

$$\cos\varepsilon_b \cong \cos(\varepsilon_\infty + \varepsilon_i) - \alpha_p \sin(\varepsilon_\infty + \varepsilon_i)\sin^2\varepsilon_\infty \sin\theta \tag{2.5.12}$$

Likewise, the sine of ε_b is written

$$\begin{aligned}\sin\varepsilon_b &= \sin(\varepsilon_\infty + \varepsilon_i)\cos(\alpha_p \sin^2\varepsilon_\infty \sin\theta) \\ &\quad + \cos(\varepsilon_\infty + \varepsilon_i)\sin(\alpha_p \sin^2\varepsilon_\infty \sin\theta)\end{aligned}$$

$$\sin\varepsilon_b \cong \sin(\varepsilon_\infty + \varepsilon_i) + \alpha_p \cos(\varepsilon_\infty + \varepsilon_i)\sin^2\varepsilon_\infty \sin\theta \tag{2.5.13}$$

Using Eqs. (2.5.3) and (2.5.9) while continuing to apply the small-angle approximation for α_p, the section lift is

$$\begin{aligned}\widetilde{L} &= \tfrac{1}{2}\rho V_b^2 c_b \widetilde{C}_L = \tfrac{1}{2}\rho V_b^2 c_b \widetilde{C}_{L,\alpha}\,\alpha_b \\ &= \tfrac{1}{2}\rho c_b \widetilde{C}_{L,\alpha}(\omega^2 r^2 + V_\infty^2 - 2\omega r V_\infty \alpha_p \sin\theta)\cos^2\varepsilon_i(\beta - \varepsilon_\infty - \varepsilon_i - \alpha_p \sin^2\varepsilon_\infty \sin\theta) \\ &\cong \tfrac{1}{2}\rho\omega^2 r^2 c_b \widetilde{C}_{L,\alpha}\left[\frac{\omega^2 r^2 + V_\infty^2}{\omega^2 r^2}(\beta - \varepsilon_\infty - \varepsilon_i - \alpha_p \sin^2\varepsilon_\infty \sin\theta)\right. \\ &\qquad \left. - 2\frac{V_\infty}{\omega r}(\beta - \varepsilon_\infty - \varepsilon_i)\alpha_p \sin\theta\right]\cos^2\varepsilon_i\end{aligned}$$

$$\begin{aligned}\widetilde{L} \cong \tfrac{1}{2}\rho\omega^2 r^2 c_b \widetilde{C}_{L,\alpha}&\left[\frac{\beta - \varepsilon_\infty - \varepsilon_i - \alpha_p \sin^2\varepsilon_\infty \sin\theta}{\cos^2\varepsilon_\infty}\right. \\ &\left. - 2(\beta - \varepsilon_\infty - \varepsilon_i)\alpha_p \tan\varepsilon_\infty \sin\theta\right]\cos^2\varepsilon_i\end{aligned} \tag{2.5.14}$$

where c_b is the local section chord length and $\widetilde{C}_{L,\alpha}$ is the local section lift slope. Using Eq. (2.5.3), the section drag can be written

$$\begin{aligned}\widetilde{D} &= \tfrac{1}{2}\rho V_b^2 c_b \widetilde{C}_D = \tfrac{1}{2}\rho c_b \widetilde{C}_D(\omega^2 r^2 + V_\infty^2 - 2\omega r V_\infty \alpha_p \sin\theta)\cos^2\varepsilon_i \\ &= \tfrac{1}{2}\rho\omega^2 r^2 c_b \widetilde{C}_D\left(\frac{\omega^2 r^2 + V_\infty^2}{\omega^2 r^2} - 2\frac{V_\infty}{\omega r}\alpha_p \sin\theta\right)\cos^2\varepsilon_i\end{aligned}$$

$$\widetilde{D} = \tfrac{1}{2}\rho\omega^2 r^2 c_b \widetilde{C}_D\left(\frac{1}{\cos^2\varepsilon_\infty} - 2\alpha_p \tan\varepsilon_\infty \sin\theta\right)\cos^2\varepsilon_i \tag{2.5.15}$$

where $\widetilde{C}_D$ is the local 2-D section parasitic drag coefficient. Remember that induced drag is included in the tilting of the lift vector.

Applying Eqs. (2.5.12), (2.5.13), (2.5.14), and (2.5.15) to Eq. (2.5.10), the axial component of section force is written

$$\begin{aligned}\widetilde{T} &= \widetilde{L}\cos\varepsilon_b - \widetilde{D}\sin\varepsilon_b = \tfrac{1}{2}\rho\omega^2 r^2 c_b \widetilde{C}_{L,\alpha} \\ &\times\left[\frac{\beta - \varepsilon_\infty - \varepsilon_i - \alpha_p \sin^2\varepsilon_\infty \sin\theta}{\cos^2\varepsilon_\infty} - 2(\beta - \varepsilon_\infty - \varepsilon_i)\alpha_p \tan\varepsilon_\infty \sin\theta\right]\cos^2\varepsilon_i \\ &\qquad \times\left[\cos(\varepsilon_\infty + \varepsilon_i) - \alpha_p \sin(\varepsilon_\infty + \varepsilon_i)\sin^2\varepsilon_\infty \sin\theta\right] \\ &- \tfrac{1}{2}\rho\omega^2 r^2 c_b \widetilde{C}_D\left(\frac{1}{\cos^2\varepsilon_\infty} - 2\alpha_p \tan\varepsilon_\infty \sin\theta\right)\cos^2\varepsilon_i \\ &\qquad \times\left[\sin(\varepsilon_\infty + \varepsilon_i) + \alpha_p \cos(\varepsilon_\infty + \varepsilon_i)\sin^2\varepsilon_\infty \sin\theta\right]\end{aligned}$$

or after rearranging and applying the small-angle approximation for α_p,

$$\widetilde{T} \cong \tfrac{1}{2}\rho\omega^2 r^2 c_b \cos^2\varepsilon_i \left\{ \left[\frac{\widetilde{C}_{L,\alpha}(\beta-\varepsilon_\infty-\varepsilon_i)\cos(\varepsilon_\infty+\varepsilon_i)-\widetilde{C}_D\sin(\varepsilon_\infty+\varepsilon_i)}{\cos^2\varepsilon_\infty} \right] \right.$$
$$-\left\{ \tan^2\varepsilon_\infty \left[(\widetilde{C}_{L,\alpha}+\widetilde{C}_D)\cos(\varepsilon_\infty+\varepsilon_i)+\widetilde{C}_{L,\alpha}(\beta-\varepsilon_\infty-\varepsilon_i)\sin(\varepsilon_\infty+\varepsilon_i) \right] \right. \qquad (2.5.16)$$
$$\left. \left. +2\tan\varepsilon_\infty \left[\widetilde{C}_{L,\alpha}(\beta-\varepsilon_\infty-\varepsilon_i)\cos(\varepsilon_\infty+\varepsilon_i)-\widetilde{C}_D\sin(\varepsilon_\infty+\varepsilon_i) \right] \right\} \alpha_p \sin\theta \right\}$$

Similarly, the circumferential component of section force is

$$\widetilde{F}_\theta = -\widetilde{L}\sin\varepsilon_b - \widetilde{D}\cos\varepsilon_b = -\tfrac{1}{2}\rho\omega^2 r^2 c_b \widetilde{C}_{L,\alpha}$$
$$\times \left[\frac{\beta-\varepsilon_\infty-\varepsilon_i-\alpha_p\sin^2\varepsilon_\infty\sin\theta}{\cos^2\varepsilon_\infty} - 2(\beta-\varepsilon_\infty-\varepsilon_i)\alpha_p\tan\varepsilon_\infty\sin\theta \right] \cos^2\varepsilon_i$$
$$\times \left[\sin(\varepsilon_\infty+\varepsilon_i)+\alpha_p\cos(\varepsilon_\infty+\varepsilon_i)\sin^2\varepsilon_\infty\sin\theta \right]$$
$$-\tfrac{1}{2}\rho\omega^2 r^2 c_b \widetilde{C}_D \left(\frac{1}{\cos^2\varepsilon_\infty} - 2\alpha_p\tan\varepsilon_\infty\sin\theta \right) \cos^2\varepsilon_i$$
$$\times \left[\cos(\varepsilon_\infty+\varepsilon_i)-\alpha_p\sin(\varepsilon_\infty+\varepsilon_i)\sin^2\varepsilon_\infty\sin\theta \right]$$

$$\widetilde{F}_\theta \cong -\tfrac{1}{2}\rho\omega^2 r^2 c_b \cos^2\varepsilon_i \left\{ \left[\frac{\widetilde{C}_D\cos(\varepsilon_\infty+\varepsilon_i)+\widetilde{C}_{L,\alpha}(\beta-\varepsilon_\infty-\varepsilon_i)\sin(\varepsilon_\infty+\varepsilon_i)}{\cos^2\varepsilon_\infty} \right] \right.$$
$$+\left\{ \tan^2\varepsilon_\infty \left[\widetilde{C}_{L,\alpha}(\beta-\varepsilon_\infty-\varepsilon_i)\cos(\varepsilon_\infty+\varepsilon_i)-(\widetilde{C}_{L,\alpha}+\widetilde{C}_D)\sin(\varepsilon_\infty+\varepsilon_i) \right] \right. \qquad (2.5.17)$$
$$\left. \left. -2\tan\varepsilon_\infty \left[\widetilde{C}_D\cos(\varepsilon_\infty+\varepsilon_i)+\widetilde{C}_{L,\alpha}(\beta-\varepsilon_\infty-\varepsilon_i)\sin(\varepsilon_\infty+\varepsilon_i) \right] \right\} \alpha_p \sin\theta \right\}$$

The thrust per unit radial distance, for the full prop-circle, is the average axial force integrated over a full revolution, multiplied by the number of blades, k. Thus, Eq. (2.5.16) is readily integrated with respect to θ to give

$$\frac{dT}{dr} = \frac{k}{2\pi}\int_{\theta=0}^{2\pi} \widetilde{T}\, d\theta$$
$$= \frac{k}{4\pi}\rho\omega^2 r^2 c_b \left[\frac{\widetilde{C}_{L,\alpha}(\beta-\varepsilon_\infty-\varepsilon_i)\cos(\varepsilon_\infty+\varepsilon_i)-\widetilde{C}_D\sin(\varepsilon_\infty+\varepsilon_i)}{\cos^2\varepsilon_\infty} \right] \cos^2\varepsilon_i \int_{\theta=0}^{2\pi} d\theta$$
$$-\frac{k}{4\pi}\rho\omega^2 r^2 c_b \left\{ \tan^2\varepsilon_\infty \left[(\widetilde{C}_{L,\alpha}+\widetilde{C}_D)\cos(\varepsilon_\infty+\varepsilon_i)+\widetilde{C}_{L,\alpha}(\beta-\varepsilon_\infty-\varepsilon_i)\sin(\varepsilon_\infty+\varepsilon_i) \right] \right.$$
$$\left. +2\tan\varepsilon_\infty \left[\widetilde{C}_{L,\alpha}(\beta-\varepsilon_\infty-\varepsilon_i)\cos(\varepsilon_\infty+\varepsilon_i)-\widetilde{C}_D\sin(\varepsilon_\infty+\varepsilon_i) \right] \right\} \alpha_p \cos^2\varepsilon_i \int_{\theta=0}^{2\pi} \sin\theta\, d\theta$$

$$\frac{dT}{dr} = \frac{k}{2}\rho\omega^2 r^2 c_b \frac{\cos^2\varepsilon_i}{\cos^2\varepsilon_\infty}\left[\widetilde{C}_{L,\alpha}(\beta-\varepsilon_\infty-\varepsilon_i)\cos(\varepsilon_\infty+\varepsilon_i)-\widetilde{C}_D\sin(\varepsilon_\infty+\varepsilon_i)\right] \quad (2.5.18)$$

and

$$\begin{aligned} T &= \int_{r=r_h}^{r_o}\frac{dT}{dr}dr \\ &= \frac{k\rho\omega^2}{2}\int_{r=r_h}^{r_o} r^2 c_b \frac{\cos^2\varepsilon_i}{\cos^2\varepsilon_\infty}\left[\widetilde{C}_{L,\alpha}(\beta-\varepsilon_\infty-\varepsilon_i)\cos(\varepsilon_\infty+\varepsilon_i)-\widetilde{C}_D\sin(\varepsilon_\infty+\varepsilon_i)\right]dr \end{aligned} \quad (2.5.19)$$

Similarly, the torque required to turn the propeller is

$$\ell = \int_{r=r_h}^{r_o}\frac{k}{2\pi}\int_{\theta=0}^{2\pi} -\widetilde{F}_\theta\, r\, d\theta\, dr$$

Applying Eq. (2.5.17), the integration with respect to θ is readily carried out to yield

$$\ell = \frac{k\rho\omega^2}{2}\int_{r=r_h}^{r_o} r^3 c_b \frac{\cos^2\varepsilon_i}{\cos^2\varepsilon_\infty}\left[\widetilde{C}_D\cos(\varepsilon_\infty+\varepsilon_i)+\widetilde{C}_{L,\alpha}(\beta-\varepsilon_\infty-\varepsilon_i)\sin(\varepsilon_\infty+\varepsilon_i)\right]dr \quad (2.5.20)$$

Comparing Eqs. (2.5.19) and (2.5.20) with Eqs. (2.3.26) and (2.3.27), we find that within the accuracy of the small-angle approximation used for α_p, the propeller thrust and torque are not affected by small changes in the propeller angle of attack.

In a similar manner we can determine the normal component of the aerodynamic force acting on a rotating propeller. This is the component of force that acts in the plane of propeller rotation and in a direction parallel to the in-plane component of the freestream velocity. From Fig. 2.5.1 we can see that the normal component of section force is equal to the circumferential component, in the direction of propeller rotation, multiplied by the sine of the rotation angle, θ,

$$\widetilde{N} = \widetilde{F}_\theta \sin\theta$$

Applying Eq. (2.5.17) to this result, we have

$$\begin{aligned} \widetilde{N} = &-\tfrac{1}{2}\rho\omega^2 r^2 c_b\left[\frac{\widetilde{C}_D\cos(\varepsilon_\infty+\varepsilon_i)+\widetilde{C}_{L,\alpha}(\beta-\varepsilon_\infty-\varepsilon_i)\sin(\varepsilon_\infty+\varepsilon_i)}{\cos^2\varepsilon_\infty}\right]\cos^2\varepsilon_i\sin\theta \\ &-\tfrac{1}{2}\rho\omega^2 r^2 c_b\Big\{\tan^2\varepsilon_\infty\left[\widetilde{C}_{L,\alpha}(\beta-\varepsilon_\infty-\varepsilon_i)\cos(\varepsilon_\infty+\varepsilon_i)-(\widetilde{C}_{L,\alpha}+\widetilde{C}_D)\sin(\varepsilon_\infty+\varepsilon_i)\right] \\ &-2\tan\varepsilon_\infty\left[\widetilde{C}_D\cos(\varepsilon_\infty+\varepsilon_i)+\widetilde{C}_{L,\alpha}(\beta-\varepsilon_\infty-\varepsilon_i)\sin(\varepsilon_\infty+\varepsilon_i)\right]\Big\}\,\alpha_p\cos^2\varepsilon_i\sin^2\theta \end{aligned}$$

The normal force per unit radial distance, for the full prop-circle, is the average section normal force per blade integrated over a full revolution, multiplied by the number of blades. Integrating from θ equals zero to 2π and multiplying by k gives

$$\frac{dN}{dr} = \frac{k}{2\pi}\int_{\theta=0}^{2\pi} \widetilde{N}\, d\theta$$

$$= -\frac{k}{4\pi}\rho\omega^2 r^2 c_b \left[\frac{\widetilde{C}_D \cos(\varepsilon_\infty+\varepsilon_i) + \widetilde{C}_{L,\alpha}(\beta-\varepsilon_\infty-\varepsilon_i)\sin(\varepsilon_\infty+\varepsilon_i)}{\cos^2\varepsilon_\infty}\right]\cos^2\varepsilon_i \int_{\theta=0}^{2\pi}\sin\theta\, d\theta$$

$$-\frac{k}{4\pi}\rho\omega^2 r^2 c_b \Big\{\tan^2\varepsilon_\infty\left[\widetilde{C}_{L,\alpha}(\beta-\varepsilon_\infty-\varepsilon_i)\cos(\varepsilon_\infty+\varepsilon_i) - (\widetilde{C}_{L,\alpha}+\widetilde{C}_D)\sin(\varepsilon_\infty+\varepsilon_i)\right]$$

$$-2\tan\varepsilon_\infty\left[\widetilde{C}_D\cos(\varepsilon_\infty+\varepsilon_i) + \widetilde{C}_{L,\alpha}(\beta-\varepsilon_\infty-\varepsilon_i)\sin(\varepsilon_\infty+\varepsilon_i)\right]\Big\}\,\alpha_p\cos^2\varepsilon_i\int_{\theta=0}^{2\pi}\sin^2\theta\, d\theta$$

$$\frac{dN}{dr} = \frac{k}{4}\rho\omega^2 r^2 c_b \Big\{2\tan\varepsilon_\infty\left[\widetilde{C}_D\cos(\varepsilon_\infty+\varepsilon_i) + \widetilde{C}_{L,\alpha}(\beta-\varepsilon_\infty-\varepsilon_i)\sin(\varepsilon_\infty+\varepsilon_i)\right]$$

$$-\tan^2\varepsilon_\infty\left[\widetilde{C}_{L,\alpha}(\beta-\varepsilon_\infty-\varepsilon_i)\cos(\varepsilon_\infty+\varepsilon_i) - (\widetilde{C}_{L,\alpha}+\widetilde{C}_D)\sin(\varepsilon_\infty+\varepsilon_i)\right]\Big\}\alpha_p\cos^2\varepsilon_i$$

Integrating this result with respect to r from the hub radius to the tip radius, the total normal force acting on the propeller is found to be

$$N = \int_{r=r_h}^{r_o}\frac{dN}{dr}dr = \frac{k\rho\omega^2}{4}\alpha_p$$

$$\times\int_{r=r_h}^{r_o} r^2 c_b\cos^2\varepsilon_i\Big\{2\tan\varepsilon_\infty\left[\widetilde{C}_D\cos(\varepsilon_\infty+\varepsilon_i) + \widetilde{C}_{L,\alpha}(\beta-\varepsilon_\infty-\varepsilon_i)\sin(\varepsilon_\infty+\varepsilon_i)\right] \qquad (2.5.21)$$

$$-\tan^2\varepsilon_\infty\left[\widetilde{C}_{L,\alpha}(\beta-\varepsilon_\infty-\varepsilon_i)\cos(\varepsilon_\infty+\varepsilon_i) - (\widetilde{C}_{L,\alpha}+\widetilde{C}_D)\sin(\varepsilon_\infty+\varepsilon_i)\right]\Big\}dr$$

While this normal force is typically quite small and is insignificant compared to the lift of the wing, it can have a very significant effect on aircraft stability.

Using Eq. (2.5.17) and following a similar procedure, it is readily shown that without sideslip, the aerodynamic side force in the plane of propeller rotation is zero,

$$Y = \int_{r=r_h}^{r_o}\frac{dY}{dr}dr = \int_{r=r_h}^{r_o}\frac{k}{2\pi}\int_{\theta=0}^{2\pi}\widetilde{Y}\, d\theta\, dr = \frac{k}{2\pi}\int_{r=r_h}^{r_o}\int_{\theta=0}^{2\pi} -\widetilde{F}_\theta\cos\theta\, d\theta\, dr = 0 \qquad (2.5.22)$$

From Eq. (2.5.16), without sideslip, the aerodynamic pitching moment about the center of the propeller disk is also zero,

$$m = \int_{r=r_h}^{r_o}\frac{k}{2\pi}\int_{\theta=0}^{2\pi}\widetilde{T}\, r\cos\theta\, d\theta\, dr = 0 \qquad (2.5.23)$$

and the aerodynamic yawing moment about the center of the propeller disk is

$$n = \int_{r=r_h}^{r_o} \frac{k}{2\pi} \int_{\theta=0}^{2\pi} \tilde{T}\, r \sin\theta \, d\theta \, dr = -\frac{k\rho\omega^2}{4} \alpha_p$$
$$\times \int_{r=r_h}^{r_o} r^3 c_b \cos^2\varepsilon_i \left\{ 2\tan\varepsilon_\infty \left[\tilde{C}_{L,\alpha} (\beta - \varepsilon_\infty - \varepsilon_i) \cos(\varepsilon_\infty + \varepsilon_i) - \tilde{C}_D \sin(\varepsilon_\infty + \varepsilon_i) \right] \right. \quad (2.5.24)$$
$$\left. + \tan^2\varepsilon_\infty \left[(\tilde{C}_{L,\alpha} + \tilde{C}_D) \cos(\varepsilon_\infty + \varepsilon_i) + \tilde{C}_{L,\alpha} (\beta - \varepsilon_\infty - \varepsilon_i) \sin(\varepsilon_\infty + \varepsilon_i) \right] \right\} dr$$

The dimensionless off-axis aerodynamic coefficients for a propeller are defined in exactly the same way as the thrust and torque coefficients. With these traditional definitions, Eqs. (2.5.21) through (2.5.24) are readily nondimensionalized to yield the following:

Side force coefficient

$$C_Y \equiv \frac{Y}{\rho(\omega/2\pi)^2 d_p^4} = 0 \quad (2.5.25)$$

Normal force coefficient

$$C_N \equiv \frac{N}{\rho(\omega/2\pi)^2 d_p^4}$$
$$= \frac{\pi^2}{8} \alpha_p \int_{\zeta=\zeta_h}^{1} \zeta^2 \hat{c}_b \cos^2\varepsilon_i \left\{ 2\tan\varepsilon_\infty \left[\tilde{C}_D \cos(\varepsilon_\infty + \varepsilon_i) + \tilde{C}_L \sin(\varepsilon_\infty + \varepsilon_i) \right] \right. \quad (2.5.26)$$
$$\left. - \tan^2\varepsilon_\infty \left[\tilde{C}_L \cos(\varepsilon_\infty + \varepsilon_i) - (\tilde{C}_{L,\alpha} + \tilde{C}_D) \sin(\varepsilon_\infty + \varepsilon_i) \right] \right\} d\zeta$$

Pitching moment coefficient

$$C_m \equiv \frac{m}{\rho(\omega/2\pi)^2 d_p^5} = 0 \quad (2.5.27)$$

Yawing moment coefficient

$$C_n \equiv \frac{n}{\rho(\omega/2\pi)^2 d_p^5}$$
$$= -\frac{\pi^2}{16} \alpha_p \int_{\zeta=\zeta_h}^{1} \zeta^3 \hat{c}_b \cos^2\varepsilon_i \left\{ 2\tan\varepsilon_\infty \left[\tilde{C}_L \cos(\varepsilon_\infty + \varepsilon_i) - \tilde{C}_D \sin(\varepsilon_\infty + \varepsilon_i) \right] \right. \quad (2.5.28)$$
$$\left. + \tan^2\varepsilon_\infty \left[(\tilde{C}_{L,\alpha} + \tilde{C}_D) \cos(\varepsilon_\infty + \varepsilon_i) + \tilde{C}_L \sin(\varepsilon_\infty + \varepsilon_i) \right] \right\} d\zeta$$

where again

$$\zeta \equiv \frac{r}{d_p/2} \tag{2.3.37}$$

$$\hat{c}_b \equiv \frac{kc_b}{d_p} \tag{2.3.38}$$

$$\beta \equiv \tan^{-1}\left(\frac{K}{\pi\zeta}\right) \tag{2.3.39}$$

$$\varepsilon_\infty \equiv \tan^{-1}\left(\frac{J}{\pi\zeta}\right) \tag{2.3.40}$$

$$K \equiv \frac{\lambda}{d_p} \tag{2.3.41}$$

$$J \equiv \frac{2\pi V_\infty}{\omega d_p} \tag{2.3.42}$$

and ε_i is determined from

$$\frac{\hat{c}_b}{8\zeta}\widetilde{C}_L - \cos^{-1}\left\{\exp\left[-\frac{k(1-\zeta)}{2\sin\beta_t}\right]\right\}\tan\varepsilon_i \sin(\varepsilon_\infty + \varepsilon_i) = 0 \tag{2.3.32}$$

Notice that both the normal force coefficient and yawing moment coefficient are directly proportional to the propeller angle of attack. By symmetry, it is easily shown that the side force and pitching moment are related to the sideslip angle in exactly the same way that the normal force and yawing moment are related to the angle of attack. The variations in the normal force and side force with angle of attack and sideslip angle become particularly important in the study of aircraft stability and control. Because of these forces, a rotating propeller that is forward of the airplane's center of gravity has a significant destabilizing effect while an aft propeller is stabilizing. This will be covered in detail in Chapter 4.

EXAMPLE 2.5.1. For the family of two-blade propellers described in Example 2.3.1, we wish to examine how the off-axis forces and moments depend on advance ratio and pitch-to-diameter ratio. For this purpose, we want to plot the change in the normal force coefficient with propeller angle of attack as a function of advance ratio. These results are to be compared for several different values of pitch-to-diameter ratio. Similar plots are to be obtained for the change in the yawing moment coefficient with respect to propeller angle of attack.

Solution. As an example calculation, we again consider the 75 percent radius section of one of these propellers with a chord-line pitch-to-diameter ratio of 0.5, operating at an advance ratio of 0.25. From Example 2.3.1, at this cross-section of the propeller we have

$$\zeta = 0.75$$

$$K = 0.591$$

$$\beta = 0.2458 = 14.08°$$

$$\varepsilon_\infty = 0.1057 = 6.06°$$

$$\hat{c}_b = 0.09922$$

$$\varepsilon_i = 0.04815 = 2.76°$$

With these results, from Eq. (2.5.26),

$$\frac{dC_{N,\alpha}}{d\zeta} = \frac{\pi^2}{8}\zeta^2\hat{c}_b\cos^2\varepsilon_i\left\{2\tan\varepsilon_\infty\left[\widetilde{C}_D\cos(\varepsilon_\infty+\varepsilon_i)+\widetilde{C}_L\sin(\varepsilon_\infty+\varepsilon_i)\right]\right.$$
$$\left.-\tan^2\varepsilon_\infty\left[\widetilde{C}_L\cos(\varepsilon_\infty+\varepsilon_i)-(\widetilde{C}_{L,\alpha}+\widetilde{C}_D)\sin(\varepsilon_\infty+\varepsilon_i)\right]\right\}$$
$$= 0.0017079$$

Integrating similar results from $\zeta = 0.1$ to 1.0, we obtain

$$C_{N,\alpha} \equiv \frac{dC_N}{d\alpha_p} = \underline{0.00273}$$

Similarly, from Eq. (2.5.28),

$$\frac{dC_{n,\alpha}}{d\zeta} = -\frac{\pi^2}{16}\zeta^3\hat{c}_b\cos^2\varepsilon_i\left\{2\tan\varepsilon_\infty\left[\widetilde{C}_L\cos(\varepsilon_\infty+\varepsilon_i)-\widetilde{C}_D\sin(\varepsilon_\infty+\varepsilon_i)\right]\right.$$
$$\left.+\tan^2\varepsilon_\infty\left[(\widetilde{C}_{L,\alpha}+\widetilde{C}_D)\cos(\varepsilon_\infty+\varepsilon_i)+\widetilde{C}_L\sin(\varepsilon_\infty+\varepsilon_i)\right]\right\}$$
$$= -0.0049410$$

$$C_{n,\alpha} \equiv \frac{dC_n}{d\alpha_p} = \underline{-0.00300}$$

After repeating these calculations for various values of the advance ratio and several different pitch-to-diameter ratios, we obtain the results that are plotted in Figs. 2.5.3 and 2.5.4.

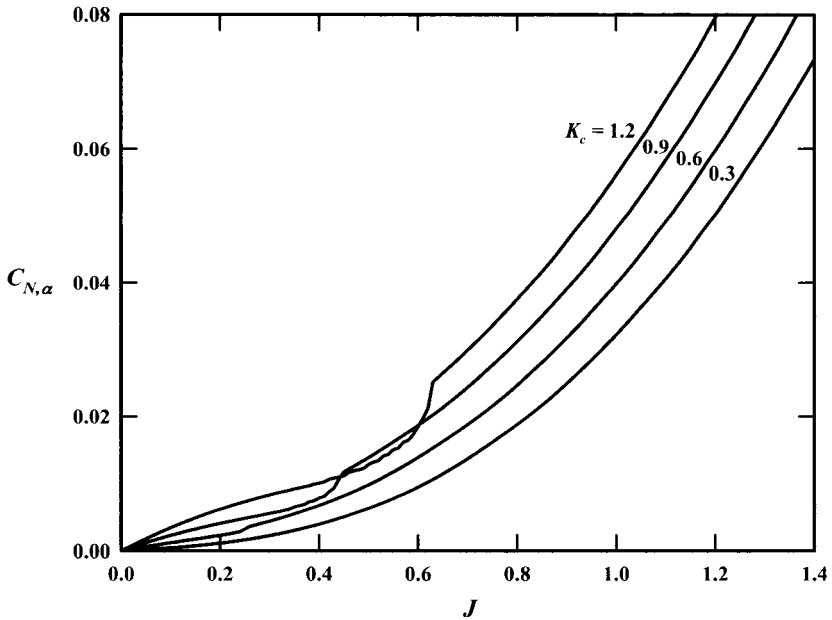


Figure 2.5.3. Dimensionless normal force derivative for the family of two-blade propellers in Example 2.5.1.

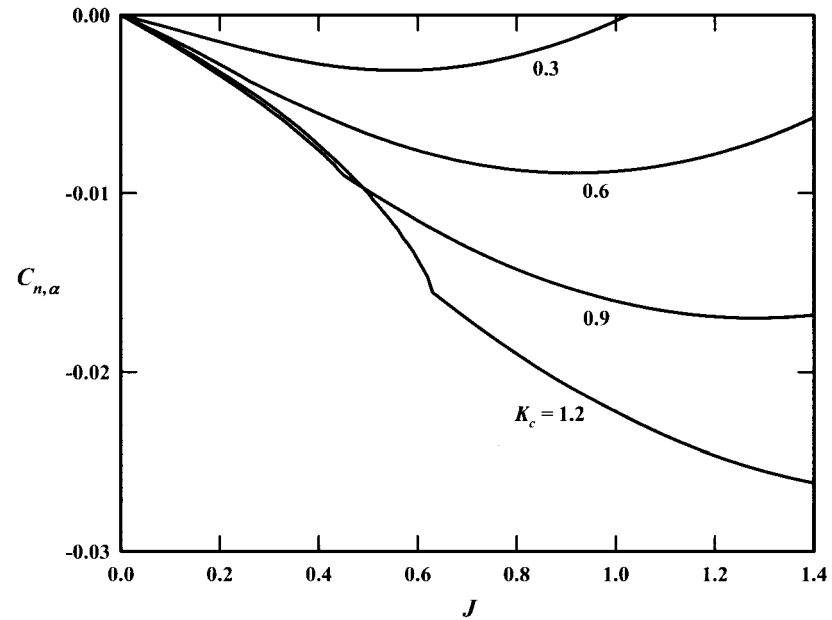


Figure 2.5.4. Dimensionless yawing-moment derivative for the family of two-blade propellers in Example 2.5.1.

2.6. Turbojet Engines: The Thrust Equation

A complete analysis for the flow of air and products of combustion through the various components of a turbojet engine is beyond the intended scope of this chapter. Here we confine our study of the turbojet engine to what is commonly called *thermodynamic cycle analysis*, which examines the thermodynamic changes in the working fluid as it flows through the components of the engine. While this type of analysis does not provide the information needed for the detailed design of individual components such as turbine and compressor blades, it does provide some valuable insight that can be useful in the study of flight mechanics. For a more detailed study of gas turbine propulsion systems, the reader is referred to the excellent text by Jack Mattingly (1996).

As shown schematically in Fig. 2.6.1, the major internal components of an installed turbojet engine are the inlet duct, compressor, combustion chamber, gas turbine, and exit nozzle. Before considering a thermodynamic cycle analysis for this propulsion system, we shall apply the momentum equation to examine the axial forces acting on such an engine mounted to the wing of a moving airplane with a strut.

Consider the control volume shown in Fig. 2.6.2. This control volume encloses the complete engine and nacelle and cuts through the mounting strut between the engine and wing. The axial forces acting on this control volume include the reaction shear force in the strut, F_r, the drag force acting on the nacelle, D_{nac}, the differential pressure force, $(p_i - p_\infty)dA_i$, integrated over the inlet area, and the differential pressure force, $(p_e - p_\infty)dA_e$, integrated over the exit area. Here dA_i and dA_e are, respectively, the differential cross-sectional areas for the inlet and exit. The pressure forces on the inlet and exit areas are defined relative to the freestream pressure, p_∞, because this is the standard convention used to define the drag force acting on the nacelle. The freestream pressure integrated over the surface of the control volume is the buoyant force, which in this case is negligible. The reaction shear force in the strut is equal to the net thrust developed by the installed engine, including the losses due to drag. This is conventionally called the *installed thrust* or *available thrust* and is traditionally denoted as T.

From Newton's second law, the summation of forces in the axial direction is equal to the net axial momentum flux. The axial momentum flux crossing the boundary of the control volume is the mass flow rate multiplied by the axial momentum per unit mass,

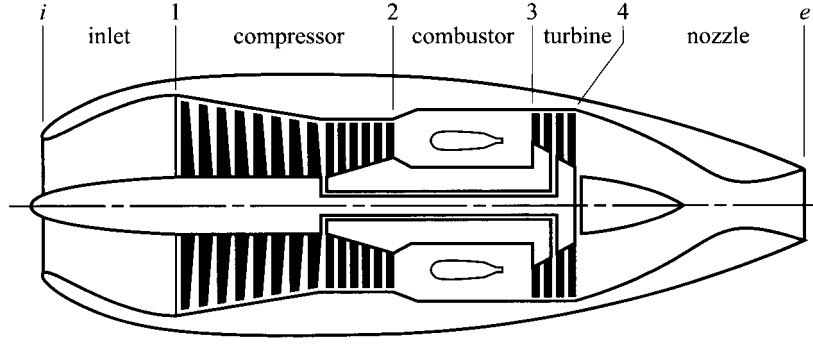


Figure 2.6.1. Components and station labeling for the turbojet engine.

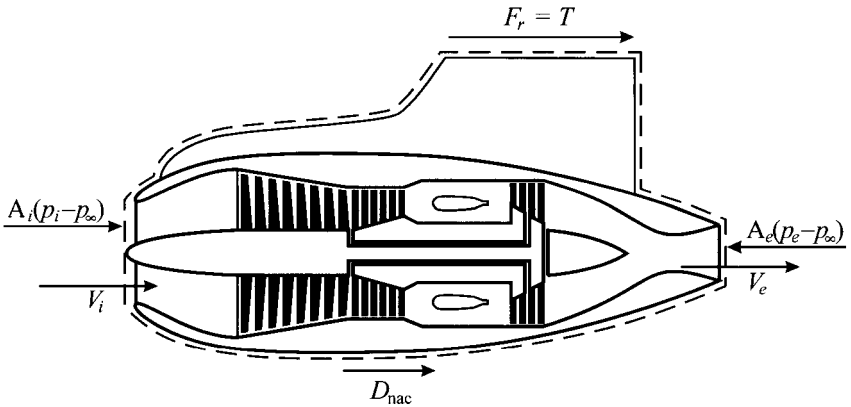


Figure 2.6.2. Control volume forces and momentum fluxes for a turbojet engine.

which is simply the axial velocity component. In the exit plane the axial momentum flux, which is considered positive leaving the control volume, is $(\rho_e V_e dA_e)V_e$ and in the inlet plane it is $(-\rho_i V_i dA_i)V_i$. Assuming uniform flow over the inlet and exit planes and neglecting the momentum of incoming fuel, Newton's second law applied to the control volume shown in Fig. 2.6.2 can be written as

$$F_r + D_{\text{nac}} + A_i(p_i - p_\infty) - A_e(p_e - p_\infty) = \rho_e A_e V_e^2 - \rho_i A_i V_i^2$$

Using the notation for mass flow rate, $\dot{m} \equiv \rho A V$, and solving for available thrust gives

$$T \equiv F_r = \dot{m}_e V_e + A_e(p_e - p_\infty) - \dot{m}_i V_i - A_i(p_i - p_\infty) - D_{\text{nac}} \tag{2.6.1}$$

In order to separate the effects of the engine and nacelle, Eq. (2.6.1) is traditionally rearranged to the form

$$T = [\dot{m}_e V_e - \dot{m}_i V_\infty + A_e(p_e - p_\infty)] - [\dot{m}_i(V_i - V_\infty) + A_i(p_i - p_\infty)] - D_{\text{nac}} \tag{2.6.2}$$

The grouping of terms in the first set of square brackets in Eq. (2.6.2) is usually called the *uninstalled thrust* and will simply be given the symbol F,

$$F \equiv \dot{m}_e V_e - \dot{m}_i V_\infty + A_e(p_e - p_\infty) \tag{2.6.3}$$

Here F is used to denote uninstalled thrust to avoid later confusion with temperature. The terms in the second set of square brackets in Eq. (2.6.2) have sometimes been called the *pre-entry drag* but are more commonly referred to as the *additive drag*, D_{add},

$$D_{\text{add}} \equiv \dot{m}_i(V_i - V_\infty) + A_i(p_i - p_\infty) \tag{2.6.4}$$

With this terminology, the installed or available thrust is equal to the uninstalled thrust less the sum of the nacelle drag and additive drag,

$$T = F - (D_{nac} + D_{add}) \tag{2.6.5}$$

Some insight into the nature of additive drag can be provided by rearranging the definition in Eq. (2.6.4). Expressing the inlet mass flow rate in terms of density, velocity, and area results in

$$D_{add} = A_i[\rho_i(V_i^2 - V_i V_\infty) + p_i - p_\infty] \tag{2.6.6}$$

Assuming that air is an ideal gas, the air density can be expressed in terms of pressure, temperature, and the ideal gas constant, R. Thus, Eq. (2.6.6) can be written

$$D_{add} = A_i\left[\frac{p_i}{RT_i}(V_i^2 - V_i V_\infty) + p_i - p_\infty\right] \tag{2.6.7}$$

The speed of sound in an ideal gas is

$$a = \sqrt{\gamma RT} \tag{2.6.8}$$

where γ is the ratio of constant-pressure specific heat to constant-volume specific heat. In view of Eq. (2.6.8), it is convenient to rearrange Eq. (2.6.7) as

$$D_{add} = A_i p_\infty\left[\gamma\frac{p_i}{p_\infty}\left(\frac{V_i^2}{\gamma RT_i} - \frac{V_i V_\infty}{\gamma R\sqrt{T_i T_\infty}}\sqrt{\frac{T_\infty}{T_i}} + \frac{1}{\gamma}\right) - 1\right]$$

or

$$D_{add} = A_i p_\infty\left[\gamma\frac{p_i}{p_\infty}\left(\mathrm{M}_i^2 - \mathrm{M}_i\,\mathrm{M}_\infty\sqrt{\frac{T_\infty}{T_i}} + \frac{1}{\gamma}\right) - 1\right] \tag{2.6.9}$$

where T_i and T_∞ are the inlet and freestream temperatures, respectively. **(Be careful not to confuse temperature and thrust.)** The pressure and temperature ratios in Eq. (2.6.9) depend on the inlet and flight Mach numbers. Assuming isentropic flow from the freestream to the inlet, the stagnation pressure, p_0, and the stagnation temperature, T_0, remain constant. Thus, Eq. (2.6.9) can be written

$$D_{add} = A_i p_\infty\left[\gamma\frac{p_i/p_{0i}}{p_\infty/p_{0\infty}}\left(\mathrm{M}_i^2 - \mathrm{M}_i\,\mathrm{M}_\infty\sqrt{\frac{T_\infty/T_{0\infty}}{T_i/T_{0i}}} + \frac{1}{\gamma}\right) - 1\right] \tag{2.6.10}$$

where, from compressible flow theory,

$$\frac{p}{p_0} = \left(1 + \frac{\gamma-1}{2}\mathrm{M}^2\right)^{\frac{-\gamma}{\gamma-1}} \quad \text{and} \quad \frac{T}{T_0} = \left(1 + \frac{\gamma-1}{2}\mathrm{M}^2\right)^{-1}$$

From Eq. (2.6.10) it can be seen that the additive drag will be zero if the inlet is designed such that the inlet Mach number, M_i, is equal to the flight Mach number, M_∞. Turbojet inlets are commonly designed to provide this match at the design cruise Mach number.

EXAMPLE 2.6.1. The inlet of a particular turbojet engine has a cross-sectional area of 46 ft^2 and is operating at standard sea level with an inlet Mach number of 0.6. Assuming that the inlet Mach number remains constant, plot the additive drag predicted from Eq. (2.6.10) as a function of flight Mach number from 0 to 1.

Solution. For this engine and the specified operating conditions, we have

$$A_i = 46 \text{ ft}^2, \quad p_\infty = 14.696 \text{ psi}, \quad M_i = 0.6, \quad \gamma = 1.4$$

and

$$\frac{p_i}{p_{0i}} = \left(1+\frac{\gamma-1}{2}M_i^2\right)^{\frac{-\gamma}{\gamma-1}} = [1+0.2(0.6)^2]^{-3.5} = 0.784004$$

$$\frac{T_i}{T_{0i}} = \left(1+\frac{\gamma-1}{2}M_i^2\right)^{-1} = [1+0.2(0.6)^2]^{-1} = 0.932836$$

As an example calculation, for a flight Mach number of 0.1, we obtain

$$\frac{p_\infty}{p_{0\infty}} = \left(1+\frac{\gamma-1}{2}M_\infty^2\right)^{\frac{-\gamma}{\gamma-1}} = [1+0.2(0.1)^2]^{-3.5} = 0.993031$$

$$\frac{T_\infty}{T_{0\infty}} = \left(1+\frac{\gamma-1}{2}M_\infty^2\right)^{-1} = [1+0.2(0.1)^2]^{-1} = 0.998004$$

$$D_{\text{add}} = A_i p_\infty \left[\gamma \frac{p_i/p_{0i}}{p_\infty/p_{0\infty}}\left(M_i^2 - M_i M_\infty \sqrt{\frac{T_\infty/T_{0\infty}}{T_i/T_{0i}}} + \frac{1}{\gamma}\right) - 1\right]$$

$$= 46(14.696\times144)\left[1.4\frac{0.784004}{0.993031}\left(0.6^2 - 0.6\times0.1\sqrt{\frac{0.998004}{0.932836}} + \frac{1}{1.4}\right) - 1\right]$$

$$= \underline{11{,}567 \text{ lbf}}$$

Repeating these calculations for different values of the flight Mach number with the inlet Mach number held constant, the results shown in Fig. 2.6.3 are obtained. The inlet static pressure is also shown in this figure as a function of the flight Mach number. Notice that the inlet pressure is below the freestream pressure for airspeeds below the design flight Mach number and above the freestream for higher Mach numbers.

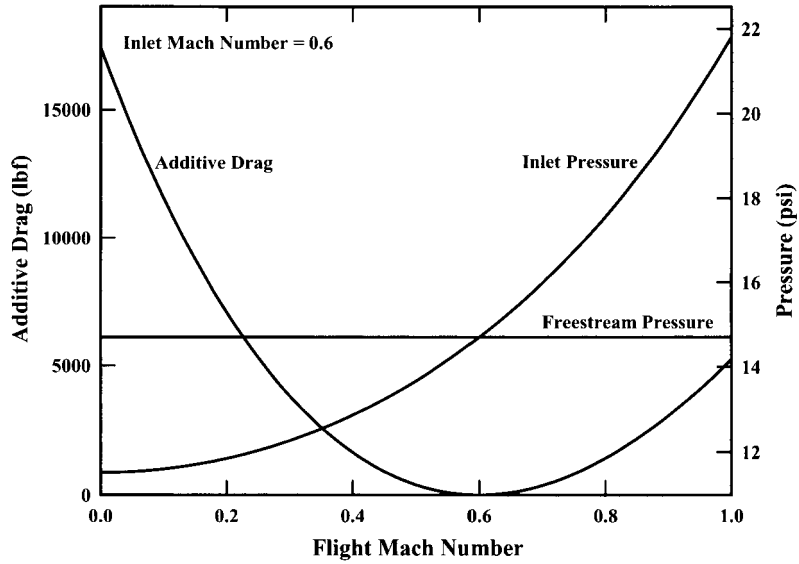


Figure 2.6.3. Inlet pressure and additive drag for Example 2.6.1.

Because the inlet area of a turbojet engine is typically larger than the exit area, the pressure component of nacelle drag will be negative, provided that the flow does not separate. In fact, it can be shown that in a completely inviscid fluid the nacelle drag would exactly offset the additive drag, and the installed thrust would be equal to the uninstalled thrust. In viscous flow, when the inlet is operating near the design Mach number, the pressure component of nacelle drag will very nearly offset the additive drag, and the installed thrust will be less than the uninstalled thrust only by an amount approximately equal to the viscous component of nacelle drag. However, when the flight Mach number is significantly different from the inlet Mach number, the airflow near the inlet must be turned through large angles. This results in flow separation with a resulting increase in nacelle drag. When the flight Mach number differs considerably from the inlet Mach number, the additive drag will dominate and the installed thrust will be substantially reduced. This is particularly significant during takeoff, when the airspeed is low and the additive drag is large. To reduce additive drag at low flight Mach numbers and increase static thrust, some turbojet installations are designed so that the inlet area can be increased for full-throttle operation on takeoff.

For efficient performance, the inlet of a turbojet engine must be designed specifically for the intended operating condition. The inlet duct must ingest air at or near the flight Mach number and reduce the velocity to a level suitable for efficient operation of the compressor. For subsonic flight, the simple divergent geometry shown in Fig. 2.6.1 is satisfactory. However, for supersonic flight, shock waves will occur as the velocity of the ingested flow is reduced. The compression process is quite inefficient if the airflow is reduced to subsonic speed through a single normal shock wave. Thus, supersonic inlets are quite different from that shown in Fig. 2.6.1 (see Mattingly 1996).

2.7. Turbojet Engines: Cycle Analysis

To gain some insight into the performance characteristics of a turbojet engine, we shall now consider the steady operation of the engine shown schematically in Fig. 2.6.1. For this analysis we consider an ideal engine having all thermodynamically reversible components. For this engine, the flow through the inlet and compressor is modeled as reversible adiabatic compression. The process in the combustion chamber is modeled as heat addition at constant stagnation pressure. The flow through the turbine and exhaust nozzle is modeled as a reversible adiabatic expansion back to ambient pressure. In terms of the station labeling shown in Fig. 2.6.1, the following assumptions are made for this ideal cycle analysis.

1. The working fluid is air, which is assumed to behave as an ideal gas with constant specific heat.

2. The flow from the freestream to the compressor inlet is assumed to be isentropic. This assumption requires that

$$\frac{T_{0\infty}}{T_\infty} = \left(\frac{p_{0\infty}}{p_\infty}\right)^{\frac{\gamma-1}{\gamma}} = 1+\frac{\gamma-1}{2}\mathrm{M}_\infty^2 \tag{2.7.1}$$

$$\frac{T_{01}}{T_{0\infty}} = \left(\frac{p_{01}}{p_{0\infty}}\right)^{\frac{\gamma-1}{\gamma}} \tag{2.7.2}$$

3. The flow through the compressor is also assumed to be isentropic, which requires that

$$\frac{T_{02}}{T_{01}} = \left(\frac{p_{02}}{p_{01}}\right)^{\frac{\gamma-1}{\gamma}} \tag{2.7.3}$$

4. The process in the combustion chamber is assumed to take place at constant stagnation pressure, and the fuel flow rate is assumed to be negligible compared to that of the air. Thus, from the combustion model we have

$$\dot{m}_e = \dot{m}_i \equiv \dot{m} \tag{2.7.4}$$

$$p_{03} = p_{02} \tag{2.7.5}$$

5. The turbine flow is assumed to be isentropic and the turbine shaft work rate, $\dot{W}_{3-4}$, is input directly to the compressor, with no loss. This requires that

$$\frac{T_{04}}{T_{03}} = \left(\frac{p_{04}}{p_{03}}\right)^{\frac{\gamma-1}{\gamma}} \tag{2.7.6}$$

$$\dot{W}_{1-2}+\dot{W}_{3-4} = 0 \tag{2.7.7}$$

6. The exhaust nozzle is modeled as an isentropic expansion from the turbine outlet pressure to ambient pressure, which requires that

$$\frac{T_{0e}}{T_{04}} = \left(\frac{p_{0e}}{p_{04}}\right)^{\frac{\gamma-1}{\gamma}} \tag{2.7.8}$$

$$\frac{T_{0e}}{T_e} = \left(\frac{p_{0e}}{p_e}\right)^{\frac{\gamma-1}{\gamma}} = 1+\frac{\gamma-1}{2}\mathrm{M}_e^2 \tag{2.7.9}$$

$$p_e = p_\infty \tag{2.7.10}$$

Since there is no shaft work or heat transfer associated with the airflow from the freestream to the compressor inlet, the first law of thermodynamics applied to this portion of the cycle requires that

$$\dot{m}\left[C_p(T_1-T_\infty)+\tfrac{1}{2}(V_1^2-V_\infty^2)\right] = \dot{m}C_p(T_{01}-T_{0\infty}) = 0$$

Combining this result with Eqs. (2.7.1) and (2.7.2), from known values of the operating conditions, T_∞, p_∞, and M_∞, the stagnation temperature and pressure at the compressor inlet are readily determined:

$$T_{01} = T_{0\infty} = T_\infty\left(1+\frac{\gamma-1}{2}\mathrm{M}_\infty^2\right) \tag{2.7.11}$$

$$p_{01} = p_{0\infty} = p_\infty\left(1+\frac{\gamma-1}{2}\mathrm{M}_\infty^2\right)^{\frac{\gamma}{\gamma-1}} \tag{2.7.12}$$

A very important design parameter for the turbojet engine is the pressure ratio across the compressor. Because the stagnation conditions at the compressor inlet are now known, the stagnation temperature and pressure at the compressor outlet can be determined directly from knowledge of this design parameter and Eq. (2.7.3):

$$T_{02} = T_{01}\left(\frac{p_{02}}{p_{01}}\right)^{\frac{\gamma-1}{\gamma}} \tag{2.7.13}$$

$$p_{02} = p_{01}\frac{p_{02}}{p_{01}} \tag{2.7.14}$$

Since there is no shaft work during combustion, using Eq. (2.7.4), the first law of thermodynamics applied to the combustion chamber yields

$$\dot{Q}_{2-3} = \dot{m}\left[C_p(T_3 - T_2) + \tfrac{1}{2}(V_3^2 - V_2^2)\right] = \dot{m}C_p(T_{03} - T_{02})$$

where $\dot{Q}_{2-3}$ is the rate of heat transfer in the combustion chamber, which results directly from the fuel that is burned. Assuming complete combustion, this heat transfer rate is known from the fuel flow rate imposed by the throttle setting and the enthalpy of combustion for the fuel. With this knowledge, stagnation temperature and pressure at the turbine inlet are obtained from this first law energy balance combined with Eq. (2.7.5) and the known combustion chamber inlet conditions:

$$T_{03} = T_{02} + \frac{\dot{Q}_{2-3}}{\dot{m}C_p} \tag{2.7.15}$$

$$p_{03} = p_{02} \tag{2.7.16}$$

Applying the first law of thermodynamics from the compressor inlet to the turbine outlet and separately for the exhaust nozzle alone yields

$$\dot{m}C_p(T_{04} - T_{01}) + \dot{W}_{1-2} + \dot{W}_{3-4} = \dot{Q}_{2-3}$$

$$\dot{m}C_p(T_{0e} - T_{04}) = 0$$

Combining these relations with Eqs. (2.7.6) through (2.7.8), the stagnation temperature and pressure in the exhaust nozzle are easily determined,

$$T_{0e} = T_{04} = T_{01} + \frac{\dot{Q}_{2-3}}{\dot{m}C_p} \tag{2.7.17}$$

$$p_{0e} = p_{04} = p_{03}\left(\frac{T_{04}}{T_{03}}\right)^{\frac{\gamma}{\gamma-1}} \tag{2.7.18}$$

Now that the stagnation pressure is known at the nozzle exit, the Mach number and static temperature at the exit can be obtained directly from Eqs. (2.7.9) and (2.7.10),

$$\mathrm{M}_e^2 = \frac{2}{\gamma - 1}\left[\left(\frac{p_{0e}}{p_\infty}\right)^{\frac{\gamma-1}{\gamma}} - 1\right] \tag{2.7.19}$$

$$T_e = T_{0e}\left(\frac{p_\infty}{p_{0e}}\right)^{\frac{\gamma-1}{\gamma}} \tag{2.7.20}$$

Three separate efficiencies are commonly defined for a turbojet engine. Because a turbojet has no net shaft work output, the thermal efficiency for a turbojet engine is traditionally defined as the net rate of increase in the kinetic energy of the working fluid divided by the rate of energy input. In view of Eq. (2.7.4), the **thermal efficiency** for the ideal turbojet engine is defined as

$$\eta_T \equiv \frac{\dot{m}(V_e^2 - V_\infty^2)/2}{\dot{Q}_{2\text{-}3}} \tag{2.7.21}$$

For an aircraft engine, propulsive power is a more significant measure of useful power output. Work is force multiplied by distance, and power is force multiplied by the rate of change of distance (i.e., velocity). Thus, the uninstalled propulsive power for a turbojet engine is defined as the uninstalled thrust multiplied by the freestream velocity. The uninstalled **propulsive efficiency** for a turbojet engine is therefore traditionally defined as the uninstalled propulsive power divided by the net rate of change in the kinetic energy of the working fluid,

$$\eta_P \equiv \frac{FV_\infty}{\dot{m}(V_e^2 - V_\infty^2)/2} \tag{2.7.22}$$

The uninstalled **overall efficiency** for a turbojet engine is defined as the uninstalled propulsive power divided by the rate of energy input,

$$\eta_O \equiv \frac{FV_\infty}{\dot{Q}_{2\text{-}3}} = \eta_T \eta_P \tag{2.7.23}$$

The net rate of increase in kinetic energy imparted to the working fluid that passes through an ideal turbojet engine is

$$\frac{\dot{m}}{2}(V_e^2 - V_\infty^2) = \frac{\dot{m}}{2}\gamma R T_\infty \left(\mathrm{M}_e^2 \frac{T_e}{T_\infty} - \mathrm{M}_\infty^2 \right) \tag{2.7.24}$$

Using Eqs. (2.7.11) through (2.7.20) and some algebraic manipulation, this result can be rearranged to give

$$\frac{\dot{m}}{2}(V_e^2 - V_\infty^2) = \dot{Q}_{2\text{-}3}\left(1 - \frac{T_\infty}{T_{02}}\right) = \dot{Q}_{2\text{-}3}\left[1 - \left(1 + \frac{\gamma - 1}{2}\mathrm{M}_\infty^2\right)^{-1}\left(\frac{p_{01}}{p_{02}}\right)^{\frac{\gamma-1}{\gamma}}\right]$$

and from the definition in Eq. (2.7.21), the thermal efficiency is

$$\eta_T = 1 - \frac{T_\infty}{T_{02}} = 1 - \left(1 + \frac{\gamma - 1}{2}\mathrm{M}_\infty^2\right)^{-1}\left(\frac{p_{01}}{p_{02}}\right)^{\frac{\gamma-1}{\gamma}} \tag{2.7.25}$$

From Eq. (2.7.25), it can be seen that the thermal efficiency of an ideal turbojet engine depends only on the freestream Mach number and the pressure ratio across the compressor. At any given flight Mach number, the thermal efficiency increases as the pressure ratio across the compressor is increased. Furthermore, for any specified compressor pressure ratio, the thermal efficiency increases with flight Mach number. One important observation that should be made from Eq. (2.7.25) is that a high pressure ratio is required to produce a reasonable thermal efficiency at low flight Mach numbers. Even with a pressure ratio of 30, the static thermal efficiency of an ideal turbojet engine is only about 62 percent. For this reason turbojet engines do not provide a particularly efficient means of propulsion for low-speed flight. However, at high Mach numbers the thermal efficiency is excellent.

Using Eqs. (2.7.4) and (2.7.10) with Eq. (2.6.3), the uninstalled thrust for the ideal turbojet engine is

$$F = \dot{m}(V_e - V_\infty) = \dot{m}\sqrt{\gamma R T_\infty}\left(\mathrm{M}_e\sqrt{\frac{T_e}{T_\infty}} - \mathrm{M}_\infty\right) \tag{2.7.26}$$

The size and weight of a turbojet engine is approximately proportional to the flow rate that must be handled. Since thrust-to-weight ratio is an important consideration for aircraft engines, an important performance parameter for turbojet engines is thrust per unit mass flow rate, which is commonly called *specific thrust*. After applying Eqs. (2.7.11) through (2.7.20) to the result expressed in Eq. (2.7.26), the uninstalled specific thrust for the ideal turbojet engine can be written as

$$\frac{F}{\dot{m}} = \sqrt{\gamma R T_\infty}\left\{\sqrt{\frac{2}{\gamma-1}\left[\left(\frac{p_{04}}{p_{03}}\right)^{\frac{\gamma-1}{\gamma}} - \left(\frac{p_{01}}{p_{02}}\right)^{\frac{\gamma-1}{\gamma}}\left(1+\frac{\gamma-1}{2}\mathrm{M}_\infty^2\right)^{-1}\right]\frac{T_{03}}{T_\infty}} - \mathrm{M}_\infty\right\} \tag{2.7.27}$$

The propulsive efficiency for an ideal turbojet engine is found by applying Eqs. (2.7.24) and (2.7.26) to the definition in Eq. (2.7.22). This gives

$$\eta_P = \frac{2\mathrm{M}_\infty}{\mathrm{M}_e\sqrt{T_e/T_\infty} + \mathrm{M}_\infty} = \frac{2V_\infty}{V_e + V_\infty} \tag{2.7.28}$$

We see from Eq. (2.7.25) that for a given ambient temperature, only by increasing the compressor outlet temperature can the thermal efficiency of an ideal turbojet engine be increased. From Eq. (2.7.27), we see that increasing turbine inlet temperature will increase specific thrust for a given pressure ratio and operating condition. Thus, high thermal efficiency and specific thrust require high operating temperatures. The maximum temperature in a turbojet engine without afterburning occurs at the turbine inlet. As a result, the performance of turbojet engines is limited by the maximum temperature that can be endured by the materials used in the construction of the turbine blades. This limits the amount of fuel that can be burned in the combustion chamber.

EXAMPLE 2.7.1. From Eqs. (2.7.25) and (2.7.27) it is seen that the pressure ratio across the compressor is an important parameter in determining the performance characteristics of a turbojet engine. However, with everything else held constant, increasing this pressure ratio will increase the turbine inlet temperature. Since maximum turbine temperature is limited by material considerations, we wish to examine the variation in ideal turbojet performance with compressor pressure ratio, under the restriction of fixed turbine inlet temperature. Consider an ideal turbojet operating under standard temperature and pressure at 30,000 feet. Plot the thermal efficiency and specific thrust as a function of compressor pressure ratio for flight Mach numbers ranging from 0.0 to 3.0. Assume that the stagnation temperature at the turbine inlet is limited to 3,000 °R.

Solution. For the specified operating conditions we have

$$T_\infty = 411.9\,^\circ\text{R}, \quad p_\infty = 4.37 \text{ psi}, \quad T_{03} = 3{,}000\,^\circ\text{R},$$
$$C_p = 0.24 \text{ Btu/lbm}\cdot{}^\circ\text{R}, \quad \gamma = 1.4$$

As an example calculation, consider a flight Mach number of 0.5 and a compressor pressure ratio of 10. From Eqs. (2.7.11) through (2.7.20) we obtain

$$T_{01} = T_{0\infty} = T_\infty\left(1+\frac{\gamma-1}{2}\mathrm{M}_\infty^2\right) = 432.5\,^\circ\text{R}$$

$$p_{01} = p_{0\infty} = p_\infty\left(1+\frac{\gamma-1}{2}\mathrm{M}_\infty^2\right)^{\frac{\gamma}{\gamma-1}} = 5.18 \text{ psi}$$

$$T_{02} = T_{01}\left(\frac{p_{02}}{p_{01}}\right)^{\frac{\gamma-1}{\gamma}} = 835.0\,^\circ\text{R}$$

$$p_{02} = p_{01}\frac{p_{02}}{p_{01}} = 51.84 \text{ psi}$$

$$\frac{\dot{Q}_{2-3}}{\dot{m}C_p} = T_{03} - T_{02} = 2{,}165.0\,^\circ\text{R}$$

$$p_{03} = p_{02} = 51.84 \text{ psi}$$

$$T_{0e} = T_{04} = T_{01} + \frac{\dot{Q}_{2-3}}{\dot{m}C_p} = 2{,}597.5\,^\circ\text{R}$$

$$p_{0e} = p_{04} = p_{03}\left(\frac{T_{04}}{T_{03}}\right)^{\frac{\gamma}{\gamma-1}} = 31.31 \text{ psi}$$

$$M_e = \sqrt{\frac{2}{\gamma-1}\left[\left(\frac{p_{0e}}{p_\infty}\right)^{\frac{\gamma-1}{\gamma}} - 1\right]} = 1.94$$

$$T_e = T_{0e}\left(\frac{p_\infty}{p_{0e}}\right)^{\frac{\gamma-1}{\gamma}} = 1{,}479.9\ ^\circ\text{R}$$

From Eq. (2.7.25), the thermal efficiency is

$$\eta_T = 1 - \frac{T_\infty}{T_{02}} = \underline{0.507}$$

The ideal gas constant is

$$R = \frac{\gamma-1}{\gamma}C_p = 0.06857\frac{\text{Btu}}{\text{lbm}\cdot{}^\circ\text{R}} = 1{,}716\frac{\text{ft}\cdot\text{lbf}}{\text{slug}\cdot{}^\circ\text{R}} = 1{,}716\frac{\text{ft}^2}{\text{sec}^2\cdot{}^\circ\text{R}}$$

From Eq. (2.7.26), the specific thrust is

$$\frac{F}{\dot{m}} = \sqrt{\gamma RT_\infty}\left(M_e\sqrt{\frac{T_e}{T_\infty}} - M_\infty\right) = 3{,}166\frac{\text{ft}}{\text{sec}} = 3{,}166\frac{\text{lbf}}{\text{slug/sec}} = \underline{98.4\frac{\text{lbf}}{\text{lbm/sec}}}$$

Similarly, we obtain the results shown in Figs. 2.7.1 and 2.7.2.

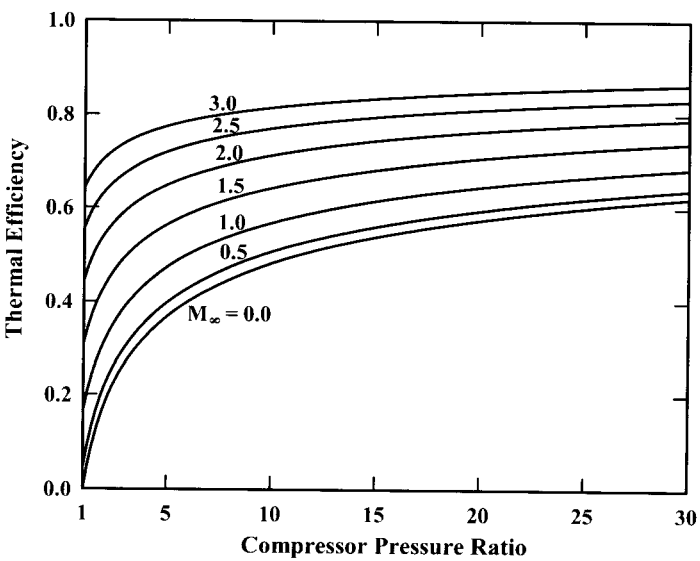


Figure 2.7.1. Thermal efficiency versus compressor pressure ratio for Example 2.7.1.

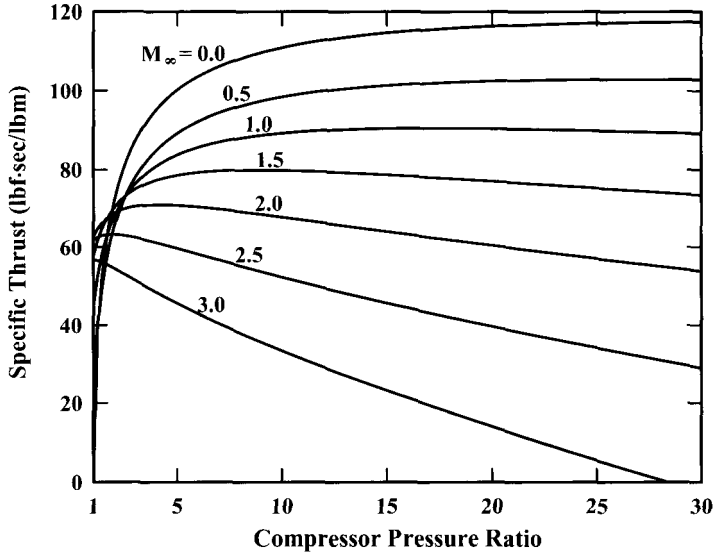


Figure 2.7.2. Specific thrust versus compressor pressure ratio for Example 2.7.1.

From the results of Example 2.7.1 it is seen that when the turbine inlet temperature is held constant, specific thrust exhibits a maximum in its variation with compressor pressure ratio. This is because as the compressor pressure ratio is increased, the burner inlet temperature is also increased. This means that the fuel-air ratio must be decreased to avoid overheating the turbine. If the compressor pressure ratio were large enough, the maximum allowable temperature would be attained at the compressor outlet and any addition of fuel would overheat the turbine. Thus, a turbojet engine with high compressor pressure ratio cannot produce thrust at high Mach numbers without exceeding the maximum allowable temperature in the turbine. Even though thermal efficiency is increased with high compressor pressure ratio, the accompanying decrease in specific thrust at high Mach number makes turbojet engines with high compressor pressure ratio impractical for supersonic flight.

From Eq. (2.7.27) it can be shown with simple calculus that the compressor pressure ratio that produces a maximum in specific thrust for a particular turbine inlet temperature and flight Mach number is given by

$$\left(\frac{p_{02}}{p_{01}}\right)_{\max(F/\dot{m})} = \left[\left(1+\frac{\gamma-1}{2}\mathrm{M}_\infty^2\right)^{-1}\sqrt{\frac{T_{03}}{T_\infty}}\right]^{\frac{\gamma}{\gamma-1}} \tag{2.7.29}$$

This optimum compressor pressure ratio decreases rapidly with increasing Mach number in supersonic flight. For subsonic flight, high compressor pressure ratio is desirable to attain better thermal efficiency and high specific thrust. However, for supersonic flight lower compressor pressure ratios are typically used to obtain higher specific thrust.

2.8. The Turbojet Engine with Afterburner

Burning additional fuel aft of the turbine in a turbojet engine will increase the specific thrust that can be developed without exceeding maximum allowable turbine temperature. The aft combustion chamber shown schematically in Fig. 2.8.1 is called an *afterburner*. The maximum temperature in the afterburner can be higher than that leaving the primary combustion chamber, because the products of combustion from the afterburner do not pass through a turbine.

Thermodynamic cycle analysis for the ideal turbojet engine with an afterburner is identical to that presented in Sec. 2.7, up through the turbine outlet at state 4. Therefore, Eqs. (2.7.11) through (2.7.16) still apply and the stagnation temperature and pressure at the turbine outlet are

$$T_{04} = T_{01} + \frac{\dot{Q}_{2-3}}{\dot{m} C_p} \tag{2.8.1}$$

$$p_{04} = p_{03}\left(\frac{T_{04}}{T_{03}}\right)^{\frac{\gamma}{\gamma-1}} \tag{2.8.2}$$

If we continue to assume an ideal or thermodynamically reversible engine, the stagnation pressure remains constant aft of the turbine and the stagnation temperature is determined from the first law. Thus, the stagnation conditions aft of the turbine are

$$T_{0e} = T_{05} = T_{04} + \frac{\dot{Q}_{4-5}}{\dot{m} C_p} \tag{2.8.3}$$

$$p_{0e} = p_{05} = p_{04} \tag{2.8.4}$$

Since the afterburner does not affect either the static or stagnation pressure at the exit of an ideal turbojet engine, the exit Mach number is not changed as a result of afterburning.

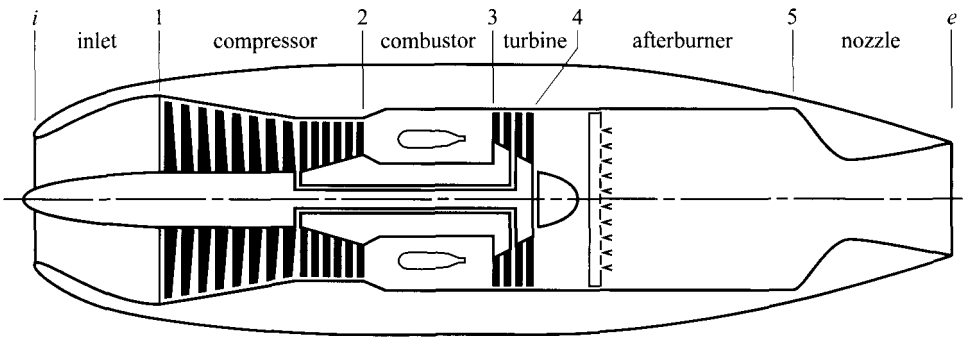


Figure 2.8.1. Components and station labeling for the turbojet engine with afterburner.

The exit velocity and thrust are increased by the afterburner only as a result of the increase in exit temperature and the accompanying increase in the speed of sound. Thus, Eqs. (2.7.19) and (2.7.20) still apply to the ideal turbojet engine with afterburner, provided that the increased stagnation temperature at the exit, which is computed from Eq. (2.8.3), is used in Eq. (2.7.20).

When the increased exit temperature is used, the kinetic energy increase can sill be computed from Eq. (2.7.24), and the thermal efficiency for an ideal turbojet engine with afterburner is

$$\eta_T \equiv \frac{\dot{m}(V_e^2 - V_\infty^2)/2}{\dot{Q}_{2\text{-}3} + \dot{Q}_{4\text{-}5}} = \frac{\dot{m}\gamma RT_\infty[\mathrm{M}_e^2(T_e/T_\infty) - \mathrm{M}_\infty^2]/2}{\dot{Q}_{2\text{-}3} + \dot{Q}_{4\text{-}5}}$$

From Eqs. (2.8.1) and (2.8.3) the total energy input can be expressed in terms of the stagnation temperature difference between states 1 and 5,

$$\dot{Q}_{2\text{-}3} + \dot{Q}_{4\text{-}5} = \dot{m}C_p(T_{05} - T_{01})$$

and the thermal efficiency is written

$$\eta_T = \frac{\gamma RT_\infty[\mathrm{M}_e^2(T_e/T_\infty) - \mathrm{M}_\infty^2]/2}{C_p(T_{05} - T_{01})} = \frac{\gamma - 1}{2}\left[\mathrm{M}_e^2\frac{T_e}{T_\infty} - \mathrm{M}_\infty^2\right]\frac{T_\infty}{T_{05} - T_{01}} \tag{2.8.5}$$

Similarly, the uninstalled thrust for an ideal turbojet engine with afterburner can still be computed from Eq. (2.7.26). Thus, specific thrust is readily computed from the known exit temperature and Mach number,

$$\frac{F}{\dot{m}} = \sqrt{\gamma RT_\infty}\left(\mathrm{M}_e\sqrt{\frac{T_e}{T_\infty}} - \mathrm{M}_\infty\right) \tag{2.8.6}$$

EXAMPLE 2.8.1. To examine the effects of an afterburner on the performance of an ideal turbojet engine, repeat Example 2.7.1 for the same operating conditions but with afterburner included. Assume that the maximum stagnation temperature aft of the turbine is limited to 4,000 °R.

Solution. For the specified operating conditions we have

$$T_\infty = 411.9\,^\circ\mathrm{R}, \quad p_\infty = 4.37 \text{ psi}, \quad T_{03} = 3{,}000\,^\circ\mathrm{R}, \quad T_{05} = 4{,}000\,^\circ\mathrm{R},$$
$$C_p = 0.24 \text{ Btu/lbm}\cdot{}^\circ\mathrm{R}, \quad \gamma = 1.4$$

As an example calculation, again we consider a flight Mach number of 0.5 and a compressor pressure ratio of 10. Following Example 2.7.1, from Eqs. (2.7.11) through (2.7.16) we obtain

$$T_{01} = 432.5\,^{\circ}\text{R} \quad \text{and} \quad p_{01} = 5.18\,\text{psi}$$

$$T_{02} = 835.0\,^{\circ}\text{R} \quad \text{and} \quad p_{03} = p_{02} = 51.84\,\text{psi}$$

$$\frac{\dot{Q}_{2-3}}{\dot{m}C_p} = T_{03} - T_{02} = 2{,}165.0\,^{\circ}\text{R}$$

From Eqs. (2.8.1) through (2.8.4) we obtain

$$T_{04} = T_{01} + \frac{\dot{Q}_{2-3}}{\dot{m}C_p} = 2{,}597.5\,^{\circ}\text{R}$$

$$p_{0e} = p_{05} = p_{04} = p_{03}\left(\frac{T_{04}}{T_{03}}\right)^{\frac{\gamma}{\gamma-1}} = 31.31\,\text{psi}$$

$$\frac{\dot{Q}_{4-5}}{\dot{m}C_p} = T_{05} - T_{04} = 1{,}402.5\,^{\circ}\text{R}$$

$$T_{0e} = T_{05} = 4{,}000\,^{\circ}\text{R}$$

From Eqs. (2.7.19) and (2.7.20) we obtain

$$\text{M}_e = \sqrt{\frac{2}{\gamma-1}\left[\left(\frac{p_{0e}}{p_\infty}\right)^{\frac{\gamma-1}{\gamma}} - 1\right]} = 1.94$$

$$T_e = T_{0e}\left(\frac{p_\infty}{p_{0e}}\right)^{\frac{\gamma-1}{\gamma}} = 2{,}278.9\,^{\circ}\text{R}$$

From Eq. (2.8.5), the thermal efficiency is

$$\eta_T = \frac{\gamma-1}{2}\left[\text{M}_e^2\frac{T_e}{T_\infty} - \text{M}_\infty^2\right]\frac{T_\infty}{T_{05} - T_{01}} = \underline{0.477}$$

and from Eq. (2.8.6), the specific thrust is

$$\frac{F}{\dot{m}} = \sqrt{\gamma R T_\infty}\left(\text{M}_e\sqrt{\frac{T_e}{T_\infty}} - \text{M}_\infty\right) = 4{,}049\frac{\text{lbf}}{\text{slug/sec}} = \underline{125.8\,\frac{\text{lbf}}{\text{lbm/sec}}}$$

Repeating similar computations for different values of compressor pressure ratio and different values of flight Mach number, we obtain the results that are shown in Figs. 2.8.2 and 2.8.3.

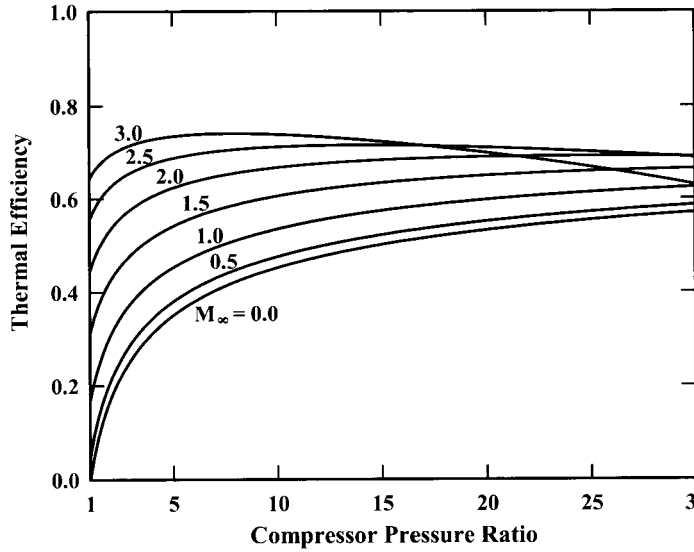


Figure 2.8.2. Thermal efficiency versus compressor pressure ratio for Example 2.8.1.

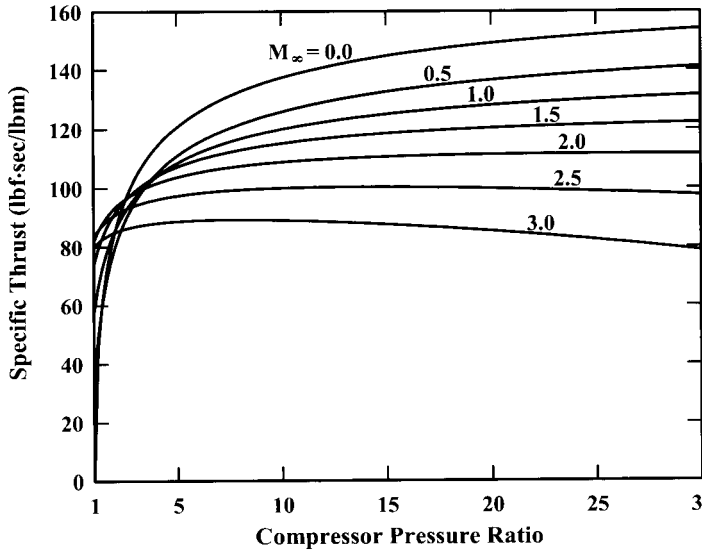


Figure 2.8.3. Specific thrust versus compressor pressure ratio for Example 2.8.1.

By comparing the results presented in Example 2.8.1 with those that were presented in Example 2.7.1, we see that afterburning increases specific thrust but reduces thermal efficiency. It can also be seen that afterburning increases the value of compressor pressure ratio that results in maximum specific thrust.

It can be shown that the compressor pressure ratio that produces maximum specific thrust for an ideal turbojet engine with afterburning depends only on the flight Mach number, ambient temperature, and stagnation temperature at the turbine inlet. The result is given by

$$\left(\frac{p_{02}}{p_{01}}\right)_{\max(F/\dot{m})} = \left\{\frac{1}{2}\left[\left(1+\frac{\gamma-1}{2}M_\infty^2\right)^{-1}\frac{T_{03}}{T_\infty}+1\right]\right\}^{\frac{\gamma}{\gamma-1}} \tag{2.8.7}$$

This optimum compressor pressure ratio is significantly higher than the optimum value without afterburning.

2.9. Turbofan Engines

The thrust developed by any propulsion system can be increased either by increasing the mass flow rate passing through the propulsion system or by increasing the velocity increment imparted to this flow. A large mass flow rate with a small velocity increment provides the best propulsive efficiency, while a larger velocity increment with a smaller mass flow rate will generally result in a higher thrust-to-weight ratio. Because of their large diameter, engine-propeller systems produce relatively high flow rates with small velocity increments and have correspondingly high propulsive efficiency. The turbojet engine, on the other hand, produces a fairly large velocity increment with a relatively low mass flow rate, providing high specific thrust. A turbofan engine is a compromise between the propeller and the turbojet. It has a diameter and flow rate that are typically less than those for an equivalent engine-propeller combination but greater than those for a turbojet of similar power. Turbofan engines are commonly used on subsonic transport aircraft, which require high efficiency for longer range. Turbojet engines are more commonly used on fighters, where thrust-to-weight ratio is typically more important than propulsive efficiency and higher speed is desired.

As shown schematically in Fig. 2.9.1, the turbofan engine has a larger turbine than a turbojet engine of similar power. As the products of combustion pass through this larger turbine more energy is extracted and the exhaust gas velocity is reduced. The extra power produced by the turbine is used to turn a ducted fan, which adds mass to the slipstream. Increasing the total mass flow rate while decreasing the velocity increment decreases specific thrust and increases propulsive efficiency. However, a larger turbine, fan, and second nozzle add weight to the engine. It can be shown that the ideal turbofan engine has the same thermal efficiency as the ideal turbojet engine. Thus, the turbofan engine has improved overall efficiency at the cost of reduced thrust-to-weight ratio.

The airflow through a turbofan engine is typically characterized in terms of a design parameter called the *bypass ratio*. This is the ratio of the mass flow rate bypassing the core, $\dot{m}_b$, to the mass flow rate passing through the core, $\dot{m}_c$,

$$\text{bypass ratio} \equiv R_b \equiv \frac{\dot{m}_b}{\dot{m}_c} \tag{2.9.1}$$

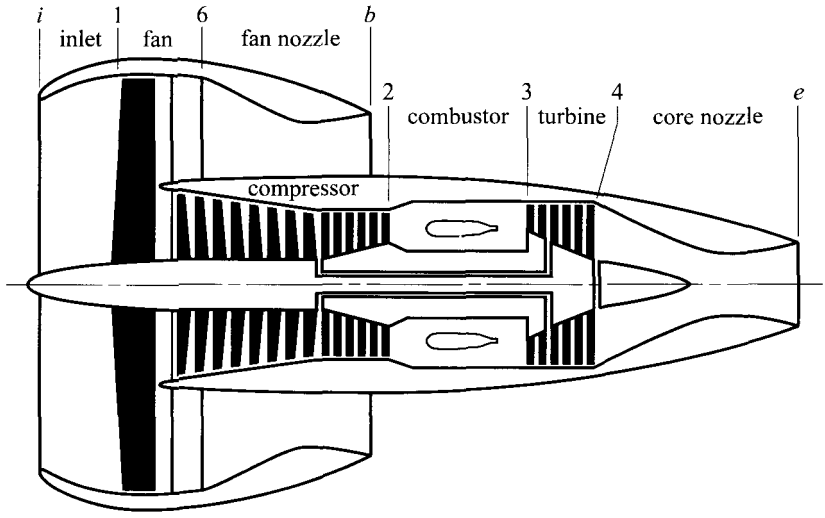


Figure 2.9.1. Components and station labeling for the turbofan engine.

Bypass ratio is sometimes given the symbol α. However, in this text, the symbol R_b is used to avoid confusion with angle of attack.

For thermodynamic cycle analysis of the ideal turbofan engine, we assume isentropic flow through the fan and fan nozzle as well as through the compressor, turbine, and core nozzle. As was the case with the ideal turbojet analysis, we assume complete expansion back to ambient pressure for both the core nozzle and the fan nozzle.

For the flow through the core, Eqs. (2.7.11) through (2.7.16) apply to the turbofan engine as well as to the turbojet. Like the compressor, the fan design is characterized by the stagnation pressure ratio. The stagnation conditions in the fan nozzle can easily be determined from this design parameter and the assumption of isentropic flow,

$$T_{0b} = T_{06} = T_{01}\left(\frac{p_{06}}{p_{01}}\right)^{\frac{\gamma-1}{\gamma}} \tag{2.9.2}$$

$$p_{0b} = p_{06} = p_{01}\frac{p_{06}}{p_{01}} \tag{2.9.3}$$

The stagnation temperature at the turbine outlet is obtained for the first law of thermodynamics applied to both the core flow and the fan flow,

$$\dot{m}_c C_p (T_{04} - T_{01}) + \dot{m}_b C_p (T_{06} - T_{01}) = \dot{Q}_{2\text{-}3}$$

Combining this relation with the assumption of isentropic flow in the core nozzle, the stagnation conditions in this nozzle are

$$T_{0e} = T_{04} = T_{01} - R_b(T_{06} - T_{01}) + \frac{\dot{Q}_{2-3}}{\dot{m}_c C_p} \tag{2.9.4}$$

$$p_{0e} = p_{04} = p_{03}\left(\frac{T_{04}}{T_{03}}\right)^{\frac{\gamma}{\gamma-1}} \tag{2.9.5}$$

The Mach number and temperature at the core and fan nozzle exits are obtained from the assumption of isentropic flow with complete expansion. From the known stagnation conditions, this gives

$$\mathrm{M}_e^2 = \frac{2}{\gamma-1}\left[\left(\frac{p_{0e}}{p_\infty}\right)^{\frac{\gamma-1}{\gamma}} - 1\right] \tag{2.9.6}$$

$$T_e = T_{0e}\left(\frac{p_\infty}{p_{0e}}\right)^{\frac{\gamma-1}{\gamma}} \tag{2.9.7}$$

$$\mathrm{M}_b^2 = \frac{2}{\gamma-1}\left[\left(\frac{p_{0b}}{p_\infty}\right)^{\frac{\gamma-1}{\gamma}} - 1\right] \tag{2.9.8}$$

$$T_b = T_{0b}\left(\frac{p_\infty}{p_{0b}}\right)^{\frac{\gamma-1}{\gamma}} \tag{2.9.9}$$

The total rate of increase in kinetic energy is the sum of that for the core stream and that for the bypass stream,

$$\frac{\dot{m}_c(V_e^2 - V_\infty^2) + \dot{m}_b(V_b^2 - V_\infty^2)}{2} = \frac{\dot{m}_c}{2}\gamma R T_\infty\left[\mathrm{M}_e^2\frac{T_e}{T_\infty} - \mathrm{M}_\infty^2 + R_b\left(\mathrm{M}_b^2\frac{T_b}{T_\infty} - \mathrm{M}_\infty^2\right)\right] \tag{2.9.10}$$

The only energy input for this engine is in the combustion chamber of the core. Thus, after applying Eq. (2.9.4) and recalling that $R = C_p(\gamma-1)/\gamma$, the thermal efficiency for the ideal turbofan engine is

$$\eta_T \equiv \frac{\dot{m}_c(V_e^2 - V_\infty^2) + \dot{m}_b(V_b^2 - V_\infty^2)}{2\dot{Q}_{2-3}} = \frac{(\gamma-1)[\mathrm{M}_e^2 T_e + R_b \mathrm{M}_b^2 T_b - (1+R_b)\mathrm{M}_\infty^2 T_\infty]}{2[T_{04} + R_b T_{06} - (1+R_b)T_{01}]}$$

Applying Eqs. (2.7.11) through (2.7.16) and Eqs. (2.9.2) through (2.9.9), this result can be expressed as

$$\eta_T = 1-\left(1+\frac{\gamma-1}{2}\mathrm{M}_\infty^2\right)^{-1}\left(\frac{p_{01}}{p_{02}}\right)^{\frac{\gamma-1}{\gamma}} \tag{2.9.11}$$

which is exactly the same result as that obtained in Sec. 2.7 for the turbojet engine. Notice from Eq. (2.9.11) that the thermal efficiency of an ideal turbofan engine does not depend on either the bypass ratio or the pressure ratio across the fan. At first the reader may find this surprising, since the net rate of increase in kinetic energy for the turbofan engine depends on the output of the fan. This result is easily justified from simple thermodynamics. The turbine of a turbofan engine extracts power from the core stream and transfers it to the bypass stream by driving the fan. Since the engine is assumed to be thermodynamically reversible, this power transfer takes place without loss and the net power output defined in terms of kinetic energy is unchanged.

Since the ideal turbofan engine has complete expansion in both the core and fan nozzles, the uninstalled thrust for this engine is

$$\begin{aligned} F &= \dot{m}_c(V_e - V_\infty) + \dot{m}_b(V_b - V_\infty) \\ &= \dot{m}_c\sqrt{\gamma RT_\infty}\left[\mathrm{M}_e\sqrt{\frac{T_e}{T_\infty}} - \mathrm{M}_\infty + R_b\left(\mathrm{M}_b\sqrt{\frac{T_b}{T_\infty}} - \mathrm{M}_\infty\right)\right] \end{aligned} \tag{2.9.12}$$

and the specific thrust is

$$\frac{F}{\dot{m}_c + \dot{m}_b} = \frac{\sqrt{\gamma RT_\infty}}{1+R_b}\left[\mathrm{M}_e\sqrt{\frac{T_e}{T_\infty}} - \mathrm{M}_\infty + R_b\left(\mathrm{M}_b\sqrt{\frac{T_b}{T_\infty}} - \mathrm{M}_\infty\right)\right] \tag{2.9.13}$$

From Eqs. (2.9.10) and (2.9.12), the propulsive efficiency for an ideal turbofan engine is

$$\eta_P \equiv \frac{2FV_\infty}{\dot{m}_c(V_e^2 - V_\infty^2) + \dot{m}_b(V_b^2 - V_\infty^2)} = \frac{2V_\infty[V_e - V_\infty + R_b(V_b - V_\infty)]}{V_e^2 - V_\infty^2 + R_b(V_b^2 - V_\infty^2)} \tag{2.9.14}$$

Since turbine inlet temperature is limited by material considerations, the available energy per unit mass in the core flow is limited as well. This places an upper limit on the fan pressure ratio that can be used with a particular bypass ratio. This upper limit is reached when expansion in the turbine is sufficient to reduce the Mach number at the core nozzle exit to zero. Once this condition has been reached, no additional power could possibly be extracted from the core flow by using a larger turbine to drive a larger fan. From Eq. (2.9.6), it can be seen that this limiting condition requires that

$$p_{0e} = p_\infty$$

Using this limit with Eqs. (2.7.11) through (2.7.16) and (2.9.2) through (2.9.5), it is readily shown that the upper limit for the fan pressure ratio is given by

$$\left(\frac{p_{06}}{p_{01}}\right)_{\max} = \left[\frac{1+R_b-\left(p_{02}/p_{01}\right)^{\frac{\gamma-1}{\gamma}}}{R_b}+\frac{\frac{T_{03}}{T_\infty}\left[1+\frac{\gamma-1}{2}\mathrm{M}_\infty^2-\left(p_{01}/p_{02}\right)^{\frac{\gamma-1}{\gamma}}\right]}{R_b\left(1+\frac{\gamma-1}{2}\mathrm{M}_\infty^2\right)^2}\right]^{\frac{\gamma}{\gamma-1}} \tag{2.9.15}$$

The turbofan engine has three important design parameters that can be varied to help meet the requirements of any particular application. These are the compressor pressure ratio, the fan pressure ratio, and the bypass ratio. The turbojet engine can be considered to be a special case of the turbofan engine, which has a bypass ratio of zero. While the thermal efficiency of the ideal turbofan engine depends only on compressor pressure ratio and flight Mach number, the bypass ratio and fan pressure ratio will significantly affect the propulsive efficiency and thus the overall efficiency of the engine. The manner in which the propulsive efficiency of an ideal turbofan engine varies with bypass ratio and fan pressure ratio is not at all obvious from inspection of Eq. (2.9.14). This is examined in the following example.

EXAMPLE 2.9.1. To explore how turbofan performance varies with bypass ratio and fan pressure ratio, consider an ideal turbofan engine operating under standard temperature and pressure at 30,000 feet. To isolate the effects of the chosen design parameters, assume a fixed flight Mach number of 0.8, a fixed compressor pressure ratio of 20, and a stagnation temperature at the turbine inlet of 3,000 °R. For these conditions, plot overall efficiency and specific thrust as a function of fan pressure ratio for several bypass ratios ranging from 0 to 12.

Solution. From the specified operating conditions and fixed design parameters, the following values are to be held constant:

$$T_\infty = 411.8\,^\circ\mathrm{R}, \quad p_\infty = 4.37 \text{ psi}, \quad \mathrm{M}_\infty = 0.8, \quad p_{02}/p_{01} = 20,$$
$$T_{03} = 3{,}000\,^\circ\mathrm{R}, \quad C_p = 0.24 \text{ Btu/lbm}\cdot{}^\circ\mathrm{R}, \quad \gamma = 1.4$$

As an example calculation, consider a bypass ratio of 4.0 and a fan pressure ratio of 3.0. From Eqs. (2.7.11) through (2.7.16) we obtain

$$T_{01} = T_{0\infty} = T_\infty\left(1+\frac{\gamma-1}{2}\mathrm{M}_\infty^2\right) = 464.5\,^\circ\mathrm{R}$$

$$p_{01} = p_{0\infty} = p_\infty\left(1+\frac{\gamma-1}{2}\mathrm{M}_\infty^2\right)^{\frac{\gamma}{\gamma-1}} = 6.66 \text{ psi}$$

$$T_{02} = T_{01}\left(\frac{p_{02}}{p_{01}}\right)^{\frac{\gamma-1}{\gamma}} = 1{,}093.2\,^\circ\mathrm{R}$$

$$p_{02} = p_{01}\frac{p_{02}}{p_{01}} = 133.23\ \text{psi}$$

$$\frac{\dot{Q}_{2-3}}{\dot{m}_c C_p} = T_{03} - T_{02} = 1{,}906.8\ ^\circ\text{R}$$

$$p_{03} = p_{02} = 133.23\ \text{psi}$$

and Eqs. (2.9.2) through (2.9.9) result in

$$T_{0b} = T_{06} = T_{01}\left(\frac{p_{06}}{p_{01}}\right)^{\frac{\gamma-1}{\gamma}} = 635.8\ ^\circ\text{R}$$

$$p_{0b} = p_{06} = p_{01}\frac{p_{06}}{p_{01}} = 19.98\ \text{psi}$$

$$T_{0e} = T_{04} = T_{01} - R_b(T_{06} - T_{01}) + \frac{\dot{Q}_{2-3}}{\dot{m}_c C_p} = 1{,}686.1\ ^\circ\text{R}$$

$$p_{0e} = p_{04} = p_{03}\left(\frac{T_{04}}{T_{03}}\right)^{\frac{\gamma}{\gamma-1}} = 17.73\ \text{psi}$$

$$\text{M}_e = \sqrt{\frac{2}{\gamma-1}\left[\left(\frac{p_{0e}}{p_\infty}\right)^{\frac{\gamma-1}{\gamma}} - 1\right]} = 1.57$$

$$T_e = T_{0e}\left(\frac{p_\infty}{p_{0e}}\right)^{\frac{\gamma-1}{\gamma}} = 1{,}130.0\ ^\circ\text{R}$$

$$\text{M}_b = \sqrt{\frac{2}{\gamma-1}\left[\left(\frac{p_{0b}}{p_\infty}\right)^{\frac{\gamma-1}{\gamma}} - 1\right]} = 1.65$$

$$T_b = T_{0b}\left(\frac{p_\infty}{p_{0b}}\right)^{\frac{\gamma-1}{\gamma}} = 411.8\ ^\circ\text{R}$$

From Eq. (2.9.11), the thermal efficiency is

$$\eta_T = 1 - \left(1 + \frac{\gamma-1}{2}\text{M}_\infty^2\right)^{-1}\left(\frac{p_{01}}{p_{02}}\right)^{\frac{\gamma-1}{\gamma}} = 0.623$$

From Eq. (2.9.13), the specific thrust is

$$\frac{F}{\dot{m}_c + \dot{m}_b} = \frac{\sqrt{\gamma RT_\infty}}{1+R_b}\left[M_e\sqrt{\frac{T_e}{T_\infty}} - M_\infty + R_b\left(M_b\sqrt{\frac{T_b}{T_\infty}} - M_\infty \right)\right] = \underline{32.1\ \frac{\text{lbf}}{\text{lbm/sec}}}$$

From Eq. (2.9.14), the propulsive efficiency is

$$\eta_P = \frac{2V_\infty[V_e - V_\infty + R_b(V_b - V_\infty)]}{V_e^2 - V_\infty^2 + R_b(V_b^2 - V_\infty^2)} = 0.576$$

and the overall efficiency is

$$\eta_O = \eta_T\eta_P = \underline{0.359}$$

Similarly, we obtain the results shown in Figs. 2.9.2 and 2.9.3. The termination of each curve with a bypass ratio greater than 3 corresponds to the maximum possible fan pressure ratio computed from Eq. (2.9.15).

Notice from Fig. 2.9.2 that for each value of bypass ratio, there is an optimum fan pressure ratio that results in the highest overall efficiency. Also notice that the overall efficiency of an engine having the optimum fan pressure ratio is improved as the bypass ratio is increased. For a bypass ratio of 12 the optimum fan pressure ratio is about 1.88, which provides an overall efficiency that is more than 220 percent of that for an ideal

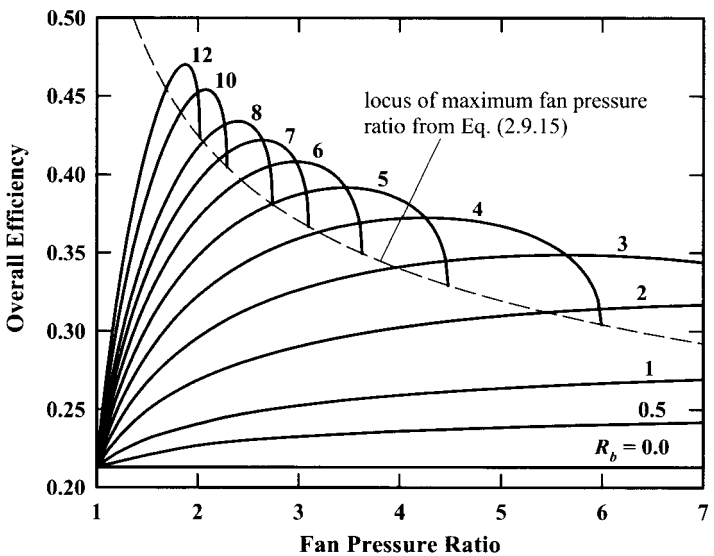


Figure 2.9.2. Overall efficiency versus fan pressure ratio for Example 2.9.1.

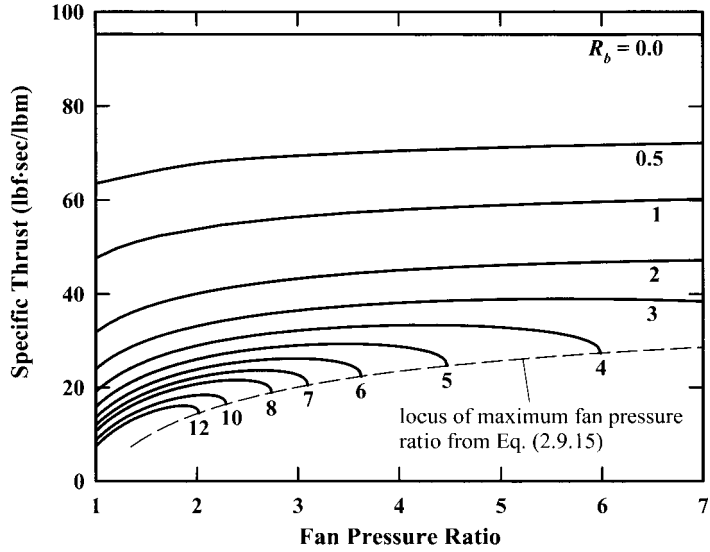


Figure 2.9.3. Specific thrust versus fan pressure ratio for Example 2.9.1.

turbojet engine with the same compressor pressure ratio. The results shown in Fig. 2.9.2 apply only for the ambient conditions, flight Mach number, compressor pressure ratio, and turbine inlet temperature specified in Example 2.9.1. However, the trends shown in this figure apply in general.

From Fig. 2.9.3 it can also be seen that for each value of bypass ratio, there is an optimum fan pressure ratio that will result in the greatest specific thrust. However, the maximum specific thrust that can be attained decreases as the bypass ratio is increased. The maximum specific thrust for the ideal turbofan engine with a bypass ratio of 12 is only about 17 percent of that produced by the ideal turbojet engine with the same compressor pressure ratio.

As it turns out, the fan pressure ratio that produces maximum specific thrust for a fixed bypass ratio is exactly the same as that which gives maximum overall efficiency. This optimum fan pressure ratio can be found by taking the partial derivative of either propulsive efficiency or specific thrust with respect to fan pressure ratio. It can be shown that this optimum fan pressure ratio is given by

$$\left(\frac{p_{06}}{p_{01}}\right)_{\text{opt}} = \left[1 - \frac{\left(p_{02}/p_{01}\right)^{\frac{\gamma-1}{\gamma}}}{1+R_b} + \frac{1+\frac{\gamma-1}{2}\mathrm{M}_\infty^2 + \frac{T_{03}}{T_\infty}\left[1+\frac{\gamma-1}{2}\mathrm{M}_\infty^2 - \left(p_{01}/p_{02}\right)^{\frac{\gamma-1}{\gamma}}\right]}{(1+R_b)\left(1+\frac{\gamma-1}{2}\mathrm{M}_\infty^2\right)^2}\right]^{\frac{\gamma}{\gamma-1}} \tag{2.9.16}$$

where R_b, M_∞, p_{02}/p_{01}, and T_{03}/T_∞ are all assumed to be fixed.

Choosing the fan pressure ratio according to Eq. (2.9.16) will provide the greatest specific thrust and overall efficiency for a fixed set of the remaining design and operating parameters. However, the best choice for bypass ratio and compressor pressure ratio depends substantially on the specific application. The design requirements that usually have the greatest effect on these two choices are the flight Mach number and desired range. If an airplane is to be designed for very long range, the engine weight will be small compared to the weight of fuel that must be carried. For such designs, overall efficiency is more important than engine weight. Thus, turbofan engines with high bypass ratios and high compressor pressure ratios are typically the optimal solution for long-range subsonic transports. On the other hand, airplanes designed for high supersonic airspeeds and short range are better fitted with turbojets or turbofans having a low bypass ratio. High supersonic Mach numbers also usually dictate lower compressor pressure ratios, because of the reduction in specific thrust with increasing compressor pressure ratios that is shown in Fig. 2.7.2.

2.10. Concluding Remarks

The study of flight mechanics requires some knowledge of propulsion and this textbook was not written under the assumption that the reader has previously completed an engineering course on propulsion. The very brief introduction to the topic of aircraft propulsion that was presented in this chapter should provide the reader with sufficient background to understand the material in the remainder of this text. However, in this chapter we have only touched on some of the concepts that are important in the design and selection of aircraft propulsion systems. For those students who intend to specialize in flight mechanics, the author would strongly suggest at least one or two engineering courses in the area of propulsion.

In this chapter, more emphasis was placed on propeller-based aircraft propulsion systems than on turbojet and turbofan systems. This may seem inappropriate in view of the fact that turbojet and turbofan propulsion systems are more commonly used on commercial and military aircraft. However, some flight testing is usually very helpful in gaining an understanding of the fundamental principles of flight mechanics. With funding for education being what it is today, it is not likely that many students will have access to turbo-powered aircraft. For this reason, the author has chosen to emphasize propellers and propeller-driven aircraft in the hope that students will experimentally investigate some of the flight mechanics concepts, which are presented in the following chapters. Knowledge gained from flight tests conducted in small general aviation airplanes is easily extended to the larger turbo-powered aircraft. This same philosophy has been applied in the remainder of this textbook.

Flight testing with small propeller-driven airplanes is more affordable than one may think. Many universities have facilities available for such flight testing. Even if your university does not, you will probably be able to locate a general aviation flight school that will be willing to provide this experience for a fee. A small general aviation airplane, with instructor included, can usually be rented at a reasonable hourly rate. Depending on the size of the airplane, two or three students could share the cost and a great deal can be learned from a well-planned flight of 20 to 30 minutes.

2.11. Problems

2.1. Write a computer program to predict the performance of a propeller using Goldstein's vortex theory as presented in Sec. 2.3. Use the secant method to solve Eq. (2.3.32) and apply an appropriate numerical integration method to integrate Eqs. (2.3.33) and (2.3.34). To define the propeller geometry and section aerodynamic coefficients, the program should use a functional relationship that can be easily changed.

2.2. Run the program written for problem 2.1 for the propeller geometry used in Example 2.3.1. Regenerate all of the figures that are presented for this example and compare your results with those presented in the text.

2.3. Run the program written for problem 2.1 for a propeller geometry that has a rectangular planform shape. The geometry is identical to that in Example 2.3.1, except that the blade has a constant chord with the same planform area as the elliptic blade used in the example ($c_b/d_p = 0.0573$). Generate all of the figures that are presented in Example 2.3.1 and compare your results with those obtained for the elliptic blade.

2.4. Modify the computer program written for problem 2.1 so that it also computes the change in normal force coefficient with propeller angle of attack and the change in yawing moment coefficient with respect to propeller angle of attack.

2.5. Run the program written for problem 2.4 for the propeller geometry used in Example 2.3.1. Regenerate the figures that are presented for Example 2.5.1 and compare your results with those presented in the text.

2.6. Run the program written for problem 2.4 for a propeller geometry that has a rectangular planform shape. The geometry is identical to that in Example 2.3.1 except that the blade has a constant chord with the same planform area as the elliptic blade used in the example ($c_b/d_p = 0.0573$). Generate the figures that are presented in Example 2.5.1 and compare your results with those obtained for the elliptic blade.

2.7. Modify the computer program written for problem 2.1 so that it will compute the rotational speed and thrust developed by the propeller as a function of propeller diameter, pitch, input brake power, and forward airspeed. To test your program, duplicate the results for the 72-inch propeller that are plotted in Fig. 2.3.14.

2.8. Use the computer program written for problem 2.7 to predict the performance for one of the three-blade propellers described in Example 2.3.2. Consider a 72-inch-diameter propeller with a 48-inch chord-line pitch, operating at standard sea level. Assuming constant brake power input of 180 horsepower, plot the rotational speed in rpm and the thrust developed by the propeller in lbf as a function of airspeed from zero to 150 mph.

2.9. Consider the propeller used in problem 2.8, operating at standard sea level. Assuming a constant rotational speed of 2,900 rpm, plot the brake power input in horsepower and the thrust developed by the propeller in lbf as a function of airspeed from zero to 200 mph.

2.10. An experimental radio-controlled airplane is to be powered by a DC electric motor turning a fixed-pitch two-blade propeller, which has the same blade geometry as that described in Example 2.3.1. The propeller is to be attached directly to the output shaft of the motor. The current that is drawn by the DC motor, I_m, is given by

$$I_m = \frac{E_m - \omega/K_v}{R_m}$$

where E_m is the voltage applied to the motor, ω is the angular velocity, K_v is a motor voltage constant, and R_m is the motor armature resistance. The brake power developed by the motor can be expressed as

$$P_m = (I_m - I_o)(E_m - I_m R_m)$$

where I_o is a motor constant normally referred to as the *no-load current*. Modify the computer program written for problem 2.1 so that it will compute the rotational speed, motor current, and thrust developed by the propeller as a function of motor voltage, propeller diameter, pitch, and forward airspeed. Assume that the motor constants, K_v, R_m, and I_o, are all known.

2.11. Use the computer program written for problem 2.10 to predict the performance for one of the motor-propeller combinations that were described in that problem. Consider a 22-inch-diameter propeller with a 19-inch chord-line pitch, operating at standard sea level with constant motor voltage of 54 volts. Use the motor constants, $K_v = 9.7$ rad/sec/volt, $R_m = 0.11$ ohm, and $I_o = 3.0$ amps, and plot the motor current in amps, rotational speed in rpm, brake horsepower, and propeller thrust in lbf, as a function of airspeed from zero to 75 mph.

2.12. The motor-propeller combination in problem 2.11 is fitted with a control system that adjusts the motor voltage to maintain a constant motor current of 30 amps. For this configuration, plot the motor voltage, rotational speed, brake horsepower, and propeller thrust, as a function of airspeed from zero to 75 mph.

2.13. Since the mechanism of a variable-pitch propeller rotates the entire blade as shown in Fig. 2.3.11, rotation of this mechanism applies an incremental pitch angle variation, $\Delta\beta$, that does not vary along the length of the blade. Thus, the incremental change in pitch length, $\Delta\lambda$, does vary with the radial coordinate according to Eq. (2.2.2). Modify the computer program written for problem 2.1 so that it can be used to predict the performance of a variable-pitch propeller.

As a test case, use a two-blade propeller with the same blade geometry and section properties that were used for the fixed-pitch propeller in Example 2.3.1 with a chord-line pitch-to-diameter ratio of 1.0. The local section chord-line pitch length for this variable-pitch propeller will be independent of ζ for only one particular setting of the variable-pitch mechanism. Thus, as an input to the program, the pitch setting is to be identified in terms of a nominal pitch length, which is defined to be equal to the local section chord-line pitch length evaluated at the 75 percent radius. With this program, generate figures similar to those that were presented in Example 2.3.1. In all figures, chord-line pitch-to-diameter ratio, K_c, should be replaced with nominal pitch-to-diameter ratio, K_n. Compare your results with those presented in Example 2.3.1. The results should be identical only when the nominal pitch-to-diameter ratio for the variable-pitch propeller is 1.0.

2.14. Modify the computer program that was written for problem 2.13 so that it will predict the performance of a 72-inch, three-blade, constant-speed propeller with the same blade geometry as that described in problem 2.13. The propeller is operating at standard sea level and the control system maintains the fuel flow and propeller pitch such that the rotational speed and brake power are held constant at 2,900 rpm and 180 hp, respectively. Plot the nominal chord-line pitch in inches, the thrust developed by the propeller in lbf, and the propulsive efficiency, as a function of airspeed from zero to 150 mph.

2.15. Use propeller momentum theory to predict the performance of the 72-inch constant-speed propeller in problem 2.14. Including the effect of slipstream rotation, plot the thrust developed by the propeller and the propulsive efficiency as a function of airspeed from zero to 150 mph. Compare the results with those predicted from propeller blade theory in problem 2.14.

2.16. Modify the computer program that was written for problem 2.1 to include the effects of section Mach number on the section lift and drag coefficients. For the section lift use Eq. (1.11.5) for $M_\infty \le 0.8$ and Eq. (1.12.18) for $M_\infty \ge 1.2$. As a rough approximation for the transonic region, use a simple linear interpolation between $M_\infty = 0.8$ and $M_\infty = 1.2$. To account for subsonic drag divergence, use the approximation

$$\frac{\tilde{C}_D}{\tilde{C}_{DM0}} = \begin{cases} 1.0, & M_\infty \le 0.80 \\ 1.0 + 160{,}000(M_\infty - 0.8)^4/27, & 0.80 \le M_\infty \le 0.95 \\ 6.0 - 800(1.0 - M_\infty)^2, & 0.95 \le M_\infty \le 1.00 \end{cases}$$

For $M_\infty \ge 1.2$, use Eq. (1.12.20) with the section geometry that was described in problem 1.45 and use simple linear interpolation between $M_\infty = 1.0$ and $M_\infty = 1.2$. Use the modified program to rework Examples 2.3.3 and 2.3.4, including this approximation for the effects of compressibility.

2.17. A large turbofan engine has an inlet area of 65 ft^2 and is operating with an inlet Mach number of 0.50. Determine the additive drag for static operation at sea level and for a flight Mach number of 0.80 at 40,000 ft. Assume standard atmospheric conditions and the same inlet Mach number for both of these operating points.

2.18. For the turbofan engine described in problem 2.17, determine the inlet mass flow rate for both of the stated operating conditions.

2.19. Determine the additive drag for an inlet area of 5.2 m^2, an inlet Mach number of 0.8, a flight Mach number of 0.2, and a standard altitude of 10,000 m.

2.20. Consider an ideal turbojet engine with a compressor pressure ratio of 12.5 and a maximum turbine inlet temperature of 1,640 °F. With the engine running at full throttle, determine the thermal efficiency and uninstalled specific thrust for static operation at standard sea level and for a flight Mach number of 2.0 at 40,000 ft with standard atmospheric conditions.

2.21. The turbojet engine described in problem 2.20 is operating with a fuel-air ratio that is 60 percent of that at full throttle. For the same two operating points, determine the thermal efficiency and uninstalled specific thrust.

2.22. The turbojet engine described in problem 2.20 has an inlet area of 10.0 ft^2. If the inlet Mach number is 0.30 at standard sea level, determine the installed static thrust. Assume zero nacelle drag.

2.23. Assuming complete combustion, determine the fuel consumption rate in pounds per hour and gallons per minute for the turbojet engine and operating condition that are described in problem 2.22. The enthalpy of combustion for the fuel is 18,400 Btu/lbm and the fuel weighs 6.7 pounds per gallon.

2.24. For the same conditions that were used in Example 2.7.1 to generate Figs. 2.7.1 and 2.7.2, plot the thrust specific fuel consumption in pounds of fuel per hour per pound of uninstalled thrust, as a function of compressor pressure ratio for different flight Mach numbers. Assume complete combustion with an enthalpy of combustion for the fuel of 18,400 Btu/lbm.

2.25. For the conditions used in Example 2.7.1, plot the compressor pressure ratio that results in maximum specific thrust as a function of Mach number.

2.26. The turbojet engine described in problem 2.20 has an afterburner installed and is operating at full throttle with the afterburner engaged. The stagnation temperature at the nozzle inlet is 3,000 °F. For the same two operating points that were specified in problem 2.20, determine the thermal efficiency and uninstalled specific thrust.

2.27. For the same conditions that were used in Example 2.8.1 to generate Figs. 2.8.2 and 2.8.3, plot the thrust specific fuel consumption in pounds of fuel per hour per pound of uninstalled thrust as a function of compressor pressure ratio for different flight mach numbers. Assume complete combustion with an enthalpy of combustion for the fuel of 18,400 Btu/lbm.

2.28. For the conditions used in Example 2.8.1, plot the compressor pressure ratio that results in maximum specific thrust as a function of Mach number.

2.29. Consider an ideal turbofan engine with a compressor pressure ratio of 26.8, fan pressure ratio of 2.31, bypass ratio 1.91, turbine inlet temperature of 2,550 °F, and airflow of 356 lbm/sec. If the flight Mach number is 0.80 with standard conditions at 40,000 ft, determine uninstalled thrust, overall efficiency, and fuel consumption rate in lbm/hr. Assume complete combustion with an enthalpy of combustion for the fuel of 18,400 Btu/lbm. What is the total fuel consumption for two of these engines in gallons per minute? The fuel weight is 6.7 lbf/gal.

2.30. Consider an ideal turbofan engine with compressor pressure ratio of 39.3, bypass ratio of 8.40, and maximum turbine inlet temperature of 2,350 °F. The fuel-air ratio at cruise is 30 percent of full throttle and the airflow is 3,037 lbm/sec. If the cruise Mach number is 0.80 at 35,000 ft and the fan pressure ratio is optimized for this operating condition, determine the uninstalled thrust, overall efficiency, and fuel consumption rate. Assume complete combustion with an enthalpy of combustion for the fuel of 18,400 Btu/lbm. If an airplane uses four of these engines, what is the total fuel consumption at cruise in gallons per minute? What is the specific range in miles per gallon? The fuel weight is 6.7 lbf/gal.

2.31. To examine how optimal turbofan performance varies with bypass ratio and Mach number, consider the ideal turbofan engine operating under standard temperature and pressure at 30,000 feet. For this comparison, assume a fixed compressor pressure ratio of 20 and a fixed stagnation temperature at the turbine inlet of 3,000 °R. Assuming that each engine has a fan pressure ratio equal to optimum value for the given bypass ratio and operating conditions, plot overall efficiency and specific thrust as a function of Mach number for the same bypass ratios used in Fig. 2.9.2.

2.32. A significant performance parameter for the turbofan engine is the ratio of the uninstalled specific thrust for the core flow to that for the bypass flow. Here, this thrust ratio will be given the symbol R_F,

$$R_F \equiv \frac{F_c/\dot{m}_c}{F_b/\dot{m}_b}$$

For the design parameters and operating conditions used in problem 2.31, plot thrust ratio as a function of Mach number for the bypass ratios used in Fig. 2.9.2.

Chapter 3
Aircraft Performance

3.1. Introduction

Now that we have some understanding of the forces and moments acting on a moving airplane, we can turn our attention to a topic that students often find more interesting, aircraft performance. In this chapter we begin to answer some important questions about how airplanes fly. How fast and how high can an airplane fly? How slow can it fly? How rapidly can it climb? How far can a given airplane fly, and how long can it remain in the air? What happens if the engines fail? How quickly and in what distance can an airplane turn? What distance is required for takeoff and landing? The engineering analysis used to answer these questions and more is usually referred to as *aircraft performance analysis* and is the topic of this chapter. The answer to each of the questions above depends on the airplane design. How large are the wings? How much does the airplane weigh? What power and thrust are developed by the engines? Airplane performance analysis is very closely related to airplane design. In performance analysis, the airplane design parameters, such as wing area and gross weight, are assumed to be known, and engineering analysis is applied to determine some performance parameter, such as rate of climb or takeoff distance. In the design process, certain performance parameters, for example minimum airspeed and maximum range, are specified as engineering design requirements, and the design parameters and operating conditions necessary to meet these requirements must be determined. Essentially the same engineering analysis is used in either case.

In the preceding two chapters we have reviewed the physical phenomena associated with the production of lift, drag, and thrust as well as the moments produced along with these aerodynamic forces. We now combine what we have learned about the aerodynamic forces and moments with what the student has learned from his or her study of calculus, differential equations, statics, and dynamics to begin our study of the movement of an aircraft as it responds to these forces and moments. The important discipline within aerospace engineering that deals with aircraft motion is commonly referred to as *flight mechanics*. This broad field of study is normally broken up into three subareas: *aircraft performance*, *aircraft stability and control*, and *flight simulation*. While these three subdisciplines are very closely related, in this text we divide our study of flight mechanics along these traditional lines. As the title indicates, this chapter deals with the study of aircraft performance. The topics of aircraft stability and control as well as flight simulation are covered in Chapters 4 through 11.

The material presented in this chapter should be thought of as only a preliminary study of airplane performance. Here, emphasis is placed on obtaining closed-form analytic solutions suitable for preliminary design. Such solutions are invaluable in helping the student to understand how a particular performance parameter is affected by different aircraft design and operating parameters. The analysis presented in this chapter makes use of some simplifying assumptions that, though reasonable, are nevertheless only approximate. While the accuracy of these approximations is quite adequate for

most preliminary design, for the final design and development of any aircraft, detailed computer simulations and wind tunnel tests are needed.

This chapter does not address all possible measures of airplane performance. The chapter is simply a collection of important examples that demonstrate how engineering analysis and mathematics can be used to evaluate and optimize certain airplane performance parameters. The methods and tools used to analyze these particular measures of performance could be used as well to study other measures of aircraft performance, and in studying this chapter students should be preparing to do exactly that. This chapter is not intended as an all-inclusive "cookbook" of aircraft performance equations. It is, rather, intended to help the student gain experience in formulating and solving engineering problems in general and flight mechanics problems in particular. The student should strive to recognize what is common to all of these examples. In each case the airplane is considered to be a rigid body on which is exerted four fundamental forces: lift, drag, thrust, and weight. The movement of the airplane as it responds to these forces is governed by Newton's second law, *force equals mass times acceleration*. Since Newton's second law is a vector equation, it provides three scalar equations that can be used to relate aircraft performance parameters to design and operating parameters. Or in the design scenario, design parameters can be related to performance and operating parameters.

The student should also become intimately familiar with another analysis technique used in many of the examples in this chapter. Once a closed-form solution for some dependent performance parameter has been obtained in terms of the associated independent design and operating parameters, the performance parameter can be optimized with respect to a particular design or operating parameter. This is done by differentiating with respect to the independent parameter of interest and setting the result to zero. For example, the rate of climb for any airplane is a function of airspeed as well as other design and operating parameters. Furthermore, the rate of climb exhibits a maximum at some particular airspeed. The airspeed that results in the maximum rate of climb can be found by differentiating the expression for rate of climb with respect to airspeed and setting the result to zero. When the resulting equation is solved for airspeed we obtain an expression for the airspeed that will produce the maximum rate of climb. A similar approach can be used to optimize other airplane performance parameters. This analysis technique is used throughout the chapter and the student is expected to be able to use the technique to solve many of the homework problems at the end of the chapter.

3.2. Thrust Required

One important performance parameter for any aircraft is the thrust required to maintain steady level flight. By *steady flight*, we mean flight at constant speed. Here, the term *level flight* will require that both the climb angle and the bank angle are zero. For steady level flight, there is no acceleration and no change in altitude. Thus, Newton's second law requires that the vector summation of forces acting on an airplane in steady level flight is zero. During level unaccelerated flight, if the thrust vector is aligned with the direction of flight, the wing must provide enough lift to balance the weight of the aircraft, and the engine or engines must provide sufficient thrust to balance the aerodynamic drag

on the aircraft. Because the aerodynamic drag varies greatly with airspeed, the thrust required to maintain steady level flight is also a strong function of airspeed. More completely, the thrust required is a function of airspeed, altitude, size, shape, and weight of the airplane.

In general, the thrust vector will be inclined upward at some angle, α_T, with respect to the direction of flight, as shown in Fig. 3.2.1. For level unaccelerated flight, the drag force, D, must equal the component of thrust in the direction of flight,

$$D = T_R \cos\alpha_T \tag{3.2.1}$$

and the lift force, L, must equal the weight of the aircraft less the component of thrust normal to the direction of flight,

$$L = W - T_R \sin\alpha_T \tag{3.2.2}$$

where T_R is the thrust required for steady level flight and W is the gross weight of the aircraft. From Eqs. (3.2.1) and (3.2.2) we can write

$$\frac{L}{D} = \frac{W - T_R \sin\alpha_T}{T_R \cos\alpha_T} \tag{3.2.3}$$

or solving for the thrust required,

$$T_R = \frac{W}{(L/D)\cos\alpha_T + \sin\alpha_T} \tag{3.2.4}$$

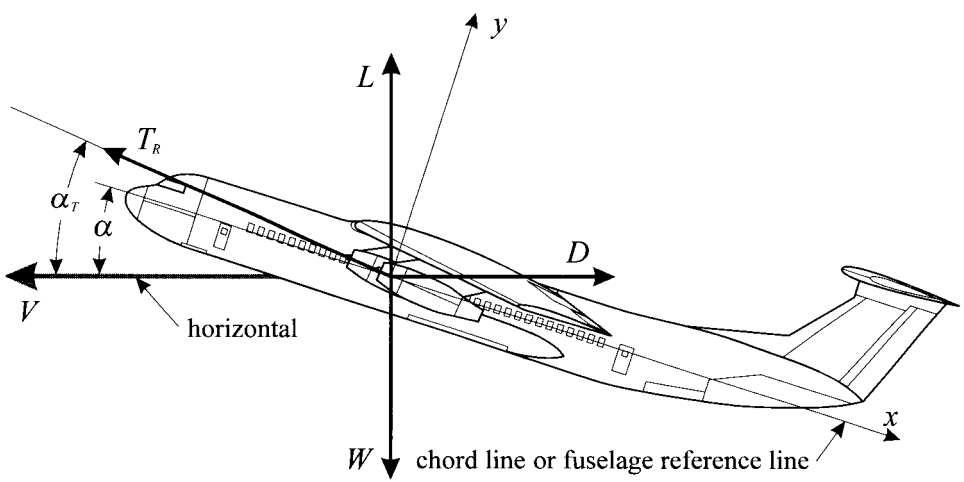


Figure 3.2.1. Forces acting on an aircraft in steady level flight, with angles exaggerated for better visibility.

Thus, we see that the thrust required for steady level flight is directly proportional to the gross weight of the aircraft. Furthermore, we see that the thrust required also depends on the ratio of lift to drag and on the thrust angle. The lift-to-drag ratio, commonly referred to as *L over D*, is a very important measure of an airplane's aerodynamic efficiency, and this ratio is a strong function of airspeed. Since the weight is clearly independent of airspeed, for any given value of α_T, the airspeed that results in the greatest *L/D* will also result in the lowest thrust required. To see how the thrust required varies with airspeed, we must examine how the ratio *L/D* varies with airspeed.

The total drag force can be written as the parasitic drag plus the induced drag,

$$D = \tfrac{1}{2}\rho V^2 S_w C_D = \tfrac{1}{2}\rho V^2 S_w \left(C_{Dp} + \frac{C_L^2}{\pi e_s R_A} \right) \tag{3.2.5}$$

where V is the airspeed, S_w is the area of the main wing, e_s is the span efficiency factor, and R_A is the aspect ratio. The parasitic drag coefficient, C_{Dp}, is very nearly a parabolic function of angle of attack. Since lift coefficient is a linear function of angle of attack, the parasitic drag coefficient can be written as a parabolic function of C_L,

$$C_{Dp} = C_{D_0} + C_{D_0,L} C_L + C_{D_0,L^2} C_L^2 \tag{3.2.6}$$

Using Eq. (3.2.6) in Eq. (3.2.5) and combining the quadratic term from the parasitic drag with the induced drag, the total drag can be written as

$$D = \tfrac{1}{2}\rho V^2 S_w \left(C_{D_0} + C_{D_0,L} C_L + \frac{C_L^2}{\pi e R_A} \right) \tag{3.2.7}$$

where e is called the *Oswald efficiency factor*. The Oswald efficiency factor for the entire aircraft is considerably less than the span efficiency factor for the wing, because it accounts for part of the parasitic drag in addition to the induced drag. From Eq. (3.2.7) we can write

$$\frac{L}{D} = \frac{\tfrac{1}{2}\rho V^2 S_w C_L}{\tfrac{1}{2}\rho V^2 S_w C_D} = \frac{C_L}{C_D} = \frac{C_L}{C_{D_0} + C_{D_0,L} C_L + \dfrac{C_L^2}{\pi e R_A}} \tag{3.2.8}$$

The aerodynamic coefficients in Eq. (3.2.8) can all depend on Mach number. However, at low Mach numbers this dependence is slight.

Even at low Mach numbers, the lift coefficient for steady level flight is a function of airspeed. For level unaccelerated flight at any given airspeed, the aircraft must be trimmed to fly at an angle of attack that will produce the correct amount of lift to just satisfy Eq. (3.2.2). If the angle of attack is too large, too much lift is generated at the given airspeed and the airplane will climb. If the angle of attack is too small, not enough lift is generated and the airplane will begin to sink.

Using the definition of lift coefficient with Eq. (3.2.2), we have

$$C_L = \frac{L}{\frac{1}{2}\rho V^2 S_w} = \frac{W - T_R \sin\alpha_T}{\frac{1}{2}\rho V^2 S_w} \tag{3.2.9}$$

Using Eq. (3.2.4) to eliminate the thrust required from Eq. (3.2.9) gives

$$C_L = \frac{W}{\frac{1}{2}\rho V^2 S_w}\left[1 - \frac{\sin\alpha_T}{(L/D)\cos\alpha_T + \sin\alpha_T}\right] = \frac{W}{\frac{1}{2}\rho V^2 S_w}\left[\frac{1}{1+(D/L)\tan\alpha_T}\right] \tag{3.2.10}$$

For most conventional airplanes, the bracketed term on the right side of Eq. (3.2.10) is very close to unity, and the lift coefficient is very nearly inversely proportional to the square of the airspeed. So we see that for steady level flight, increasing the airspeed will require the angle of attack and the corresponding lift coefficient to decrease.

Using Eqs. (3.2.8) and (3.2.10), we can numerically determine both C_L and L/D as a function of airspeed. A plot of the lift-to-drag ratio versus airspeed for a typical general aviation aircraft at sea level is shown in Fig. 3.2.2. Notice that L/D has a well-defined maximum at some particular airspeed. This characteristic is common to all airplanes. While the maximum value of L/D and the airspeed at which this maximum occurs vary with aircraft design, all airplanes exhibit a maximum in the lift-to-drag ratio at some particular airspeed.

The maximum lift-to-drag ratio and the airspeed that results in this maximum are both important aircraft design parameters. We can find the lift coefficient that will result in maximum L/D by differentiating Eq. (3.2.8) with respect to C_L and setting the result to zero. This gives

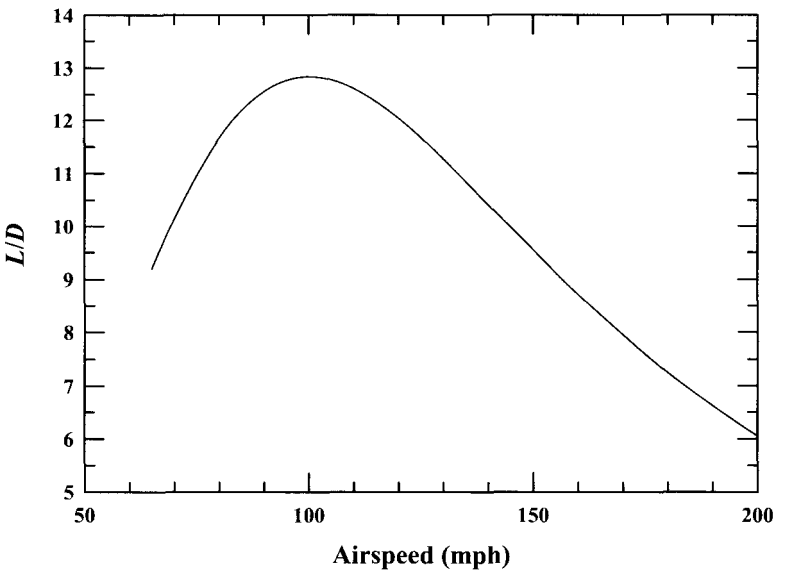


Figure 3.2.2. Lift-to-drag ratio at standard sea level.

$$\frac{\partial(L/D)}{\partial C_L} = \frac{\left(C_{D_0} + C_{D_{0,L}} C_L + \frac{C_L^2}{\pi e R_A}\right) - C_L\left(C_{D_{0,L}} + \frac{2C_L}{\pi e R_A}\right)}{\left(C_{D_0} + C_{D_{0,L}} C_L + \frac{C_L^2}{\pi e R_A}\right)^2} = 0 \qquad (3.2.11)$$

or

$$C_{D_0} = \frac{C_L^2}{\pi e R_A} \qquad (3.2.12)$$

The term on the right-hand side of Eq. (3.2.12) is often referred to as the *induced drag* even though, strictly speaking, it is the induced drag plus the quadratic portion of the parasitic drag. Using this terminology, it is said that maximum lift-to-drag ratio occurs at the airspeed that makes the induced drag equal to the parasitic drag at zero lift. Using Eq. (3.2.12) to eliminate the lift coefficient from Eq. (3.2.8), we obtain an expression for the maximum lift-to-drag ratio,

$$(L/D)_{\max} = \frac{\sqrt{\pi e R_A}}{2\sqrt{C_{D_0}} + C_{D_{0,L}}\sqrt{\pi e R_A}} \qquad (3.2.13)$$

The airspeed at which an aircraft must be flown in order to attain maximum lift-to-drag ratio is found by solving Eq. (3.2.10) for the airspeed and using Eqs. (3.2.12) and (3.2.13) to eliminate C_L and L/D. This gives

$$V_{MD} = \frac{\sqrt{2}}{\sqrt[4]{\pi e R_A C_{D_0}}}\sqrt{\frac{W/S_w}{\rho}}\sqrt{1\Big/\left[1 + \left(2\sqrt{\frac{C_{D_0}}{\pi e R_A}} + C_{D_{0,L}}\right)\tan\alpha_T\right]} \qquad (3.2.14)$$

where V_{MD} is usually referred to as the *minimum drag airspeed* or the *best L over D airspeed*. The parameter W/S_w, called the *wing loading*, is another very important parameter in aircraft design. Note that the best L over D airspeed for any airplane is proportional to the square root of the wing loading divided by the air density. This means that the higher an airplane flies and the greater its wing loading, the faster it must be flown to achieve best L over D. We can see from Eq. (3.2.13), however, that the maximum lift-to-drag ratio for any airplane is independent of both wing loading and altitude. The maximum lift-to-drag ratio is a function only of the aircraft design. No matter how heavily the plane is loaded or how high it is flown, the maximum lift-to-drag ratio is always the same. For this reason maximum lift-to-drag ratio is a commonly used measure of aerodynamic efficiency for an airplane.

This maximum value for L/D is often referred to simply as the *lift-to-drag ratio* for the aircraft. For example, you may hear it said that a particular airplane has a lift-to-drag ratio of 12. This manner of speaking could erroneously lead the student to believe that this airplane will always produce 1 pound of drag for each 12 pounds of aircraft

weight. Nothing could be further from the truth. As we have seen in Fig. 3.2.2, the ratio of lift to drag for an airplane varies greatly with airspeed. It must be remembered that when an aerodynamicist specifies an unqualified lift-to-drag ratio for an aircraft, he or she is referring to the maximum lift-to-drag ratio for that aircraft.

For most conventional airplanes, the change in drag coefficient with respect to lift coefficient at zero lift is either zero or a very small negative value. Thus, from Eq. (3.2.13) we see that the maximum lift-to-drag ratio can be increased only by decreasing the parasitic drag coefficient or by increasing the aspect ratio and Oswald efficiency factor. For this reason, the problem of designing an aircraft for high L over D is as much a structures problem as it is an aerodynamics problem. From an aerodynamics viewpoint, we want to build a very streamlined airplane with a very high aspect ratio. From a structures viewpoint, the longer and thinner the wing must be, the more difficult it is to design the wing so that it will support the weight of the aircraft and payload.

From Eq. (3.2.4) we see that because maximum lift-to-drag ratio is independent of both wing area and altitude, the minimum thrust required is also independent of wing area and altitude. Figure 3.2.3 shows how the thrust required varies with airspeed and altitude for a typical general aviation aircraft. Wing area affects the thrust required in the same way as air density. Thus, a plot of thrust required as a function of airspeed for constant weight and different values of wing area would look very much like Fig. 3.2.3, with higher wing loading moving the curve to the right.

We have now seen that there is an optimum airspeed that results in maximum L/D and minimum thrust required. Similarly, we can show from Eq. (3.2.4) that there is an optimum thrust angle that can be used to minimize the thrust required. To find the value

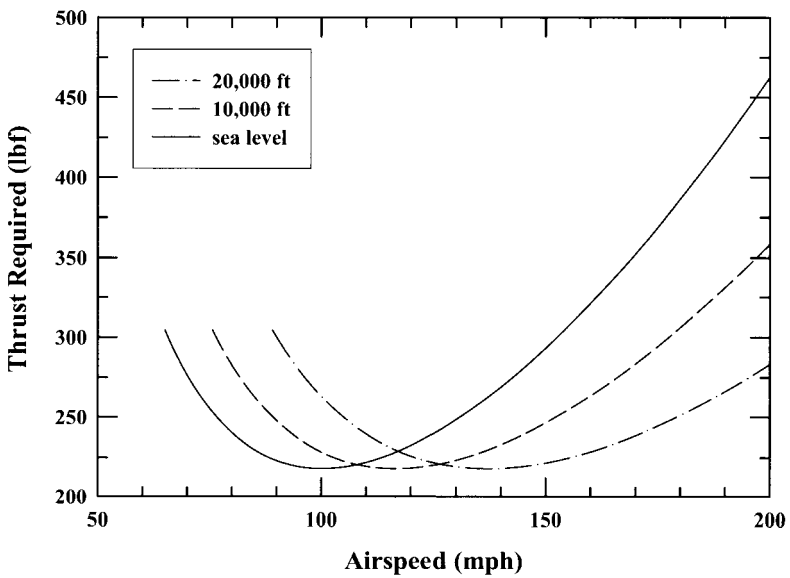


Figure 3.2.3. Thrust required at altitude.

of α_T that will result in minimum thrust required, we differentiate Eq. (3.2.4) with respect to α_T and set the result to zero. This gives

$$\frac{\partial T_R}{\partial \alpha_T} = \frac{W\left[(L/D)\sin\alpha_T - \cos\alpha_T\right]}{\left[(L/D)\cos\alpha_T + \sin\alpha_T\right]^2} = 0 \tag{3.2.15}$$

or

$$\alpha_T = \tan^{-1}(D/L) \tag{3.2.16}$$

So we see that to completely minimize the thrust required, the thrust vector should not be aligned exactly with the direction of flight. Rather, the thrust vector should be tilted upward slightly, at an angle equal to the arctangent of the inverse of the lift-to-drag ratio for the aircraft. However, for a well-designed airplane, the lift-to-drag ratio is fairly high. Most modern airplanes will have maximum lift-to-drag ratios between 8 and 24, with even higher values for some specialty aircraft. Thus, the optimum thrust angle for most conventional airplanes is very small (between 2 and 7 degrees, with even smaller values for airplanes with very high aerodynamic efficiency).

Since α_T and D/L are both small for conventional airplanes, for the purpose of making preliminary calculations for airplane performance, we often use the small-angle approximations

$$\cos\alpha_T = 1 - \frac{\alpha_T^2}{2!} + \frac{\alpha_T^4}{4!} - \frac{\alpha_T^6}{6!} + \cdots \cong 1 \tag{3.2.17}$$

$$\sin\alpha_T = \alpha_T - \frac{\alpha_T^3}{3!} + \frac{\alpha_T^5}{5!} - \frac{\alpha_T^7}{7!} + \cdots \cong \alpha_T \tag{3.2.18}$$

$$(D/L)\sin\alpha_T \cong \alpha_T^2 \cong 0 \tag{3.2.19}$$

This will be called the *small-thrust-angle approximation* and is based on neglecting all terms of order α_T squared and smaller when compared to unity. Notice that we are not making the approximation $\sin\alpha_T \cong 0$, but rather, $\sin\alpha_T \cong \alpha_T$ and $(D/L)\sin\alpha_T \cong 0$. Since both $\sin\alpha_T$ and D/L are of the same order of magnitude as the angle of attack (10^{-1} for most conventional airplanes), we clearly should not neglect either $\sin\alpha_T$ or D/L when compared to unity. The product of D/L with $\sin\alpha_T$, on the other hand, is of the same order as the angle of attack squared, and neglecting this product compared to unity is consistent with the other small-angle approximations that we used previously. With this approximation, Eqs. (3.2.1) and (3.2.10) reduce to

$$T_R = D \tag{3.2.20}$$

$$L = W \tag{3.2.21}$$

Thus, for small thrust angles, the equations of motion for level unaccelerated flight simply require that the thrust must equal the drag and the lift must equal the weight. Therefore, the thrust required is simply the gross weight divided by the lift-to-drag ratio for the airplane.

$$T_R = \frac{W}{L/D} \tag{3.2.22}$$

Using Eq. (3.2.8) in Eq. (3.2.22), for small thrust angles we can write the thrust required for steady level flight as

$$T_R = \frac{C_D}{C_L} W = \left(\frac{C_{D_0}}{C_L} + C_{D_0,L} + \frac{C_L}{\pi e R_A} \right) W \tag{3.2.23}$$

Using the small-thrust-angle approximation with Eq. (3.2.10) gives

$$C_L = \frac{W}{\frac{1}{2}\rho V^2 S_w} \tag{3.2.24}$$

Using Eq. (3.2.24) in Eq. (3.2.23), we can write the thrust required for small thrust angles as a function of airspeed:

$$T_R = \left(\frac{\frac{1}{2}\rho V^2 C_{D_0}}{W/S_w} + C_{D_0,L} + \frac{W/S_w}{\frac{1}{2}\pi e R_A \rho V^2} \right) W \tag{3.2.25}$$

Using Eq. (3.2.13) in Eq. (3.2.22), the minimum thrust required for small thrust angles can be closely approximated as

$$T_{R_{\min}} = \left(2\sqrt{\frac{C_{D_0}}{\pi e R_A}} + C_{D_0,L} \right) W \tag{3.2.26}$$

Using Eq. (3.2.19) in Eq. (3.2.14), the minimum drag airspeed for small thrust angles becomes

$$V_{MD} = \left(\frac{4}{\pi e R_A C_{D_0}} \right)^{1/4} \sqrt{\frac{W/S_w}{\rho}} \tag{3.2.27}$$

As mentioned previously, the change in drag coefficient with respect to lift coefficient at zero lift is either zero or a very small negative value. Thus, for the purpose of making preliminary performance calculations, the value of $C_{D_0,L}$ in Eqs. (3.2.25) and (3.2.26) is often assumed to be zero.

EXAMPLE 3.2.1. A turbojet engine produces a thrust that is nearly independent of airspeed. As a first approximation, we can model a turbojet engine as a device that produces an available thrust, T_A, that is constant with airspeed, V, and directly proportional to the air density, ρ,

$$T_A = \tau \frac{\rho}{\rho_0} T_{A0}$$

where τ is a throttle setting expressed as a fraction of the full-throttle thrust, ρ_0 is the air density at standard sea level, and T_{A0} is the full-throttle thrust developed at standard sea level.

Consider an executive business jet having the following properties:

$$S_w = 320 \text{ ft}^2, \quad b_w = 54 \text{ ft}, \quad W = 20{,}000 \text{ lbf}, \quad T_{A0} = 6{,}500 \text{ lbf},$$
$$C_{D_0} = 0.023, \quad C_{D_0,L} = 0.0, \quad e = 0.82$$

Using the small-thrust-angle approximation with the foregoing approximation for the thrust available, determine the airspeed for this aircraft in steady level flight with a 60 percent throttle setting, for both sea level and 20,000 feet.

Solution. For steady level flight, the thrust required must equal the thrust available. For small thrust angles, the thrust required is given by Eq. (3.2.25), and for this example, the thrust available is given by the relation above. Thus we can write

$$\left(\frac{\frac{1}{2}\rho V^2 C_{D_0}}{W/S_w} + C_{D_0,L} + \frac{W/S_w}{\frac{1}{2}\pi e R_A \rho V^2} \right) W = \tau \frac{\rho}{\rho_0} T_{A0}$$

This equation can be written in terms of a dimensionless velocity ratio

$$R_V \equiv V \Big/ \sqrt{\frac{W/S_w}{\rho}}$$

and a dimensionless thrust-to-weight ratio

$$R_{T/W} \equiv \frac{T_A}{W} = \tau \frac{\rho}{\rho_0} \frac{T_{A0}}{W}$$

With these definitions, the balance between thrust required and thrust available can be written as

$$C_{D_0} R_V^4 - 2(R_{T/W} - C_{D_0,L}) R_V^2 + \frac{4}{\pi e R_A} = 0$$

This gives a quadratic equation for the dimensionless velocity ratio squared and we have

$$R_V^2 = \frac{R_{T/W} - C_{D_0,L}}{C_{D_0}} \pm \sqrt{\left(\frac{R_{T/W} - C_{D_0,L}}{C_{D_0}}\right)^2 - \frac{4}{\pi e R_A C_{D_0}}}$$

The airspeed for steady level flight is then

$$V = \sqrt{\frac{R_{T/W} - C_{D_0,L}}{C_{D_0}} \pm \sqrt{\left(\frac{R_{T/W} - C_{D_0,L}}{C_{D_0}}\right)^2 - \frac{4}{\pi e R_A C_{D_0}}}} \sqrt{\frac{W/S_w}{\rho}}$$

From this equation we see that in the absence of stall, there may be two steady level airspeeds that can be sustained by the aircraft with a given thrust. The reason for this is made clear by reviewing Fig. 3.2.3. The airspeed of interest is the larger of these two roots. For the aircraft in this example, the aspect ratio is

$$R_A = \frac{b_w^2}{S_w} = \frac{(54\text{ ft})^2}{320\text{ ft}^2} = 9.1125$$

the wing loading is

$$\frac{W}{S_w} = \frac{20{,}000\text{ lbf}}{320\text{ ft}^2} = 62.5\text{ lbf/ft}^2$$

and the thrust-to-weight ratio for 60 percent of maximum thrust at standard sea level is

$$R_{T/W} = \frac{T_A}{W} = \tau \frac{\rho}{\rho_0} \frac{T_{A0}}{W} = 0.6 \frac{0.0023769\text{ slug/ft}^3}{0.0023769\text{ slug/ft}^3} \frac{6{,}500\text{ lbf}}{20{,}000\text{ lbf}} = 0.195$$

Thus, at sea level, the steady airspeed that can be sustained in level flight with 60 percent of maximum thrust is

$$V = \sqrt{\frac{0.195 - 0.0}{0.023} + \sqrt{\left(\frac{0.195 - 0.0}{0.023}\right)^2 - \frac{4}{\pi(0.82)9.1125(0.023)}}} \sqrt{\frac{62.5\text{ lbf/ft}^2}{0.0023769\text{ slug/ft}^3}}$$

$$= \underline{659\text{ ft/sec} = 449\text{ mph} = 390\text{ knots} = 723\text{ km/hr}}$$

At 20,000 feet, the thrust-to-weight ratio for 60 percent of maximum thrust is

$$\frac{T_A}{W} = \tau \frac{\rho}{\rho_0} \frac{T_{A0}}{W} = 0.6 \frac{0.0012673 \text{ slug/ft}^3}{0.0023769 \text{ slug/ft}^3} \frac{6{,}500 \text{ lbf}}{20{,}000 \text{ lbf}} = 0.104$$

and

$$V = \sqrt{\frac{0.104 - 0.0}{0.023} + \sqrt{\left(\frac{0.104 - 0.0}{0.023}\right)^2 - \frac{4}{\pi(0.82)9.1125(0.023)}}} \sqrt{\frac{62.5 \text{ lbf/ft}^2}{0.0012673 \text{ slug/ft}^3}}$$

$$= \underline{633 \text{ ft/sec} = 432 \text{ mph} = 375 \text{ knots} = 695 \text{ km/hr}}$$

Thus we see that while the available thrust produced by this turbojet engine is reduced by nearly 50 percent in going from sea level to 20,000 feet, the corresponding airspeed is only reduced by about 4 percent.

3.3. Power Required

Another important performance parameter for any aircraft is the power required to maintain level, unaccelerated flight. This parameter is also a strong function of airspeed. The power delivered by a jet engine or any engine-propeller combination is just the rate of work that results from the thrust force acting on the aircraft moving through the air. The work is the force multiplied by the distance through which it acts as the aircraft moves through the air. The work rate, or power, is then the dot product of the force vector and velocity vector. The power required is then the thrust required multiplied by the airspeed and the cosine of the thrust angle,

$$P_R = T_R V \cos\alpha_T = DV \tag{3.3.1}$$

where P_R is defined as the power required for steady level flight. Using the small-thrust-angle approximation, for steady level flight we have

$$C_L = \frac{W}{\frac{1}{2}\rho V^2 S_w} \tag{3.3.2}$$

Solving Eq. (3.3.2) for the airspeed, we obtain

$$V = \sqrt{\frac{2(W/S_w)}{\rho C_L}} \tag{3.3.3}$$

Using Eq. (3.3.3) in Eq. (3.3.1) along with the small-thrust-angle approximation gives

$$P_R = T_R \sqrt{\frac{2(W/S_w)}{\rho C_L}} \tag{3.3.4}$$

From Eq. (3.2.23), the thrust required for small thrust angles is given by

$$T_R = \frac{C_D}{C_L} W = \left(\frac{C_{D_0}}{C_L} + C_{D_0,L} + \frac{C_L}{\pi e R_A} \right) W \tag{3.3.5}$$

Using Eq. (3.3.5) in Eq. (3.3.4), we have

$$P_R = \sqrt{2} \left(\frac{C_{D_0}}{C_L^{3/2}} + \frac{C_{D_0,L}}{C_L^{1/2}} + \frac{C_L^{1/2}}{\pi e R_A} \right) W \sqrt{\frac{W/S_w}{\rho}} \tag{3.3.6}$$

Using Eq. (3.3.2) in Eq. (3.3.6), we can write the power required for steady level flight as a function of airspeed,

$$P_R = \left(\frac{C_{D_0} \rho V^3}{2(W/S_w)} + C_{D_0,L} V + \frac{2(W/S_w)}{\pi e R_A \rho V} \right) W \tag{3.3.7}$$

Since the first two terms on the right of Eq. (3.3.7) increase with airspeed while the third term decreases with airspeed, the power required will also have a minimum at some particular airspeed. Figure 3.3.1 shows the power required as a function of airspeed for a typical general aviation aircraft at sea level.

We can find the aircraft lift coefficient that results in minimum power required by differentiating Eq. (3.3.6) with respect to C_L and setting the result to zero. This gives

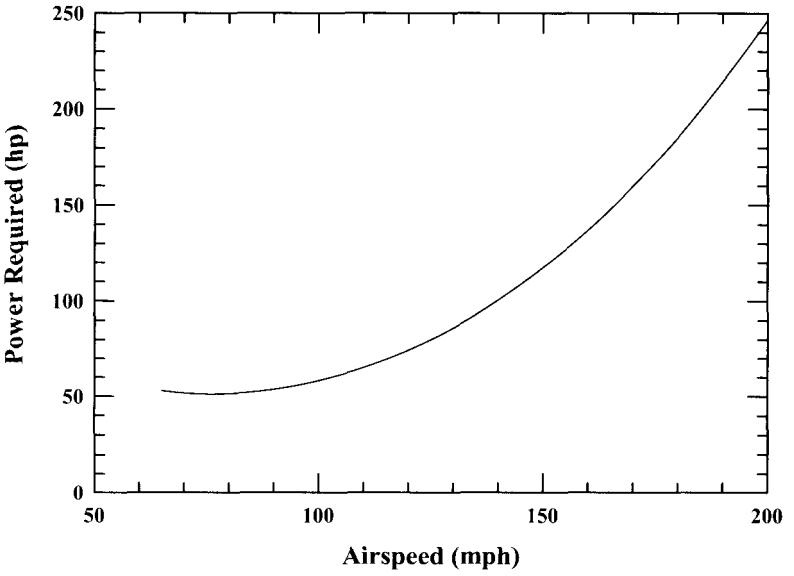


Figure 3.3.1. Power required at standard sea level.

$$\frac{\partial P_R}{\partial C_L} = \sqrt{2}\left(-\frac{3}{2}\frac{C_{D_0}}{C_L^{5/2}} - \frac{1}{2}\frac{C_{D_0,L}}{C_L^{3/2}} + \frac{1}{2}\frac{1}{\pi e R_A C_L^{1/2}}\right) W\sqrt{\frac{W/S_w}{\rho}} = 0 \tag{3.3.8}$$

or

$$3C_{D_0} + C_{D_0,L}\,C_L = \frac{C_L^2}{\pi e R_A} \tag{3.3.9}$$

Because $C_{D_0,L}$ is very nearly zero, from Eq. (3.3.9) we see that at the airspeed which requires minimum power, the induced drag is approximately three times the zero-lift drag. After solving Eq. (3.3.9) for the lift coefficient that is required when the airplane is flying at minimum power, we have

$$C_L = \frac{\pi e R_A}{2}\left(C_{D_0,L} + \sqrt{C_{D_0,L}^2 + \frac{12C_{D_0}}{\pi e R_A}}\right) \tag{3.3.10}$$

Using the lift coefficient from Eq. (3.3.10) in Eq. (3.3.6), we can obtain the minimum power required. The basic features of this relationship can be more easily examined by considering the usual approximation $C_{D_0,L} = 0$. Using this approximation, the minimum power required becomes

$$P_{R_{\min}} = (DV)_{\min} \cong \frac{4\sqrt{2}\,C_{D_0}^{1/4}}{(3\pi e R_A)^{3/4}} W\sqrt{\frac{W/S_w}{\rho}} \tag{3.3.11}$$

From this equation we see that as was the case for minimum thrust required, the minimum power required for a given weight can be made smaller by decreasing the parasitic drag or increasing the aspect ratio and Oswald efficiency factor. However, the minimum thrust required was independent of both wing loading and air density. The minimum power required, on the other hand, increases with both wing loading and altitude. Thus, when designing an aircraft for very high payload-to-power ratio, we not only want the highest possible aspect ratio and the lowest possible parasitic drag but the lowest possible wing loading as well. Without a doubt, the ultimate in low-powered aircraft designs have been the human-powered aircraft (Gossamer Condor and Gossamer Albatross) designed and built by Paul MacCready and his colleagues. The wing loading for these aircraft was on the order of ¼ pound per square foot. This is in contrast to a wing loading on the order of 100 pounds per square foot for modern high-powered fighter aircraft.

The airspeed at which an aircraft must fly in order to attain minimum power required is found by combining Eqs. (3.3.3) and (3.3.10). This gives

$$V_{MDV} = \frac{2}{\sqrt{\pi e R_A C_{D_0,L} + \sqrt{(\pi e R_A C_{D_0,L})^2 + 12\pi e R_A C_{D_0}}}}\sqrt{\frac{W/S_w}{\rho}} \tag{3.3.12}$$

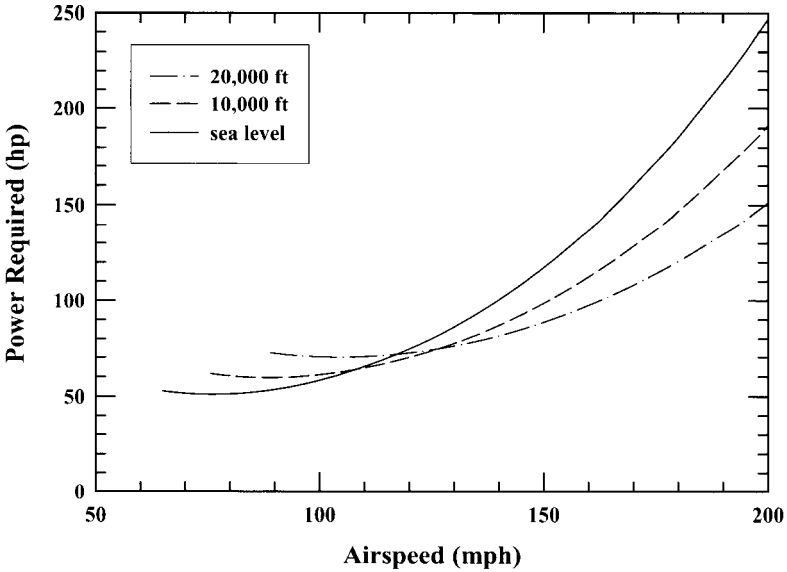


Figure 3.3.2. Power required at altitude.

where V_{MDV} is the airspeed for minimum power required, which means minimum DV product. Note that as was the case for the minimum thrust airspeed, the minimum power airspeed is proportional to the square root of the wing loading divided by the air density. The minimum power airspeed is typically about 75 to 80 percent of the minimum thrust airspeed. Note that both the minimum power airspeed and the minimum power required increase with altitude. Figure 3.3.2 shows how the power required varies with altitude for a typical general aviation aircraft.

EXAMPLE 3.3.1. For small thrust angles, the propulsive power available from an aircraft power plant is equal to the thrust available multiplied by the airspeed. An engine combined with a variable-pitch propeller can be adjusted, either manually by the pilot or automatically with a governor mechanism, to produce an available power that is nearly independent of airspeed over the range of airspeeds encountered in normal flight. As a first approximation, we can model this type of power plant as a device that produces an available power, P_A, that is constant with airspeed, V, and directly proportional to the air density, ρ,

$$P_A = \tau \frac{\rho}{\rho_0} P_{A0}$$

where τ is a throttle setting expressed as a fraction of the full-throttle power available, ρ_0 is the air density at standard sea level, and P_{A0} is the full-throttle power available at standard sea level.

Consider a general aviation aircraft having such a power plant and the following properties:

$$S_w = 180\ \text{ft}^2, \quad b_w = 33\ \text{ft}, \quad W = 2{,}700\ \text{lbf}, \quad P_{A0} = 180\ \text{hp},$$
$$C_{D_0} = 0.023, \quad C_{D_0,L} = 0.0, \quad e = 0.82$$

Using the small-thrust-angle approximation, determine the maximum airspeed that can be sustained by this aircraft in steady level flight for both sea level and 10,000 feet.

Solution. For steady level flight, the power required must equal the power available. For small thrust angles, the power required is given by Eq. (3.3.7), and for this example, the power available is given by the relation above. Thus we can write

$$\left(\frac{C_{D_0} \rho V^3}{2(W/S_w)} + C_{D_0,L} V + \frac{2(W/S_w)}{\pi e R_A \rho V} \right) W = \tau \frac{\rho}{\rho_0} P_{A0}$$

This equation can be written in terms of the dimensionless velocity ratio

$$R_V \equiv V \Big/ \sqrt{\frac{W/S_w}{\rho}}$$

and a dimensionless power-to-weight ratio

$$R_{P/W} \equiv P_A \Big/ \left(W \sqrt{\frac{W/S_w}{\rho}} \right) = \tau \frac{\rho}{\rho_0} P_{A0} \Big/ \left(W \sqrt{\frac{W/S_w}{\rho}} \right)$$

Thus, the balance between power required and power available can be written

$$\frac{C_{D_0}}{2} R_V^3 + C_{D_0,L} R_V + \frac{2}{\pi e R_A} R_V^{-1} = R_{P/W} \tag{3.3.13}$$

This does not reduce to a simple quadratic equation, as was the case for the turbojet engine in Example 3,2.1. However, the equation can quickly be solved for the velocity ratio by using Newton's method.

Let the left-hand side of Eq. (3.3.13) be $f(R_V)$. Then we have

$$f'(R_V) \equiv \frac{\partial f}{\partial R_V} = \frac{3C_{D_0}}{2} R_V^2 + C_{D_0,L} - \frac{2}{\pi e R_A} R_V^{-2}$$

Newton's method allows us to obtain an improved estimate for the dimensionless velocity ratio, from some initial estimate, by using Newton's corrector equation,

$$R_{V_{i+1}} = R_{V_i} + \frac{R_{P/W} - f(R_{V_i})}{f'(R_{V_i})} \tag{3.3.14}$$

As was the case for the turbojet engine in Example 3.2.1, there may be two positive roots to Eq. (3.3.13). The airspeed of interest is associated with the larger of these two roots. To ensure that Newton's method converges on the larger root, we obtain our initial estimate for the dimensionless velocity ratio by neglecting all but the highest-order term on the left-hand side of Eq. (3.3.13). Retaining only the cubic term, this gives

$$R_{V0} = \left(\frac{2R_{P/W}}{C_{D_0}}\right)^{1/3} \tag{3.3.15}$$

For the aircraft in this example, the aspect ratio is

$$R_A = \frac{b_w^2}{S_w} = \frac{(33\text{ ft})^2}{180\text{ ft}^2} = 6.05$$

the wing loading is

$$\frac{W}{S_w} = \frac{2{,}700\text{ lbf}}{180\text{ ft}^2} = 15.0\text{ lbf/ft}^2$$

and the full-throttle power available at standard sea level is

$$P_A = P_{A0} = 180\text{ hp} = 99{,}000\text{ ft}\cdot\text{lbf/sec}$$

This gives a dimensionless power-to-weight ratio of

$$R_{P/W} \equiv P_A \Big/ \left(W\sqrt{\frac{W/S_w}{\rho}}\right)$$

$$= 99{,}000\text{ ft}\cdot\text{lbf/sec} \Big/ \left(2{,}700\text{ lbf}\sqrt{\frac{15.0\text{ lbf/ft}^2}{0.0023769\text{ slug/ft}^3}}\right)$$

$$= \frac{99{,}000\text{ ft}\cdot\text{lbf/sec}}{214{,}488\text{ ft}\cdot\text{lbf/sec}} = 0.462$$

and from Eq. (3.3.15), the initial estimate for the dimensionless velocity ratio at sea level is

$$R_{V0} = \left(\frac{2R_{P/W}}{C_{D_0}}\right)^{1/3} = \left(\frac{2(0.462)}{0.023}\right)^{1/3} = 3.4249$$

Using this initial estimate and iteratively applying Eq. (3.3.14) gives

i	R_{Vi}	$f(R_{Vi})$	$f'(R_{Vi})$	R_{Vi+1}
0	3.4249	0.49947	0.39374	3.3297
1	3.3297	0.46309	0.37093	3.3268
2	3.3268	0.46200	0.37024	3.3268

Thus, at standard sea level, the maximum airspeed that can be sustained by the aircraft in steady level flight is

$$V = R_V\sqrt{\frac{W/S_w}{\rho}} = 3.3268\sqrt{\frac{15.0\ \text{lbf/ft}^2}{0.0023769\ \text{slug/ft}^3}}$$
$$= \underline{264\ \text{ft/sec} = 180\ \text{mph} = 156\ \text{knots} = 290\ \text{km/hr}}$$

Repeating the calculations for 10,000 feet, we have

$$P_A = \tau\frac{\rho}{\rho_0}P_{A0}$$
$$= 1.0\frac{0.0017556\ \text{slug/ft}^3}{0.0023769\ \text{slug/ft}^3}180\ \text{hp} = 132.95\ \text{hp} = 73{,}122\ \text{ft lbf/sec}$$

$$R_{P/W} \equiv P_A\Big/\left(W\sqrt{\frac{W/S_w}{\rho}}\right)$$
$$= 73{,}122\cdot\text{ft lbf/sec}\Big/\left(2{,}700\ \text{lbf}\sqrt{\frac{15.0\ \text{lbf/ft}^2}{0.0017556\ \text{slug/ft}^3}}\right)$$
$$= \frac{73{,}122\ \text{ft}\cdot\text{lbf/sec}}{249{,}572\ \text{ft}\cdot\text{lbf/sec}} = 0.293$$

$$R_{V0} = \left(\frac{2R_{P/W}}{C_{D_0}}\right)^{1/3} = \left(\frac{2(0.293)}{0.023}\right)^{1/3} = 2.9425$$

i	R_{Vi}	$f(R_{Vi})$	$f'(R_{Vi})$	R_{Vi+1}
0	2.9425	0.33661	0.28390	2.7889
1	2.7889	0.29548	0.25185	2.7791
2	2.7791	0.29300	0.24984	2.7791

$$V = R_V\sqrt{\frac{W/S_w}{\rho}} = 2.7791\sqrt{\frac{15.0\ \text{lbf/ft}^2}{0.0017556\ \text{slug/ft}^3}}$$
$$= \underline{257\ \text{ft/sec} = 175\ \text{mph} = 152\ \text{knots} = 282\ \text{km/hr}}$$

For this propeller-driven airplane, the available power is reduced by more than 25 percent in going from sea level to 10,000 feet, while the corresponding maximum airspeed is reduced by only about 3 percent. This is because, as is seen in Fig. 3.3.2, the power required at high airspeeds is also significantly reduced with altitude.

3.4. Rate of Climb and Power Available

The rate at which an airplane can climb is another important performance parameter. As we should expect, the rate of climb is a function not only of the aerodynamic design and weight of the aircraft but is also a function of the power available from the airplane's engines. This power depends on engine type and design as well as on airspeed, air density, and throttle setting.

To determine the steady rate of climb, we consider an airplane in unaccelerated climbing flight, as is shown in Fig. 3.4.1. The flight path relative to the surrounding air is inclined at an angle of γ to the horizontal, and the airplane's airspeed along this flight path is V. The drag force must equal the component of thrust parallel to the flight path less the component of the airplane's weight that is aligned with the flight path,

$$D = T_A \cos\alpha_T - W \sin\gamma \tag{3.4.1}$$

where T_A is the thrust available. The lift must support the airplane's weight component that is normal to the flight path less the component of thrust normal to the flight path,

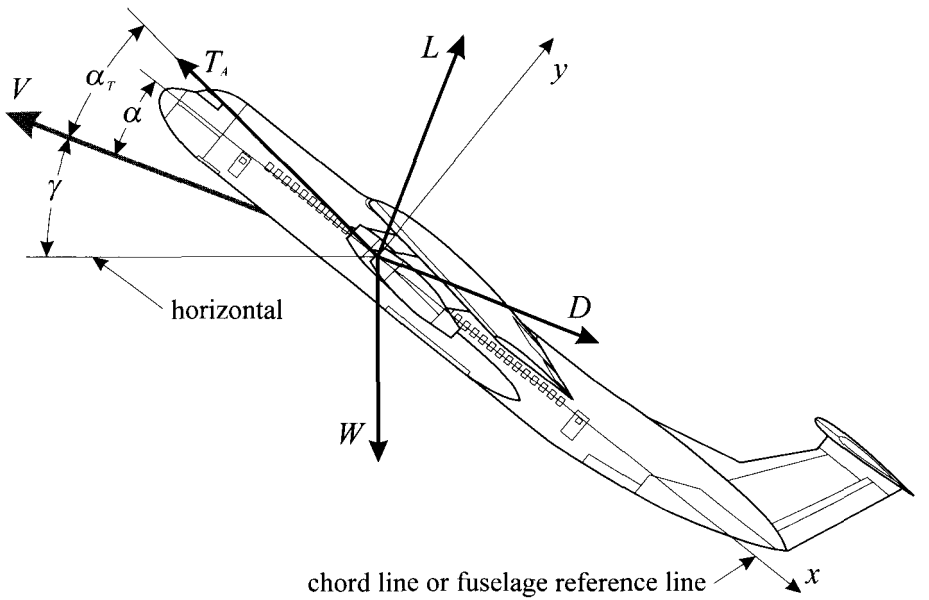


Figure 3.4.1. Forces acting on an aircraft in steady climbing flight.

$$L = W\cos\gamma - T_A \sin\alpha_T \tag{3.4.2}$$

Combining Eqs. (3.4.1) and (3.4.2) with Eq. (3.2.7) and the definition of lift coefficient, we have the **general formulation for steady climbing flight**,

$$\tfrac{1}{2}\rho V^2 S_w \left(C_{D_0} + C_{D_{0,L}} C_L + \frac{C_L^2}{\pi e R_A} \right) = T_A \cos\alpha_T - W\sin\gamma \tag{3.4.3}$$

$$\tfrac{1}{2}\rho V^2 S_w C_L = W\cos\gamma - T_A \sin\alpha_T \tag{3.4.4}$$

Equations (3.4.3) and (3.4.4) can be used to solve for the unknown lift coefficient and one additional unknown. If the airspeed and thrust available are known, we could use this formulation to solve for the climb angle. If the thrust available is known, we could also use the formulation to obtain the equilibrium airspeed for a given climb angle. On the other hand, we could also employ Eqs. (3.4.3) and (3.4.4) to determine the thrust necessary to support a given climb angle at a given airspeed.

The drag experienced during climbing flight is somewhat less than that for level flight. This is because, as can be seen from Eq. (3.4.4), the lift for climbing flight is less than the lift for level flight. Since the lift is reduced during climbing flight, the induced drag is also reduced and, as a result, the total drag is reduced. For example, consider an aircraft in a vertical climb having the thrust vector aligned with the direction of flight. For this special case, Eq. (3.4.4) shows that the lift, and hence the induced drag, are exactly zero. Of course, as Eq. (3.4.3) predicts, a vertical climb requires a thrust-to-weight ratio greater than 1. However, most airplanes have a thrust-to-weight ratio much less than 1. For such aircraft, the climb angle is always small and we can obtain an approximation for the rate of climb by using the level flight drag in Eq. (3.4.1).

Solving Eq. (3.4.1) for $\sin\gamma$, we have

$$\sin\gamma = \frac{T_A \cos\alpha_T - D}{W} \tag{3.4.5}$$

The rate of climb, V_c, is the vertical component of the airplane's velocity, i.e., the airspeed multiplied by the sine of the flight path angle. Thus, from Eq. (3.4.5) we have

$$V_c \equiv V\sin\gamma = \frac{VT_A\cos\alpha_T - VD}{W} \tag{3.4.6}$$

For an aircraft with low thrust-to-weight ratio, the climb angle is always small and we can obtain a conservative estimate for the rate of climb by using the level flight drag in Eq. (3.4.6). The level flight drag is related to the thrust required for level flight, T_R, according to Eq. (3.2.1). Thus, the rate of climb is approximated as

$$V_c = \frac{VT_A\cos\alpha_T - VT_R\cos\alpha_T}{W} \tag{3.4.7}$$

The airspeed multiplied by the thrust available and the cosine of the thrust angle is the dot product of the thrust vector with the velocity vector, which is the power available, P_A. The airspeed multiplied by the thrust required for level flight and the cosine of the thrust angle is the power required for level flight, as defined by Eq. (3.3.1). Thus we can write Eq. (3.4.7) as

$$V_c = \frac{P_A - P_R}{W} \tag{3.4.8}$$

The difference between the power available and the power required for level flight is called the *excess power*. For small thrust-to-weight ratio, the rate of climb can be approximated as the excess power divided by the total aircraft weight. This equation is not as simple as it looks. In general, both the power available and the power required are functions of airspeed and air density. The power required for steady level flight has been discussed and can be computed from either Eq. (3.3.6) or Eq. (3.3.7). In general, the power available and its dependence on airspeed, density, and throttle setting needs to be determined from engine tests.

In any case, at very high airspeeds the power required always exceeds the power available and the rate of climb is negative. This means that such airspeeds can only be achieved in a dive. The airspeed at which the full throttle power available matches the power required is the maximum level flight airspeed at the given altitude. The maximum rate of climb can be found graphically by plotting both the power available and the power required as a function of airspeed and finding the point at which the difference is maximum. If the power available is known in the form of an equation, we can find the maximum climb rate and the maximum climb rate airspeed analytically or numerically. Figures 3.4.2 and 3.4.3 shows how the thrust and power available might vary with airspeed and throttle setting for a typical general aviation aircraft at sea level.

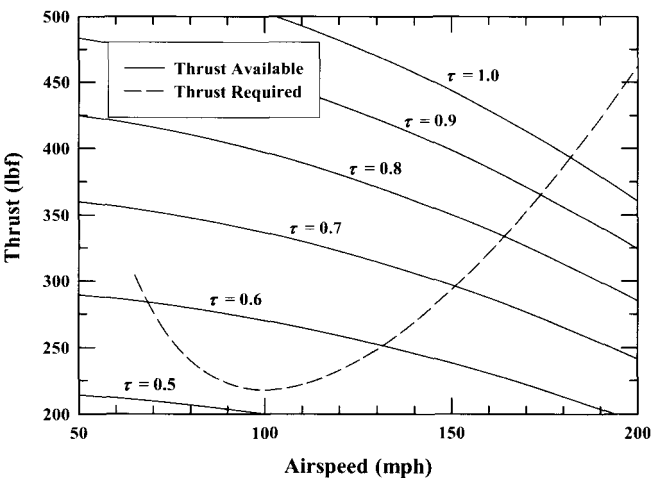


Figure 3.4.2. Thrust available and thrust required at standard sea level.

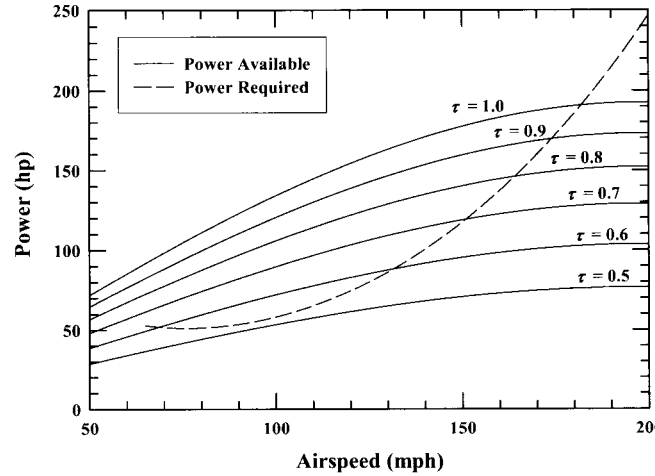


Figure 3.4.3. Power available and power required at standard sea level.

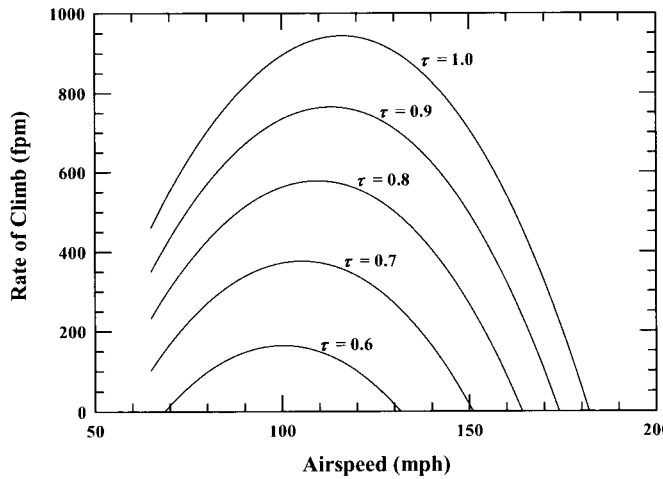


Figure 3.4.4. Rate of climb at standard sea level.

At any throttle setting, in steady level flight, the airplane will fly at the airspeed where the power available is just equal to the power required. If the power available exceeds the power required, the aircraft will accelerate or climb. If the power required exceeds the power available, the aircraft must decelerate or descend. The rate of climb, from Eq. (3.4.8), is the excess power divided by the weight and is shown in Fig. 3.4.4. Notice that the airspeed that results in the maximum rate of climb is greater than that for minimum power required. This is because for this particular power plant and operating point, the power available is increasing with airspeed.

As altitude increases, the power required increases and the power available decreases. Thus, the rate of climb will decrease with altitude. Figure 3.4.5 shows the power available and the power required, for the present aircraft, at 10,000 feet and Fig. 3.4.6 shows the rate of climb at the same altitude.

Notice that for this aircraft and power plant, the maximum rate of climb is reduced from more than 900 feet per minute at sea level to about 500 feet per minute at 10,000 feet. Since the rate of climb decreases with altitude, at some altitude the power available at the best climb airspeed will just match the power required and the airplane will not be

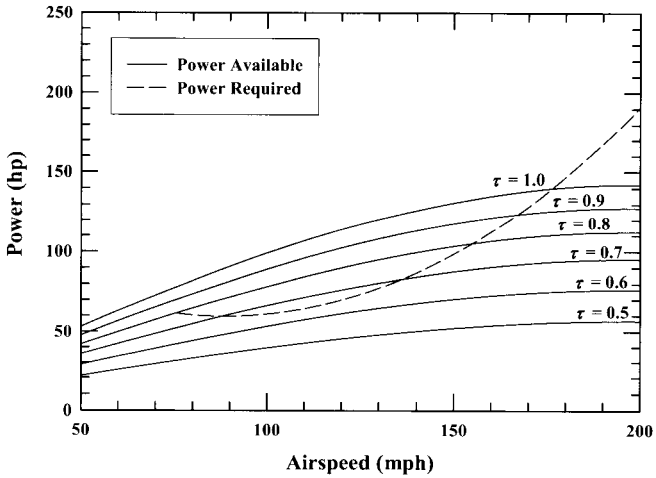


Figure 3.4.5. Power available and power required at 10,000 feet.

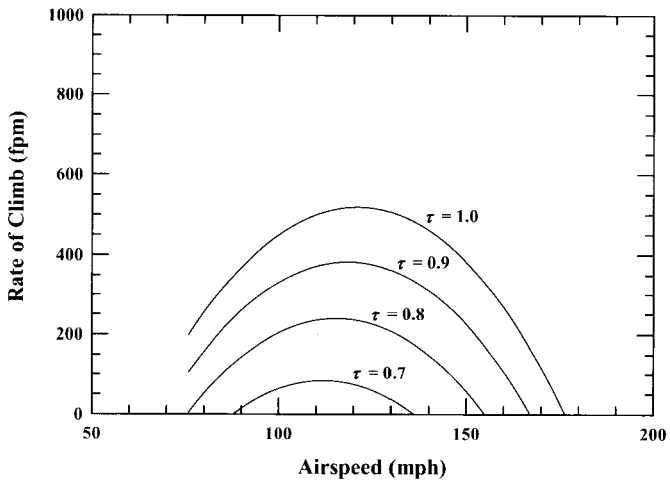


Figure 3.4.6. Rate of climb at 10,000 feet.

able to climb higher. This altitude is called the *absolute ceiling* for the aircraft. The *service ceiling* for an aircraft is defined to be the altitude at which the maximum rate of climb is reduced to 100 feet per minute.

Figures 3.4.4 and 3.4.6 show that at a given altitude and throttle setting, there are two airspeeds which can result in zero rate of climb. In most cases, only the faster of these two airspeeds is possible because the lower airspeed is usually less than stall.

When an airplane is flying in steady level flight at any given throttle setting, the power available is just equal to the power required, making the rate of climb zero. If the pilot slowly pulls back on the stick, the aircraft will slow down and climb. As the pilot continues to pull back on the stick, the airspeed will continue to decrease and the climb rate will increase until the maximum rate of climb for that throttle setting is reached. If the pilot continues to pull back on the stick after reaching the maximum rate of climb, the airspeed will continue to decrease but now the climb rate will begin to decrease as well. If the process continues, the wing will eventually stall.

Of course, this analysis was based on the assumption of a small climb angle, which means low thrust-to-weight ratio. Some fighter aircraft have a thrust-to-weight ratios greater than 1 and are capable of accelerating at a 90-degree climb angle. When the thrust-to-weight ratio is large, a climb analysis can still be carried out but Eq. (3.4.8) is no longer valid. For an aircraft with large thrust-to-weight ratio, Eqs. (3.4.3) and (3.4.4) must be used to compute the lift and induced drag. The thrust required for steady level flight cannot be substituted for the drag force in Eq. (3.4.6). The resulting analysis is somewhat more complex but still manageable.

For both jet engines and reciprocating engine-propeller combinations, power available is a function of throttle setting, airspeed, and air density. The actual maximum rate of climb for any aircraft must be determined either numerically or graphically from experimental data for the particular engine or engines used.

EXAMPLE 3.4.1. Consider the turbojet aircraft described in Example 3.2.1. For this aircraft the thrust available was approximated as being constant with airspeed and directly proportional to air density,

$$T_A = \tau \frac{\rho}{\rho_0} T_{A0}$$

where τ is a throttle setting expressed as a fraction of the full-throttle thrust and T_{A0} is the full-throttle thrust available at standard sea level. Assuming a thrust vector aligned with the flight path, determine the full-throttle rate of climb for an airspeed of 360 mph at sea level. Compute the rate of climb both with and without using the small-climb-angle approximation.

Solution. For this executive business jet we have

$$S_w = 320 \text{ ft}^2, \quad b_w = 54 \text{ ft}, \quad W = 20{,}000 \text{ lbf}, \quad T_{A0} = 6{,}500 \text{ lbf},$$
$$C_{D_0} = 0.023, \quad C_{D_0,L} = 0.0, \quad e = 0.82, \quad R_A = 9.1125,$$

$$V = 360 \text{ mph} = 528 \text{ ft/sec},$$

$$\sqrt{\frac{W/S_w}{\rho}} = \sqrt{\frac{20{,}000 \text{ lbf}/320 \text{ ft}^2}{0.0023769 \text{ slug/ft}^3}} = 162.16 \text{ ft/sec}, \quad R_V \equiv V \Big/ \sqrt{\frac{W/S_w}{\rho}} = 3.2561$$

Using the small-climb-angle approximation, the rate of climb computed from Eq. (3.4.8) is

$$V_c = \frac{P_A - P_R}{W}$$

For small thrust angles, the power available is the thrust available multiplied by the airspeed and the power required for steady level flight is given by Eq. (3.3.7). Thus we have

$$\begin{aligned} V_c &= \frac{T_A}{W} V - \frac{C_{D_0} \rho V^3}{2(W/S_w)} - C_{D_{0,L}} V - \frac{2(W/S_w)}{\pi e R_A \rho V} \\ &= \left(\frac{T_A}{W} R_V - \frac{C_{D_0}}{2} R_V^3 - C_{D_{0,L}} R_V - \frac{2}{\pi e R_A R_V} \right) \sqrt{\frac{W/S_w}{\rho}} \\ &= \left[\frac{6{,}500}{20{,}000} 3.2561 - \frac{0.023}{2} 3.2561^3 - 0.0 - \frac{2}{\pi(0.82)9.1125(3.2561)} \right] 162.16 \\ &= \underline{103.0 \text{ ft/sec} = 6{,}179 \text{ ft/min}} \end{aligned}$$

To obtain the rate of climb for this airplane and operating condition without using the small-climb-angle approximation, we start with Eqs. (3.4.3) and (3.4.4). Equation (3.4.4) can be solved for the cosine of the climb angle. For a thrust vector aligned with the flight path, this gives

$$\cos\gamma = \frac{\frac{1}{2}\rho V^2 S_w}{W} C_L \tag{3.4.9}$$

Using this result in Eq. (3.4.3) and rearranging, we have

$$\frac{\frac{1}{2}\rho V^2 S_w}{W} \left(C_{D_0} + C_{D_{0,L}} C_L + \frac{C_L^2}{\pi e R_A} \right) + \sqrt{1 - \left(\frac{\frac{1}{2}\rho V^2 S_w}{W} C_L \right)^2} = \frac{T_A}{W}$$

Using the known values for the aircraft, this equation reduces to

$$\sqrt{1.0 - 28.102 C_L^2} = 0.2031 - 0.2258 C_L^2$$

This is easily solved to yield the lift coefficient

$$C_L = 0.1850$$

Using this lift coefficient in Eq. (3.4.9), we have

$$\cos\gamma = \frac{\frac{1}{2}\rho V^2 S_w}{W} C_L = 0.9807$$

and

$$\gamma = 11.27^\circ$$

The rate of climb is the airspeed multiplied by the sine of the climb angle. Thus,

$$V_c = V\sin\gamma = \underline{103.2 \text{ ft/sec} = 6{,}194 \text{ ft/min}}$$

Notice that for this example, with a thrust-to-weight ratio of 0.325, the small-climb-angle approximation used in Eq. (3.4.8) is accurate to within 1 percent.

EXAMPLE 3.4.2. Consider the general aviation airplane described in Example 3.3.1. For this propeller driven aircraft the power available was approximated as being constant with airspeed and directly proportional to air density,

$$P_A = \tau\frac{\rho}{\rho_0}P_{A0}$$

where τ is a throttle setting expressed as a fraction of the full-throttle power available and P_{A0} is the full throttle power available at standard sea level. Using the small-climb-angle approximation, determine the maximum rate of climb for this airplane at both sea level and 10,000 feet.

Solution. For this airplane

$$S_w = 180 \text{ ft}^2, \quad b_w = 33 \text{ ft}, \quad W = 2{,}700 \text{ lbf}, \quad P_{A0} = 180 \text{ hp} = 99{,}000 \text{ ft}\cdot\text{lbf/sec},$$
$$C_{D_0} = 0.023, \quad C_{D_0,L} = 0.0, \quad e = 0.82, \quad R_A = 6.05, \quad W/S_w = 15.0 \text{ lbf/ft}^2$$

With the small-climb-angle approximation, the rate of climb is computed by using the power required from Eq. (3.3.7) in Eq. (3.4.8). For this airplane, we have

$$V_c = \frac{P_A - P_R}{W} = \tau\frac{\rho}{\rho_0}\frac{P_{A0}}{W} - \frac{C_{D_0}\rho V^3}{2(W/S_w)} - \frac{2(W/S_w)}{\pi e R_A \rho V}$$

Here again it is convenient to use the dimensionless velocity ratio

$$R_V \equiv V \Big/ \sqrt{\frac{W/S_w}{\rho}}$$

and the dimensionless power-to-weight ratio

$$R_{P/W} \equiv P_A \Big/ \left(W\sqrt{\frac{W/S_w}{\rho}} \right) = \tau \frac{\rho}{\rho_0} P_{A0} \Big/ \left(W\sqrt{\frac{W/S_w}{\rho}} \right)$$

Thus, for this airplane, the rate of climb can be written as

$$V_c = \left(R_{P/W} - \frac{C_{D0}}{2} R_V^3 - \frac{2}{\pi e R_A R_V} \right) \sqrt{\frac{W/S_w}{\rho}} \tag{3.4.10}$$

The velocity ratio that results in maximum rate of climb is found by differentiating the rate of climb with respect to velocity ratio and setting the result equal to zero. This gives

$$\frac{\partial V_c}{\partial R_V} = \left(-\frac{3C_{D0}}{2} R_V^2 + \frac{2}{\pi e R_A R_V^2} \right) \sqrt{\frac{W/S_w}{\rho}} = 0$$

or

$$R_V = \left(\frac{4}{3\pi e R_A C_{D0}} \right)^{1/4} = \left(\frac{4}{3\pi(0.82)(6.05)(0.023)} \right)^{1/4} = 1.3887$$

The maximum rate of climb is found by using this result in Eq. (3.4.10). For this airplane at sea level

$$R_{P/W} \equiv P_A \Big/ \left(W\sqrt{\frac{W/S_w}{\rho}} \right) = 0.462$$

$$(V_c)_{\max} =$$

$$\left(0.462 - \frac{0.023}{2}(1.3887)^3 - \frac{2}{\pi(0.82)(6.05)(1.3887)} \right) \sqrt{\frac{15.0 \text{ lbf/ft}^2}{0.0023769 \text{ slug/ft}^3}}$$

$$= \underline{26.91 \text{ ft/sec} = 1{,}615 \text{ ft/min}}$$

and at 10,000 feet

$$R_{P/W} \equiv P_A \Big/ \left(W\sqrt{\frac{W/S_w}{\rho}} \right) = 0.293$$

$$(V_c)_{\max} =$$

$$\left(0.293 - \frac{0.023}{2}(1.3887)^3 - \frac{2}{\pi(0.82)(6.05)(1.3887)}\right)\sqrt{\frac{15.0 \text{ lbf/ft}^2}{0.0017556 \text{ slug/ft}^3}}$$

$$= \underline{15.69 \text{ ft/sec} = 942 \text{ ft/min}}$$

EXAMPLE 3.4.3. For the turbojet aircraft described in Examples 3.2.1 and 3.4.1, use the small-climb-angle approximation and determine the maximum rate of climb at both sea level and 20,000 feet.

Solution. For this executive business jet at full throttle

$$R_{T/W} \equiv \frac{T_A}{W} = \frac{\rho}{\rho_0}\frac{T_{A0}}{W},$$

$$S_w = 320 \text{ ft}^2, \quad b_w = 54 \text{ ft}, \quad W = 20{,}000 \text{ lbf}, \quad T_{A0} = 6{,}500 \text{ lbf},$$

$$C_{D_0} = 0.023, \quad C_{D_{0,L}} = 0.0, \quad e = 0.82, \quad R_A = 9.1125,$$

$$W/S_w = 62.5 \text{ lbf/ft}^2$$

Using the small-climb-angle approximation, the rate of climb for this aircraft is

$$V_c = \frac{T_A}{W}V - \frac{C_{D_0}\rho V^3}{2(W/S_w)} - C_{D_{0,L}}V - \frac{2(W/S_w)}{\pi e R_A \rho V}$$

$$= \left(R_{T/W}R_V - \frac{C_{D_0}}{2}R_V^3 - C_{D_{0,L}}R_V - \frac{2}{\pi e R_A R_V}\right)\sqrt{\frac{W/S_w}{\rho}}$$

The velocity ratio at maximum climb rate is found from

$$\frac{\partial V_c}{\partial R_V} = \left(R_{T/W} - \frac{3C_{D_0}}{2}R_V^2 + \frac{2}{\pi e R_A R_V^2}\right)\sqrt{\frac{W/S_w}{\rho}} = 0$$

or

$$\frac{3C_{D_0}}{2}R_V^4 - R_{T/W}R_V^2 - \frac{2}{\pi e R_A} = 0$$

This equation is quadratic in the velocity ratio squared. Thus, at maximum rate of climb,

$$R_V^2 = \frac{R_{T/W}}{3C_{D_0}} \pm \sqrt{\left(\frac{R_{T/W}}{3C_{D_0}}\right)^2 + \frac{4}{3\pi e R_A C_{D_0}}}$$

where only the positive root is of interest. For this airplane at standard sea level,

$$R_{T/W} \equiv \frac{T_A}{W} = \frac{\rho}{\rho_0}\frac{T_{A0}}{W} = 0.325$$

$$R_V = \sqrt{\frac{R_{T/W}}{3C_{D_0}} + \sqrt{\left(\frac{R_{T/W}}{3C_{D_0}}\right)^2 + \frac{4}{3\pi e R_A C_{D_0}}}} = 3.11055$$

$$(V_c)_{\max} = \left(R_{T/W} R_V - \frac{C_{D_0}}{2} R_V^3 - C_{D_0,L} R_V - \frac{2}{\pi e R_A R_V}\right)\sqrt{\frac{W/S_w}{\rho}} = \underline{8{,}487 \text{ ft/min}}$$

and at 20,000 feet,

$$R_{T/W} \equiv \frac{T_A}{W} = \frac{\rho}{\rho_0}\frac{T_{A0}}{W} = 0.173$$

$$R_V = \sqrt{\frac{R_{T/W}}{3C_{D_0}} + \sqrt{\left(\frac{R_{T/W}}{3C_{D_0}}\right)^2 + \frac{4}{3\pi e R_A C_{D_0}}}} = 2.33800$$

$$(V_c)_{\max} = \left(R_{T/W} R_V - \frac{C_{D_0}}{2} R_V^3 - C_{D_0,L} R_V - \frac{2}{\pi e R_A R_V}\right)\sqrt{\frac{W/S_w}{\rho}} = \underline{4{,}066 \text{ ft/min}}$$

3.5. Fuel Consumption and Endurance

Another important performance parameter for an aircraft is fuel consumption during steady level flight. Fuel consumption is sometimes specified in terms of endurance. Endurance is defined as the total time that an aircraft can stay in the air on a tank of fuel. We can maximize endurance, for a given aircraft and fuel capacity, by minimizing the fuel consumption per unit time.

For fuel consumption analysis it is convenient to define the power-specific fuel consumption for a power plant, q_P, to be the weight of fuel consumption per unit time divided by the propulsive power available. In general, the power-specific fuel consumption for a given power plant is a function of air density, throttle setting, and airspeed,

$$q_P \equiv \frac{\dot{Q}}{P_A} = q_P(\rho, \tau, V) \tag{3.5.1}$$

where $\dot{Q}$ is the total weight of fuel consumed per unit time and P_A is the propulsive power available. The specific fuel consumption and its dependence on air density,

throttle setting, and airspeed for any particular power plant must be determined from power plant tests. Figure 3.5.1 shows how this specific fuel consumption for an internal combustion engine with a fixed-pitch propeller might vary with airspeed and throttle setting at sea level.

The empirical relation implied by Eq. (3.5.1) and shown hypothetically in Fig. 3.5.1 provides one equation relating the fuel consumption rate to the air density, throttle setting, and airspeed. Steady level flight imposes a second relationship between air density, throttle setting, and airspeed. The power available from the power plant can also be expressed as an empirical function of air density, throttle setting, and airspeed,

$$P_A = P_A(\rho, \tau, V) \tag{3.5.2}$$

In steady level flight, the power available must equal the power required. Using the small-thrust-angle approximation, from Eq. (3.3.7) the power required is given by

$$P_R = \left(\frac{C_{D_0} \rho V^3}{2(W/S_w)} + C_{D_0,L} V + \frac{2(W/S_w)}{\pi e R_A \rho V} \right) W \tag{3.5.3}$$

Thus, combining Eqs. (3.5.2) and (3.5.3), steady level flight requires that

$$P_A(\rho, \tau, V) = \left(\frac{C_{D_0} \rho V^3}{2(W/S_w)} + C_{D_0,L} V + \frac{2(W/S_w)}{\pi e R_A \rho V} \right) W \tag{3.5.4}$$

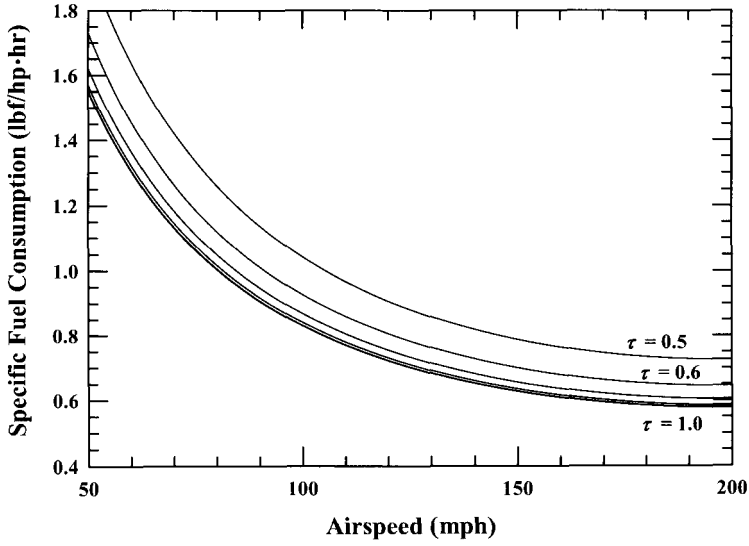


Figure 3.5.1. Specific fuel consumption for an aircraft power plant at standard sea level.

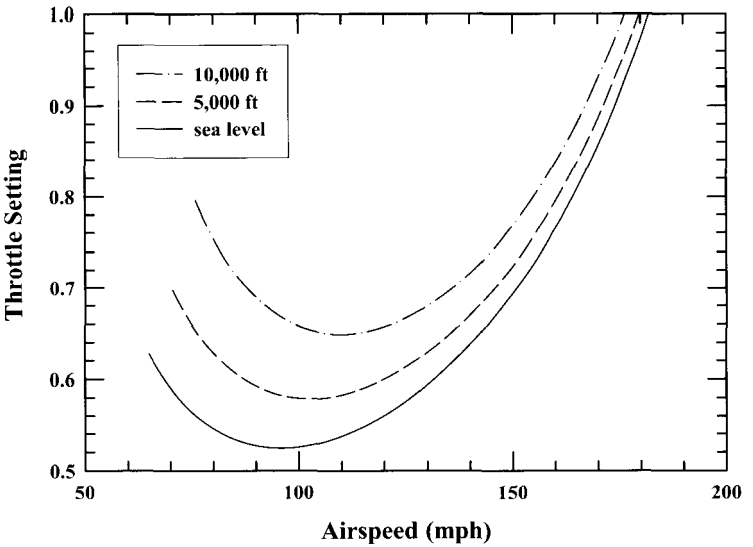


Figure 3.5.2. Throttle setting required for steady level flight.

Thus, steady level flight imposes a second relationship among the air density, throttle setting, and airspeed, as given by Eq. (3.5.4). At any given altitude and airspeed, this empirical relation determines the throttle setting necessary to maintain steady level flight. Figure 3.5.2 shows how the throttle setting required for steady level flight might vary with airspeed and altitude for a typical general aviation aircraft.

Combining the specific fuel consumption relation implied by Eq. (3.5.1) and the steady level flight requirement implied by Eq. (3.5.4), for a given aircraft and power plant we can eliminate the throttle setting and express specific fuel consumption for steady level flight as a function of only the airspeed and air density. Combining the specific fuel consumption relation shown in Fig. 3.5.1 with the steady level flight requirement shown in Fig. 3.5.2, we obtain the specific fuel consumption relation for steady level flight shown in Fig. 3.5.3.

The total fuel consumption rate is then found by multiplying the specific fuel consumption for steady level flight by the power required for steady level flight at the same airspeed. Figure 3.5.4 shows the total fuel consumption rate as a function of airspeed and altitude for the present example.

We notice that for this example, the fuel consumption rate has a minimum at some value of airspeed that is somewhat faster than the airspeed for minimum power required. This is because, for this example, the specific fuel consumption is decreasing with airspeed. If the specific fuel consumption were independent of airspeed, the airspeed for minimum fuel consumption rate would be equal to the airspeed for minimum power required. We also notice that the minimum fuel consumption rate and the airspeed required to attain minimum fuel consumption rate both increase with altitude for this example.

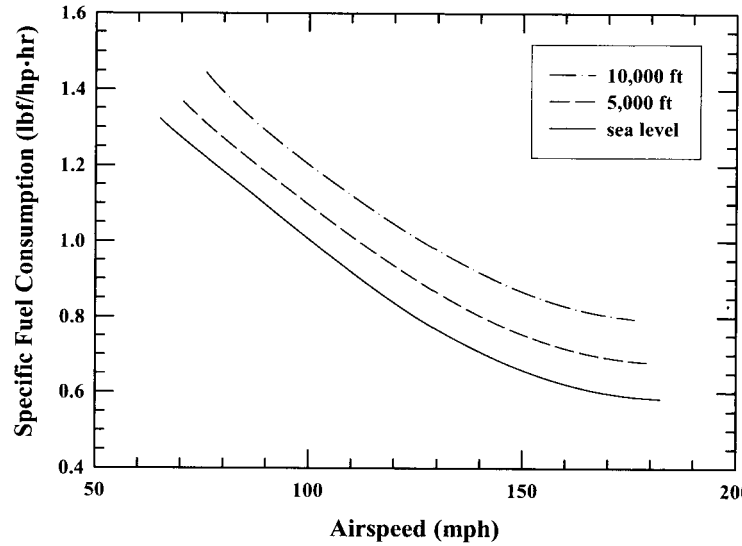


Figure 3.5.3. Specific fuel consumption for steady level flight.

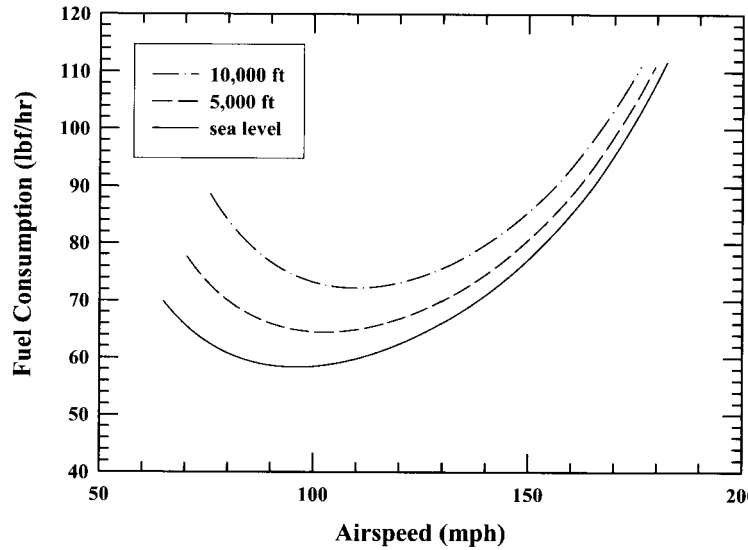


Figure 3.5.4. Fuel consumption rate for steady level flight.

It is also important to recognize that because fuel consumption depends on power required and power required depends on weight, the fuel consumption rate will vary with the gross weight of the aircraft. For the example considered here, Figure 3.5.5 shows the fuel consumption at sea level as a function of airspeed for three different values of gross vehicle weight. Notice that the fuel consumption rate, at any airspeed, increases

with gross vehicle weight (GVW). Also notice that the airspeed required to attain minimum fuel consumption rate increases with gross vehicle weight. This means that to maximize endurance, the pilot should gradually decrease airspeed as fuel is burned off and the gross vehicle weight is decreased. Figure 3.5.6 shows how the airspeed at sea level should be varied with gross weight for the aircraft under consideration.

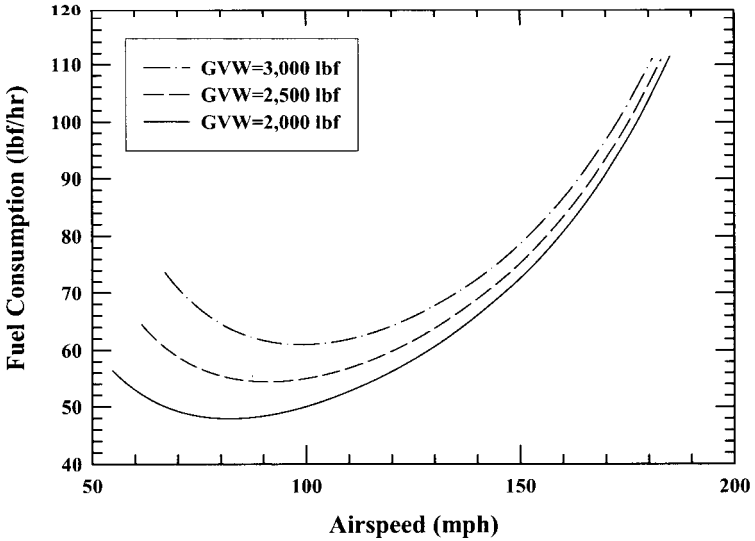


Figure 3.5.5. Effect of gross weight on the fuel consumption rate at sea level.

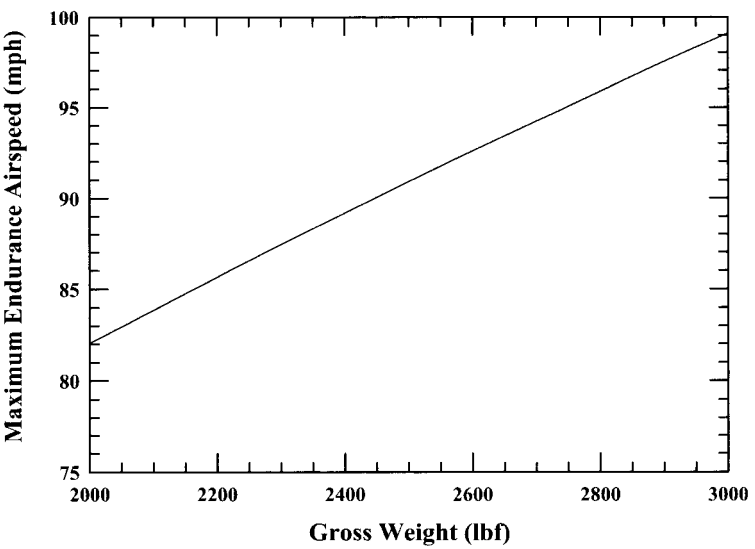


Figure 3.5.6. Maximum endurance airspeed as a function of gross weight at sea level.

The weight of the aircraft decreases with time as a result of the fuel that is burned. Thus, the time rate of change in the gross aircraft weight is the negative of the fuel consumption rate,

$$\frac{dW}{dt} = -\dot{Q} \tag{3.5.5}$$

The maximum endurance, E_{max}, is the time required to decrease the aircraft weight from the gross weight with fuel tanks full, W_f, to the gross weight with fuel tanks empty, W_e. This is found by rearranging Eq. (3.5.5) and integrating,

$$E_{max} = \int_0^{E_{max}} dt = -\int_{W_f}^{W_e} \frac{1}{\dot{Q}} dW = \int_{W_e}^{W_f} \frac{1}{\dot{Q}} dW \tag{3.5.6}$$

The inverse of the total fuel consumption rate, which appears in Eq. (3.5.6), is the instantaneous specific endurance, i.e., the flight time per unit weight of fuel burned. Figure 3.5.7 shows how the specific endurance varies with gross weight at sea level for this same hypothetical aircraft. The result shown in this figure is based on maintaining the maximum endurance airspeed at all times. Therefore, it represents the maximum possible specific endurance. As specified by Eq. (3.5.6), the total maximum endurance is simply the area under this curve between W_e and W_f.

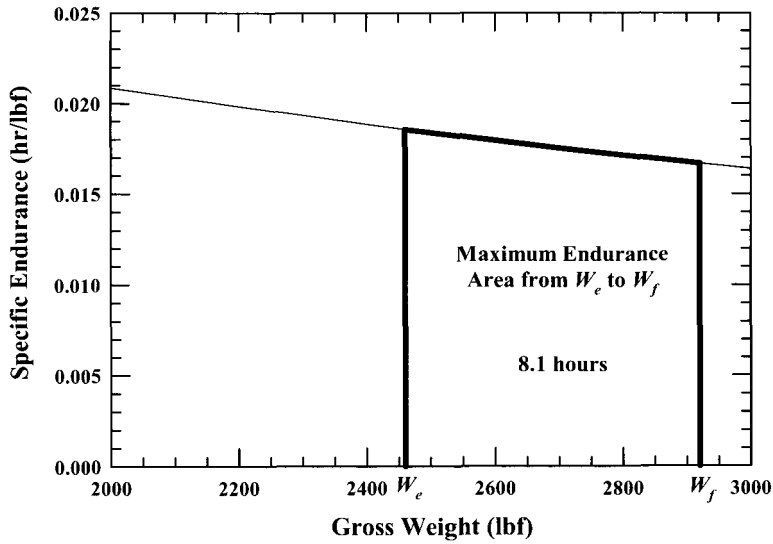


Figure 3.5.7. Maximum specific endurance as a function of gross weight at sea level. The maximum total endurance is the area under this curve between the aircraft gross weight with fuel tanks empty and the aircraft gross weight with fuel tanks full.

EXAMPLE 3.5.1. As discussed in Example 3.3.1, an internal combustion engine combined with a variable-pitch propeller can be adjusted, either manually by the pilot or automatically with a governor mechanism, to produce an available power that is nearly independent of airspeed over the range of airspeeds encountered in normal flight. For such a power plant, the specific fuel consumption based on propulsive power available can be written as

$$q_P \equiv \dot{Q}/P_A = \dot{Q}/\eta_p P_b = q_b/\eta_p$$

where η_p is the propeller efficiency, P_b is the brake power developed by the engine, and q_b is the specific fuel consumption for the engine based on brake power. With the fuel mixture and propeller pitch properly adjusted, both the specific fuel consumption for the engine and the propeller efficiency are very nearly independent of airspeed and altitude. Thus, as a first approximation, we can model this type of power plant as having a specific fuel consumption based on propulsive power available that is constant with both airspeed and air density.

Consider the general aviation aircraft described in Example 3.3.1. The specific fuel consumption for the engine based on brake power is 0.5 lbf/hp·hr and the propeller efficiency is 80 percent. The dry weight for the airplane is 2,300 lbf and the fuel capacity is 400 lbf. Assuming that the pilot maintains the maximum endurance airspeed at all times, determine the total endurance at sea level.

Solution. For this airplane

$$S_w = 180 \text{ ft}^2, \quad b_w = 33 \text{ ft}, \quad W_f = 2{,}700 \text{ lbf}, \quad W_e = 2{,}300 \text{ lbf},$$
$$C_{D_0} = 0.023, \quad C_{D_0,L} = 0.0, \quad e = 0.82, \quad R_A = 6.05,$$
$$q_P = q_b/\eta_p = 0.625 \text{ lbf/hp·hr} = 3.157 \times 10^{-7} \text{ ft}^{-1}$$

The specific endurance is the inverse of the total fuel consumption rate and, for steady level flight, the power available must equal the power required,

$$1/\dot{Q} = 1/q_P P_A = 1/q_P P_R$$

For this airplane the power required is

$$P_R = DV$$
$$= \tfrac{1}{2}\rho V^2 S_w \left(C_{D_0} + \frac{C_L^2}{\pi e R_A} \right) V = \tfrac{1}{2}\rho V^2 S_w \left[C_{D_0} + \frac{1}{\pi e R_A} \left(\frac{W}{\tfrac{1}{2}\rho V^2 S_w} \right)^2 \right] V$$
$$= \left(\frac{C_{D_0}\rho V^3}{2(W/S_w)} + \frac{2(W/S_w)}{\pi e R_A \rho V} \right) W = \left(\frac{C_{D_0}}{2} R_V^3 + \frac{2}{\pi e R_A R_V} \right) W \sqrt{\frac{W/S_w}{\rho}}$$

Thus, for this airplane, the specific endurance is

$$\frac{1}{\dot{Q}} = \frac{1}{q_P P_R} = \frac{1}{q_P\left(\frac{C_{D_0}}{2}R_V^3 + \frac{2}{\pi e R_A R_V}\right)W\sqrt{\frac{W/S_w}{\rho}}} \tag{3.5.7}$$

The velocity ratio that results in maximum specific endurance is found by differentiating the specific endurance with respect to velocity ratio and setting the result equal to zero. This gives

$$R_V = \left(\frac{4}{3\pi e R_A C_{D_0}}\right)^{1/4}$$

Using this result in Eq. (3.5.7), the maximum instantaneous specific endurance for this airplane is

$$\frac{1}{\dot{Q}} = \frac{(3\pi e R_A)^{3/4}\sqrt{\rho}}{\sqrt{32}\, q_P C_{D_0}^{1/4} W\sqrt{W/S_w}}$$

From Eq. (3.5.6) the maximum constant-altitude endurance at sea level is

$$E_{\max} = \int_{W_e}^{W_f}\frac{1}{\dot{Q}}dW = \int_{W_e}^{W_f}\frac{(3\pi e R_A)^{3/4}\sqrt{\rho}}{\sqrt{32}\, q_P C_{D_0}^{1/4} W\sqrt{W/S_w}}dW$$

$$= \frac{(3\pi e R_A)^{3/4}\sqrt{\rho S_w}}{\sqrt{32}\, q_P C_{D_0}^{1/4}}\int_{W_e}^{W_f}\frac{dW}{W^{3/2}}$$

$$= \frac{2(3\pi e R_A)^{3/4}}{\sqrt{32}\, C_{D_0}^{1/4}}\left(\frac{1}{\sqrt{W_e}} - \frac{1}{\sqrt{W_f}}\right)\frac{\sqrt{\rho S_w}}{q_P}$$

$$= \frac{2[3\pi(0.82)(6.05)]^{3/4}}{\sqrt{32}\,(0.023)^{1/4}}\left(\frac{1}{\sqrt{2{,}300\ \text{lbf}}} - \frac{1}{\sqrt{2{,}700\ \text{lbf}}}\right) \times \frac{\sqrt{0.0023769\ \text{slug/ft}^3\,(180\ \text{ft}^2)}}{3.157\times10^{-7}\ \text{ft}^{-1}}$$

$$= \underline{54{,}030\ \text{sec} = 15.0\ \text{hr}}$$

It should be noted that for this propeller-driven aircraft, the maximum endurance is proportional to the square root of the air density. Thus, endurance is shortened as altitude is increased.

3.6. Fuel Consumption and Range

For most aircraft applications, it is not appropriate to optimize fuel consumption in terms of endurance. Fuel consumption is usually specified in terms of range. *Range* is defined as the total distance that an aircraft can travel on a tank of fuel. We can maximize range for a given aircraft and fuel capacity by minimizing fuel consumption per unit distance. While fuel consumption with time is normally expressed as a fuel consumption rate, for example in pounds per hour, the consumption of fuel with distance is not usually expressed in terms of fuel consumption per unit distance but rather, in terms of distance per unit fuel consumption. For an automobile this is commonly expressed in miles per gallon. For an aircraft, weight is more important than volume, so it is convenient to express the fuel consumption with distance in terms of distance traveled per unit weight of fuel consumed. This is the specific range for the aircraft, r_s, or the inverse of the fuel consumption per unit distance. Distance traveled over the ground per unit weight of fuel consumed is the distance traveled per unit time or the ground speed, V_g, divided by the weight of fuel consumed per unit time,

$$r_s \equiv \frac{V_g}{\dot{Q}} \tag{3.6.1}$$

In the performance measures that we have considered to this point, the only velocity that has been important has been the airspeed of the aircraft. Here we see that the range of an aircraft depends not only on airspeed but on ground speed as well. For level flight, the relationship among ground speed, airspeed, and wind speed is shown in Fig. 3.6.1.

We see from Fig. 3.6.1 that ground speed for an aircraft depends on the speed and direction of the wind as well as airspeed and heading. If an aircraft is flying directly into a headwind, the ground speed will be less than the airspeed by an amount equal to the wind speed. If an aircraft is flying directly with a tailwind, the ground speed will be equal to the sum of the airspeed and wind speed. A crosswind will also affect the ground speed of an aircraft because, to maintain a specified track over the ground, the pilot must *crab* into the wind at an angle to the desired line of flight. When flying in a direct crosswind, only one component of the airspeed contributes to the ground speed. The other component must balance the crosswind to keep the aircraft from drifting off track.

In Fig. 3.6.1 the angle ψ_g is called the *ground track*, ψ is called the *heading*, and ψ_w is the wind direction. The angle φ_c is called the *crab angle*, and is equal to the difference between the heading and the ground track. The angle φ_w, the *wind-track angle*, is equal to the difference between the wind direction and the ground track. From this figure we see that the ground speed, V_g, is related to the airspeed, V, and the wind speed, V_w, according to

$$V_g = \sqrt{V^2 - V_w^2 \sin^2 \varphi_w} - V_w \cos \varphi_w \tag{3.6.2}$$

The fuel consumption per unit time is the specific fuel consumption multiplied by the power available. For an aircraft in steady level flight, the power available must equal the power required, which is the product of the drag and the airspeed. Thus, the fuel consumption per unit time for steady level flight can be written as

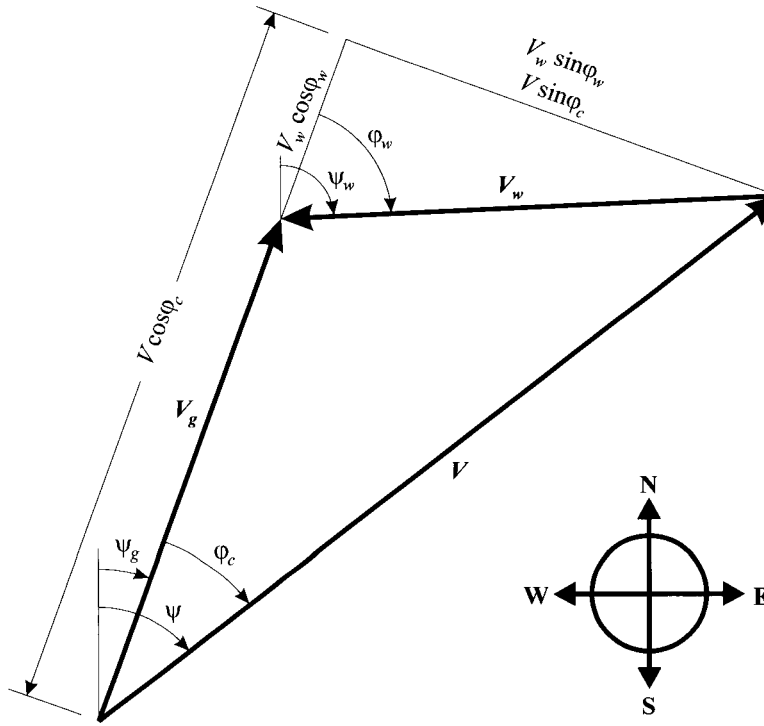


Figure 3.6.1. Relationship among ground speed, airspeed, and wind speed for level flight.

$$\dot{Q} = q_P D V \tag{3.6.3}$$

Using the small-thrust-angle approximation, the drag is equal to the thrust required as given by Eq. (3.2.25),

$$D = \left(\frac{\frac{1}{2}\rho V^2 C_{D_0}}{W/S_w} + C_{D_{0,L}} + \frac{W/S_w}{\frac{1}{2}\pi e R_A \rho V^2} \right) W \tag{3.6.4}$$

Combining Eqs. (3.6.1) and (3.6.3), the specific range can be written

$$r_s = \frac{V_g}{q_P D V} \tag{3.6.5}$$

From Eqs. (3.6.4) and (3.6.5) we see that because the drag has a minimum at some particular value of airspeed, the specific range will exhibit a maximum with airspeed. However, the maximum range airspeed is not necessarily the minimum drag airspeed.

To find the airspeed that will maximize the specific range for any particular wind speed and direction, we differentiate Eq. (3.6.5) with respect to airspeed and set the result to zero,

$$\frac{\partial r_s}{\partial V} = \frac{1}{q_P DV}\frac{\partial V_g}{\partial V} - \frac{V_g}{q_P^2 DV}\frac{\partial q_P}{\partial V} - \frac{V_g}{q_P D^2 V}\frac{\partial D}{\partial V} - \frac{V_g}{q_P DV^2} = 0 \tag{3.6.6}$$

or

$$\frac{V}{D}\frac{\partial D}{\partial V} = \frac{V}{V_g}\frac{\partial V_g}{\partial V} - \frac{V}{q_P}\frac{\partial q_P}{\partial V} - 1 \tag{3.6.7}$$

From Eq. (3.6.2) we can write

$$\frac{V}{V_g}\frac{\partial V_g}{\partial V} = \left(\frac{V}{\sqrt{V^2 - V_w^2 \sin^2\varphi_w} - V_w \cos\varphi_w}\right)\left(\frac{V}{\sqrt{V^2 - V_w^2 \sin^2\varphi_w}}\right) = \frac{V}{V - V_{eh}} \tag{3.6.8}$$

where V_{eh} can be thought of as an *effective headwind*, that is, the velocity of a pure headwind that would produce the same ground speed as the actual wind. This effective headwind speed is given by

$$V_{eh} = V_w\left[\cos\varphi_w\sqrt{1-(V_w/V)^2\sin^2\varphi_w} + (V_w/V)\sin^2\varphi_w\right] \tag{3.6.9}$$

Using Eqs. (3.6.8) and (3.6.4) in Eq. (3.6.7), at the airspeed that gives maximum specific range, we require that

$$\begin{aligned}\frac{V}{D}\frac{\partial D}{\partial V} &= \left(\frac{\rho V^2 C_{D_0}}{W/S_w} - \frac{4W/S_w}{\pi e R_A \rho V^2}\right)\Bigg/\left(\frac{\frac{1}{2}\rho V^2 C_{D_0}}{W/S_w} + C_{D_{0,L}} + \frac{W/S_w}{\frac{1}{2}\pi e R_A \rho V^2}\right) \\ &= \frac{V}{V - V_{eh}} - \frac{V}{q_P}\frac{\partial q_P}{\partial V} - 1 = \frac{V_{eh}}{V - V_{eh}} - \frac{V}{q_P}\frac{\partial q_P}{\partial V}\end{aligned} \tag{3.6.10}$$

Figure 3.6.2 shows how the term on the left-hand side of Eq. (3.6.10) varies with airspeed for a typical general aviation aircraft. From this figure we see that the left-hand side of Eq. (3.6.10) is a monotonically increasing function of airspeed. We also see that increasing altitude moves the curve to the right, in the direction of higher airspeed. The exact shape and position of the curves will vary with aircraft design and operating conditions, but these general characteristics hold for any aircraft. Since the left-hand side of Eq. (3.6.10) is always increasing with airspeed, anything that causes the right-hand side of this equation to increase will cause the maximum range airspeed to increase and anything that will cause the right-hand side to decrease will cause the maximum range airspeed to decrease.

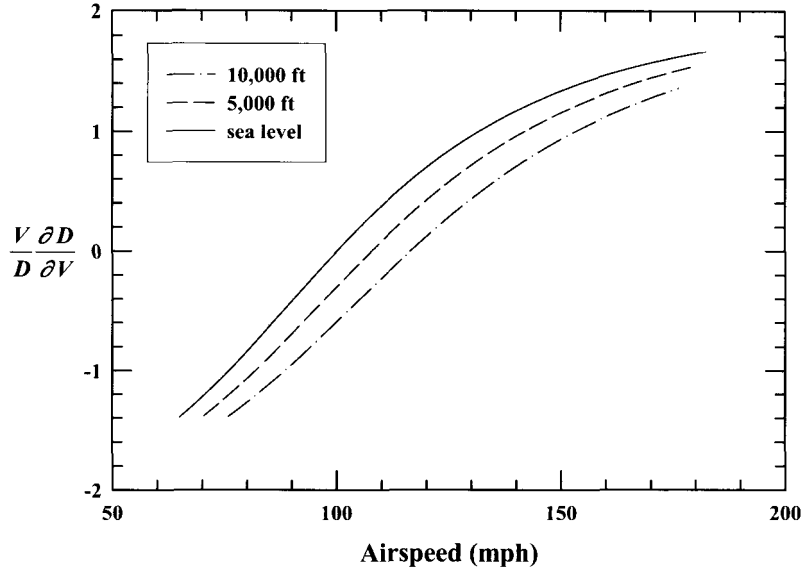


Figure 3.6.2. Left-hand side of Eq. (3.6.10).

Thus we see from Eq. (3.6.10) that if both the change in specific fuel consumption with respect to airspeed and the wind speed are zero, the maximum range airspeed will be equal to the airspeed that results in minimum drag. We see further that the maximum range airspeed will increase as the change in specific fuel consumption with respect to airspeed decreases. Furthermore, a headwind will increase the maximum range airspeed, a tailwind will decrease the maximum range airspeed, and any crosswind will always increase the airspeed required for maximum range.

Before we can determine the maximum range airspeed and the maximum specific range for any particular aircraft, we must know how the thrust available and the specific fuel consumption depend on air density, throttle setting, and airspeed for the specific power plant that is being used. As has been mentioned previously, these relationships need to be determined from engine tests. Once these experimental relationships are available, we can find the throttle setting that will result in steady level flight at any given airspeed and altitude, by setting the power available from the power plant equal to the power required by the airframe for steady level flight. For the example that we have been considering, this relationship among throttle setting, airspeed, and altitude is shown in Fig. 3.5.2.

Using this relationship for throttle setting as a function of airspeed and air density, which is imposed by the condition of steady level flight, we can eliminate throttle setting from the relationship for specific fuel consumption as a function of air density, throttle setting, and airspeed. This gives the specific fuel consumption for steady level flight as a function of only airspeed and air density. Figure 3.5.3 shows this relationship for the present example.

We can now use this relationship with Eqs. (3.6.2) and (3.6.4) in Eq. (3.6.5) to obtain the specific range as a function of airspeed, air density, wind speed, and wind direction. For the aircraft that we have been using, Fig. 3.6.3 shows how the specific range depends on airspeed and altitude for zero wind. Figure 3.6.4 shows the specific range at sea level for four different wind conditions. Notice that the wind affects both the maximum specific range and the maximum range airspeed. As the wind speed approaches the minimum drag airspeed for the airframe, this effect becomes very large.

The airspeed that results in maximum specific range can be found by solving Eq. (3.6.10) for the airspeed. As was the case for the maximum endurance airspeed, the maximum range airspeed is a function of aircraft gross weight. In general, the maximum range airspeed will be a function of weight, wind, and air density. For the current example, Fig. 3.6.5 shows the maximum range airspeed at sea level as a function of gross weight under four different wind conditions. For the purpose of comparison, the maximum endurance airspeed is also included here.

Comparing Figs. 3.2.2 and 3.6.4 we see that the airspeed required for maximum range, even with a 50-mile per hour tailwind, is considerably higher than the minimum drag airspeed. This is a function of the performance of the power plant. For this example, with a gross weight of 3,000 pounds, the airframe has minimum drag at about 100 miles per hour. If the specific fuel consumption were independent of airspeed, this would be the maximum range airspeed for no wind. However, as can be seen from Fig. 3.5.1, the specific fuel consumption for this power plant is minimum at an airspeed of almost 200 miles per hour. The net result is a trade-off between minimizing the drag and minimizing the specific fuel consumption, which results in a no-wind maximum range airspeed of about 135 mph.

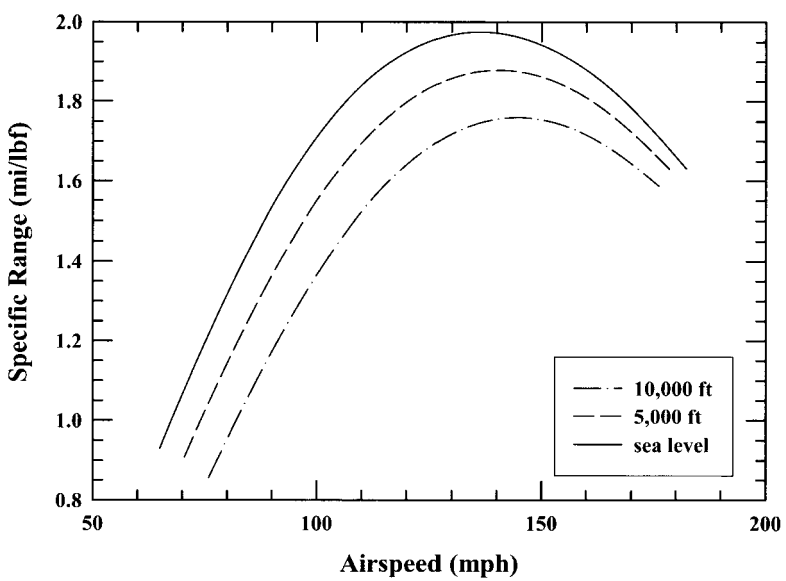


Figure 3.6.3. Specific range as a function of airspeed and altitude with zero wind.

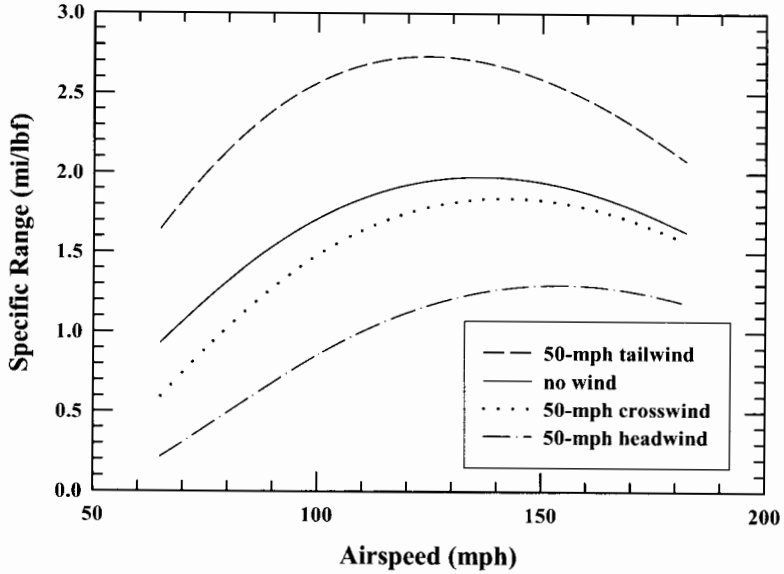


Figure 3.6.4. Specific range at sea level as a function of airspeed and wind.

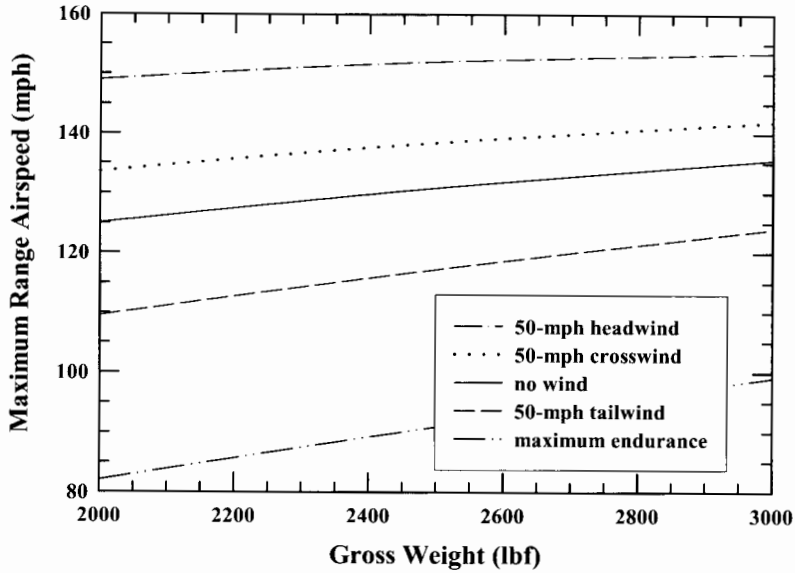


Figure 3.6.5. Maximum range airspeed as a function of gross weight at sea level.

It is also important to notice that the airspeed required for maximum range is considerably higher than that required for maximum endurance, with the same engine and airframe. This is true in general, independent of the power plant performance characteristics. The zero wind maximum range airspeed is related to the minimum drag

airspeed in the same way that the maximum endurance airspeed is related to the airspeed for minimum power required. Since the airspeed for minimum power required is always less then the airspeed for minimum drag, the maximum endurance airspeed will always be less than the zero wind maximum range airspeed.

Using the maximum range airspeed in Eq. (3.6.5), we obtain the maximum possible specific range for a given weight, wind, and air density. For this example, Fig. 3.6.6 shows how the maximum specific range at sea level varies with gross weight and wind.

As the aircraft travels, fuel is burned and the gross weight of the aircraft decreases. The specific range is the negative of the change in distance with respect to gross weight,

$$\frac{dx_f}{dW} = -r_s \tag{3.6.11}$$

where x_f is the distance traveled over the ground. The maximum range, $R_{\max}$, is found by integrating Eq. (3.6.11) from the gross weight with fuel tanks full, W_f, to the gross weight with fuel tanks empty, W_e,

$$R_{\max} = \int_0^{R_{\max}} dx_f = -\int_{W_f}^{W_e} r_s \, dW = \int_{W_e}^{W_f} r_s \, dW \tag{3.6.12}$$

Thus, the maximum range for any of the wind conditions shown in Fig. 3.6.6 would be the area under the curve for that wind condition between W_e and W_f. This is shown for no wind at standard sea level in Fig. 3.6.7. Figure 3.6.8 shows how the maximum range at sea level is affected by wind.

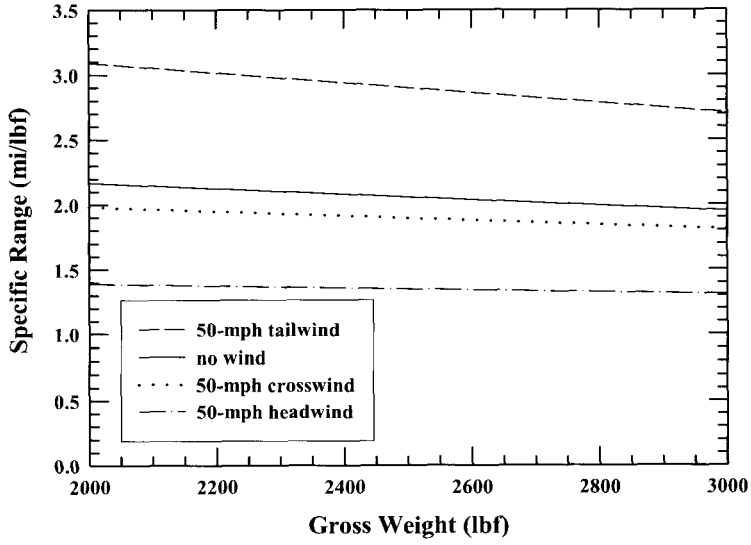


Figure 3.6.6. Maximum specific range as a function of gross weight at sea level.

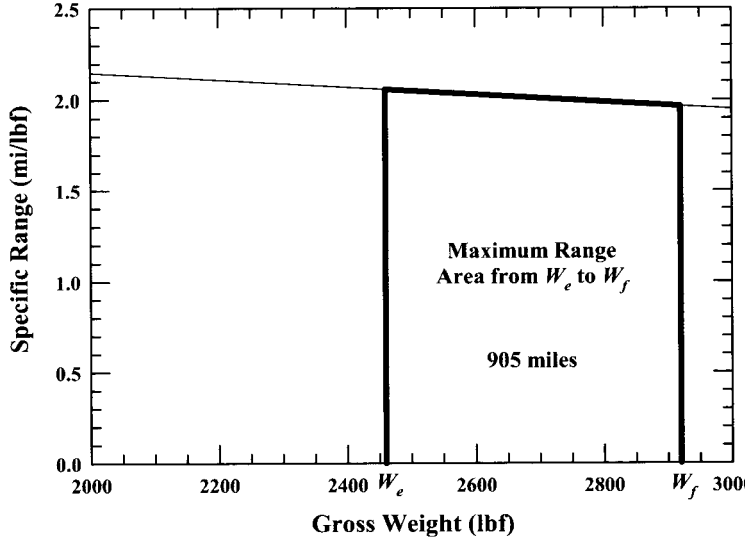


Figure 3.6.7. Maximum range for no wind at sea level.

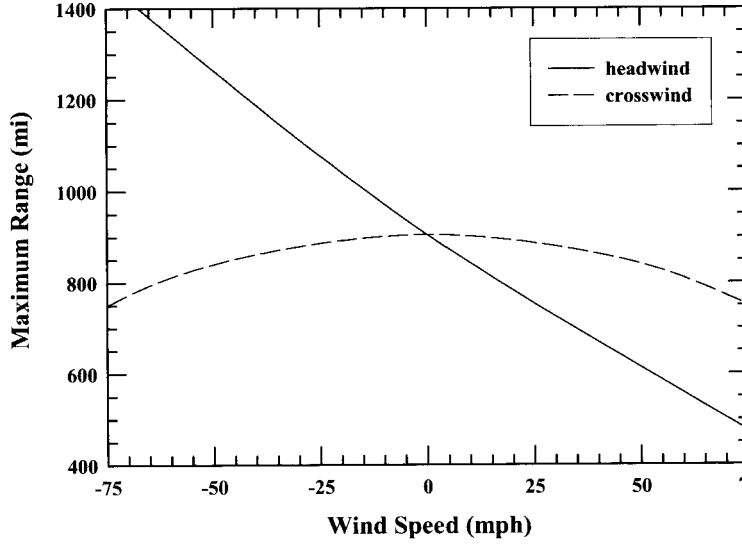


Figure 3.6.8. Effect of wind on maximum range.

EXAMPLE 3.6.1. For the propeller-driven general aviation aircraft and power plant described in Example 3.5.1, assuming that the pilot maintains the maximum range airspeed at all times, determine the maximum range for this aircraft with no wind at sea level.

Solution. For this airplane

$$S_w = 180 \text{ ft}^2, \quad b_w = 33 \text{ ft}, \quad W_f = 2{,}700 \text{ lbf}, \quad W_e = 2{,}300 \text{ lbf},$$
$$C_{D_0} = 0.023, \quad C_{D_0,L} = 0.0, \quad e = 0.82, \quad R_A = 6.05,$$
$$q_P = q_b/\eta_p = 0.625 \text{ lbf/hp·hr} = 3.157\times10^{-7} \text{ ft}^{-1}$$

The specific range is the ground speed divided by the total fuel consumption rate. The total fuel consumption rate is the specific fuel consumption multiplied by the power available. However, for steady level flight with no wind, the power available is equal to the power required and the ground speed is equal to the airspeed. Thus, we have

$$r_s \equiv \frac{V_g}{\dot{Q}} = \frac{V_g}{q_P P_A} = \frac{V}{q_P P_R}$$

For this airplane the power required is

$$\begin{aligned} P_R &= DV = \tfrac{1}{2}\rho V^2 S_w \left(C_{D_0} + \frac{C_L^2}{\pi e R_A} \right) V \\ &= \tfrac{1}{2}\rho V^2 S_w \left[C_{D_0} + \frac{1}{\pi e R_A} \left(\frac{W}{\frac{1}{2}\rho V^2 S_w} \right)^2 \right] V \\ &= \left(\frac{C_{D_0}\rho V^3}{2(W/S_w)} + \frac{2(W/S_w)}{\pi e R_A \rho V} \right) W = \left(\frac{C_{D_0}}{2} R_V^3 + \frac{2}{\pi e R_A R_V} \right) W \sqrt{\frac{W/S_w}{\rho}} \end{aligned}$$

Thus, for this airplane, the no-wind specific range is

$$\begin{aligned} r_s &= \frac{V}{q_P P_R} = \frac{V}{q_P \left(\frac{C_{D_0}}{2} R_V^3 + \frac{2}{\pi e R_A R_V} \right) W \sqrt{\frac{W/S_w}{\rho}}} \\ &= \frac{R_V}{q_P \left(\frac{C_{D_0}}{2} R_V^3 + \frac{2}{\pi e R_A R_V} \right) W} \end{aligned} \tag{3.6.13}$$

The velocity ratio that results in maximum specific range is found by differentiating the specific range with respect to velocity ratio and setting the result equal to zero. This gives

$$R_V = \left(\frac{4}{\pi e R_A C_{D_0}} \right)^{1/4}$$

Using this result in Eq. (3.6.13), the maximum instantaneous specific range for this airplane is

$$r_s = \sqrt{\frac{\pi e R_A}{4C_{D_0}}}\,\frac{1}{q_P W}$$

From Eq. (3.6.12) the maximum range is

$$R_{\max} = \int_{W_e}^{W_f} r_s\,dW = \int_{W_e}^{W_f} \sqrt{\frac{\pi e R_A}{4C_{D_0}}}\,\frac{1}{q_P W}\,dW = \sqrt{\frac{\pi e R_A}{4C_{D_0}}}\,\frac{1}{q_P}\int_{W_e}^{W_f}\frac{dW}{W}$$

$$= \sqrt{\frac{\pi e R_A}{4C_{D_0}}}\,\frac{1}{q_P}\ln\left(\frac{W_f}{W_e}\right)$$

$$= \sqrt{\frac{\pi(0.82)(6.05)}{4(0.023)}}\,\frac{1}{3.157\times10^{-7}\ \text{ft}^{-1}}\ln\left(\frac{2{,}700\ \text{lbf}}{2{,}300\ \text{lbf}}\right)$$

$$= \underline{6.611\times10^{6}\ \text{ft} = 1{,}252\ \text{mi}}$$

It should be noted that while the maximum endurance for this particular propeller-driven aircraft is proportional to the square root of air density, the maximum range is completely independent of air density. This is a result of the performance characteristics of the particular power plant being used. A very different result is obtained for a turbojet engine, as seen in the next example.

EXAMPLE 3.6.2. As discussed in Example 3.2.1, a turbojet engine produces a thrust that is nearly independent of airspeed and directly proportional to air density. The fuel consumption rate for a turbojet engine is very nearly proportional to the thrust produced by the engine, independent of airspeed or altitude. For this reason, fuel consumption for a turbojet engine is often expressed in terms of a thrust-specific fuel consumption, q_T,

$$q_T \equiv \frac{\dot{Q}}{T_A}$$

As a first approximation, we can assume that the thrust-specific fuel consumption for a turbojet engine is constant. Thus, for a turbojet engine, the specific fuel consumption based on propulsive power available can be conveniently written as

$$q_P \equiv \frac{\dot{Q}}{P_A} = \frac{\dot{Q}}{T_A V} = \frac{q_T}{V}$$

Consider the executive business jet described in Example 3.2.1. The thrust-specific fuel consumption for the engine is 0.6 lbf-fuel/hr/lbf-thrust, the dry weight

of the airplane is 12,000 lbf, and the fuel capacity is 8,000 lbf. Assuming that the pilot maintains the maximum range airspeed at all times, determine the maximum range for this aircraft with no wind at both sea level and 20,000 feet.

Solution. For this airplane

$$S_w = 320\ \text{ft}^2, \quad b_w = 54\ \text{ft}, \quad W_f = 20{,}000\ \text{lbf}, \quad W_e = 12{,}000\ \text{lbf},$$
$$C_{D_0} = 0.023, \quad C_{D_{0,L}} = 0.0, \quad e = 0.82, \quad R_A = 9.1125,$$
$$q_T = 0.6\ \text{lbf/hr}\cdot\text{lbf} = 1.667\times10^{-4}\ \text{sec}^{-1}$$

With no wind, the specific range for this aircraft is

$$r_s \equiv \frac{V_g}{\dot{Q}} = \frac{V_g}{q_P P_A} = \frac{V}{q_P P_R} = \frac{V^2}{q_T P_R}$$

Following Example 3.6.1, the power required is

$$P_R = \left(\frac{C_{D_0}\rho V^3}{2(W/S_w)} + \frac{2(W/S_w)}{\pi e R_A \rho V}\right) W = \left(\frac{C_{D_0}}{2} R_V^3 + \frac{2}{\pi e R_A R_V}\right) W \sqrt{\frac{W/S_w}{\rho}}$$

Thus, for this jet, the specific range is

$$\begin{aligned} r_s &= \frac{V^2}{q_T P_R} = \frac{V^2}{q_T\left(\dfrac{C_{D_0}}{2} R_V^3 + \dfrac{2}{\pi e R_A R_V}\right) W \sqrt{\dfrac{W/S_w}{\rho}}} \\ &= \frac{R_V^2}{q_T\left(\dfrac{C_{D_0}}{2} R_V^3 + \dfrac{2}{\pi e R_A R_V}\right) W \sqrt{\dfrac{W/S_w}{\rho}}} \end{aligned} \tag{3.6.14}$$

and the velocity ratio that results in maximum specific range is

$$R_V = \left(\frac{12}{\pi e R_A C_{D_0}}\right)^{1/4}$$

Using this result in Eq. (3.6.14), the maximum instantaneous specific range for the turbojet is

$$r_s = \frac{3}{2}\left(\frac{\pi e R_A}{12 C_{D_0}^3}\right)^{1/4} \frac{1}{q_T W}\sqrt{\frac{W/S_w}{\rho}}$$

From Eq. (3.6.12), for constant altitude, the maximum range at sea level is

$$R_{\max} = \int_{W_e}^{W_f} r_s \, dW = \int_{W_e}^{W_f} \frac{3}{2}\left(\frac{\pi e R_A}{12 C_{D_0}^3}\right)^{1/4} \frac{1}{q_T W}\sqrt{\frac{W/S_w}{\rho}}\, dW$$

$$= \frac{3}{2}\left(\frac{\pi e R_A}{12 C_{D_0}^3}\right)^{1/4} \frac{1}{q_T\sqrt{\rho S_w}} \int_{W_e}^{W_f} \frac{dW}{\sqrt{W}} = 3\left(\frac{\pi e R_A}{12 C_{D_0}^3}\right)^{1/4} \frac{\sqrt{W_f} - \sqrt{W_e}}{q_T\sqrt{\rho S_w}}$$

$$= 3\left[\frac{\pi(0.82)(9.1125)}{12(0.023)^3}\right]^{1/4} \frac{\sqrt{20{,}000 \text{ lbf}} - \sqrt{12{,}000 \text{ lbf}}}{1.667\times10^{-4} \text{ sec}^{-1}\sqrt{0.0023769 \text{ slug/ft}^3\,(320 \text{ ft}^2)}}$$

$$= \underline{1.317\times10^7 \text{ ft} = 2{,}495 \text{ mi} = 4{,}015 \text{ km}}$$

Repeating these calculation for 20,000 feet ($\rho = 0.0012673$ slug/ft^3) and again assuming constant altitude, the maximum range at this altitude is found to be

$$R_{\max} = 3\left(\frac{\pi e R_A}{12 C_{D_0}^3}\right)^{1/4} \frac{\sqrt{W_f} - \sqrt{W_e}}{q_T\sqrt{\rho S_w}} = \underline{1.804\times10^7 \text{ ft} = 3{,}416 \text{ mi} = 5{,}498 \text{ km}}$$

Note that for the turbojet in Example 3.6.2, the predicted maximum range was inversely proportional to the square root of air density. At 20,000 feet the maximum range for this turbojet was about 37 percent greater than that at sea level. Clearly, there is a significant advantage to flying such airplanes at higher altitudes. Typical cruising altitudes for subsonic commercial jets are in the range of 30,000 to 40,000 feet. In the example it was assumed that the density altitude remained constant for the entire flight. This neglects the fuel required for takeoff, climb, descent, and landing. When all phases of the flight are accounted for, the optimal flight profile (speed and altitude) depends on the length of the flight as well as the variations in thrust-specific fuel consumption with airspeed and altitude, which are encountered for the more common turbofan engine.

3.7. Power Failure and Gliding Flight

We have now seen that the steady rate of climb that an airplane can sustain depends on the power produced by the airplane's engines. We have also seen that the velocity that an airplane can sustain in steady level flight is dependent on engine power. An obvious question that one might ask is: What happens if the engines fail?

In the previous analysis for rate of climb, there was no restriction that the power available be positive and nonzero. Equation (3.4.8) can be used to predict the rate of climb for any aircraft with low thrust-to-weight ratio. Thus, this equation applies equally well to the case of an airplane with zero thrust-to-weight ratio. From Eqs. (3.3.1) and (3.4.8), for zero power available we have

$$V_c = -\frac{P_R}{W} = -\frac{DV}{W} \tag{3.7.1}$$

Since the drag, the airspeed, and the weight are always positive, the steady rate of climb in powerless flight is always negative. The negative of the rate of climb is called the sink rate, V_s,

$$V_s = \frac{P_R}{W} = \frac{DV}{W} \tag{3.7.2}$$

So we see that to minimize sink rate, we minimize power required or the DV product. Using Eq. (3.3.7) for the power required in Eq. (3.7.2), we have

$$V_s = \frac{P_R}{W} = \frac{C_{D_0}\rho V^3}{2(W/S_w)} + C_{D_0,L}V + \frac{2(W/S_w)}{\pi e R_A \rho V} \tag{3.7.3}$$

The sink rate as a function of airspeed and altitude for a typical general aviation aircraft is shown in Fig. 3.7.1.

Since the weight is independent of airspeed, the minimum sink airspeed, V_{MS}, is the same as the airspeed for minimum power required, and from Eq. (3.3.12) we have

$$V_{MS} = V_{MDV} = \frac{2}{\sqrt{\pi e R_A C_{D_0,L} + \sqrt{(\pi e R_A C_{D_0,L})^2 + 12\pi e R_A C_{D_0}}}} \sqrt{\frac{W/S_w}{\rho}} \tag{3.7.4}$$

The minimum sink rate is found by using this airspeed in Eq. (3.7.3). Using the common approximation that $C_{D_0,L}$ is zero, this gives

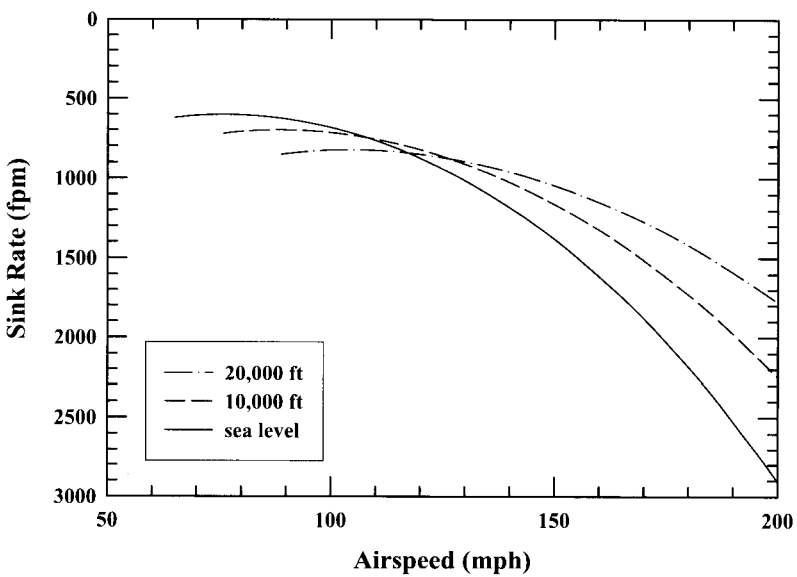


Figure 3.7.1. Variation in sink rate with airspeed and altitude.

$$(V_s)_{\min} = \frac{(DV)_{\min}}{W} \cong \frac{4\sqrt{2}\,C_{D_0}^{1/4}}{(3\pi e R_A)^{3/4}}\sqrt{\frac{W/S_w}{\rho}} \tag{3.7.5}$$

If the pilot flies at the minimum sink airspeed after the engine fails, he or she can maximize the time that the airplane will remain in the air. If the plane is very near a good landing field, this may be a good strategy. It would give the pilot the maximum possible time to restart the engine and it would give people on the ground the maximum possible time to prepare for an emergency landing. However, the pilot may not be near a good landing field when the engine fails. In this case the pilot may want to maximize distance traveled over the ground, not time in the air.

To consider distance traveled over the ground, we return to Eqs. (3.4.1) and (3.4.2). Setting the thrust available to zero, we have

$$D = -W\sin\gamma \tag{3.7.6}$$

and

$$L = W\cos\gamma \tag{3.7.7}$$

The horizontal component of the plane's airspeed, V_h, is

$$V_h = V\cos\gamma \tag{3.7.8}$$

The vertical component of the plane's airspeed, V_s, is the sink rate

$$V_s = -V\sin\gamma \tag{3.7.9}$$

Here we should recall that the sink rate is positive in the downward direction and γ, the angle of climb relative to the surrounding air, is negative for powerless flight. Thus, Eq. (3.7.9) gives positive values of V_s for a gliding plane.

If there is no wind, the plane's velocity over the ground is just the horizontal component of the plane's airspeed. However, when a wind is present, the ground speed, V_g, is related to the horizontal component of the plane's airspeed, V_h, the wind speed, V_w, and wind-track angle, φ_w, as shown in Fig. 3.7.2. From this figure, the ground speed is

$$V_g = \sqrt{V_h^2 - V_w^2\sin^2\varphi_w} - V_w\cos\varphi_w \tag{3.7.10}$$

The glide ratio, R_G, is defined as the airplane's horizontal velocity over the ground divided by the sink rate,

$$R_G \equiv \frac{V_g}{V_s} \tag{3.7.11}$$

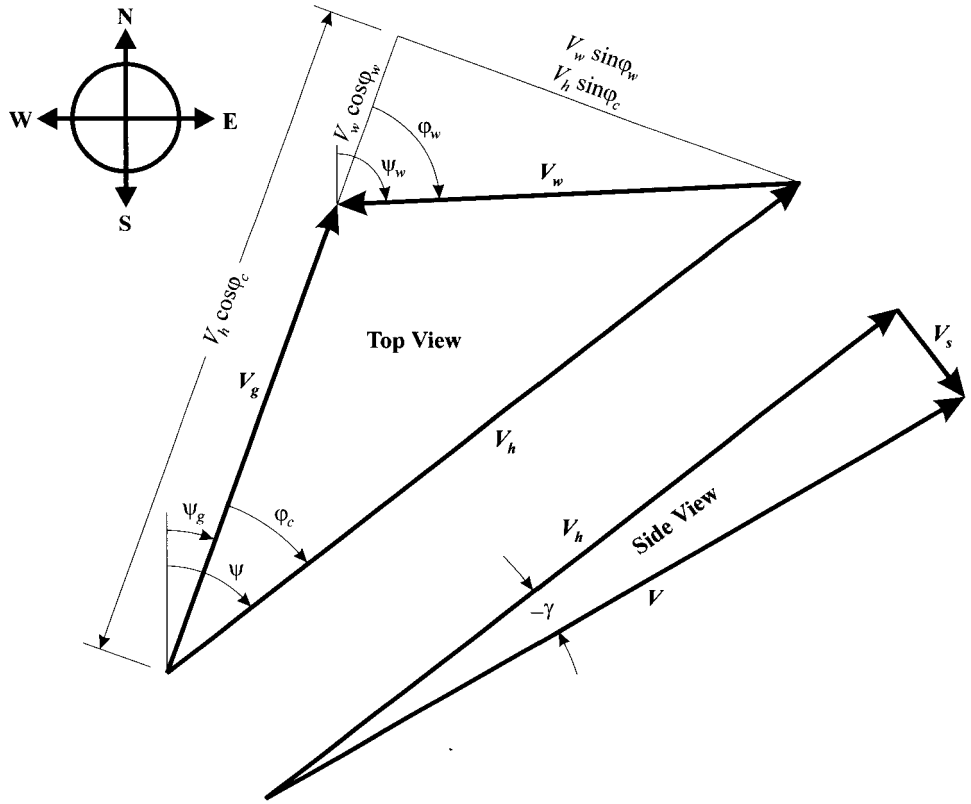


Figure 3.7.2. Relationship among ground speed, airspeed, and wind speed for gliding flight.

Using Eqs. (3.7.8), (3.7.9), and (3.7.10) in Eq. (3.7.11), the glide ratio is related to the airspeed, climb angle, and the wind:

$$R_G = \frac{\sqrt{V_h^2 - V_w^2 \sin^2 \varphi_w} - V_w \cos\varphi_w}{V_s} = \frac{\sqrt{V^2 \cos^2 \gamma - V_w^2 \sin^2 \varphi_w} - V_w \cos\varphi_w}{-V \sin\gamma} \tag{3.7.12}$$

From Eq. (3.7.6) we can write

$$\sin\gamma = -\frac{D}{W} \tag{3.7.13}$$

and from Eq. (3.7.7) we can write

$$\cos\gamma = \frac{L}{W} \tag{3.7.14}$$

Using Eqs. (3.7.13) and (3.7.14) in Eq. (3.7.12) gives

$$\begin{aligned} R_G &= \frac{\sqrt{V^2(L/W)^2 - V_w^2 \sin^2 \varphi_w} - V_w \cos \varphi_w}{V(D/W)} \\ &= \frac{L}{D}\left(\sqrt{1 - \frac{V_w^2 \sin^2 \varphi_w}{V^2(L/W)^2}} - \frac{V_w \cos \varphi_w}{V(L/W)}\right) \end{aligned} \tag{3.7.15}$$

For most aircraft, the lift-to-drag ratio is large enough so that the glide angle is small and the lift is very nearly equal to the weight. Thus, we can closely approximate the glide ratio as

$$\begin{aligned} R_G &\cong \frac{L}{D}\left(\sqrt{1 - \frac{V_w^2 \sin^2 \varphi_w}{V^2}} - \frac{V_w \cos \varphi_w}{V}\right) \\ &= \frac{C_L}{C_D}\left(\sqrt{1 - \frac{V_w^2 \sin^2 \varphi_w}{V^2}} - \frac{V_w \cos \varphi_w}{V}\right) \end{aligned} \tag{3.7.16}$$

From Eq. (3.7.15) or Eq. (3.7.16) we see that the zero-wind glide ratio, R_{G0}, is equal to the lift-to-drag ratio. We further see that a headwind or crosswind will decrease the glide ratio while a tailwind will increase it. From Eq. (3.2.8),

$$\frac{L}{D} = \frac{C_L}{C_D} = \frac{C_L}{C_{D_0} + C_{D_{0,L}} C_L + \dfrac{C_L^2}{\pi e R_A}} = \left(\frac{C_{D_0}}{C_L} + C_{D_{0,L}} + \frac{C_L}{\pi e R_A}\right)^{-1} \tag{3.7.17}$$

For small glide angles, the lift is very nearly equal to the weight and

$$\frac{C_L}{C_D} \cong \left(\frac{\frac{1}{2}\rho V^2 C_{D_0}}{W/S_w} + C_{D_{0,L}} + \frac{W/S_w}{\frac{1}{2}\pi e R_A \rho V^2}\right)^{-1} \tag{3.7.18}$$

The maximum zero-wind glide ratio is simply the maximum lift-to-drag ratio for the aircraft. From Eq. (3.2.13) this gives

$$(R_{G0})_{\max} = (C_L/C_D)_{\max} = \frac{\sqrt{\pi e R_A}}{2\sqrt{C_{D_0}} + C_{D_{0,L}}\sqrt{\pi e R_A}} \tag{3.7.19}$$

The zero-wind best glide airspeed, V_{BG0}, is the airspeed that gives maximum lift-to-drag ratio. This is the airspeed resulting in the lift coefficient that will satisfy Eq. (3.2.12). For small glide angles, the lift is very nearly equal to the weight, and we can write

$$V_{BG0} = V_{MD} \cong \frac{\sqrt{2}}{\sqrt[4]{\pi e R_A C_{D_0}}} \sqrt{\frac{W/S_w}{\rho}} \tag{3.7.20}$$

We see from Eqs. (3.7.19) and (3.7.20) that the zero-wind maximum glide ratio is independent of wing loading and air density, while the zero-wind best glide airspeed is proportional to the square root of the wing loading divided by the air density. The glide ratio as a function of airspeed and altitude for a typical general aviation aircraft is shown in Fig. 3.7.3, for the case of zero wind.

Including the effects of wind, we compute the glide ratio for the airplane by using Eq. (3.7.18) in Eq. (3.7.16). This gives

$$R_G \cong \frac{\sqrt{1 - \dfrac{V_w^2 \sin^2 \varphi_w}{V^2}} - \dfrac{V_w \cos \varphi_w}{V}}{\dfrac{\frac{1}{2}\rho V^2 C_{D_0}}{W/S_w} + C_{D_0,L} + \dfrac{W/S_w}{\frac{1}{2}\pi e R_A \rho V^2}} \tag{3.7.21}$$

Figure 3.7.4 shows the glide ratio at sea level, for a typical general aviation aircraft, as a function of airspeed for several different wind conditions.

To find the best glide airspeed, we differentiate Eq. (3.7.21) with respect to airspeed and set the result to zero. This gives an equation that can be solved numerically for the best glide airspeed,

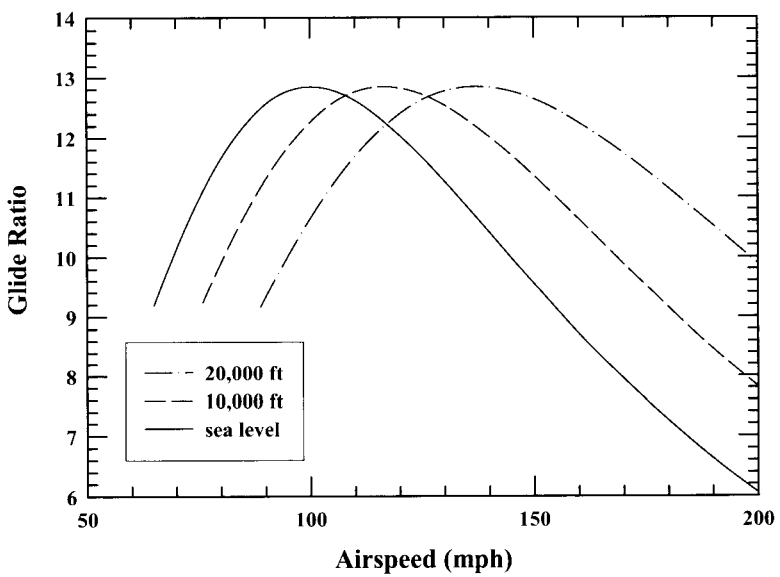


Figure 3.7.3. Variation in zero-wind glide ratio with airspeed and altitude.

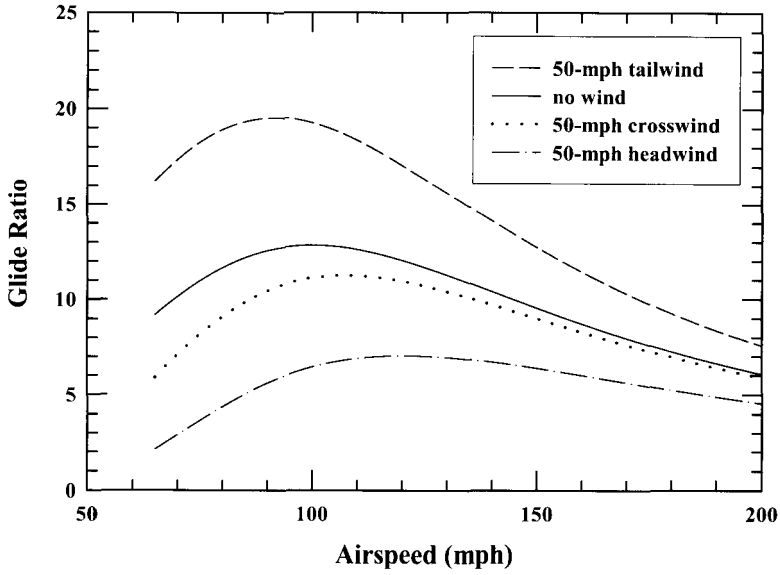


Figure 3.7.4. Variation in glide ratio at sea level with airspeed and wind.

$$2\left(V^4 - V_{MD}^4\right)V - \left(3V^4 - V_{MD}^4\right)V_w\left(\cos\varphi_w\sqrt{1-\frac{V_w^2\sin^2\varphi_w}{V^2}} + \frac{V_w\sin^2\varphi_w}{V}\right) = 0 \quad (3.7.22)$$

To obtain the maximum glide ratio, we use the best glide airspeed in Eq. (3.7.21). Figure 3.7.5 shows the best glide airspeed at sea level as a function of wind speed. Figure 3.7.6 shows the maximum glide ratio as a function of wind speed for the same general aviation aircraft.

We can see from Eq. (3.7.21) that, in general, the glide ratio is a function of wing loading. Figure 3.7.7 shows how the maximum glide ratio varies with headwind and gross weight for the same general aviation aircraft that was used for the other figures in this chapter. Notice that the heaviest wing loading results in the largest glide ratio when there is a headwind. It may seem counterintuitive that increasing the weight of an aircraft could increase its glide ratio under any conditions. However, this is in fact the case. Added weight affects the maximum glide ratio of an aircraft in two ways. Added weight, of course, increases the induced drag, but it also increases the potential energy of the aircraft at any given altitude. In gliding flight, it is the decrease in potential energy of the aircraft that provides the energy required to move the aircraft through the air. A heavier aircraft gives up more potential energy for each foot of elevation lost. Thus, a heavier aircraft can do more work against the drag for each foot of elevation lost. Even though the heavier weight produces greater drag, it also provides additional potential energy needed to move the aircraft against that drag. Since increasing drag at constant weight would decrease the glide ratio and increasing the weight at constant drag would increase the glide ratio, it is not immediately obvious what net effect increased wing loading will

have on the glide ratio. As it turns out, increasing wing loading improves maximum glide ratio in a headwind and degrades maximum glide ratio in a tailwind. With no wind, the maximum glide ratio for any aircraft is independent of wing loading.

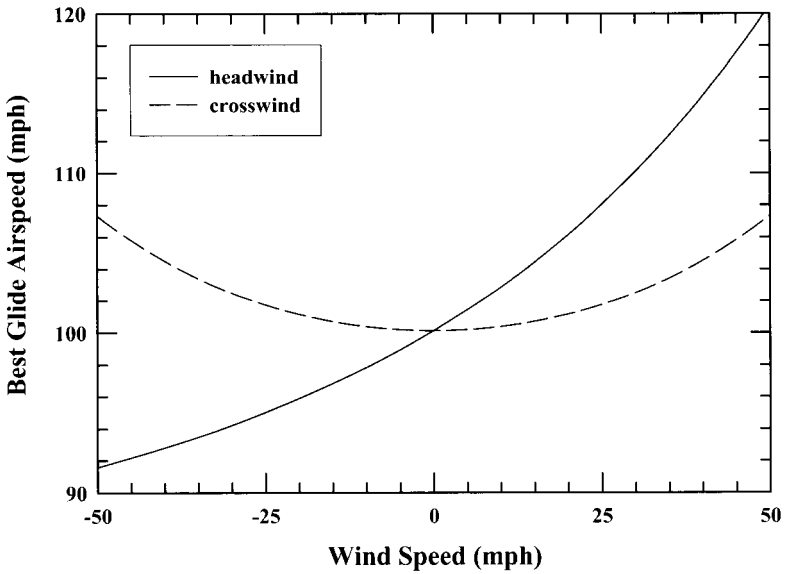


Figure 3.7.5. Variation in best glide airspeed at sea level with wind speed.

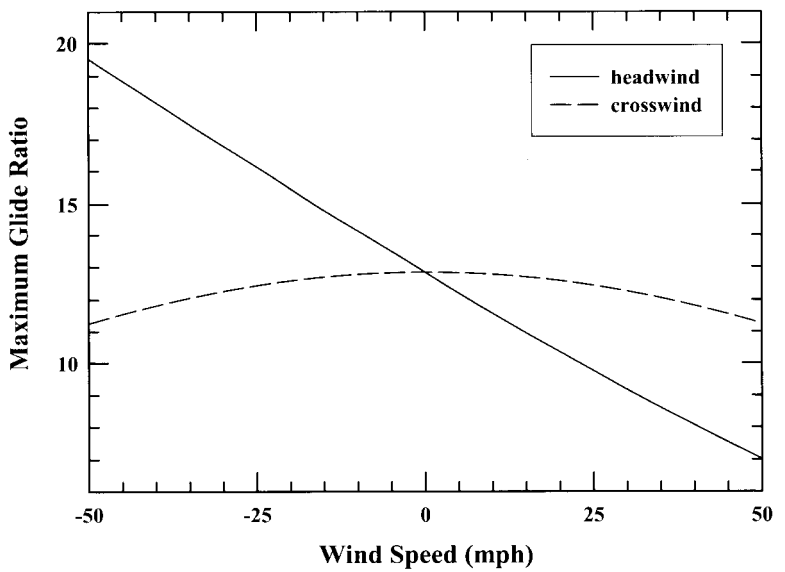


Figure 3.7.6. Variation in maximum glide ratio at sea level with wind speed.

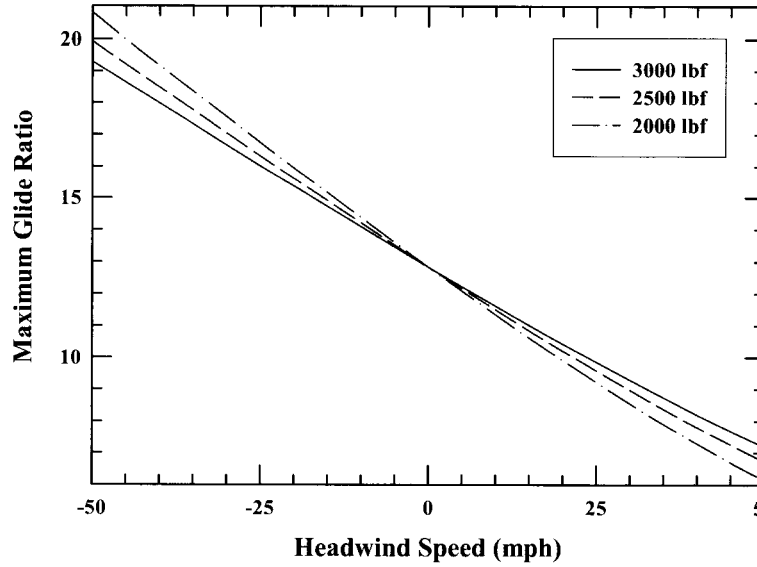


Figure 3.7.7. Variation in the maximum glide ratio at sea level with headwind speed and aircraft gross weight.

EXAMPLE 3.7.1. For the general aviation aircraft described in Example 3.5.1, determine the best glide airspeed at sea level and the maximum glide ratio with fuel tanks full, for the case of no wind, with a 60-mph headwind, and with a 60-mph tailwind.

Solution. For this airplane

$$S_w = 180\ \text{ft}^2, \quad b_w = 33\ \text{ft}, \quad W_f = 2{,}700\ \text{lbf}, \quad W_f/S_w = 15.0\ \text{lbf/ft}^2,$$
$$C_{D_0} = 0.023, \quad C_{D_0,L} = 0.0, \quad e = 0.82, \quad R_A = 6.05$$

With no wind, the glide ratio is equal to the lift-to-drag ratio for the airplane. Using the small glide angle approximation, from Eq. (3.7.18) we have

$$\begin{aligned} R_G &= \frac{C_L}{C_D} = \left(\frac{\frac{1}{2}\rho V^2 C_{D_0}}{W/S_w} + C_{D_0,L} + \frac{W/S_w}{\frac{1}{2}\pi e R_A \rho V^2} \right)^{-1} \\ &= \left(\frac{C_{D_0}}{2} R_V^2 + \frac{2}{\pi e R_A R_V^2} \right)^{-1} \end{aligned} \tag{3.7.23}$$

Differentiating with respect to velocity ratio and setting the result to zero, we obtain the velocity ratio for maximum glide ratio,

$$R_V = \left(\frac{4}{\pi e R_A C_{D_0}}\right)^{1/4} \tag{3.7.24}$$

Thus, the best glide airspeed with no wind is

$$\begin{aligned} V_{BG} &= R_V\sqrt{\frac{W/S_w}{\rho}} = \left(\frac{4}{\pi e R_A C_{D_0}}\right)^{1/4}\sqrt{\frac{W/S_w}{\rho}} \\ &= \left(\frac{4}{\pi(0.82)(6.05)(0.023)}\right)^{1/4}\sqrt{\frac{15.0\ \text{lbf/ft}^2}{0.0023769\ \text{slug/ft}^3}} \\ &= \underline{145\ \text{ft/sec} = 99\ \text{mph} = 86\ \text{knots} = 159\ \text{km/hr}} \end{aligned}$$

Using Eq. (3.7.24) in Eq. (3.7.23), the maximum glide ratio with no wind is

$$R_G = \sqrt{\frac{\pi e R_A}{4C_{D_0}}} = \sqrt{\frac{\pi(0.82)(6.05)}{4(0.023)}} = \underline{13.0}$$

With a headwind, V_{hw}, from Eq. (3.7.16),

$$\begin{aligned} R_G &= \frac{C_L}{C_D}\left(1-\frac{V_{hw}}{V}\right) = \left(\frac{C_{D_0}}{2}R_V^2 + \frac{2}{\pi e R_A R_V^2}\right)^{-1}\left(1-\frac{V_{hw}}{V}\right) \\ &= \left(\frac{C_{D_0}}{2}R_V^2 + \frac{2}{\pi e R_A R_V^2}\right)^{-1}\left(1-\frac{R_{V_{hw}}}{R_V}\right) \end{aligned} \tag{3.7.25}$$

where

$$R_{V_{hw}} \equiv V_{hw}\Big/\sqrt{\frac{W/S_w}{\rho}}$$

Differentiating the glide ratio with respect to velocity ratio and setting the result to zero, we obtain an equation for the best glide velocity ratio with a headwind,

$$C_{D_0}R_V^5 - \frac{3C_{D_0}R_{V_{hw}}}{2}R_V^4 - \frac{4}{\pi e R_A}R_V + \frac{2R_{V_{hw}}}{\pi e R_A} = 0 \tag{3.7.26}$$

For a 60-mph headwind,

$$R_{V_{hw}} \equiv V_{hw}\Big/\sqrt{\frac{W/S_w}{\rho}} = 88\ \text{ft/sec}\Big/\sqrt{\frac{15.0\ \text{lbf/ft}^2}{0.0023769\ \text{slug/ft}^3}} = 1.108$$

and Eq. (3.7.26) becomes

$$0.023R_V^5 - 0.038226R_V^4 - 0.25665R_V + 0.142184 = 0$$

This is easily solved using Newton's method to give the best glide velocity ratio,

$$R_V = 2.3325$$

Thus the best glide airspeed with a 60-mph headwind is

$$V_{BG} = R_V\sqrt{\frac{W/S_w}{\rho}} = 2.3325\sqrt{\frac{15.0 \text{ lbf/ft}^2}{0.0023769 \text{ slug/ft}^3}}$$
$$= \underline{185 \text{ ft/sec} = 126 \text{ mph} = 110 \text{ knots} = 203 \text{ km/hr}}$$

Using this result in Eq. (3.7.25), the maximum glide ratio with a 60-mph headwind is found to be

$$(R_G)_{\max} = \left(\frac{C_{D_0}}{2}R_V^2 + \frac{2}{\pi e R_A R_V^2}\right)^{-1}\left(1 - \frac{R_{V_{hw}}}{R_V}\right)$$
$$= \left(\frac{0.023}{2}(2.3325)^2 + \frac{2}{\pi(0.82)(6.05)(2.3325)^2}\right)^{-1}\left(1 - \frac{1.108}{2.3325}\right) = \underline{6.1}$$

For a 60-mph tailwind,

$$R_{V_{hw}} \equiv V_{hw}\Big/\sqrt{\frac{W/S_w}{\rho}} = -88 \text{ ft/sec}\Big/\sqrt{\frac{15.0 \text{ lbf/ft}^2}{0.0023769 \text{ slug/ft}^3}} = -1.108$$

Eq. (3.7.26) becomes

$$0.023R_V^5 + 0.038226R_V^4 - 0.25665R_V - 0.142184 = 0$$

and

$$R_V = 1.6508$$

Thus the best glide airspeed with a 60-mph tailwind is

$$V_{BG} = R_V\sqrt{\frac{W/S_w}{\rho}} = 1.6508\sqrt{\frac{15.0 \text{ lbf/ft}^2}{0.0023769 \text{ slug/ft}^3}}$$
$$= \underline{131 \text{ ft/sec} = 89 \text{ mph} = 78 \text{ knots} = 144 \text{ km/hr}}$$

and the maximum glide ratio with a 60-mph tailwind is

$$(R_G)_{\max} = \left(\frac{C_{D_0}}{2}R_V^2 + \frac{2}{\pi e R_A R_V^2}\right)^{-1}\left(1 - \frac{R_{V_{hw}}}{R_V}\right)$$

$$= \left(\frac{0.023}{2}(1.6508)^2 + \frac{2}{\pi(0.82)(6.05)(1.6508)^2}\right)^{-1}\left(1 + \frac{1.108}{1.6508}\right) = \underline{21.3}$$

In summary,

V_{hw} (mph)	$R_{V_{hw}}$	R_V	V_{BG} (mph)	$(R_g)_{\max}$
−60	−1.108	1.6508	89	21.3
0	0.0	1.8277	99	13.0
60	1.108	2.3325	126	6.1

3.8. Airspeed, Wing Loading, and Stall

In previous sections we have discussed several important airspeeds. Two of these airspeeds are independent of engine thrust. One is the airspeed that results in the minimum value of the drag-airspeed product for steady level flight when the thrust is aligned with the direction of flight,

$$V_{MDV} = \frac{2}{\sqrt{\pi e R_A C_{D_0,L} + \sqrt{(\pi e R_A C_{D_0,L})^2 + 12\pi e R_A C_{D_0}}}}\sqrt{\frac{W/S_w}{\rho}} \tag{3.8.1}$$

Another important airspeed is that which results in minimum level flight drag when the thrust is aligned with the direction of flight,

$$V_{MD} = \frac{\sqrt{2}}{\sqrt[4]{\pi e R_A C_{D_0}}}\sqrt{\frac{W/S_w}{\rho}} \tag{3.8.2}$$

The airspeed, V_{MDV}, will result in the minimum power required for steady level flight and the minimum sink rate for gliding flight. This airspeed would also result in maximum endurance for an aircraft if the power-specific fuel consumption were independent of airspeed. The airspeed, V_{MD}, will result in minimum thrust required for steady level flight and maximum zero-wind glide ratio for gliding flight. The V_{MD} airspeed will also result in maximum range for no wind and an aircraft with power-specific fuel consumption independent of airspeed.

There is another important airspeed that is independent of engine thrust. This is the level flight stall speed for thrust aligned with the direction of flight. The stall speed is the minimum airspeed at which the airplane can fly. It can be evaluated from Eq. (3.3.3) by setting the lift coefficient equal to the maximum possible lift coefficient,

$$V_{\min} = \sqrt{\frac{2}{C_{L\max}}}\sqrt{\frac{W/S_w}{\rho}} \tag{3.8.3}$$

Notice that all three of the airspeeds above are proportional to the square root of the wing loading divided by the air density. These airspeeds also depend on the parasitic drag coefficient, the Oswald efficiency, the aspect ratio, and the maximum lift coefficient. However, these other parameters are limited by factors, such as structural strength and wing section design, and cannot be varied over a wide range to adjust the design airspeed of an airplane. The primary factor that the designer uses to control airspeed is wing loading.

The aspect ratio for modern subsonic airplanes and sailplanes varies from about 5 to 24, but is typically between 6 and 8 for most general aviation and transport aircraft. The Oswald efficiency for modern aircraft can vary from about 0.7 to as high as 0.95 but is typically in the range of 0.8 for most subsonic airplanes. The zero-lift parasitic drag coefficient for today's subsonic airplanes and sailplanes ranges from about 0.01 to 0.10, with typical values usually between 0.02 and 0.05 for general aviation and transport aircraft. The maximum lift coefficient for modern airfoils can be as low as 0.8 for thin symmetric airfoils without flaps, and as high as 5 for airfoils with both leading edge and trailing edge high-lift mechanisms in landing configuration. However, most modern airfoils in cruise configuration have a maximum lift coefficient in the range between 1.2 and 1.6. The wing loading, on the other hand, can vary from less than 1 pound per square foot for slow-flying ultralights to over 100 pounds per square foot for high-speed jet transports.

We now see that airplane wing loading is the only design parameter that can be varied widely to control the design airspeed of a particular airplane. We also see from Eqs. (3.8.1) through (3.8.3) that all three critical airspeeds are proportional to the square root of wing loading. Thus, if an airplane is to be designed for very low takeoff and landing speeds, suitable for rough landing fields, then it will need to have a low wing loading. If, on the other hand, a high cruise speed is desired, the plane will need to be designed with a high wing loading.

If any one of the three airspeeds given by Eqs. (3.8.1) through (3.8.3) is known as a design constraint, then we can use the appropriate equation for that airspeed to help fix the wing area. For example, if we were designing for minimum drag at a particular cruise speed, Eq. (3.8.2) could be used to determine the required wing loading.

EXAMPLE 3.8.1. We wish to design an airplane to have a minimum drag cruise speed of 100 miles per hour at sea level with a gross weight of 3,000 pounds. Assume that for structural reasons, the aspect ratio has been fixed at 7. For these initial calculations, use typical values of 0.8 for the Oswald efficiency and 0.03 for the zero-lift parasitic drag coefficient. Estimate the wing area required for this airplane.

Solution. From Eq. (3.8.2) we can compute an initial estimate for the required wing area,

$$S_w = \frac{2}{\sqrt{\pi e R_A C_{D_0}}} \frac{W}{\rho V_{MD}^2}$$

$$= \frac{2}{\sqrt{\pi(0.8)(7.0)(0.03)}} \frac{3{,}000 \text{ lbf}}{0.0023769 \text{ slug/ft}^3 \left(100 \frac{5{,}280}{3{,}600} \text{ ft/sec}\right)^2} = \underline{162 \text{ ft}^2}$$

As the design is refined and the parasitic drag coefficient and Oswald efficiency become known more accurately, the wing area may change somewhat. However, if the airplane is to have minimum drag at 100 miles per hour, with a gross weight of 3,000 pounds, the wing area cannot be far from this value.

3.9. The Steady Coordinated Turn

In a steady coordinated turn, the wings of an airplane are banked at a constant angle, ϕ, as shown in Fig. 3.9.1. In a perfectly coordinated turn there is no side force. Since the wings are banked at the angle ϕ, the lift vector is also inclined at the angle ϕ toward the center of the turn. The horizontal component of lift produces a constant acceleration

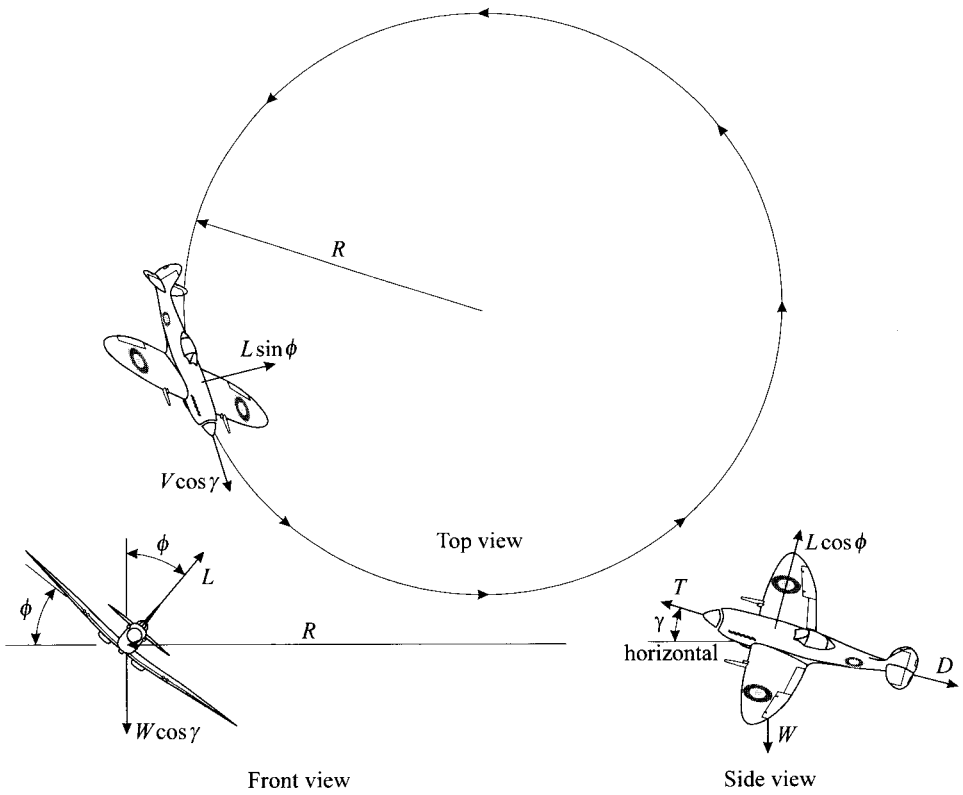


Figure 3.9.1. The steady coordinated turn.

normal to the flight path, causing the airplane to turn at constant airspeed along a circular or spiral path of radius R. For this steady turn, the radial acceleration is equal to the circumferential velocity squared divided by the turning radius. Thus, summing forces in the radial direction, we can write

$$L\sin\phi = \frac{W}{g}\frac{(V\cos\gamma)^2}{R} \tag{3.9.1}$$

Using the small-thrust-angle approximation and summing forces in the direction of flight gives

$$T = D + W\sin\gamma = \tfrac{1}{2}\rho V^2 S_w\left(C_{D_0} + C_{D_{0,L}}C_L + \frac{C_L^2}{\pi e R_A}\right) + W\sin\gamma \tag{3.9.2}$$

and summing forces in a direction normal to both the direction of flight and the radial direction,

$$L\cos\phi = W\cos\gamma \tag{3.9.3}$$

Solving Eq. (3.9.3) for the lift, we have

$$L = \frac{W\cos\gamma}{\cos\phi} \tag{3.9.4}$$

and the lift coefficient is

$$C_L \equiv \frac{L}{\tfrac{1}{2}\rho V^2 S_w} = \frac{W\cos\gamma}{\tfrac{1}{2}\rho V^2 S_w\cos\phi} \tag{3.9.5}$$

Using Eq. (3.9.4) to eliminate the lift from Eq. (3.9.1) and solving for the turning radius, we have

$$R = \frac{V^2\cos\gamma}{g\tan\phi} \tag{3.9.6}$$

Using Eq. (3.9.5) in Eq. (3.9.2), the thrust required to maintain constant airspeed is

$$T = \tfrac{1}{2}\rho V^2 S_w C_{D_0} + C_{D_{0,L}}\frac{W\cos\gamma}{\cos\phi} + \frac{1}{\tfrac{1}{2}\pi e R_A \rho V^2 S_w}\left(\frac{W\cos\gamma}{\cos\phi}\right)^2 + W\sin\gamma \tag{3.9.7}$$

Solving Eq. (3.9.7) for $\sin\gamma$ gives

$$\sin\gamma = \frac{T - \left[\frac{1}{2}\rho V^2 S_w C_{D_0} + C_{D_{0,L}} \frac{W\cos\gamma}{\cos\phi} + \frac{1}{\frac{1}{2}\pi e R_A \rho V^2 S_w}\left(\frac{W\cos\gamma}{\cos\phi}\right)^2\right]}{W} \tag{3.9.8}$$

For any **steady coordinated turn**, Eqs. (3.9.6) and (3.9.8) can be used to obtain the turning radius and the climb angle as a function of bank angle, airspeed, and thrust.

The sine of γ multiplied by the airspeed is the rate of climb, V_c, and the thrust multiplied by the airspeed is the power available, P_A. Thus, multiplying Eq. (3.9.8) by the airspeed, we have

$$V_c = \frac{P_A - \left[\frac{1}{2}\rho V^3 S_w C_{D_0} + C_{D_{0,L}} V \frac{W\cos\gamma}{\cos\phi} + \frac{1}{\frac{1}{2}\pi e R_A \rho V S_w}\left(\frac{W\cos\gamma}{\cos\phi}\right)^2\right]}{W} \tag{3.9.9}$$

Most turns executed in normal flight are close to being level, i.e., γ is small. Thus, applying the usual small-angle approximation, $\cos\gamma \cong 1$, to Eqs. (3.9.6) and (3.9.9), for a ***nearly level*** **steady coordinated turn**, the turning radius and the rate of climb are given by

$$R = \frac{V^2}{g\tan\phi} \tag{3.9.10}$$

and

$$V_c = \frac{P_A - \left[\frac{1}{2}\rho V^3 S_w C_{D_0} + C_{D_{0,L}} V \frac{W}{\cos\phi} + \frac{1}{\frac{1}{2}\pi e R_A \rho V S_w}\left(\frac{W}{\cos\phi}\right)^2\right]}{W} \tag{3.9.11}$$

Notice from Eq. (3.9.10) that turning radius for a nearly level coordinated turn is independent of the thrust or power available. The turning radius depends only on bank angle and airspeed. However, from Eq. (3.9.11), we see that the rate of climb in such a turn is a function of power available as well as bank angle and airspeed. The bracketed term in Eq. (3.9.11) is the power that would be required for a steady level coordinated turn with the same bank angle and airspeed. The difference between the power available and the power required for a level turn is called the *excess power* for the turn. Thus, as was the case for straight flight, the rate of climb for turning flight is equal to the excess

power divided by the gross weight. However, since the cosine of ϕ is always less than unity in a turn, the power required for level flight is always greater in a turn than it is for straight flight. Because the lift required in a turn is always greater than the lift required for straight flight at the same rate of climb, the drag and the power required to maintain constant airspeed are also greater in a turn. The excess power in a turn can be either positive or negative. If the power required for steady level turning flight is greater than the power available, then the rate of climb for the steady turn will simply be negative.

In executing a turn, the pilot can manipulate the throttle and elevator as well as the ailerons and rudder. The throttle and elevator can be used together to control the rate of climb and the airspeed. The rudder is normally used only to eliminate the side force and coordinate the turn. The ailerons are used primarily to control the bank angle, which controls the turning radius at any given airspeed. From Eq. (3.9.10) we see that for a given airspeed, the turning radius is made smaller by increasing the bank angle. There are, however, limits to how large a bank angle may be used in a steady coordinated turn.

From Eq. (3.9.5) we see that as the bank angle goes to 90 degrees, the lift coefficient would need to go to infinity. Since the lift coefficient has a maximum value, the bank angle will have a maximum value as well. Using the maximum lift coefficient in Eq. (3.9.5) and applying the small-climb-angle approximation, for a nearly level coordinated turn we can write

$$\cos\phi_{\max} = \frac{W}{\frac{1}{2}\rho V^2 S_w C_{L_{\max}}} \tag{3.9.12}$$

This is one obvious limit to the bank angle. If this bank angle is exceeded, the airplane will stall. Hence, the maximum bank angle computed from Eq. (3.9.12) is called the *stall-limited bank angle.*

There is also another important limit to the bank angle in a coordinated turn. This is related to the structural strength of the aircraft. During any maneuver in which the airplane travels along a curved path, there is a component of acceleration normal to the flight path. If the vector sum of the airplane's acceleration and the acceleration of gravity falls in a plane normal to the wing span, there is no spanwise component of total acceleration and the maneuver is said to be *coordinated.* The component of the airplane's acceleration that is normal to the flight path can either add to or subtract from the acceleration of gravity. Such maneuvers load the aircraft in a manner similar to what would be encountered if the airplane were flying straight and level in a gravitational field with a strength equal to the vector sum of the airplane's acceleration and the acceleration of gravity. Therefore, such maneuvers are usually rated in terms of what is called the *load factor*, n, which is defined as the lift generated during the maneuver divided by the aircraft weight,

$$n \equiv \frac{L}{W} = \frac{\frac{1}{2}\rho V^2 S_w C_L}{W} = \frac{\frac{1}{2}\rho V^2}{W/S_w} C_L \tag{3.9.13}$$

Load factor is usually stated in terms of "g's." For example, if a maneuver produces a lift force of five times the aircraft weight, the maneuver is said to be a "5-g maneuver."

From Eq. (3.9.3) we see that the load factor for a steady coordinated turn is a function only of bank angle and climb angle. For a nearly level turn, we use the small-climb-angle approximation and rearrange Eq. (3.9.3) to give

$$n \equiv \frac{L}{W} = \frac{1}{\cos\phi} \tag{3.9.14}$$

Obviously, there is a limit to the lift force that can be applied to the wings without causing structural damage. This limit is usually specified in terms of a load factor at maximum gross weight, $W_{\max}$. Because the wings are not always symmetric with respect to positive and negative loading, we usually specify both a positive load limit,

$$n_{pll} \equiv \frac{L_{pll}}{W_{\max}} \tag{3.9.15}$$

and a negative load limit,

$$n_{nll} \equiv \frac{L_{nll}}{W_{\max}} \tag{3.9.16}$$

where L_{pll} is the maximum allowable positive lift and L_{nll} is the minimum allowable negative lift. In a conventional coordinated turn, the lift and load factor are both positive. Thus, rearranging Eq. (3.9.14), we find the maximum bank angle that can be used without exceeding the structural limit is given by

$$\cos\phi_{\max} = \frac{1}{n_{\max}} = \frac{W}{L_{pll}} = \frac{W}{n_{pll} W_{\max}} \tag{3.9.17}$$

The bank angle limit imposed by Eq. (3.9.17) is the load-limited bank angle. The maximum allowable bank angle in a nearly level coordinated turn is the smaller of the stall-limited bank angle, given by Eq. (3.9.12), and the load-limited bank angle, given by Eq. (3.9.17). Figure 3.9.2 shows the stall-limited bank angle and the load-limited bank angle, at maximum gross weight, as a function of airspeed for a typical general aviation aircraft with a 5-g positive load limit.

The turning radius for a steady coordinated turn can be expressed in terms of load factor as well as bank angle. Squaring Eqs. (3.9.1) and (3.9.3) and adding the two equations together, we have

$$L^2(\sin^2\phi + \cos^2\phi) = L^2 = \left(\frac{WV^2\cos^2\gamma}{gR}\right)^2 + W^2\cos^2\gamma \tag{3.9.18}$$

Solving Eq. (3.9.18) for the turning radius gives

$$R = \frac{WV^2\cos^2\gamma}{g\sqrt{L^2 - W^2\cos^2\gamma}} = \frac{V^2\cos^2\gamma}{g\sqrt{n^2 - \cos^2\gamma}} \tag{3.9.19}$$

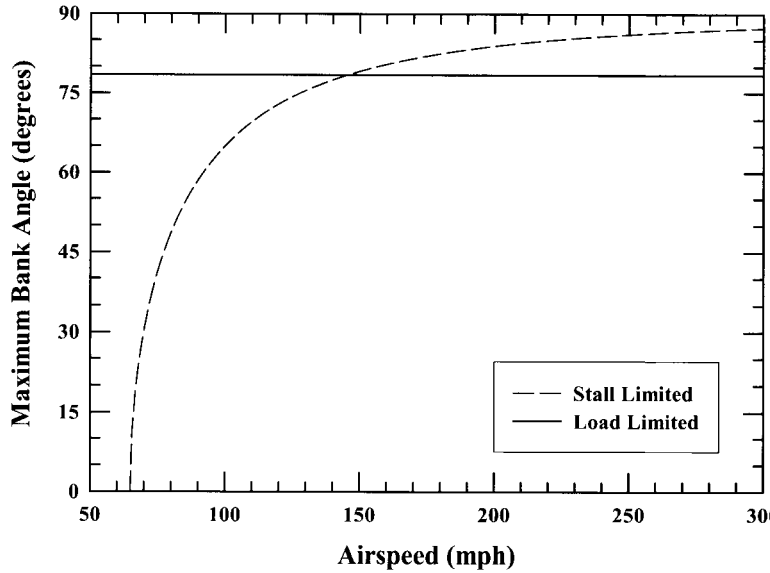


Figure 3.9.2. Stall-limited and load-limited maximum bank angles for a coordinated turn at maximum gross weight.

Using the small-climb-angle approximation in Eq. (3.9.19), a nearly level coordinated turn has a turning radius that can be expressed as a function of airspeed and load factor,

$$R = \frac{V^2}{g\sqrt{n^2 - 1}} \tag{3.9.20}$$

Load factor is an important parameter for all maneuvers involving curved flight. At low airspeed, the maximum possible load factor is limited by stall,

$$n_{\max} = \frac{L_{\max}}{W} = \frac{\frac{1}{2}\rho V^2}{W/S_w} C_{L_{\max}} \tag{3.9.21}$$

Since the wing can also stall at negative angles of attack, there is a low-speed negative limit for the load factor that will also result in stall,

$$n_{\min} = \frac{L_{\min}}{W} = \frac{\frac{1}{2}\rho V^2}{W/S_w} C_{L_{\min}} \tag{3.9.22}$$

At higher airspeeds the load factor is limited by structural constraints,

$$n_{\max} = \frac{L_{pll}}{W} = \frac{L_{pll}}{W_{\max}} \frac{W_{\max}}{W} = n_{pll} \frac{W_{\max}}{W} \tag{3.9.23}$$

and,

$$n_{\min} = \frac{L_{nll}}{W} = \frac{L_{nll}}{W_{\max}} \frac{W_{\max}}{W} = n_{nll} \frac{W_{\max}}{W} \tag{3.9.24}$$

The stall-limited and load-limited load factors are shown as a function of airspeed in Fig. 3.9.3, for the same aircraft and weight as that used for Fig. 3.9.2. This plot, called a *V-n diagram*, graphically displays the allowable flight envelope for the aircraft. Any flight maneuver, corresponding to an operating point that is below both the positive stall limit and the positive load limit while being above both negative limits, is an allowable maneuver, provided that some maximum allowable airspeed is not exceeded. Maneuvers that result in operating points above the positive stall limit or below the negative stall limit are not possible, because the wing will stall. Maneuvers that result in operating points above the positive load limit and below the positive stall limit are aerodynamically possible but may result in structural damage. Likewise, structural damage may result from any maneuver with an operating point that is below the negative load limit and above the negative stall limit. The velocity corresponding to the vertical line on the right-hand side of the *V-n* diagram is called the *VNE airspeed* or the *velocity to never exceed.* At flight velocities higher than this limit, the dynamic pressure is above the design limit for the aircraft. The VNE airspeed is a "red-line" airspeed that, by design, should always be higher than the maximum level flight airspeed by at least a factor of 1.2. For some aircraft, such as fighters and stunt planes, the VNE airspeed may be as high as the terminal airspeed in a vertical dive.

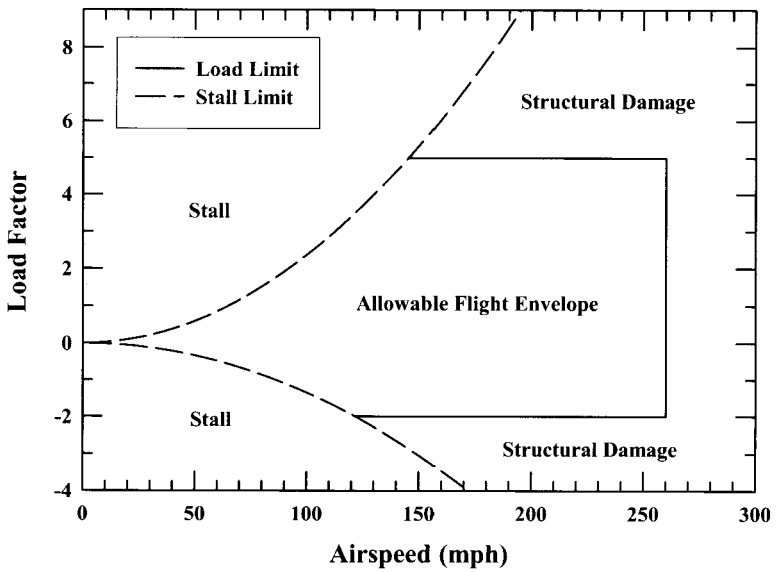


Figure 3.9.3. *V-n* diagram for a general aviation aircraft at maximum gross weight.

The airspeed at which the maximum allowable load factor changes from the positive stall limit to the positive load limit is often called the *corner velocity* for positive-*g* maneuvers. More commonly this airspeed is called the *maneuvering speed.* This terminology comes about because this is the airspeed at which the airplane can perform the tightest and fastest maneuvers without stalling the wing or risking structural damage to the aircraft. Furthermore, if the maneuvering speed is not exceeded during a positive-*g* maneuver, structural damage to the aircraft cannot occur as a result of aerodynamic lift. Here this airspeed will be designated as V_M. Setting the maximum load factor obtained from Eq. (3.9.21) equal to that obtained from Eq. (3.9.23) and solving for the airspeed, we have

$$V_M = \sqrt{\frac{2n_{pll}}{C_{L_{\max}}}}\sqrt{\frac{W_{\max}/S_w}{\rho}} = \sqrt{n_{pll}}\,V_{\text{smgw}} \tag{3.9.25}$$

where V_{smgw} is the level-flight stall speed at maximum gross weight.

The allowable flight envelope for any aircraft changes with actual gross weight. As the gross weight of the aircraft is decreased below the maximum gross weight, the allowable flight envelope is broadened. Decreasing gross weight at any airspeed increases the allowable load factor based on both stall and structural strength. This is shown in Fig. 3.9.4. In this figure, the *V-n* diagram is shown for both maximum gross weight and 75 percent of maximum gross weight. Notice that the maneuvering speed and the VNE airspeed do not change with the actual gross weight of the aircraft. When the gross weight of an airplane is reduced below the maximum gross weight, the stall

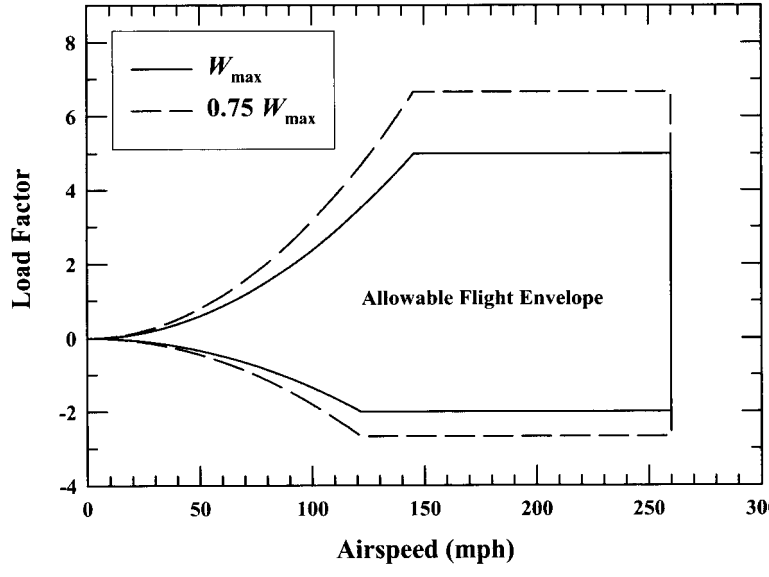


Figure 3.9.4. *V-n* diagram at two different gross weights for a typical general aviation aircraft, showing that the maneuvering speed is independent of gross weight.

speed at any given load factor is reduced. In addition, since the strength of the airplane remains constant with weight, the maximum allowable load factor based on structural strength will always increase when the gross weight is decreased. The net effect of these two changes in the *V-n* diagram is that the maneuvering speed does not change with the aircraft gross weight.

As seen from Eq. (3.9.25), the true airspeed at the maneuvering speed does change with air density. However, airspeed indicators are always calibrated for standard sea level and a density error is experienced unless the actual air density matches the air density at standard sea level. This density error is inversely proportional to the square root of air density. Because the maneuvering speed is also inversely proportional to the square root of air density, the indicated airspeed at the maneuvering speed does not change with either gross weight or altitude. Thus, indicated airspeed at the maneuvering speed is a design feature, independent of operating conditions.

The maneuvering speed given by Eq. (3.9.25) represents a critical dividing line. At airspeeds below V_M, the airplane cannot be structurally damaged by the production of positive lift. The wing will always stall before the structural limit is reached. At airspeeds above V_M, lift can be generated that may structurally damage the aircraft, and the pilot must be careful to avoid maneuvers that will generate such lift. The maneuvering speed is the highest airspeed at which the pilot can manipulate the controls arbitrarily without any risk of damaging the aircraft through excessive aerodynamic loading. The maneuvering speed is also the highest airspeed at which structural damage cannot occur from excessive aerodynamic loading due to turbulent gusts. Whenever severe turbulence is encountered, the pilot is always well advised to adjust the airspeed to match the maneuvering speed. This gives the best possible control without risk of structural damage.

EXAMPLE 3.9.1. For both the general aviation aircraft described in Example 3.5.1 and the executive business jet described in Example 3.6.2, determine the minimum turning radius for a nearly level turn at sea level with fuel tanks full and with fuel tanks empty. Assume that both airplanes are designed for a positive load limit of 4 *g*'s with fuel tanks full and have a maximum lift coefficient in cruise configuration of 1.2.

Solution. From Eq. (3.9.20), the turning radius is

$$R = \frac{V^2}{g\sqrt{n^2 - 1}}$$

The stall-limited maximum load factor is given by Eq. (3.9.21) and the load-limited maximum load factor is given by Eq. (3.9.23). Thus, the stall-limited turning radius is

$$(R_{\min})_{\text{stall}} = 1 \Bigg/ g\sqrt{\left(\frac{\rho C_{L_{\max}}}{2W/S_w}\right)^2 - \frac{1}{V^4}} \tag{3.9.26}$$

and the load-limited turning radius is

$$(R_{\min})_{\text{load}} = V^2 \Big/ g\sqrt{\left(n_{pll}\frac{W_{\max}}{W}\right)^2 - 1} \tag{3.9.27}$$

The stall-limited turning radius decreases with increasing airspeed, while the load-limited turning radius increases with increasing airspeed. This can be seen in Fig. 3.9.5 for the present general aviation airplane with fuel tanks full.

From Fig. 3.9.5 we see that the minimum possible turning radius is achieved at the airspeed where the stall-limited turning radius is equal to the load-limited turning radius. This is the maneuvering speed. Notice that increasing the strength of this airplane would not significantly decrease the minimum turning radius.

Setting the turning radius from Eq. (3.9.26) equal to that from Eq. (3.9.27) and solving for airspeed,

$$V_{R_{\min}} = V_M = \sqrt{\frac{2n_{pll}}{C_{L_{\max}}}}\sqrt{\frac{W_{\max}/S_w}{\rho}}$$

Using this result for the airspeed in either Eq. (3.9.26) or (3.9.27), we obtain the minimum turning radius that can be achieved at any airspeed, without stalling the wing or structurally damaging the airplane,

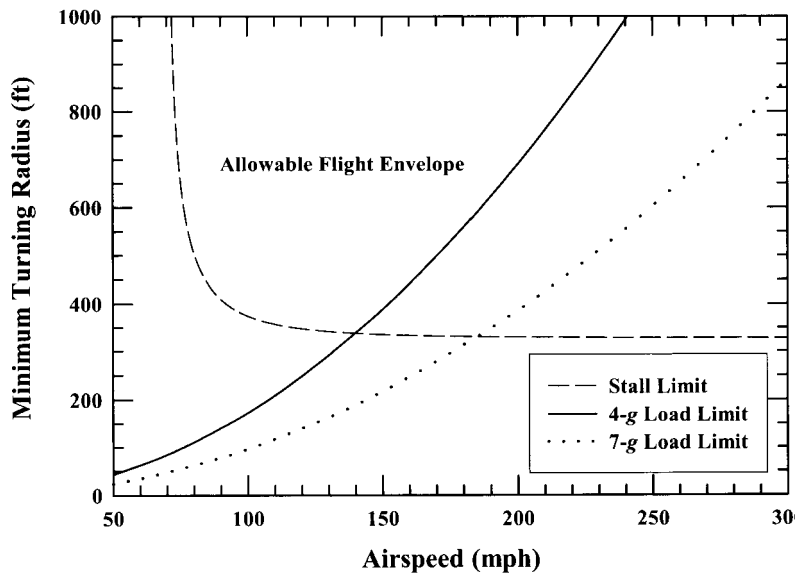


Figure 3.9.5. Minimum turning radius in a coordinated turn at sea level for the general aviation airplane in Example 3.9.1 with fuel tanks full.

$$R_{\min} = \frac{2n_{pll}}{C_{L_{\max}}\sqrt{n_{pll}^2 - (W/W_{\max})^2}} \frac{W/S_w}{\rho g} \tag{3.9.28}$$

For the general aviation airplane,

$$C_{L_{\max}} = 1.2, \quad n_{pll} = 4.0, \quad W_f/S_w = 15.0 \text{ lbf/ft}^2, \quad W_e/S_w = 12.8 \text{ lbf/ft}^2$$

$$(R_{\min})_{\text{full}} = \frac{2(4.0)}{1.2\sqrt{4.0^2 - (15.0/15.0)^2}} \frac{15.0 \text{ lbf/ft}^2}{0.0023769 \text{ slug/ft}^3 (32.2 \text{ ft/sec}^2)} = \underline{337 \text{ ft}}$$

$$(R_{\min})_{\text{empty}} = \frac{2(4.0)}{1.2\sqrt{4.0^2 - (12.8/15.0)^2}} \frac{12.8 \text{ lbf/ft}^2}{0.0023769 \text{ slug/ft}^3 (32.2 \text{ ft/sec}^2)} = \underline{285 \text{ ft}}$$

and for the business jet,

$$C_{L_{\max}} = 1.2, \quad n_{pll} = 4.0, \quad W_f/S_w = 62.5 \text{ lbf/ft}^2, \quad W_e/S_w = 37.5 \text{ lbf/ft}^2$$

$$(R_{\min})_{\text{full}} = \frac{2(4.0)}{1.2\sqrt{4.0^2 - (62.5/62.5)^2}} \frac{62.5 \text{ lbf/ft}^2}{0.0023769 \text{ slug/ft}^3 (32.2 \text{ ft/sec}^2)} = \underline{1{,}406 \text{ ft}}$$

$$(R_{\min})_{\text{empty}} = \frac{2(4.0)}{1.2\sqrt{4.0^2 - (37.5/62.5)^2}} \frac{37.5 \text{ lbf/ft}^2}{0.0023769 \text{ slug/ft}^3 (32.2 \text{ ft/sec}^2)} = \underline{826 \text{ ft}}$$

While turning radius is an important consideration in analyzing the turning performance of an aircraft, it is not the only important consideration. We are often also concerned with turning rate. *Turning rate* is simply the angular velocity of the airplane as it executes a turn. While turning radius is a measure of the distance required to turn an aircraft, turning rate is a measure of the time required to turn the aircraft.

The angular velocity of the airplane as it moves along a curved path is simply the translational velocity divided by the radius of curvature. Thus, using the result given in Eq. (3.9.20), the turning rate for a nearly level steady coordinated turn is

$$\Omega = \frac{V\cos\gamma}{R} \cong \frac{V}{R} = \frac{g\sqrt{n^2 - 1}}{V} \tag{3.9.29}$$

Using the stall-limited load factor from Eq. (3.9.21) in Eq. (3.9.29), we obtain the stall-limited maximum turning rate,

$$(\Omega_{\max})_{\text{stall}} = g\sqrt{\left(\frac{\rho C_{L_{\max}}}{2W/S_w}\right)^2 V^2 - \frac{1}{V^2}} \tag{3.9.30}$$

and using the load-limited load factor from Eq. (3.9.23) in Eq. (1.8.29), we obtain the load-limited maximum turning rate,

$$(\Omega_{\max})_{\text{load}} = \frac{g}{V}\sqrt{\left(n_{pll}\frac{W_{\max}}{W}\right)^2 - 1} \tag{3.9.31}$$

Figure 3.9.6 shows both the stall-limited and load-limited turning rates plotted as a function of airspeed for the general aviation airplane used in Example 3.9.1. Note that as was the case for the minimum turning radius, the maximum turning rate is achieved at the airspeed where the stall limit is equal to the load limit, i.e., the maneuvering speed. Setting the maximum turning rate from Eq. (3.9.30) equal to that from Eq. (3.9.31), we have

$$V_{\Omega_{\max}} = V_M = \sqrt{\frac{2n_{pll}}{C_{L_{\max}}}}\sqrt{\frac{W_{\max}/S_w}{\rho}} \tag{3.9.32}$$

Using this result for the airspeed in either Eq. (3.9.30) or (3.9.31), we obtain the maximum attainable turning rate,

$$\Omega_{\max} = \sqrt{\frac{C_{L_{\max}}}{2}\left(\frac{n_{pll}W_{\max}}{W} - \frac{W}{n_{pll}W_{\max}}\right)}\, g\sqrt{\frac{\rho}{W/S_w}} \tag{3.9.33}$$

Notice that both the minimum turning radius and the maximum turning rate are functions of the maximum lift coefficient, the positive load limit, the air density, and the

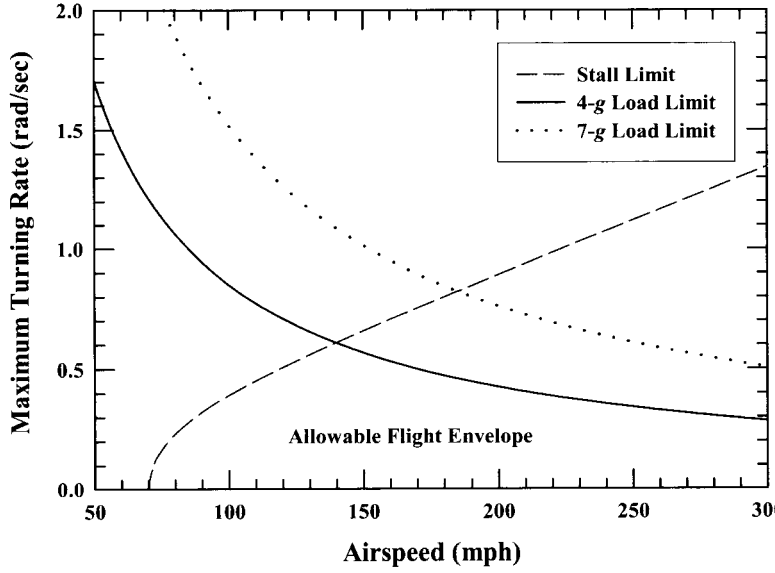


Figure 3.9.6. Maximum turning rate in a coordinated turn at sea level for the general aviation airplane in Example 3.9.1 with fuel tanks full.

wing loading. The designer has no control over air density and little control over the maximum lift coefficient. Most airplanes in cruise configuration will have a maximum lift coefficient between about 1.2 and 1.6. Thus, the primary features that the designer must use to control the turning performance of a conventional airplane are the wing loading and the load limit. Furthermore, as can be seen from Fig. 3.9.5, the minimum turning radius is not significantly affected by increasing the load limit beyond about 4. The only design parameter that can be used to significantly change the minimum turning radius of a conventional airplane is the wing loading. To provide a short turning radius in a conventional coordinated turn, the wing loading must be kept low.

Turning rate is not usually an important consideration in civilian aircraft. If an airplane needs to maneuver, take off, and land in small confined spaces, such as a small mountain valley, a short turning radius can be important. The maximum turning rate, however, has little effect on an airplane's ability to maneuver in tight places. Since increasing the load limit beyond about 4 cannot significantly reduce the minimum turning radius, load limit has little effect on the turning performance of most civilian airplanes. The positive load limit for civilian transports and general aviation airplanes is normally in the range from about 2.5 to 4.5.

On the other hand, turning rate can be a very important consideration for combat airplanes. As can be seen in Fig. 3.9.6, the maximum turning rate for an airplane is significantly improved by increasing the load limit well beyond 4. At large load factors, the maximum turning rate increases in proportion to the square root of the positive load limit. Thus, good turning performance for a combat airplane requires a high positive load limit as well as a low wing loading. The absolute upper limit for turning rate in a human-piloted aircraft is affected more by the pilot than by our ability to build an airplane capable of withstanding high load factor. A 9-g maneuver is about the maximum that a human pilot can endure without passing out. The positive load limit for modern fighter airplanes is normally in the range from about 6.5 to 9.0. Wing loading is always a trade-off in fighter airplanes because high wing loading facilitates high speed, but low wing loading facilitates agility.

EXAMPLE 3.9.2. For both the general aviation airplane and the business jet that were considered in Example 3.9.1, determine the indicated airspeed that should be used to achieve the highest turning rate. Also compute the maximum turning rate at 10,000 feet, for both aircraft, with fuel tanks full and with fuel tanks empty.

Solution. Assuming a nearly level coordinated turn, from Eq. (3.9.32) the airspeed that allows the highest turning rate is the maneuvering speed

$$V_{\Omega_{\max}} = V_M = \sqrt{\frac{2n_{pll}}{C_{L_{\max}}}}\sqrt{\frac{W_{\max}/S_w}{\rho}}$$

From Eq. (3.9.33) the maximum turning rate that can be achieved without stalling the wing or structurally damaging the airplane is

$$\Omega_{\max} = \sqrt{\frac{C_{L_{\max}}}{2}\left(\frac{n_{pll}W_{\max}}{W} - \frac{W}{n_{pll}W_{\max}}\right)}\, g\sqrt{\frac{\rho}{W/S_w}}$$

Airspeed indicators are always calibrated for the air density at standard sea level. Thus, for the general aviation airplane,

$$C_{L_{\max}} = 1.2, \quad n_{pll} = 4.0, \quad W_f/S_w = 15.0 \text{ lbf/ft}^2, \quad W_e/S_w = 12.8 \text{ lbf/ft}^2$$

$$(V_M)_{\text{indicated}} = \sqrt{\frac{2(4.0)}{1.2}}\sqrt{\frac{15.0 \text{ lbf/ft}^2}{0.0023769 \text{ slug/ft}^3}} = \underline{205 \text{ ft/sec} = 140 \text{ mph} = 122 \text{ knots}}$$

$$(\Omega_{\max})_{\text{full}} = \sqrt{\frac{1.2}{2}\left(\frac{(4.0)15.0}{15.0} - \frac{15.0}{(4.0)15.0}\right)}(32.2 \text{ ft/sec}^2)\sqrt{\frac{0.0017556 \text{ slug/ft}^3}{15.0 \text{ lbf/ft}^2}}$$

$$= \underline{0.5225 \text{ rad/sec}}$$

$$(\Omega_{\max})_{\text{empty}} = \sqrt{\frac{1.2}{2}\left(\frac{(4.0)15.0}{12.8} - \frac{12.8}{(4.0)15.0}\right)}(32.2 \text{ ft/sec}^2)\sqrt{\frac{0.0017556 \text{ slug/ft}^3}{12.8 \text{ lbf/ft}^2}}$$

$$= \underline{0.6179 \text{ rad/sec}}$$

and for the business jet,

$$C_{L_{\max}} = 1.2, \quad n_{pll} = 4.0, \quad W_f/S_w = 62.5 \text{ lbf/ft}^2, \quad W_e/S_w = 37.5 \text{ lbf/ft}^2$$

$$(V_M)_{\text{indicated}} = \sqrt{\frac{2(4.0)}{1.2}}\sqrt{\frac{62.5 \text{ lbf/ft}^2}{0.0023769 \text{ slug/ft}^3}} = \underline{419 \text{ ft/sec} = 285 \text{ mph} = 248 \text{ knots}}$$

$$(\Omega_{\max})_{\text{full}} = \sqrt{\frac{1.2}{2}\left(\frac{(4.0)62.5}{62.5} - \frac{62.5}{(4.0)62.5}\right)}(32.2 \text{ ft/sec}^2)\sqrt{\frac{0.0017556 \text{ slug/ft}^3}{62.5 \text{ lbf/ft}^2}}$$

$$= \underline{0.2560 \text{ rad/sec}}$$

$$(\Omega_{\max})_{\text{empty}} = \sqrt{\frac{1.2}{2}\left(\frac{(4.0)62.5}{37.5} - \frac{37.5}{(4.0)62.5}\right)}(32.2 \text{ ft/sec}^2)\sqrt{\frac{0.0017556 \text{ slug/ft}^3}{37.5 \text{ lbf/ft}^2}}$$

$$= \underline{0.4357 \text{ rad/sec}}$$

For both of the examples that were presented in this section, the turning analysis was based on the assumption of a nearly level turn. That is, the small-climb-angle approximation, $\cos\gamma = 1$, was used. This approximation simplified the turning analysis by making both the turning radius and the turning rate independent of the power or thrust available from the engines. For steeply climbing or diving turns we must return to the more general result that was given by Eq. (3.9.19). Using Eqs. (3.9.21) and (3.9.23) in Eq. (3.9.19), we obtain the stall-limited and load-limited turning radii for steeply climbing or diving turns,

$$(R_{\min})_{\text{stall}} = \cos^2\gamma \Big/ g\sqrt{\left(\frac{\rho C_{L_{\max}}}{2W/S_w}\right)^2 - \frac{\cos^2\gamma}{V^4}} \tag{3.9.34}$$

$$(R_{\min})_{\text{load}} = V^2\cos^2\gamma \Big/ g\sqrt{\left(n_{pll}\frac{W_{\max}}{W}\right)^2 - \cos^2\gamma} \tag{3.9.35}$$

Using these results in the general form of Eq. (3.9.29), we obtain the stall-limited and load-limited turning rates for steeply climbing or diving turns,

$$(\Omega_{\max})_{\text{stall}} = \frac{g}{\cos\gamma}\sqrt{\left(\frac{\rho C_{L_{\max}}}{2W/S_w}\right)^2 V^2 - \frac{\cos^2\gamma}{V^2}} \tag{3.9.36}$$

$$(\Omega_{\max})_{\text{load}} = \frac{g}{V\cos\gamma}\sqrt{\left(n_{pll}\frac{W_{\max}}{W}\right)^2 - \cos^2\gamma} \tag{3.9.37}$$

Thus, we see that for steeply climbing or diving turns, the minimum turning radius is smaller and the maximum turning rate is larger than for nearly level turns. However, for steady turns of this type, the minimum turning radius and the maximum turning rate depend on the climb angle, which in turn depends on the thrust available. The general relation between the turning climb angle and the thrust available for a steady turn is given by Eq. (3.9.8). The general relation for load factor in a steady climbing or diving turn, as obtained from Eq. (3.9.3), is

$$n \equiv \frac{L}{W} = \frac{\cos\gamma}{\cos\phi} \tag{3.9.38}$$

Using Eq. (3.9.38) in Eq. (3.9.8), the turning climb angle is related to the thrust available and the load factor according to

$$\sin\gamma = \frac{T - \left(\frac{1}{2}\rho V^2 S_w C_{D_0} + C_{D_{0,L}} nW + \dfrac{n^2W^2}{\frac{1}{2}\pi e R_A \rho V^2 S_w}\right)}{W} \tag{3.9.39}$$

Using Eqs. (3.9.21) and (3.9.23) in Eq. (3.9.39), we obtain the stall-limited and load-limited climb angles for steady climbing or diving turns,

$$(\sin\gamma)_{\text{stall-limit}} = \frac{T - \frac{1}{2}\rho V^2 S_w\left(C_{D_0} + C_{D_{0,L}} C_{L\max} + \dfrac{C_{L\max}^2}{\pi e R_A}\right)}{W} \tag{3.9.40}$$

$$(\sin\gamma)_{\text{load-limit}} = \frac{T - \left(\frac{1}{2}\rho V^2 S_w C_{D_0} + C_{D_{0,L}} n_{pll} W_{\max} + \frac{n_{pll}^2 W_{\max}^2}{\frac{1}{2}\pi e R_A \rho V^2 S_w} \right)}{W} \tag{3.9.41}$$

Thus, for a steeply climbing or diving turn with constant airspeed, Eqs. (3.9.40) and (3.9.41) can be used to eliminate the climb angle from Eqs. (3.9.34) through (3.9.37) and express the limiting values for turning radius and turning rate as a function of thrust and airspeed.

While a steeply climbing or diving turn can result in reduced turning radius and increased turning rate, such turns are not typically used with civilian aircraft. However, such turns are routinely employed with combat airplanes. Furthermore, pilots of combat airplanes often execute what are called *dynamic turns* in which the airspeed and angle of attack change very rapidly. In such maneuvers the aircraft may reach velocities near zero and angles of attack as high as 90 degrees. Maneuvers that involve angles of attack greater than stall are called *post-stall maneuvers*. Such maneuvers, of course, violate the constant-airspeed assumption that has been used throughout this section.

An example of a post-stall dynamic turn called the *cobra maneuver* is shown in Fig. 3.9.7. In this maneuver the pilot pitches the aircraft up rapidly and decelerates, slowing to extremely low speeds while executing the turn. As the angle of attack approaches 90 degrees the aircraft is rolled approximately 90 degrees about the velocity

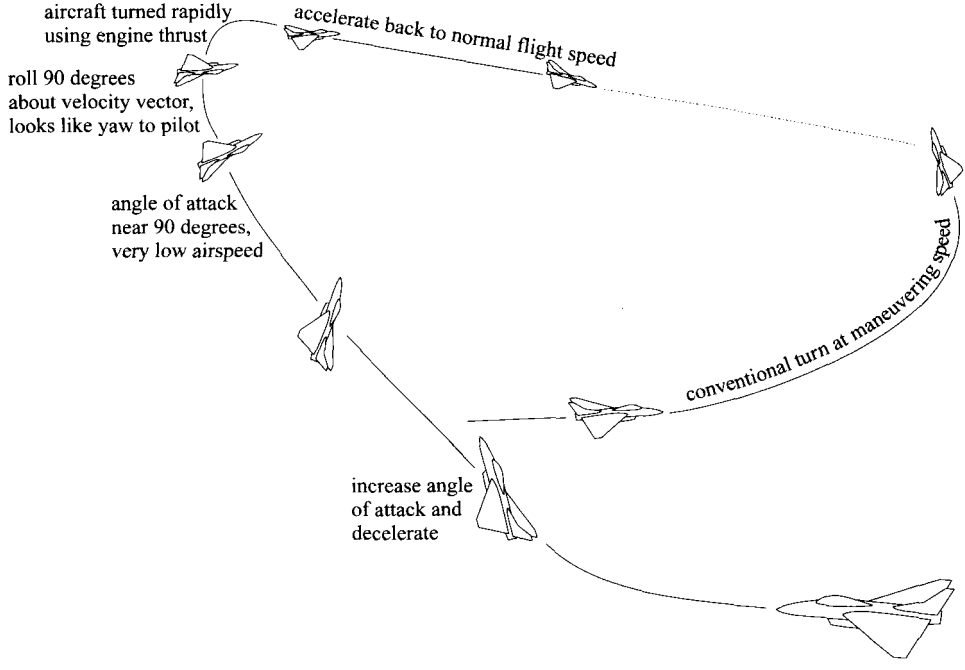


Figure 3.9.7. A post-stall dynamic turn called the cobra maneuver.

vector. This roll looks like a 90-degree yaw to the pilot because of the nearly 90-degree angle of attack. At the top of the maneuver, the aircraft is turned very rapidly using engine thrust until the nose is pointing at the target aircraft. The pilot then takes the shot and accelerates out of the high angle of attack and back to normal flight speed. Such maneuvers, of course, cannot be treated using a constant-airspeed turning analysis.

It should also be noted that there is another somewhat more subtle assumption implied in the turning analysis that was presented in this section. This assumption was implicitly introduced with Eq. (3.9.5). In using this equation for the lift coefficient we have implied that the airspeed is the same at every spanwise section of the wing.

In reality, when an airplane is turning, the outer wingtip is moving faster than the center of gravity, and the inner wingtip is moving slower than the center of gravity. If the turning radius is large compared to the semispan, then this effect is very small and can be neglected in the turning analysis. For most airplanes, with typical values of wing loading and span, this assumption is well justified. However, the minimum turning radius is proportional to wing loading, and some specialty aircraft with low wing loading and large span can violate this approximation.

The spanwise distribution of airspeed across the wing of a turning airplane varies linearly with distance from the axis of the turn,

$$V(r) = V_{cg}\, r/R \tag{3.9.42}$$

where V_{cg} is the airspeed for the center of gravity, r is the local distance from the turn axis, and R is the distance from the turn axis to the center of gravity, i.e., the turning radius. Thus, the airspeed at the inner wingtip is

$$V_{\text{inner}} = V_{cg}\left(1-\frac{b}{2R}\cos\phi\right) \tag{3.9.43}$$

and the airspeed at the outer wingtip is

$$V_{\text{outer}} = V_{cg}\left(1+\frac{b}{2R}\cos\phi\right) \tag{3.9.44}$$

For airplanes with typical wing loading and span, this airspeed difference is slight and is easily countered with a little aileron deflection to increase the lift coefficient on the inside wing. However, when flying an airplane with low wing loading and large span, the decrease in airspeed at the inside wingtip can cause this wingtip to stall at a load factor considerably less than that predicted by Eq. (3.9.21). This type of wingtip stall often leads to a spin.

A modification to Eq. (3.9.21) that can approximately account for the spanwise variation in airspeed is

$$n_{\max} = \frac{\frac{1}{2}\rho V_{\text{inner}}^2}{W/S_w} C_{L_{\max}} = \frac{\frac{1}{2}\rho V^2}{W/S_w}\left(1-\frac{b}{2R}\cos\phi_{\max}\right)^2 C_{L_{\max}} \tag{3.9.45}$$

Using Eqs. (3.9.14) and (3.9.20) to eliminate the bank angle and the turning radius from this result, Eq. (3.9.45) can be rearranged to yield

$$n_{\max} - \frac{bg}{2V^2}\sqrt{n_{\max}^2 - 1} - \sqrt{\frac{2W/S_w}{\rho V^2 C_{L_{\max}}}}\sqrt{n_{\max}^3} = 0 \tag{3.9.46}$$

Equation (3.9.46) can be solved numerically to yield the stall-limited load factor as a function of airspeed. This result can be used in Eq. (3.9.20) to obtain the stall-limited turning radius as a function of airspeed. Combining the stall-limited load factor from Eq. (3.9.46) with the load-limited load factor from Eq. (3.9.23), we obtain an equation for the airspeed at which the minimum turning radius is attained,

$$V^2 - \sqrt{\frac{2n_{pll} W_{\max}/S_w}{\rho C_{L\max}}}\, V - \frac{bg}{2}\sqrt{1 - \left(\frac{W}{n_{pll} W_{\max}}\right)^2} = 0 \tag{3.9.47}$$

The airspeed that allows for the minimum turning radius without stalling the inside wingtip or causing structural damage to the aircraft is approximated as the positive root of Eq. (3.9.47),

$$V_{R_{\min}} = \sqrt{\frac{n_{pll} W_{\max}/S_w}{2\rho C_{L_{\max}}}} + \sqrt{\frac{n_{pll} W_{\max}/S_w}{2\rho C_{L_{\max}}} + \frac{bg}{2}\sqrt{1 - \left(\frac{W}{n_{pll} W_{\max}}\right)^2}} \tag{3.9.48}$$

The minimum turning radius is approximated by using this airspeed in Eq. (3.9.27) and the maximum turning rate is approximated by using this airspeed in Eq. (3.9.31).

Accounting for wingtip stall always increases the stall-limited turning radius. For most airplanes this increase is small and can be ignored. Figure 3.9.8 shows the effect of wingtip stall on the minimum turning radius for the general aviation airplane described in Example 3.9.1. The solid line shows the stall-limited turning radius predicted by Eq. (3.9.26), and the dashed line shows the stall-limited turning radius obtained from the solution to Eq. (3.9.46). For this airplane, with a relatively low wing loading of 15 lbf/ft^2, the effect of the spanwise variation in airspeed is perceptible but small. Most commercial and military airplanes have significantly higher wing loading, and the effect of wingtip stall on the turning performance of these airplanes is even smaller. The effect of wingtip stall becomes more important in the design of airplanes with very low wing loading and large span.

The turning characteristics of an airplane with large span and low wing loading are much different from those of more typical airplanes. For such aircraft, the turning analysis must account for the variation in airspeed with position along the span. For example, a turn is usually initiated with a deflection of the ailerons. To initiate a right turn the left aileron is deflected down and the right aileron is deflected up. This increases the lift and drag coefficients on the outboard portion of the left wing and decreases the lift and drag coefficients on the outboard portion of the right wing. For airplanes with

typical wing loading and span, this increases the lift and drag on the left wing and decreases the lift and drag on the right wing, banking the airplane to the right and yawing it to the left. The tendency of an airplane to yaw left when being banked right is called *adverse yaw*. This leftward yawing motion decreases the airspeed over the outboard portion of the left wing and increases the airspeed over the outboard portion of the right wing. While the differential in lift coefficient between the outboard portions of the right and left wings will tend to bank the plane right, the differential in airspeed between the outboard portions of the right and left wings will tend to bank the plane left. For an airplane with typical wing loading and span, the lift coefficient differential dominates and the plane banks right. However, for an airplane with very large span and very low wing loading, the airspeed differential may actually dominate the lift coefficient differential, causing the airplane to bank left and yaw left as the result of what would normally be thought of as a right-turning aileron deflection. This is only one of many possible effects that may result from spanwise airspeed variation during a turn.

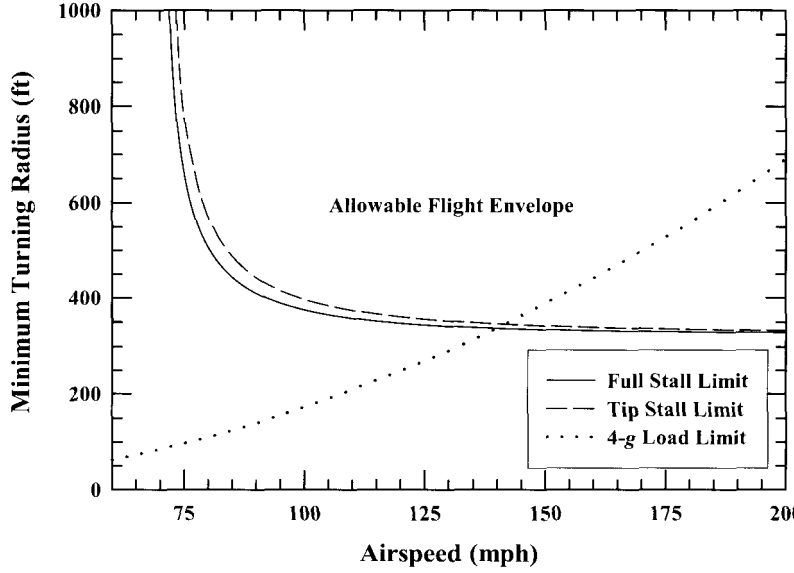


Figure 3.9.8. Effect of wingtip stall on minimum turning radius in a coordinated turn at sea level for the general aviation airplane in Example 3.9.1 with fuel tanks full.

3.10. Takeoff and Landing Performance

One important aspect of airplane design and performance analysis is takeoff and landing distances. The liftoff distance is defined as the distance along the ground required for an airplane, starting with zero ground speed, to accelerate to flight speed, rotate to liftoff attitude, and lift from the ground. This total distance, referred to as the *ground roll*, is designated here as s_g. This total ground roll distance can be divided into two segments, the acceleration distance, s_a, and the rotation distance, s_r.

For aircraft with the commonly used tricycle landing gear, during the acceleration phase of the ground roll, the angle of attack and lift coefficient are fixed by the landing gear. The case of tail-dragger landing gear is addressed later. Once the airplane has accelerated to flight speed, the pilot initiates an elevator deflection to rotate the airplane and increase the angle of attack. During the rotation phase of the ground roll, the angle of attack and lift coefficient are constantly increasing as a result of the moment applied to the airplane through the elevator deflection. As the airplane rotates, the angle of attack and lift coefficient continue to increase until the lift is equal to the weight and the airplane lifts from the ground.

Maximum thrust is nearly always used for takeoff, so once the extent of engagement for the high-lift devices is fixed, the lift and drag coefficients during the acceleration run are functions only of airplane design. Thus, the acceleration distance is controlled almost entirely by the design of the airplane and can easily be determined. The rotation distance, on the other hand, depends mostly on the pilot. Maximum elevator deflection is seldom used. However, the rotation distance is a small fraction of the total ground roll, and by making some appropriate assumption concerning pilot input, a reasonable estimate for the rotation distance can be made.

To determine the acceleration distance, we apply Newton's second law in the direction of motion. The mass of the airplane multiplied by its acceleration must equal the summation of forces in the direction of motion. For a zero thrust angle and constant headwind speed, V_{hw}, we have

$$\frac{W}{g}\frac{dV_g}{dt} = \frac{W}{g}\frac{d}{dt}(V - V_{hw}) = \frac{W}{g}\frac{dV}{dt} = T - D - F_r \tag{3.10.1}$$

where V_g is ground speed, V is airspeed, and the force terms on the far right-hand side are respectively, the engine thrust, the aerodynamic drag, and the rolling friction between the tires and the ground. Each of these forces is shown schematically in Fig. 3.10.1.

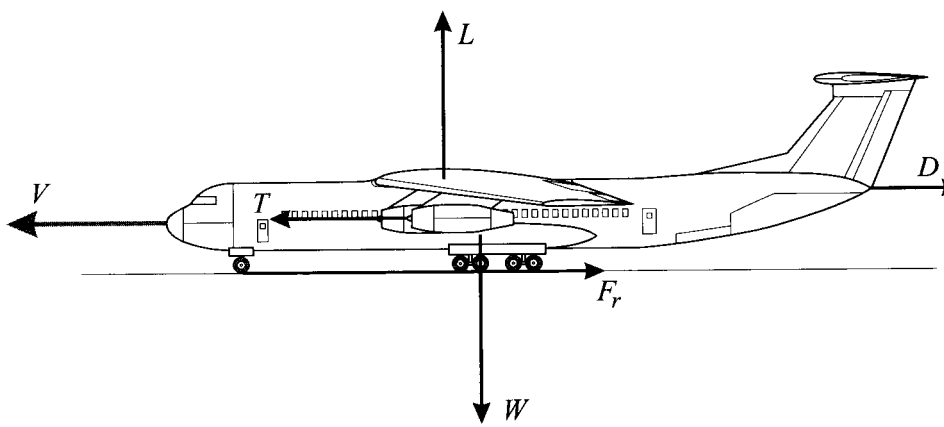


Figure 3.10.1. Forces acting on an airplane with tricycle landing gear during the acceleration run or landing ground roll.

The change in airspeed with respect to time can be written as

$$\frac{dV}{dt} = \frac{ds}{dt}\frac{dV}{ds} = (V - V_{hw})\frac{dV}{ds} \tag{3.10.2}$$

where s is distance traveled along the ground. Using Eq. (3.10.2) in Eq. (3.10.1) and rearranging, we obtain

$$\frac{ds}{dV} = \frac{W(V - V_{hw})}{g(T - D - F_r)} \tag{3.10.3}$$

Separating variables and integrating between any two points along the runway gives

$$s_{i+1} - s_i = \frac{W}{g}\int_{V_i}^{V_{i+1}} \frac{(V - V_{hw})\,dV}{T - D - F_r} \tag{3.10.4}$$

Here, we have neglected the fuel that is burned off during takeoff and are assuming constant weight. The integral in Eq. (3.10.4) can be evaluated numerically, if we know how the thrust, the drag, and the rolling friction depend on airspeed. Figure 3.10.2 shows how these forces might vary with airspeed for a typical general aviation airplane.

The total drag on the airplane is the parasitic drag plus the induced drag. However, during the takeoff run, the induced drag is diminished by a phenomenon known as *ground effect*. When a moving wing is close to the ground, the strength of the trailing vortices is decreased as a result of interaction with the ground. Since these vortices

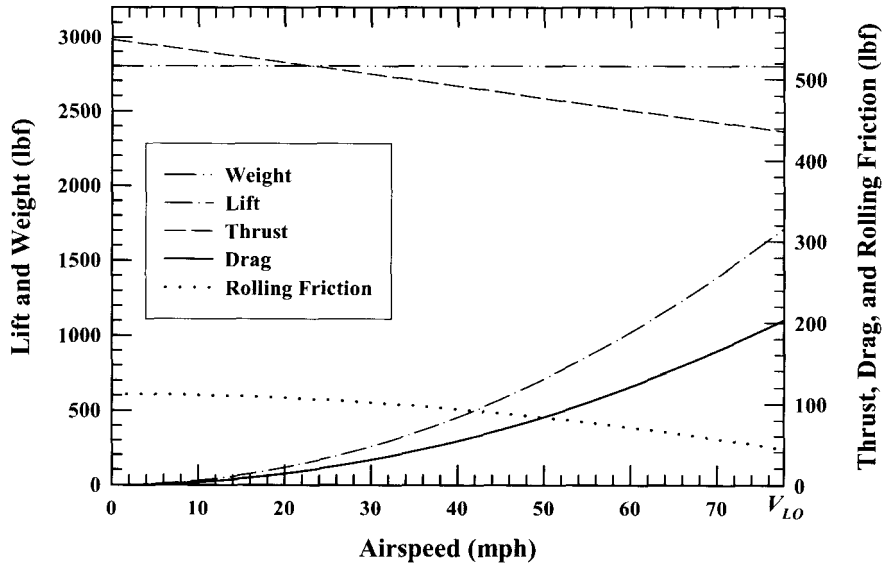


Figure 3.10.2. Variation in forces with airspeed during the acceleration run.

induce the downwash that generates induced drag, the downwash and associated induced drag are reduced when an airplane is close to the ground. An approximate equation for the drag on an airplane in ground effect is

$$D = \tfrac{1}{2}\rho V^2 S_w C_D \cong \tfrac{1}{2}\rho V^2 S_w \left(C_{D_0} + C_{D_{0,L}} C_L + \frac{(16 h_w/b_w)^2}{1+(16 h_w/b_w)^2} \frac{C_L^2}{\pi e R_A} \right) \tag{3.10.5}$$

where h_w is the height of the wing above the ground and b_w is the wingspan. During ground roll, the zero-lift drag coefficient is typically higher than in cruise configuration, because the landing gear is extended and high-lift devices are engaged.

During the ground roll, the rolling friction force is given by

$$F_r = \mu_r (W - L) = \mu_r (W - \tfrac{1}{2}\rho V^2 S_w C_L) \tag{3.10.6}$$

where μ_r is the coefficient of rolling friction and $W - L$ is the net normal force between the tires and the ground. Experiments have shown that the coefficient of rolling friction, on takeoff, varies from about 0.04 for paved surfaces to 0.10 for grass landing fields. For rough landing fields with soft or loose soil, even higher values of μ_r should be used.

The lift coefficient remains fairly constant during the acceleration phase of the takeoff run, so both the lift and the drag vary approximately as the square of the airspeed. The actual value of the lift coefficient during the acceleration run is controlled by the angle of attack that is maintained by the landing gear and by the extent to which high-lift devices are engaged during takeoff. Hence, the lift coefficient for the acceleration run is essentially a design feature of the airplane. Increasing the lift coefficient for the acceleration run will reduce the rolling friction but will increase the drag. Depending on the airplane design, the lift coefficient for the acceleration run could vary from less than 0.1 to as much as 70 percent of $C_{L_{\max}}$. In any case, as the airplane accelerates down the runway, the lift coefficient remains constant at this design value until the airplane reaches the rotation speed. Thus, during the acceleration run, both the drag and the rolling friction are linear functions of the airspeed squared.

The manner in which thrust depends on airspeed is a function of the power plant being used. For turbojet engines, the thrust remains relatively constant with airspeed. For a piston engine combined with a constant-pitch propeller, the thrust decreases nearly linearly with airspeed. A turbofan engine produces thrust that varies almost as a parabolic function of airspeed. Normally, the relation between engine thrust and airspeed is determined experimentally and provided in tabular form. For most power plants, the variation in thrust with airspeed can be approximated as parabolic over a fairly broad range of airspeed and, in general, we could describe thrust as a piecewise parabolic function of airspeed. If the acceleration run is divided into small segments and the thrust is assumed parabolic with airspeed over each segment, then for segment i,

$$T = (T_0)_i + (T')_i V + (T'')_i V^2 \tag{3.10.7}$$

where T_0, T', and T'' are experimentally determined coefficients.

Applying Eqs. (3.10.5) through (3.10.7) to Eq. (3.10.4), we have

$$s_{i+1} - s_i = \frac{1}{g}\int_{V_i}^{V_{i+1}} \frac{(V - V_{hw})\,dV}{(K_0)_i + (K_1)_i V + (K_2)_i V^2} \tag{3.10.8}$$

where

$$(K_0)_i = \frac{(T_0)_i}{W} - \mu_r \tag{3.10.9}$$

$$(K_1)_i = \frac{(T')_i}{W} \tag{3.10.10}$$

$$(K_2)_i = \frac{(T'')_i}{W} + \frac{\rho}{2W/S_w}(C_L\mu_r - C_D) \tag{3.10.11}$$

The integration on the right-hand side of Eq. (3.10.8) is easily carried out to yield

$$s_{i+1} - s_i = \frac{(K_T)_i - V_{hw}(K_W)_i}{g} \tag{3.10.12}$$

where

$$(K_T)_i = \begin{cases} \begin{cases} \dfrac{(V^2)_{i+1} - (V^2)_i}{2(K_0)_i}, & (K_1)_i = 0 \\ \dfrac{(K_0)_i}{(K_1)_i^2}\ln\left(\dfrac{f_i}{f_{i+1}}\right) + \dfrac{(V)_{i+1} - (V)_i}{(K_1)_i}, & (K_1)_i \neq 0 \end{cases}, & (K_2)_i = 0 \\ \dfrac{1}{2(K_2)_i}\ln\left(\dfrac{f_{i+1}}{f_i}\right) - \dfrac{(K_1)_i (K_W)_i}{2(K_2)_i}, & (K_2)_i \neq 0 \end{cases} \tag{3.10.13}$$

$$(K_W)_i = \begin{cases} \begin{cases} \dfrac{(V)_{i+1} - (V)_i}{(K_0)_i}, & (K_1)_i = 0 \\ \dfrac{1}{(K_1)_i}\ln\left(\dfrac{f_{i+1}}{f_i}\right), & (K_1)_i \neq 0 \end{cases}, & (K_2)_i = 0 \\ \dfrac{1}{\sqrt{-(K_R)_i}}\ln\left[\dfrac{\left(f'_{i+1} - \sqrt{-(K_R)_i}\right)\left(f'_i + \sqrt{-(K_R)_i}\right)}{\left(f'_{i+1} + \sqrt{-(K_R)_i}\right)\left(f'_i - \sqrt{-(K_R)_i}\right)}\right], & (K_R)_i < 0 \\ \dfrac{2}{f'_i} - \dfrac{2}{f'_{i+1}}, & (K_R)_i = 0 \\ \dfrac{2}{\sqrt{(K_R)_i}}\left[\tan^{-1}\left(\dfrac{f'_{i+1}}{\sqrt{(K_R)_i}}\right) - \tan^{-1}\left(\dfrac{f'_i}{\sqrt{(K_R)_i}}\right)\right], & (K_R)_i > 0 \end{cases} \tag{3.10.14}$$

$$f_i = (K_0)_i + (K_1)_i (V)_i + (K_2)_i (V^2)_i \tag{3.10.15}$$

$$f_{i+1} = (K_0)_i + (K_1)_i (V)_{i+1} + (K_2)_i (V^2)_{i+1} \tag{3.10.16}$$

$$f_i' = (K_1)_i + 2(K_2)_i (V)_i \tag{3.10.17}$$

$$f_{i+1}' = (K_1)_i + 2(K_2)_i (V)_{i+1} \tag{3.10.18}$$

$$(K_R)_i = 4(K_0)_i (K_2)_i - (K_1)_i^2 \tag{3.10.19}$$

To obtain the total acceleration distance, Eq. (3.10.4) must be integrated from zero ground speed to the rotation speed. The change in airspeed during rotation is usually quite small, so the rotation speed is very close to the liftoff speed. Thus, for computing the ground roll, the rotation speed is usually assumed to be equal to the liftoff speed. The airspeed at liftoff must be at least 1.1 times the stall speed for the airplane in takeoff configuration,

$$V_{LO} = 1.1\sqrt{\frac{2}{C_{L\max}}}\sqrt{\frac{W/S_w}{\rho}} \tag{3.10.20}$$

Here $C_{L\max}$ is the maximum lift coefficient for the airplane in takeoff configuration. Remember that the landing gear and tail configuration may limit the maximum angle of attack, and hence the maximum lift coefficient for takeoff.

For best accuracy, the acceleration distance should be broken up into many small segments with the length of each segment computed from Eq. (3.10.12). However, for most power plants, the variation in thrust with airspeed is nearly parabolic over the entire acceleration run. Thus, a good approximation for the acceleration distance is obtained by applying Eq. (3.10.12) over the full acceleration run as a single step. To obtain a parabolic approximation for the thrust over the full acceleration run, the coefficients in Eq. (3.10.7) can be computed as

$$T_0 = T_S \tag{3.10.21}$$

$$T' = \frac{6\overline{T} - 4T_S - 2T_{LO}}{V_{LO}} \tag{3.10.22}$$

$$T'' = \frac{3T_S + 3T_{LO} - 6\overline{T}}{V_{LO}^2} \tag{3.10.23}$$

where T_S is the static thrust, T_{LO} is the thrust at liftoff, and $\overline{T}$ is the average thrust,

$$\overline{T} \equiv \frac{1}{V_{LO}} \int_0^{V_{LO}} T\, dV \tag{3.10.24}$$

For the critical case of **no wind**, this gives

$$s_a = \frac{K_T}{g} \tag{3.10.25}$$

where

$$K_T = \begin{cases} \left\{ \begin{array}{ll} \dfrac{V_{LO}^2}{2K_0}, & K_1 = 0 \\ \dfrac{K_0}{K_1^2}\ln\left(\dfrac{f_S}{f_{LO}}\right) + \dfrac{V_{LO}}{K_1}, & K_1 \neq 0 \end{array} \right\}, & K_2 = 0 \\ \dfrac{1}{2K_2}\ln\left(\dfrac{f_{LO}}{f_S}\right) - \dfrac{K_1 K_W}{2K_2}, & K_2 \neq 0 \end{cases} \tag{3.10.26}$$

$$K_W = \begin{cases} \dfrac{1}{\sqrt{-K_R}}\ln\left[\dfrac{\left(f'_{LO} - \sqrt{-K_R}\right)\left(f'_S + \sqrt{-K_R}\right)}{\left(f'_{LO} + \sqrt{-K_R}\right)\left(f'_S - \sqrt{-K_R}\right)}\right], & K_R < 0 \\ \dfrac{2}{f'_S} - \dfrac{2}{f'_{LO}}, & K_R = 0 \\ \dfrac{2}{\sqrt{K_R}}\left[\tan^{-1}\left(\dfrac{f'_{LO}}{\sqrt{K_R}}\right) - \tan^{-1}\left(\dfrac{f'_S}{\sqrt{K_R}}\right)\right], & K_R > 0 \end{cases} \tag{3.10.27}$$

$$f_S = K_0 = \frac{T_S}{W} - \mu_r \tag{3.10.28}$$

$$f_{LO} = K_0 + K_1 V_{LO} + K_2 V_{LO}^2 = \frac{T_{LO}}{W} - \mu_r + \frac{\rho V_{LO}^2}{2W/S_w}(\mu_r C_L - C_D) \tag{3.10.29}$$

$$f'_S = K_1 = \frac{6\bar{T} - 4T_S - 2T_{LO}}{WV_{LO}} \tag{3.10.30}$$

$$f'_{LO} = K_1 + 2K_2 V_{LO} = \frac{2T_S + 4T_{LO} - 6\bar{T}}{WV_{LO}} + \frac{\rho V_{LO}}{W/S_w}(C_L\mu_r - C_D) \tag{3.10.31}$$

$$K_0 = \frac{T_S}{W} - \mu_r \tag{3.10.32}$$

$$K_1 = \frac{T'}{W} = \frac{6\bar{T} - 4T_S - 2T_{LO}}{WV_{LO}} \tag{3.10.33}$$

$$K_2 = \frac{T''}{W} + \frac{\rho}{2W/S_w}(C_L\mu_r - C_D)$$
$$= \frac{3T_S + 3T_{LO} - 6\bar{T}}{WV_{LO}^2} + \frac{\rho}{2W/S_w}(C_L\mu_r - C_D) \tag{3.10.34}$$

$$K_R = 4K_0K_2 - K_1^2 \tag{3.10.35}$$

When the airplane has accelerated to flight speed, the pilot initiates an elevator deflection to rotate the airplane, increasing the angle of attack and lift coefficient to the point where the lift is equal to the weight and the airplane lifts from the ground. The rotation distance is a small fraction of the total ground roll and, as previously mentioned, the change in airspeed during rotation is usually quite small. Thus, for computing the ground roll, the rotation is usually assumed to take place at a constant airspeed equal to the liftoff speed given by Eq. (3.10.20). The rotation rate depends almost entirely on the pilot. Maximum elevator deflection is almost never used during rotation. In computing ground roll, the designer should allow the pilot a rotation time in proportion to the size of the airplane. For small general aviation aircraft and fighter planes, a rotation time on the order of 1 second is adequate, but for large transports and bombers, the rotation time should be increased to about 3 seconds. For the very largest airplanes, as much as 4 seconds should probably be allowed for rotation. Thus, the rotation distance is computed simply as the time allowed for rotation multiplied by the ground speed at the liftoff airspeed,

$$s_r = (V_{LO} - V_{hw})t_r \tag{3.10.36}$$

where t_r is the assumed rotation time. The total ground roll is the sum of the acceleration distance and the rotation distance,

$$s_g = s_a + s_r \tag{3.10.37}$$

To gain some additional insight into the parameters that affect takeoff performance, consider a further simplification to Eq. (3.10.25). As we have seen from Fig. 3.10.2, the drag increases with airspeed while the rolling friction decreases with airspeed. Furthermore, for many power plants, the change in thrust during takeoff is small. Thus, as a first approximation for the acceleration distance, we can neglect the variation in net force with airspeed (i.e., $K_1 \cong K_2 \cong 0$). With this approximation, the no-wind acceleration distance from Eq. (3.10.25) reduces to

$$s_a = \frac{K_T}{g} \cong \frac{V_{LO}^2}{2gK_0} \cong \frac{WV_{LO}^2}{2g(T - D - F_r)} \tag{3.10.38}$$

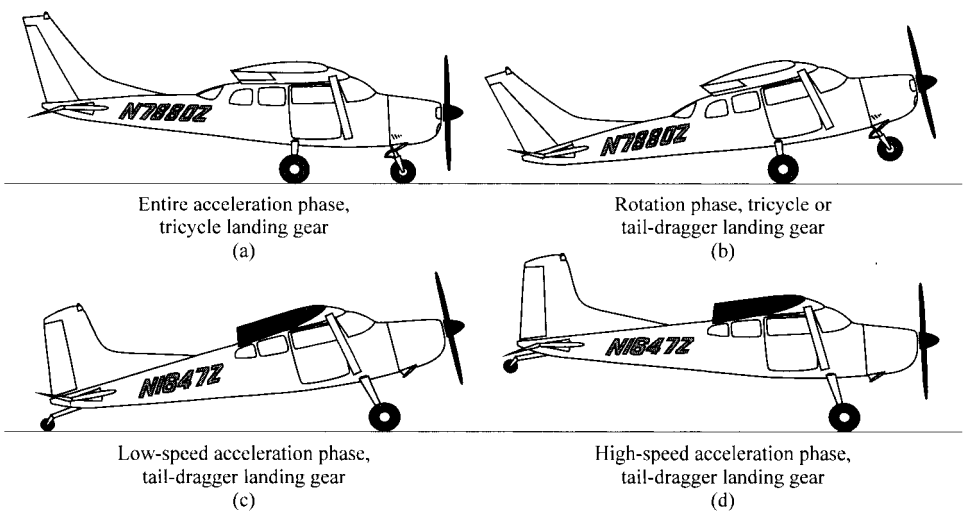
Equation (3.10.38) gives a reasonable first estimate for the acceleration distance even when there is some variation in the net force with airspeed, provided that the net force is

evaluated at about 70 percent of the liftoff airspeed. Using the liftoff speed from Eq. (3.10.20) and adding the rotation distance from Eq. (3.10.36), an approximate first estimate for the no-wind ground roll on takeoff is

$$s_g \cong \frac{1.21W^2}{\rho g S_w C_{L_{\max}} (T - D - F_r)_{0.7V_{LO}}} + 1.1 t_r \sqrt{\frac{2}{C_{L_{\max}}}} \sqrt{\frac{W/S_w}{\rho}} \tag{3.10.39}$$

From Eq. (3.10.39) we note that the acceleration distance increases as the square of the gross weight. If we double the weight of an airplane, the acceleration distance will quadruple. We also see that acceleration distance varies inversely with air density. Since the thrust also decreases with decreasing density, this effect is much greater than would at first appear from looking at Eq. (3.10.39). In fact, the acceleration distance varies almost as the inverse square of the air density. As a result, hot summer days and high-altitude airports require significantly longer acceleration runs. We can also see from Eq. (3.10.39) that the acceleration distance is inversely proportional to the wing area. Thus, if we require a short takeoff distance, low wing loading is important.

The no-wind acceleration distance computed from Eqs. (3.10.25) through (3.10.35) is for an airplane with tricycle landing gear, as shown in Fig. 3.10.3a and b. In obtaining this relation, it was assumed that the angle of attack remains constant for the entire acceleration run. This is a good assumption for tricycle landing gear, because this type of gear holds the attitude of the airplane constant prior to rotation. For a tail dragger, however, this assumption is not valid. A tail dragger starts the acceleration run at a high angle of attack with the tail wheel on the ground, as shown in Fig 3.10.3c. During this initial phase of the acceleration run, the lift and drag coefficients are quite large,



Entire acceleration phase, tricycle landing gear (a)

Rotation phase, tricycle or tail-dragger landing gear (b)

Low-speed acceleration phase, tail-dragger landing gear (c)

High-speed acceleration phase, tail-dragger landing gear (d)

Figure 3.10.3. Aircraft attitude during different phases of the takeoff ground roll for airplanes with tricycle and tail-dragger landing gear.

due to this high angle of attack. The tail must remain on the ground to provide steering until sufficient airspeed is developed to afford adequate steering with the rudder. This airspeed is called the *minimum ground control speed.* At this airspeed the pilot initiates an elevator deflection to lift the tail, as shown in Fig 3.10.3d, decreasing the angle of attack and the associated lift and drag coefficients. The remainder of the acceleration run takes place at this reduced angle of attack to keep the drag low. Once the airplane has accelerated to flight speed, the pilot initiates a second elevator deflection, this time to increase the angle of attack and rotate the plane to liftoff, as shown in Fig. 3.10.3b. This final rotation phase of the ground roll is similar to that for an airplane with tricycle landing gear.

While Eq. (3.10.25) does not apply directly to a tail-dragger, Eq. (3.10.12) can still be used independently over each phase of the acceleration run. The low-speed phase starts at a ground speed of zero (i.e., an airspeed equal to the headwind speed) and continues until the airspeed is equal to the minimum ground control speed. During this phase, the angle of attack, the lift coefficient, and the drag coefficient are held constant at the values associated with the tail-down attitude. The lift coefficient for the low-speed phase of the acceleration run should be very close to $C_{L_{max}}$. The high-speed phase of the acceleration run starts at an airspeed equal to the minimum ground control speed and continues to the liftoff speed. During this phase, we assume constant lift and drag coefficients associated with the lower angle of attack in the tail-up attitude. The total acceleration distance is the sum of that for both the low-speed phase and the high-speed phase. The details of this calculation are left as an exercise for the student.

EXAMPLE 3.10.1. Consider the takeoff performance of the general aviation airplane described in Example 3.3.1. For this airplane in takeoff configuration, the zero-lift drag coefficient is 0.036, the maximum lift coefficient is 1.40, and the wing is 6.0 feet above the ground. During takeoff, the propeller pitch is fixed at the value that gives best takeoff performance. The thrust is proportional to air density, and with this pitch setting, the power plant produces a static thrust at sea level of 1,200 lbf. The sea-level thrust decreases linearly with airspeed at the rate of 4.0 lbf for each 1.0 ft/sec of airspeed.

As previously discussed, the angle of attack and lift coefficient for the acceleration run are fixed by the design of the tricycle landing gear. Depending on the relative height of the nose wheel and main gear, the angle of attack for the acceleration run can be fixed at any desired value. For this airplane, determine the lift coefficient that could be used to minimize the acceleration distance. Using this lift coefficient, determine the total no-wind ground roll required for takeoff at both sea level and at 5,000 feet. Also compute the total no-wind ground roll at sea level for both a lift coefficient of zero and a lift coefficient of two times the optimum value. Assume that μ_r is 0.04.

Solution. The lift coefficient that will result in the shortest acceleration distance is the lift coefficient that results in the lowest value of drag and rolling friction combined. Adding the values given by Eqs. (3.10.5) and (3.10.6) and rearranging, we have

$$D+F_r = \mu_r W + \tfrac{1}{2}\rho V^2 S_w\left[C_{D_0} + (C_{D_0,L} - \mu_r)C_L + \frac{(16h_w/b_w)^2}{1+(16h_w/b_w)^2}\frac{C_L^2}{\pi e R_A}\right]$$

Differentiating with respect to lift coefficient and setting the result to zero gives the optimum lift coefficient,

$$(C_L)_{opt} = \pi e R_A \frac{1+(16h_w/b_w)^2}{2(16h_w/b_w)^2}(\mu_r - C_{D_0,L})$$

For this airplane in takeoff configuration,

$$S_w = 180\ \text{ft}^2,\quad b_w = 33\ \text{ft},\quad h_w = 6.0\ \text{ft},\quad W = 2{,}700\ \text{lbf},$$
$$W/S_w = 15\ \text{lbf/ft}^2,\quad R_A = 6.05,\quad C_{D_0} = 0.036,\quad C_{D_0,L} = 0.0,$$
$$e = 0.82,\quad C_{L_{\max}} = 1.4,\quad \mu_r = 0.04$$

The optimum lift coefficient for the acceleration run is

$$(C_L)_{\text{opt}} = \pi(0.82)(6.05)\frac{1+[16(6/33)]^2}{2[16(6/33)]^2}(0.04-0.0) = 0.3485$$

and the corresponding total drag coefficient for the acceleration run is

$$C_D = C_{D_0} + C_{D_0,L}\,C_L + \frac{(16h_w/b_w)^2}{1+(16h_w/b_w)^2}\frac{C_L^2}{\pi e R_A}$$
$$= 0.036 + 0.0 + \frac{[16(6/33)]^2}{1+[16(6/33)]^2}\frac{0.3485^2}{\pi(0.82)(6.05)} = 0.042969$$

From Eq. (3.10.20), the liftoff velocity at sea level is

$$V_{LO} = 1.1\sqrt{\frac{2}{C_{L_{\max}}}}\sqrt{\frac{W/S_w}{\rho}}$$
$$= 1.1\sqrt{\frac{2}{1.4}}\sqrt{\frac{15\ \text{lbf/ft}^2}{0.0023769\ \text{slug/ft}^3}} = 104.444\ \text{ft/sec}$$

For this airplane the thrust is a linear function of airspeed, and at sea level

$$T_S = 1{,}200\ \text{lbf},\qquad T' = -4.0\ \text{lbf}\cdot\text{sec/ft},\qquad T'' = 0.0$$

Using Eq. (3.10.25) to compute the acceleration distance gives

$$K_0 = \frac{T_S}{W} - \mu_r = \frac{1{,}200 \text{ lbf}}{2{,}700 \text{ lbf}} - 0.04 = 0.40444$$

$$K_1 = \frac{T'}{W} = \frac{-4.0 \text{ lbf}\cdot\text{sec/ft}}{2{,}700 \text{ lbf}} = -0.0014815 \text{ sec/ft}$$

$$K_2 = \frac{T''}{W} + \frac{\rho}{2W/S_w}(C_L\mu_r - C_D) = \frac{\rho}{2W/S_w}(\mu_r C_L - C_D)$$

$$= \frac{0.0023769 \text{ slug/ft}^3}{2(15 \text{ lbf/ft}^2)}[0.04(0.3485) - 0.042969]$$

$$= -2.3000\times10^{-6} \text{ sec}^2/\text{ft}^2$$

$$K_R = 4K_0K_2 - K_1^2$$

$$= 4(0.40444)(-2.3000\times10^{-6} \text{ sec}^2/\text{ft}^2) - (-0.0014815 \text{ sec/ft})^2$$

$$= -5.9157\times10^{-6} \text{ sec}^2/\text{ft}^2$$

$$\sqrt{-K_R} = 0.0024322 \text{ sec/ft}$$

$$f_S = K_0 = 0.40444$$

$$f_{LO} = K_0 + K_1V_{LO} + K_2V_{LO}^2$$

$$= 0.40444 - 0.0014815(104.444) - 2.3000\times10^{-6}(104.444)^2$$

$$= 0.22462$$

$$f'_S = K_1 = -0.0014815 \text{ sec/ft}$$

$$f'_{LO} = K_1 + 2K_2V_{LO}$$

$$= -0.0014815 + 2(-2.3000\times10^{-6} \text{ sec}^2/\text{ft}^2)(104.444 \text{ ft/sec})$$

$$= -0.0019619 \text{ sec/ft}$$

$$K_W = \frac{1}{\sqrt{-K_R}}\ln\left[\frac{\left(f'_{LO} - \sqrt{-K_R}\right)\left(f'_S + \sqrt{-K_R}\right)}{\left(f'_{LO} + \sqrt{-K_R}\right)\left(f'_S - \sqrt{-K_R}\right)}\right]$$

$$= \frac{1}{0.0024322 \text{ sec/ft}}\ln\left[\frac{\left(-0.001962 - 0.002432\right)\left(-0.001482 + 0.002432\right)}{\left(-0.001962 + 0.002432\right)\left(-0.001482 - 0.002432\right)}\right]$$

$$= 336.98 \text{ ft/sec}$$

$$K_T = \frac{1}{2K_2}\ln\left(\frac{f_{LO}}{f_S}\right) - \frac{K_1K_W}{2K_2}$$

$$= \frac{\ln(0.22462/0.40444) + 0.0014815 \text{ sec/ft}(336.98 \text{ ft/sec})}{2(-2.3000\times10^{-6} \text{ sec}^2/\text{ft}^2)}$$

$$= 19{,}317 \text{ ft}^2/\text{sec}^2$$

$$s_a = \frac{K_T}{g} = \frac{19{,}317 \text{ ft}^2/\text{sec}^2}{32.2 \text{ ft/sec}^2} = 600 \text{ ft}$$

The total ground roll is the acceleration distance plus the rotation distance,

$$s_g = s_a + V_{LO}\, t_r = 600 \text{ ft} + (104 \text{ ft/sec})(1 \text{ sec}) = \underline{704 \text{ ft}}$$

Repeating the calculations for 5,000 feet, we have

$$V_{LO} = 112.513 \text{ ft/sec}$$
$$T_S = 1{,}034.05 \text{ lbf}$$
$$T' = -3.4468 \text{ lbf} \cdot \text{sec/ft}$$
$$K_0 = 0.34298$$
$$K_1 = -0.0012766 \text{ sec/ft}$$
$$K_2 = -1.9819 \times 10^{-6} \text{ sec}^2/\text{ft}^2$$
$$K_R = -4.3487 \times 10^{-6} \text{ sec}^2/\text{ft}^2$$
$$\sqrt{-K_R} = 0.0020854 \text{ sec/ft}$$
$$f_S = 0.34298$$
$$f_{LO} = 0.17426$$
$$f'_S = -0.0012766 \text{ sec/ft}$$
$$f'_{LO} = -0.0017226 \text{ sec/ft}$$
$$K_W = 444.17 \text{ ft/sec}$$
$$K_T = 27{,}777 \text{ ft}^2/\text{sec}^2$$
$$s_a = 863 \text{ ft}$$
$$s_g = \underline{975 \text{ ft}}$$

Repeating the calculations for sea level and $C_L = 0.0$, we obtain

$$s_g = \underline{712 \text{ ft}}$$

and repeating the calculations for sea level and $C_L = 2(0.3485)$ gives

$$s_g = \underline{712 \text{ ft}}$$

Two things should be noted from Example 3.10.1. First, notice that there is a very significant increase in the ground roll required for takeoff at 5,000 feet over that required at sea level. Both the designer and the pilot should always remember this fact. Second, notice that while there is an optimum angle of attack for the acceleration run, this optimum is quite flat. The lift coefficient can be widely varied on either side of this optimum without increasing the ground roll a great deal. In Example 3.10.1, doubling this lift coefficient or reducing it to zero increases the ground roll by only about 1 percent. This is because increasing the angle of attack for the acceleration run will decrease the rolling friction and increase the drag. Thus, the net effect of changing the angle of attack is quite small.

EXAMPLE 3.10.2. For the general aviation airplane considered in Example 3.10.1, determine the total ground roll required for takeoff at sea level with a 20-mph headwind. Assume the optimum lift coefficient and a μ_r value of 0.04.

Solution. With a headwind the initial airspeed for the acceleration run is not zero but equal to the headwind speed. Thus, we cannot use Eq. (3.10.25) but must return to the more general result given by Eq. (3.10.12). From Example 3.10.1 and the given headwind,

$$S_w = 180\ \text{ft}^2,\quad b_w = 33\ \text{ft},\quad h_w = 6.0\ \text{ft},\quad W = 2{,}700\ \text{lbf},\quad W/S_w = 15\ \text{lbf/ft}^2,$$
$$R_A = 6.05,\quad C_{D_0} = 0.036,\quad C_{D_0,L} = 0.0,\quad e = 0.82,\quad C_{L_{\max}} = 1.4,$$
$$C_L = 0.3485,\quad \mu_r = 0.04,\quad C_D = 0.042969,\quad V_{LO} = 104.44\ \text{ft/sec},$$
$$V_{hw} = 29.33\ \text{ft/sec},\quad V_1 = 29.33\ \text{ft/sec},\quad V_2 = 104.44\ \text{ft/sec},$$
$$T_0 = 1{,}200\ \text{lbf},\quad T' = -4.0\ \text{lbf}\cdot\text{sec/ft},\quad T'' = 0.0$$

Using Eq. (3.10.12) to compute the acceleration distance, we have

$$K_0 = \frac{T_0}{W} - \mu_r = 0.40444$$

$$K_1 = \frac{T'}{W} = -0.0014815\ \text{sec/ft}$$

$$K_2 = \frac{T''}{W} + \frac{\rho}{2W/S_w}(C_L\mu_r - C_D) = -2.3000\times10^{-6}\ \text{sec}^2/\text{ft}^2$$

$$K_R = 4K_0K_2 - K_1^2 = -5.9157\times10^{-6}\ \text{sec}^2/\text{ft}^2$$

$$\sqrt{-K_R} = 0.0024322\ \text{sec/ft}$$

$$f_1 = K_0 + K_1V_1 + K_2V_1^2 = 0.35901$$

$$f_2 = K_0 + K_1V_2 + K_2V_2^2 = 0.22462$$

$$f_1' = K_1 + 2K_2V_1 = -0.0016164\ \text{sec/ft}$$

$$f_2' = K_1 + 2K_2V_2 = -0.0019619\ \text{sec/ft}$$

$$K_W = \frac{1}{\sqrt{-K_R}}\ln\left[\frac{\left(f_2' - \sqrt{-K_R}\right)\left(f_1' + \sqrt{-K_R}\right)}{\left(f_2' + \sqrt{-K_R}\right)\left(f_1' - \sqrt{-K_R}\right)}\right] = 260.14\ \text{ft/sec}$$

$$K_T = \frac{1}{2K_2}\ln\left(\frac{f_2}{f_1}\right) - \frac{K_1K_W}{2K_2} = 18{,}160\ \text{ft}^2/\text{sec}^2$$

$$s_2 - s_1 = \frac{K_T - V_{hw}K_W}{g} = 327\ \text{ft}$$

The total ground roll is this 327-ft acceleration distance plus the rotation distance. The rotation distance is the time allowed for rotation multiplied by the ground speed at liftoff,

$$s_g = s_2 - s_1 + (V_{LO} - V_{hw})t_r = \underline{402 \text{ ft}}$$

This compares to a ground roll of 704 ft with no headwind.

The landing ground roll can be analyzed in a manner similar to that used for takeoff. The main differences are that during deceleration, the thrust is set to the idle value or in the case of large airplanes, some reverse thrust, and the coefficient of rolling friction is increased to about 0.4 to account for braking. Sometimes spoilers are also used to increase the drag and reduce the lift, imposing greater weight on the tires and increasing the friction force. With these differences, Eqs. (3.10.8) through (3.10.19) still apply and can be used to obtain the braking distance, s_b.

For best accuracy, the braking distance can be broken up into small segments with the length of each segment computed from Eq. (3.10.12). Normally, thrust reversal can be applied only above some cutoff speed, and the braking distance must be divided into at least two segments. The total braking distance is the distance required to reduce the ground speed from the touchdown value to zero. To allow for a margin of safety, the touchdown airspeed, V_{TD}, should be about 15 percent above the stall speed for the aircraft in landing configuration (a margin of only 10 percent is normally used for military aircraft). The maximum lift coefficient for the landing configuration is typically larger than that for takeoff configuration, because the high-lift devices are fully engaged for landing. Thus the stall speed for landing is typically less than that for takeoff.

For airplanes without thrust reversal, the idle thrust is quite small and can usually be ignored. For this type of aircraft, the braking distance can be determined by applying Eq. (3.10.12) over the full braking distance as a single step. Thus, for the critical case of **no wind and no thrust reversal**, this gives

$$s_b = \begin{cases} \dfrac{V_{TD}^2}{2g\mu_r}, & C_L = \dfrac{C_D}{\mu_r} \\ \dfrac{W/S_w}{\rho g(C_D - \mu_r C_L)} \ln\left[1 + \dfrac{\rho V_{TD}^2}{2W/S_w}\left(\dfrac{C_D}{\mu_r} - C_L\right)\right], & C_L \neq \dfrac{C_D}{\mu_r} \end{cases} \tag{3.10.40}$$

In computing the total ground roll for landing, the designer should allow for a short "free roll" to account for the reaction time required for the pilot to apply the brakes and engage the spoilers and the thrust reversers. This reaction time, t_f, is typically on the order of 1 to 3 seconds, depending on the complexity of the braking system. The free-roll distance is usually approximated as this assumed reaction time multiplied by the ground speed at the touchdown airspeed,

$$s_f = (V_{TD} - V_{hw})t_f \tag{3.10.41}$$

The total ground roll for landing is the sum of the free-roll and the braking distances,

$$s_g = s_f + s_b \tag{3.10.42}$$

EXAMPLE 3.10.3. Consider the landing performance of the executive business jet described in Example 3.2.1. For this airplane, during the landing ground roll, the total drag coefficient is 0.040, the lift coefficient is 0.10, and the maximum lift coefficient is 2.10. The airplane is equipped with a thrust reversal system that delivers a constant thrust of –2,000 lbf at sea level. However, to avoid reingestion of the exhaust gases, this can only be used at airspeeds above 100 ft/sec. Estimate the total no-wind ground roll for this aircraft on landing at sea level. Because of the complexity of this braking system, allow a full 3 seconds for pilot reaction time. Assume that μ_r is 0.4.

Solution. For this airplane,

$$S_w = 320 \text{ ft}^2, \quad b_w = 54 \text{ ft}, \quad W = 20{,}00 \text{ lbf}, \quad W/S_w = 62.5 \text{ lbf/ft}^2,$$
$$C_D = 0.040, \quad C_L = 0.10, \quad C_{L_{\max}} = 2.10, \quad \mu_r = 0.4$$
$$V_{TD} = 1.15\sqrt{\frac{2}{C_{L_{\max}}}}\sqrt{\frac{W/S_w}{\rho}} = 1.15\sqrt{\frac{2}{2.1}}\sqrt{\frac{62.5 \text{ lbf/ft}^2}{0.0023769 \text{ slug/ft}^3}} = 181.99 \text{ ft/sec}$$
$$s_f = V_{TD}\, t_f = 181.99 \text{ ft/sec}(3 \text{sec}) = 546.0 \text{ ft}$$

After this initial free roll, the thrust force remains constant at –2,000 lbf from the touchdown velocity to 100 ft/sec. At that point the engines are throttled back to idle and the thrust reversers are disengaged. For the remainder of the ground roll, the thrust is assumed to be zero. Thus, the braking distance is determined by using Eq. (3.10.12) over two segments.

$$V_1 = 181.99 \text{ ft/sec}, \quad V_2 = 100.00 \text{ ft/sec}, \quad V_3 = 0.00 \text{ ft/sec},$$
$$T_{1\text{-}2} = -2{,}000.0 \text{ lbf}, \quad T_{2\text{-}3} = 0.0 \text{ lbf}$$
$$(K_0)_1 = -0.5, \quad (K_0)_2 = -0.4$$
$$(K_1)_1 = 0.0, \quad (K_1)_2 = 0.0$$
$$(K_2)_1 = 0.0, \quad (K_2)_2 = 0.0$$

Because K_2 is zero for both segments and since there is no wind, there is no need to compute K_W. In addition, since K_1 is also zero for both segments, K_T is given by

$$(K_T)_1 = \frac{V_2^2 - V_1^2}{2(K_0)_1} = 23{,}120 \text{ ft}^2/\text{sec}^2, \quad (K_T)_2 = \frac{V_3^2 - V_2^2}{2(K_0)_2} = 12{,}500 \text{ ft}^2/\text{sec}^2$$

and the braking distance for each segment is

$$s_2 - s_1 = \frac{(K_T)_1}{g} = 718.0 \text{ ft}, \quad s_3 - s_2 = \frac{(K_T)_2}{g} = 388.2 \text{ ft}$$

The total ground roll distance for the landing is the sum of the free roll and the two segments of the braking roll,

$$s_g = s_f + (s_2 - s_1) + (s_3 - s_2) = 546.0 \text{ ft} + 718.0 \text{ ft} + 388.2 \text{ ft} = \underline{1{,}652 \text{ ft}}$$

3.11. Accelerating Climb and Balanced Field Length

The takeoff ground-roll distance discussed in Sec. 3.10 is the actual distance traveled along the runway, from brake release until the wheels of the aircraft leave the ground. Obviously, for safety reasons, the wheels of the aircraft should not leave the ground right at the end of the runway. This quite naturally raises another question. What is the minimum runway length required for the safe operation of any particular aircraft? This depends not only on the ability of the aircraft to accelerate along the ground, but also on the ability of the aircraft to climb. Since there could be an obstacle at the end of the runway, the aircraft should climb to some minimum *obstacle clearance altitude* before passing over the end of the runway, as shown in Fig. 3.11.1. This minimum obstacle clearance altitude is usually 35 feet for commercial airplanes and 50 feet for small general aviation airplanes and military aircraft. Transport aircraft, which are certified under Federal Air Regulations (FAR) Part 25, are required to accelerate during this initial climb, from an airspeed at liftoff that is at least 10 percent above stall to an airspeed that is at least 20 percent above stall at the obstacle clearance altitude. The total running distance measured along the ground, s_{OC}, from brake release until the airplane has reached the obstacle clearance altitude is usually called the *FAR takeoff distance*.

The minimum runway length required for a transport aircraft operating under FAR Part 25 is also influenced by the possibility of engine failure. If one engine were to fail just prior to liftoff, the airplane should be capable of continuing the takeoff with one engine inoperative, because the distance required to stop the aircraft from a speed close to the liftoff speed may be too great. However, if one engine were to fail just after the acceleration run was started, the pilot could more easily abort the takeoff and stop the

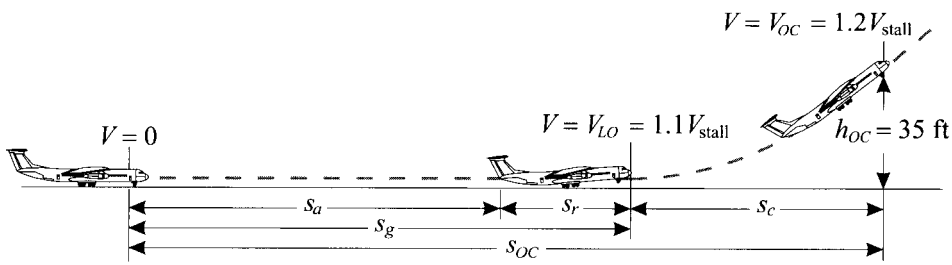


Figure 3.11.1. FAR Part 25 takeoff.

aircraft. This is because in the early part of the acceleration run, the ground speed is still low and the distance required to stop the aircraft is much less than the distance required to continue the takeoff with one engine inoperative. As the point of engine failure moves further into the acceleration run, the speed of the aircraft at engine failure is increased. As the engine failure speed increases, the distance required to continue the takeoff with one engine inoperative is decreased and the distance required to stop the airplane from the point of engine failure is increased. At some point along the acceleration run, the airplane reaches a speed where the distance required to continue the takeoff and climb to the obstacle clearance altitude with one engine inoperative is exactly equal to the distance required to stop the airplane from that same speed. This speed is called the *critical engine failure speed.* The distance required to accelerate an airplane from rest to the critical engine failure speed, using all engines, and then to continue the takeoff and climb to the obstacle clearance altitude, with one engine inoperative, is called the *balanced field length.* The two equilateral options that determine the balanced field length are shown in Fig. 3.11.2. This balanced field length is considered to be the minimum runway length required for safe takeoff of the aircraft and is significantly longer than the FAR takeoff distance with all engines operative.

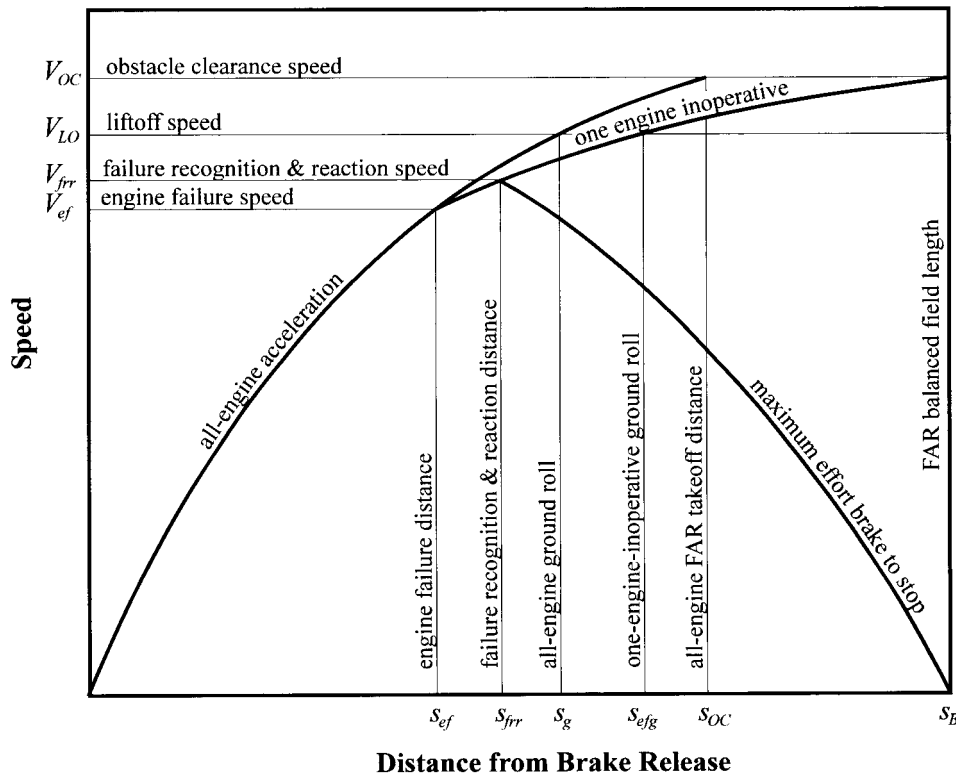


Figure 3.11.2. The two equilateral options defining balanced field length.

If one engine fails at any speed below the critical engine failure speed, the takeoff should always be aborted. If one engine fails at any speed above the critical engine failure speed, the takeoff should be continued with one engine inoperative. In any case, if these requirements are adhered to, the distance required to complete the takeoff and climb to the obstacle clearance altitude or brake the aircraft to a complete stop, in the event of engine failure, will always be less than or equal to the balanced field length.

In determining the balanced field length for transport aircraft operating under FAR Part 25, the use of reverse thrust is not permitted. In addition, we must account for the time required for the pilot to recognize the engine failure and react. For example, the time required for the pilot to realize that an engine has failed might be on the order of 1 second, with an additional second required for the pilot to react and apply the maximum braking force. Notice that the balanced field length for a twin-engine aircraft will be significantly longer than that for, say, a four-engine aircraft having the same total thrust. This is because the twin loses half its thrust on engine failure, while the quad loses only 25 percent of its thrust on engine failure.

To estimate the FAR takeoff distance and the balanced field length for an aircraft, we must be able to estimate the distance traveled while climbing to the obstacle clearance altitude. This phase of the takeoff is usually referred to as the *transition phase*, because it encompasses the transition from horizontal motion along the runway to the steady climbing flight that takes place following the takeoff. Since FAR Part 25 requires the airspeed to increase from at least 1.1 V_{stall} at liftoff to 1.2 V_{stall} at the obstacle clearance altitude, the airplane must accelerate in both the axial and normal directions during transition. The forces acting on an airplane during such an accelerating climb are shown in Fig. 3.11.3.

For the critical case of **no wind**, Newton's second law applied to the direction of flight requires that

$$\frac{W}{g}\frac{dV}{dt} = T - D - W\sin\gamma \tag{3.11.1}$$

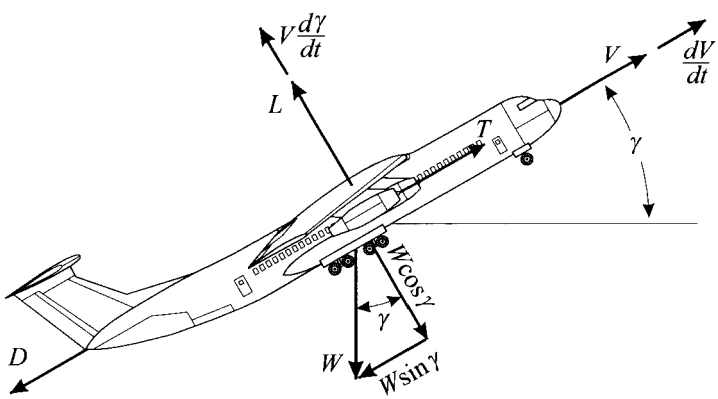


Figure 3.11.3. Forces acting on an airplane during accelerating climb.

In the direction normal to the curved flight path, the centripetal acceleration is supported by the difference between the lift and the normal component of weight,

$$\frac{W}{g}\frac{V^2}{R} = \frac{W}{g}\frac{V^2}{V/\Omega} = \frac{W}{g}V\frac{d\gamma}{dt} = L - W\cos\gamma \tag{3.11.2}$$

where R is the radius of curvature of the flight path and $\Omega = d\gamma/dt$ is the angular velocity. Solving Eq. (3.11.1) for $\sin\gamma$, we have

$$\sin\gamma = \frac{T-D}{W} - \frac{1}{g}\frac{dV}{dt} \tag{3.11.3}$$

The vertical component of velocity is

$$\frac{dh}{dt} = V\sin\gamma \tag{3.11.4}$$

and the horizontal component of velocity is

$$\frac{ds}{dt} = V\cos\gamma \tag{3.11.5}$$

Using Eq. (3.11.3) in Eq. (3.11.4) gives

$$\frac{dh}{dt} = \frac{T-D}{W}V - \frac{V}{g}\frac{dV}{dt} \tag{3.11.6}$$

Applying Eq. (3.11.5) to Eq. (3.11.6) and rearranging gives

$$\frac{T-D}{\cos\gamma}\frac{ds}{dt} = W\frac{dh}{dt} + \frac{W}{g}V\frac{dV}{dt} \tag{3.11.7}$$

After integrating both sides of Eq. (3.11.7) from liftoff to the obstacle clearance altitude, we obtain

$$\int_{s_{LO}}^{s_{OC}} \frac{T-D}{\cos\gamma}\,ds = \int_0^{h_{OC}} W\,dh + \frac{1}{g}\int_{V_{LO}}^{V_{OC}} WV\,dV \tag{3.11.8}$$

where the subscripts LO and OC refer to the liftoff point and the obstacle clearance point, respectively. Assuming constant aircraft weight, the integration on the right-hand side of Eq. (3.11.8) is readily carried out to yield

$$\int_{s_{LO}}^{s_{OC}} \frac{T-D}{\cos\gamma}\,ds = Wh_{OC} + \frac{W}{2g}(V_{OC}^2 - V_{LO}^2) \tag{3.11.9}$$

From Eq. (3.11.9) we see that the work done by the aircraft engines, in excess of that dissipated by the drag force, can be used to increase potential energy, kinetic energy, or both. The exact flight path that is followed during the climb to obstacle clearance altitude depends on pilot technique. Both the climb angle, γ, and the velocity, V, are changing with time during this portion of the takeoff. The thrust force depends on velocity, and the drag force depends on both velocity and climb angle. Thus, if we knew exactly how the velocity and the climb angle varied with position during the climb from liftoff to obstacle clearance altitude, we could evaluate the integral on the left-hand side of Eq. (3.11.9) numerically. Unfortunately, this variation in velocity and climb angle depends on pilot technique and is not known. However, by examining the integrand on the left-hand side of Eq. (3.11.9), we can make a reasonable assumption that allows us to perform the required integration.

Because of induced drag, the drag coefficient increases with lift coefficient, which increases with load factor. Solving Eq. (3.11.2) for the load factor gives

$$\frac{L}{W} = \cos\gamma + \frac{V}{g}\frac{d\gamma}{dt} \tag{3.11.10}$$

From Eq. (3.11.10), we see that the load factor is a function of both the climb angle and the time rate of change of the climb angle. The first term on the right in Eq. (3.11.10) tends to reduce the load factor and induced drag during transition, while the second term tends to increase the load factor and induced drag. In addition, the decrease in ground effect, which occurs as the airplane climbs, tends to increase the drag somewhat. The small increase in velocity that takes place during transition reduces the thrust and increases the drag. The net effect is that the increase in climb angle and airspeed together with the decrease in ground effect, which all take place during transition, combine to cause a slight decrease in the numerator of the integrand in Eq. (3.11.9). However, since the climb angle is increasing, the denominator in this integrand is also decreasing during transition. Thus, because of these counteracting effects and because climb angle and velocity changes are typically small, the integrand in Eq. (3.11.9) changes only slightly during the transition phase. As a result, it is reasonable to assume that the integrand on the left-hand side of Eq. (3.11.9) is a linear function of the distanced traveled, s. With this assumption, the integration can be performed to give

$$\overline{F}_c s_c = Wh_{OC} + \frac{W}{2g}(V_{OC}^2 - V_{LO}^2) \tag{3.11.11}$$

where $\overline{F}_c$ is an effective net force during transition,

$$\overline{F}_c = \frac{T_{LO} - D_{LO} + (T_{OC} - D_{OC})/\cos(\gamma_{OC})}{2} \tag{3.11.12}$$

and s_c is the distance traveled over the ground during the climb from liftoff to obstacle clearance altitude, $s_{OC} - s_{LO}$. From Eq. (3.11.11) the distance required to climb to obstacle clearance altitude is

$$s_c = \frac{W}{\overline{F}_c}\left[h_{OC} + \frac{V_{OC}^2 - V_{LO}^2}{2g}\right] \tag{3.11.13}$$

The climb angle at obstacle clearance should be the steady climb angle for the aircraft in takeoff configuration, corresponding to the airspeed at the obstacle clearance altitude. From Eq. (3.11.3) this gives

$$\gamma_{OC} = \sin^{-1}\left(\frac{T_{OC} - D_{OC}}{W}\right) \tag{3.11.14}$$

From the requirements of FAR Part 25, the altitude and the airspeed are known at both liftoff and obstacle clearance. Thus, the thrust force and the drag can be determined at these two points, including the effects of climb angle and ground effect. Using these results with Eqs. (3.11.12) and (3.11.14), the effective net force during transition is readily determined. This effective net force is then used in Eq. (3.11.13) to determine the distance traveled over the ground during the climb from liftoff to the obstacle clearance altitude.

Since the effective net force during transition is decreased by the angular acceleration and increased by the climb angle and ground effect, a reasonable first approximation for this effective net force can be obtained by using the values for steady level flight in the absence of ground effect,

$$\overline{F}_c \cong \frac{(T_A - T_R)_{LO} + (T_A - T_R)_{OC}}{2} \tag{3.11.15}$$

where T_A is the thrust available and T_R is the thrust required for steady level flight as determined in Sec. 3.2.

EXAMPLE 3.11.1. For the executive business jet described in Example 3.2.1, determine the FAR takeoff distance at standard sea level with no wind. This airplane is fitted with turbojet engines that produce a thrust that is independent of airspeed. For the takeoff acceleration run at standard sea level, use the following properties:

$$S_w = 320\ \text{ft}^2, \quad b_w = 54\ \text{ft}, \quad h_w = 6.0\ \text{ft}, \quad W = 20{,}000\ \text{lbf}, \quad T_A = 6{,}500\ \text{lbf},$$
$$C_{D_0} = 0.033, \quad C_{D_0,L} = 0.0, \quad e = 0.74, \quad C_{L_{\max}} = 1.6, \quad C_L = 0.4,$$
$$\mu_r = 0.04, \quad t_r = 1\ \text{sec}$$

Solution. The ground roll is found following the solution to Example 3.10.1,

$$C_D = C_{D_0} + C_{D_0,L}\,C_L + \frac{(16h_w/b_w)^2}{1+(16h_w/b_w)^2}\frac{C_L^2}{\pi e R_A} = 0.038737$$

$$V_{LO} = 1.1\sqrt{\frac{2}{C_{L_{\max}}}}\sqrt{\frac{W/S_w}{\rho}} = 199.43 \text{ ft/sec}$$

$$T_S = 6{,}500 \text{ lbf}, \qquad T' = 0.0, \qquad T'' = 0.0$$

$$K_0 = \frac{T_S}{W} - \mu_r = 0.28500$$

$$K_1 = \frac{T'}{W} = 0.0$$

$$K_2 = \frac{T''}{W} + \frac{\rho}{2W/S_w}(C_L\mu_r - C_D) = -4.323552\times10^{-7} \text{ sec}^2/\text{ft}^2$$

$$f_S = K_0 = 0.28500$$

$$f_{LO} = K_0 + K_1 V_{LO} + K_2 V_{LO}^2 = 0.2678049$$

$$K_T = \frac{1}{2K_2}\ln\left(\frac{f_{LO}}{f_S}\right) - \frac{K_1 K_W}{2K_2} = 71{,}967 \text{ ft}^2/\text{sec}^2$$

$$s_a = \frac{K_T}{g} = 2{,}235.0 \text{ ft}$$

$$s_g = s_a + V_{LO} t_r = 2{,}434.4 \text{ ft}$$

The velocity at the obstacle clearance altitude is

$$V_{OC} = 1.2\sqrt{\frac{2}{C_{L_{\max}}}}\sqrt{\frac{W/S_w}{\rho}} = 217.56 \text{ ft/sec}$$

As a first approximation, the lift and drag coefficients at obstacle clearance are taken as those for steady level flight in the absence of ground effect,

$$C_{L_{OC}} \cong \frac{W}{\frac{1}{2}\rho V_{OC}^2 S_w} = 1.1111$$

$$C_{D_{OC}} \cong C_{D_0} + C_{D_{0,L}} C_{L_{OC}} + \frac{C_{L_{OC}}^2}{\pi e R_A} = 0.091272$$

Our first approximation for the drag force at obstacle clearance is then

$$D_{OC} \cong \tfrac{1}{2}\rho V_{OC}^2 S_w C_{D_{OC}} = 1{,}643 \text{ lbf}$$

and, from Eq. (3.11.14), our first estimate for the climb angle at obstacle clearance altitude is

$$\gamma_{OC} \cong \sin^{-1}\left(\frac{T_{OC} - D_{OC}}{W}\right) = 14.1^\circ$$

Using this value for the climb angle, we can obtain an improved estimate for the lift and drag coefficients at the obstacle clearance altitude of 35 feet,

$$C_{L_{OC}} = \frac{W\cos(\gamma_{OC})}{\frac{1}{2}\rho V_{OC}^2 S_w} = 1.0778$$

$$C_{D_{OC}} = C_{D_0} + C_{D_0,L}\, C_{L_{OC}} + \frac{[16(h_w + h_{OC})/b_w]^2}{1+[16(h_w + h_{OC})/b_w]^2}\frac{C_{L_{OC}}^2}{\pi e R_A} = 0.087467$$

The improved estimate for the drag force at obstacle clearance is

$$D_{OC} = \tfrac{1}{2}\rho V_{OC}^2 S_w C_{D_{OC}} = 1{,}574 \text{ lbf}$$

and the improved estimate for the climb angle at obstacle clearance is

$$\gamma_{OC} = \sin^{-1}\left(\frac{T_{OC} - D_{OC}}{W}\right) = 14.3°$$

The lift and drag coefficients at liftoff are

$$C_{L_{LO}} = \frac{W}{\frac{1}{2}\rho V_{LO}^2 S_w} = 1.3223$$

$$C_{D_{LO}} = C_{D_0} + C_{D_0,L}\, C_{L_{LO}} + \frac{(16 h_w/b_w)^2}{1+(16 h_w/b_w)^2}\frac{C_{L_{LO}}^2}{\pi e R_A} = 0.095694$$

The drag force at liftoff is then

$$D_{LO} = \tfrac{1}{2}\rho V_{LO}^2 S_w C_{D_{LO}} = 1{,}447 \text{ lbf}$$

The integrand in Eq. (3.11.9), evaluated at both liftoff and obstacle clearance, is

$$\left(\frac{T-D}{\cos\gamma}\right)_{LO} = \frac{6{,}500 \text{ lbf} - 1{,}447 \text{ lbf}}{1.0} = 5{,}053 \text{ lbf}$$

$$\left(\frac{T-D}{\cos\gamma}\right)_{OC} = \frac{6{,}500 \text{ lbf} - 1{,}574 \text{ lbf}}{0.96954} = 5{,}082 \text{ lbf}$$

From Eq. (3.11.12), the average effective net force during transition is then

$$\overline{F_c} = \frac{T_{LO} - D_{LO} + (T_{OC} - D_{OC})/\cos(\gamma_{OC})}{2} = 5{,}067 \text{ lbf}$$

and from Eq. (3.11.13), the distance required to climb to obstacle clearance altitude is

$$s_c = \frac{W}{\bar{F}_c}\left[h_{OC} + \frac{V_{OC}^2 - V_{LO}^2}{2g}\right] = 601.5 \text{ ft}$$

This gives a FAR takeoff distance of

$$s_{OC} = s_g + s_c = \underline{3{,}036 \text{ ft}}$$

EXAMPLE 3.11.2. The executive business jet in Example 3.11.1 is powered by two turbojet engines. Assuming that one engine fails during a no-wind takeoff at standard sea level, plot the total field length required to stop the aircraft after engine failure and the total field length required to continue the FAR takeoff on the remaining engine, as a function of the engine failure recognition speed. Use an obstacle clearance altitude of 35 feet and assume 1 second for engine failure recognition and another second for the pilot to react and apply the brakes. What are the *critical engine failure recognition speed* and the balanced field length for this aircraft?

Solution. The acceleration distance prior to engine failure and the acceleration distance after engine failure are found using Eq. (3.10.12). From Example 3.11.1, we have

$$S_w = 320 \text{ ft}^2, \quad b_w = 54 \text{ ft}, \quad h_w = 6.0 \text{ ft}, \quad W = 20{,}000 \text{ lbf}, \quad C_{D_0} = 0.033,$$
$$C_{D_0,L} = 0.0, \quad e = 0.74, \quad C_{L_{\max}} = 1.6, \quad C_L = 0.4, \quad (\mu_r)_a = 0.04,$$
$$(\mu_r)_b = 0.4, \quad t_r = 1 \text{ sec}, \quad C_D = 0.038737, \quad V_{LO} = 199.43 \text{ ft/sec},$$
$$(T_A)_{2\text{-engines}} = 6{,}500 \text{ lbf}, \quad (T_A)_{1\text{-engine}} = 3{,}250 \text{ lbf}$$

Equation (3.10.12) is applied separately over the two segments of the acceleration run, from zero velocity to engine failure and from engine failure to liftoff speed. For example, an engine failure speed of 50 ft/sec would give

$$V_1 = 0.00 \text{ ft/sec}, \quad V_2 = 50.00 \text{ ft/sec}, \quad V_3 = 199.43 \text{ ft/sec},$$
$$T_{1\text{-}2} = 6{,}500 \text{ lbf}, \quad T_{2\text{-}3} = 3{,}250 \text{ lbf}$$
$$(K_0)_1 = 0.28500, \quad (K_0)_2 = 0.12250$$
$$(K_1)_1 = 0.0, \quad (K_1)_2 = 0.0$$
$$(K_2)_1 = -4.323552\times10^{-7} \text{ sec}^2/\text{ft}^2, \quad (K_2)_2 = -4.323552\times10^{-7} \text{ sec}^2/\text{ft}^2$$
$$(K_T)_1 = 4{,}394 \text{ ft}^2/\text{sec}^2, \quad (K_T)_2 = 164{,}666 \text{ ft}^2/\text{sec}^2$$
$$(s_a)_1 = 136.5 \text{ ft}, \quad (s_a)_2 = 5{,}113.9 \text{ ft}$$
$$s_g = (s_a)_1 + (s_a)_2 + V_{LO}\, t_r = 5{,}449.8 \text{ ft}$$

Following Example 3.11.1 and computing the distance required to climb to 35 feet with only one engine, we obtain

$$V_{OC} = 217.56 \text{ ft/sec}$$
$$\gamma_{OC} = 4.6°$$
$$s_c = 1{,}777.8 \text{ ft}$$

Thus, the FAR takeoff distance for engine failure at 50 ft/sec is

$$s_{OC} = s_g + s_c = \underline{7{,}228 \text{ ft}}$$

To determine the engine failure recognition speed we return to Newton's second law stated in Eq. (3.10.1),

$$\frac{W}{g}\frac{dV}{dt} = T - D - F_r$$

Rearranging, we have

$$\frac{dV}{dt} = g\frac{T - D - F_r}{W}$$

Since the engine failure recognition time is very short, we can assume a constant net force and this can be integrated to yield the engine failure recognition speed, V_{fr},

$$V_{fr} = V_{ef} + g\frac{T - D - F_r}{W}(t_{fr} - t_{ef}) = V_{ef} + g(K_0 + K_1 V + K_2 V^2)(t_{fr} - t_{ef})$$

For the present example with engine failure at 50 ft/sec, the engine failure recognition speed, V_{fr}, is

$$\begin{aligned} V_{fr} &= V_{ef} + g(K_0 + K_1 V_{ef} + K_2 V_{ef}^2)(t_{fr} - t_{ef}) \\ &= 50 \text{ ft/sec} + 32.2 \text{ ft/sec}^2[0.12250 + 0.0 - 4.323552 \times 10^{-7}(50^2)]1.0 \text{ sec} \\ &= 53.9 \text{ ft/sec} \end{aligned}$$

In a similar manner the engine failure recognition and reaction speed, V_{frr}, is

$$\begin{aligned} V_{frr} &= V_{fr} + g(K_0 + K_1 V_{fr} + K_2 V_{fr}^2)(t_{frr} - t_{fr}) \\ &= 53.9 \text{ ft/sec} + 32.2 \text{ ft/sec}^2[0.12250 + 0.0 - 4.323552 \times 10^{-7}(53.9^2)]1.0 \text{ sec} \\ &= 57.8 \text{ ft/sec} \end{aligned}$$

The distance traveled during the failure recognition and reaction time is also found by using Eq. (3.10.12). This gives

$$s_{frr} - s_{ef} = 107.8 \text{ ft}$$

Similarly, using Eq. (3.10.12), the distance required to brake to a full stop from the failure recognition and reaction speed of 57.8 ft/sec is

$$s_b = 131.0 \text{ ft}$$

The total field length required to abort a takeoff after engine failure at 50 ft/sec is then, the distance required to accelerate to 50 ft/sec with both engines, plus the distance traveled during the failure recognition and reaction time with one engine inoperative, plus the distance required to brake to a full stop from the failure recognition and reaction speed,

$$s_{\text{abort}} = (s_a)_1 + (s_{frr} - s_{ef}) + s_b = \underline{375 \text{ ft}}$$

These calculations are repeated for engine failure speeds ranging from zero to the liftoff speed, in increments of 1 foot per second. Sample results are shown in Table 3.11.1, and all results are plotted in Fig. 3.11.4. The speed at which the field length required to abort the takeoff is equal to the field length required to complete the FAR takeoff is the critical engine failure recognition speed, and the corresponding FAR takeoff distance is the balanced field length. For this airplane

V_{ef}	V_{fr}	s_{OC}	s_{abort}
0.0000	3.9445	7,409.3660	10.3049
1.0000	4.9445	7,409.2950	13.0142
2.0000	5.9444	7,409.0770	15.9040
3.0000	6.9444	7,408.7170	18.9874
4.0000	7.9443	7,408.2090	22.2509
⋮	⋮	⋮	⋮
50.0000	53.9097	7,227.5340	375.3876
⋮	⋮	⋮	⋮
193.0000	196.4259	4,436.2270	4,244.8180
194.0000	197.4205	4,402.0580	4,289.1900
195.0000	198.4151	4,367.6350	4,333.8480
196.0000	199.4097	4,332.9600	4,378.7940
197.0000	200.4042	4,298.0250	4,424.0300
198.0000	201.3987	4,262.8370	4,469.5600
199.0000	202.3932	4,227.3920	4,515.3830

Table 3.11.1. Sample data used to construct the plot in Fig. 3.11.4.

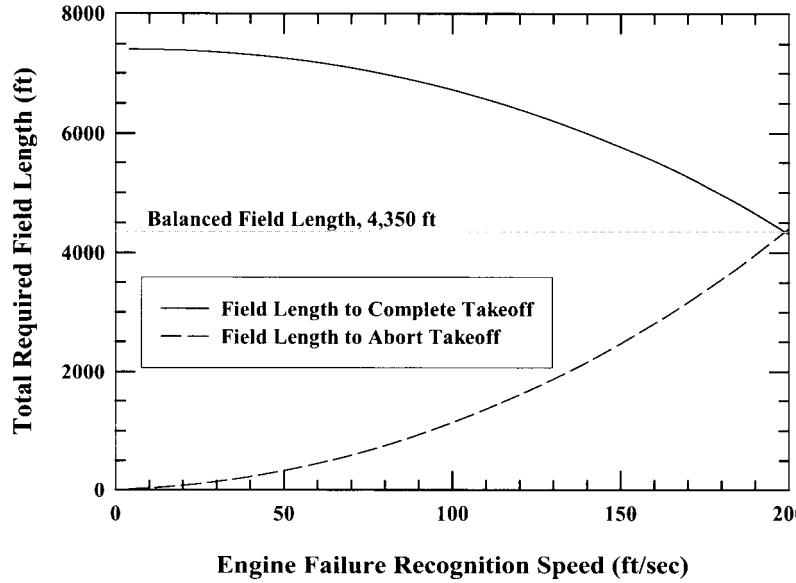


Figure 3.11.4. Graphical determination of balanced field length for the twin-engine airplane in Example 3.11.2.

at sea level, the critical engine failure recognition speed is about 199 ft/sec and the balanced field length is about 4,350 ft, which is 43 percent greater than the FAR takeoff distance for the same aircraft with both engines operational, as determined in Example 3.11.1.

For the twin-engine executive business jet in Example 3.11.2, the critical engine failure recognition speed was found to be almost exactly equal to the liftoff speed. This means that if the pilot recognizes an engine failure while the aircraft is still on the ground, the takeoff should always be aborted. Even if the airplane has reached liftoff speed when the failure is detected, the pilot could still stop the aircraft in the same distance that would be required to complete the takeoff to obstacle clearance altitude. The decision to stop the aircraft rather than continue the takeoff with one engine inoperative is seen to be even more appropriate when one considers the relative consequences associated with coming up short. If the pilot elects to continue the takeoff with one engine inoperative and does not quite clear an obstacle, a very serious airborne collision will result. On the other hand, if the pilot decides to abort the takeoff and is not able to completely stop the aircraft before the end of the runway, the consequence of going off the runway at this much lower speed will be substantially less severe.

The high critical engine failure recognition speed that was found in Example 3.11.2 is typical of twin-engine aircraft. This is a direct consequence of the simple fact that when one engine fails on a twin, the airplane loses half of its power. When one engine fails on an airplane with three or more engines, the fraction of total power lost is much

less. This significantly reduces the critical engine failure recognition speed and the balanced field length. For example, Fig. 3.11.5 shows how the aircraft in Example 3.11.2 would perform under conditions of engine failure if the same total thrust were provided by four engines instead of two. In this case the critical engine failure recognition speed would be reduced to about 180 ft/sec, and the balanced field length would be reduced to about 3,570 feet.

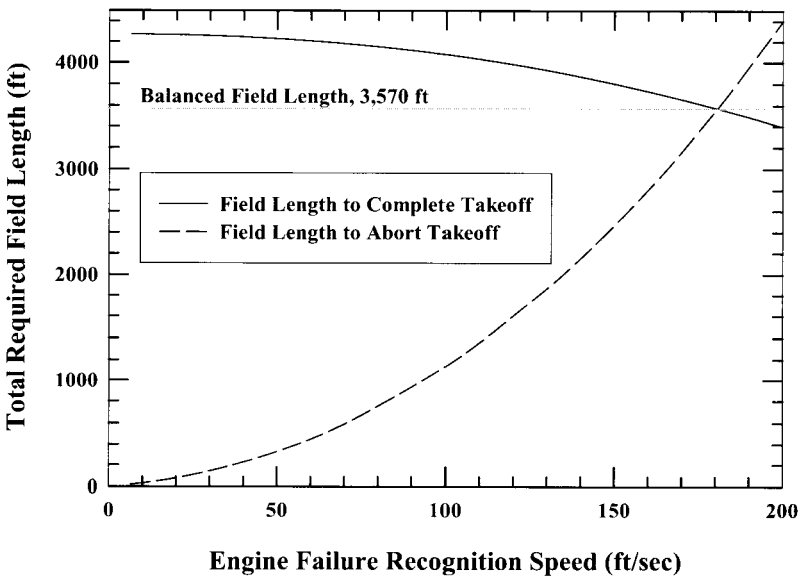


Figure 3.11.5. Balanced field length for the airplane in Example 3.11.2 assuming four engines instead of two.

3.12. Problems

3.1. Consider the executive business jet described in Example 3.2.1. Using the small-thrust-angle approximation and assuming that the wing does not stall, compute the lift coefficient, drag coefficient, thrust required, and power required for steady level flight at sea level for airspeeds of 200, 300, 400, and 500 mph.

3.2. For the executive business jet described in Example 3.2.1, using the small-thrust-angle approximation, compute the minimum thrust required and the airspeed at which it occurs for both sea level and 20,000 feet.

3.3. For the executive business jet described in Example 3.2.1, using the small-thrust-angle approximation, compute the minimum power required and the airspeed at which it occurs for both sea level and 20,000 feet.

3.4. Consider the general aviation airplane described in Example 3.3.1. Using the small-thrust-angle approximation and assuming that the wing does not stall, compute the lift coefficient, drag coefficient, thrust required, and power required for steady level flight at sea level for airspeeds of 50, 100, 150, and 200 mph.

3.5. For the general aviation airplane described in Example 3.3.1, using the small-thrust-angle approximation, compute the minimum thrust required and the airspeed at which it occurs for both sea level and 10,000 feet.

3.6. For the general aviation airplane described in Example 3.3.1, using the small-thrust-angle approximation, compute the minimum power required and the airspeed at which it occurs for both sea level and 10,000 feet.

3.7. A small jet transport has the following properties in cruise configuration:

$$S_w = 950 \text{ ft}^2, \quad b_w = 75 \text{ ft}, \quad W = 73{,}000 \text{ lbf},$$
$$C_{D_0} = 0.020, \quad C_{D_{0,L}} = 0.0, \quad e = 0.67$$

Using the small-thrust-angle approximation and assuming that the wing does not stall, compute the lift coefficient, the drag coefficient, the thrust required, and the power required for steady level flight at 30,000 ft for airspeeds of 400, 600, and 800 ft/sec.

3.8. For the jet transport described in problem 3.7, using the small-thrust-angle approximation, compute the minimum thrust required and the airspeed at which it occurs for both sea level and 30,000 feet.

3.9. For the jet transport described in problem 3.7, using the small-thrust-angle approximation, compute the minimum power required and the airspeed at which it occurs for both sea level and 30,000 feet.

3.10. A large jet transport, similar to the Boeing 747, has the following properties in cruise configuration:

$$S_w = 5{,}500 \text{ ft}^2, \quad b_w = 196 \text{ ft}, \quad W = 636{,}600 \text{ lbf},$$
$$C_{D_0} = 0.020, \quad C_{D_{0,L}} = 0.0, \quad e = 0.72$$

Using the small-thrust-angle approximation and assuming that the wing does not stall, compute the lift coefficient, the drag coefficient, the thrust required, and the power required for steady level flight at 30,000 ft for airspeeds of 400, 600, and 800 ft/sec.

3.11. For the jet transport described in problem 3.10, using the small-thrust-angle approximation, compute the minimum thrust required and the airspeed at which it occurs for both sea level and 30,000 feet.

3.12. For the jet transport described in problem 3.10, using the small-thrust-angle approximation, compute the minimum power required and the airspeed at which it occurs for both sea level and 30,000 feet.

3.13. The jet transport in problem 3.7 is fitted with turbojet engines that produce a thrust that is independent of airspeed and directly proportional to air density. The total full-throttle thrust available from these engines is given by the equation

$$T_A = \frac{\rho}{\rho_0} 27{,}700 \text{ lbf}$$

where ρ is the air density and ρ_0 is the air density at standard sea level. Using the small-climb-angle approximation, find the rate of climb at sea level and 30,000 feet for airspeeds of 400, 600, and 800 ft/sec.

3.14. For the jet transport described in problem 3.13, using the small-climb-angle approximation, compute the maximum rate of climb and the airspeed at which it occurs for both sea level and 30,000 feet.

3.15. Assume that the jet transport described in problem 3.10 is fitted with turbojet engines that produce a thrust that is independent of airspeed. Suppose that the total full-throttle thrust available from these engines is given by the equation

$$T_A = \left(\frac{\rho}{\rho_0}\right)^{0.8} 250{,}000 \text{ lbf}$$

where ρ is the air density and ρ_0 is the air density at standard sea level. Using the small-climb-angle approximation, find the rate of climb at sea level and 30,000 feet for airspeeds of 400, 600, and 800 ft/sec.

3.16. For the jet transport described in problem 3.15, using the small-climb-angle approximation, compute the maximum rate of climb and the airspeed at which it occurs for both sea level and 30,000 feet.

3.17. A propeller-driven transport has the following properties in cruise configuration:

$$S_w = 945 \text{ ft}^2, \quad b_w = 96 \text{ ft}, \quad W = 40{,}000 \text{ lbf}, \quad C_{D_0} = 0.025, \quad C_{D_{0,L}} = 0.0,$$
$$e = 0.80, \quad T_A = (\rho/\rho_0)(10{,}000 \text{ lbf} - 12.0 \text{ lbf} \cdot \text{sec/ft } V)$$

Using the small-climb-angle approximation, compute the rate of climb at both sea level and 10,000 feet for airspeeds of 200, 250, 300, and 350 ft/sec.

3.18. For the propeller-driven transport described in problem 3.17, using the small-climb-angle approximation, compute the maximum rate of climb and the airspeed at which it occurs for both sea level and 10,000 feet.

3.19. A human athlete can produce more than 1 horsepower for a few seconds. However, in sustained aerobic exercise, a human athlete is capable of delivering only about 0.33 hp. In the development of the human-powered airplane (Gossamer Condor) designed by Paul MacCready and his colleagues, the power delivered by the pilot was converted to propulsive power available with an efficiency of about 70 percent. Assuming that a human-powered airplane could be built with the following reasonable properties,

$$R_A = 12, \quad W = 200 \text{ lbf}, \quad P_A = 0.70(0.33 \text{ hp})$$
$$C_{D_0} = 0.010, \quad C_{D_0,L} = 0.0, \quad e = 0.80$$

estimate the wing area required for the airplane and the airspeed at which it should be flown at standard sea level. What is the minimum power that the pilot would need to provide to fly this airplane in Denver Colorado, at an elevation of 5,000 feet?

3.20. For the human-powered airplane in problem 3.19, assuming that the pilot can produce 0.6 hp for a short time during takeoff and climb, estimate the rate of climb for this aircraft at sea level.

3.21. For the small jet transport described in problem 3.7, the maximum usable fuel weight is 29,500 lbf and the thrust-specific fuel consumption is 0.69 lbf of fuel per hour per lbf of thrust. This airplane has the following properties in cruise configuration:

$$S_w = 950 \text{ ft}^2, \quad b_w = 75 \text{ ft}, \quad W_f = 73{,}000 \text{ lbf}, \quad W_e = 43{,}500 \text{ lbf},$$
$$q_T = 0.69 \text{ lbf/lbf-hr}, \quad C_{D_0} = 0.020, \quad C_{D_0,L} = 0.0, \quad e = 0.67$$

Assuming that the thrust-specific fuel consumption is independent of both airspeed and altitude, compute the maximum endurance airspeed with maximum fuel weight and with minimum fuel weight for both sea level and 30,000 feet.

3.22. For the jet transport described in problem 3.21, assuming that the pilot maintains the maximum endurance airspeed at all times, determine the maximum endurance for this airplane at 30,000 feet.

3.23. For the large jet transport described in problem 3.10, the total fuel capacity is 330,700 pounds and thrust-specific fuel consumption is 0.66 pound of fuel per hour per pound of thrust. Because some fuel must be held in reserve, the maximum usable fuel weight is 304,200 lbf. This airplane has the following properties in cruise configuration:

$$S_w = 5{,}500 \text{ ft}^2, \quad b_w = 196 \text{ ft}, \quad W_f = 636{,}600 \text{ lbf}, \quad W_e = 332{,}400 \text{ lbf},$$
$$q_T = 0.66 \text{ lbf/lbf} \cdot \text{hr}, \quad C_{D_0} = 0.020, \quad C_{D_0,L} = 0.0, \quad e = 0.72$$

Assuming that the thrust-specific fuel consumption is independent of both airspeed and altitude, compute the minimum fuel consumption rate, in gallons per minute, with maximum fuel weight and with minimum fuel weight for both sea level and 30,000 feet. Jet fuel weighs 6.67 pounds per gallon.

3.24. For the jet transport described in problem 3.23, assuming that the pilot maintains the no-wind maximum range airspeed at all times, compute the fuel consumption rate, in gallons per minute, with maximum fuel weight and with minimum fuel weight for both sea level and 30,000 feet.

3.25. For the propeller-driven airplane and power plant described in Example 3.5.1, if the pilot maintains the maximum endurance airspeed at all times, determine the total distance that the airplane will travel on a tank of fuel at sea level.

3.26. For the propeller-driven airplane and power plant described in Example 3.5.1, if the pilot maintains the maximum range airspeed at all times, determine the total time required for the airplane to fly a distance equal to the maximum range with no wind at sea level.

3.27. To attain maximum range, the airspeed of an airplane must be decreased as fuel is burned off and gross weight is decreased. For the executive business jet that is described in Example 3.6.2, determine the maximum range airspeed with fuel tanks full and with fuel tanks empty, for no wind at 20,000 feet.

3.28. For the executive business jet described in Example 3.6.2, determine the maximum range at 20,000 feet, with a 100-mph headwind and with a 100-mph tailwind.

3.29. For the jet transport described in problem 3.21, assuming that the pilot maintains the maximum range airspeed at all times, determine the no-wind maximum range for this airplane at 30,000 feet.

3.30. For the jet transport described in problem 3.23, assuming that the pilot maintains the maximum range airspeed at all times, determine the no-wind maximum range for this airplane at 30,000 feet. Also determine the average fuel consumption rate in gallons per minute and the average specific range in miles per gallon. If this airplane is carrying 500 passengers, what is the average specific range in passenger miles per gallon? Compare this with an automobile carrying one person that gets 20 miles per gallon.

3.31. For the jet transport in problem 3.30, assuming that the pilot maintains a constant airspeed equal to the maximum range airspeed based on average weight, determine the no-wind range for this airplane flying at 30,000 ft. Also determine the no-wind range for the same altitude, if the pilot maintains a constant airspeed of 100 feet per second more than the maximum range airspeed based on average weight. Compare these values with the maximum range found in problem 3.30.

3.32. A commercial airplane such as the Boeing 747 is not usually flown at the maximum range airspeed. The reason for this is purely economic. The jet transport in problem 3.31 costs \$150,000,000 and is flown 14 hr/day. Using a 30-year life and a 7 percent interest rate, what is the investment cost per hour of flight time? The total personnel cost for the crew, including fringe benefits, is \$1,200 per hour and the cost of jet fuel is \$1.00 per gallon. Determine the sum of the investment cost, the personnel cost, and the fuel cost in dollars per hour and in dollars per mile, assuming no wind and a constant airspeed equal to the maximum range airspeed based on average weight. Also determine the same costs for a constant airspeed equal to 100 feet per second more than the maximum range airspeed based on average weight. Repeat the problem assuming that the cost of jet fuel goes to \$2.00 per gallon.

3.33. For the propeller-driven transport described in problem 3.17, the maximum usable fuel weight is 8,000 lbf and the power-specific fuel consumption based on propulsive power is 0.52 lbf/hp·hr. This airplane has the following properties in cruise configuration:

$$S_w = 945\ \text{ft}^2, \quad b_w = 96\ \text{ft}, \quad W_f = 40{,}000\ \text{lbf}, \quad W_e = 32{,}000\ \text{lbf},$$
$$q_P = 0.52\ \text{lbf/hp}\cdot\text{hr}, \quad C_{D_0} = 0.025, \quad C_{D_{0,L}} = 0.0, \quad e = 0.80$$

Assuming that the power-specific fuel consumption is independent of both airspeed and altitude, and that the pilot maintains the maximum range airspeed at all times, determine the no-wind maximum range for this airplane at 10,000 feet. Also determine the average specific range in miles per gallon. Use a fuel weight of 5.64 pounds per gallon.

3.34. For the general aviation aircraft described in Example 3.5.1, determine the best glide airspeed at sea level and the maximum glide ratio with *fuel tanks empty*, for no wind, for a 60-mph headwind, and for a 60-mph tailwind.

3.35. For the executive business jet described in Example 3.6.2, determine the best glide airspeed and maximum glide ratio at 20,000 feet with *fuel tanks full*, for no wind, for a 100-mph headwind, and for a 100-mph tailwind.

3.36. For the executive business jet described in Example 3.6.2, determine the best glide airspeed and maximum glide ratio at 20,000 feet with *fuel tanks empty*, for no wind, for a 100 mph-headwind, and for a 100-mph tailwind.

3.37. For the small jet transport described in problem 3.7, determine the following performance parameters for no-power gliding flight:

a) Calculate the minimum sink airspeed at sea level and 30,000 feet.
b) Calculate the minimum sink rate at sea level and 30,000 feet.
c) Calculate the no-wind best glide airspeed at sea level and 30,000 feet.
d) Calculate the no-wind maximum glide ratio at sea level and 30,000 feet.

3.38. For the large jet transport described in problem 3.10, determine the following performance parameters for no-power gliding flight:
a) Calculate the minimum sink airspeed at sea level and 30,000 feet.
b) Calculate the minimum sink rate at sea level and 30,000 feet.
c) Calculate the no-wind best glide airspeed at sea level and 30,000 feet.
d) Calculate the no-wind maximum glide ratio at sea level and 30,000 feet.

3.39. For the propeller-driven transport described in problem 3.17, determine the following performance parameters for no-power gliding flight:
a) Calculate the minimum sink airspeed at sea level and 10,000 feet.
b) Calculate the minimum sink rate at sea level and 10,000 feet.
c) Calculate the no-wind best glide airspeed at sea level and 10,000 feet.
d) Calculate the no-wind maximum glide ratio at sea level and 10,000 feet.

3.40. For the human-powered airplane described in problem 3.19, determine the following performance parameters for no-power gliding flight:
a) Calculate the minimum sink airspeed at sea level.
b) Calculate the minimum sink rate at sea level.
c) Calculate the no-wind best glide airspeed at sea level.
d) Calculate the no-wind maximum glide ratio at sea level.

3.41. For the small jet transport described in problem 3.7, determine the best glide airspeed and the maximum glide ratio at sea level with a 50-mph headwind, with no wind, and with a 50-mph tailwind.

3.42. For the large jet transport described in problem 3.10, determine the best glide airspeed and the maximum glide ratio at sea level with a 50-mph headwind, with no wind, and with a 50-mph tailwind.

3.43. For the propeller-driven transport described in problem 3.17, determine the best glide airspeed and the maximum glide ratio at sea level with a 50-mph headwind, with no wind, and with a 50-mph tailwind.

3.44. For the human-powered airplane described in problem 3.19, determine the best glide airspeed and the maximum glide ratio at sea level with a 10-mph headwind, with no wind, and with a 10-mph tailwind.

3.45. Determine the stall speed at standard sea level for each of the airplanes described in problems 3.7, 3.10, 3.17, and 3.19. For the sake of this comparison, assume that all four airplanes have a maximum lift coefficient of 1.2.

3.46. For the jet transport described in problem 3.7, compute the maneuvering speed, the minimum turning radius, and the maximum turning rate for maximum gross weight at both sea level and 30,000 feet. Assume a maximum lift coefficient of 1.2 and a positive load factor limit of 4.0.

3.47. For the jet transport described in problem 3.10, compute the maneuvering speed, the minimum turning radius, and the maximum turning rate for maximum gross weight at both sea level and 30,000 feet. Assume a maximum lift coefficient of 1.2 and a positive load factor limit of 4.0.

3.48. For the propeller-driven transport described in problem 3.17, compute the maneuvering speed, the minimum turning radius, and the maximum turning rate for maximum gross weight at both sea level and 30,000 feet. For this airplane, assume a maximum lift coefficient of 1.6 and a positive load factor limit of 4.0.

3.49. The propeller-driven transport in problem 3.48 is flying at an airspeed equal to the minimum power airspeed for straight and level flight. For this airspeed, compute the minimum turning radius and the maximum bank angle at both sea level and 30,000 feet.

3.50. For the human-powered airplane described in problem 3.19, compute the maneuvering speed, the minimum turning radius, and the maximum turning rate for maximum gross weight at sea level. Assume a maximum lift coefficient of 1.2 and a positive load factor limit of 1.1.

3.51. The human-powered airplane in problem 3.50 is flying at an airspeed equal to the minimum power airspeed for straight and level flight. For this airspeed, compute the minimum turning radius and the maximum bank angle at sea level.

3.52. The jet transport described in problem 3.7 is fitted with turbofan engines. Determine the total no-wind ground roll required for takeoff at sea level and at 5,000 feet. For this airplane in takeoff configuration,

$$S_w = 950 \text{ ft}^2, \quad b_w = 75 \text{ ft}, \quad h_w = 6.0 \text{ ft}, \quad W = 73{,}000 \text{ lbf}, \quad \mu_r = 0.04,$$
$$C_{D_0} = 0.033, \quad C_{D_0,L} = 0.0, \quad e = 0.64, \quad C_L = 0.10, \quad C_{L_{\max}} = 1.86,$$
$$T_A = (\rho/\rho_0)[27{,}700 \text{ lbf} - (21.28 \text{ lbf}\cdot\text{sec/ft})\,V + (0.01117 \text{ lbf}\cdot\text{sec}^2/\text{ft}^2)\,V^2]$$

3.53. The large jet transport described in problem 3.10 is fitted with turbofan engines. Determine the total no-wind ground roll required for takeoff at sea level and at 5,000 feet. For this airplane in takeoff configuration,

$$S_w = 5{,}500 \text{ ft}^2, \quad b_w = 196 \text{ ft}, \quad h_w = 16 \text{ ft}, \quad W = 636{,}600 \text{ lbf}, \quad \mu_r = 0.04,$$
$$C_{D_0} = 0.033, \quad C_{D_0,L} = 0.0, \quad e = 0.64, \quad C_L = 0.30, \quad C_{L_{\max}} = 1.94,$$
$$T_A = (\rho/\rho_0)^{0.741}[199{,}000 \text{ lbf} - (177.6 \text{ lbf}\cdot\text{sec/ft})\,V + (0.1193 \text{ lbf}\cdot\text{sec}^2/\text{ft}^2)\,V^2]$$

3.54. Consider the takeoff performance of the propeller-driven transport that was described in problem 3.17. Determine the total ground roll required for takeoff at sea level and at 5,000 feet, with no wind. For this airplane in takeoff configuration,

$$S_w = 945 \text{ ft}^2, \quad b_w = 96 \text{ ft}, \quad h_w = 12 \text{ ft}, \quad W = 40{,}000 \text{ lbf}, \quad \mu_r = 0.04,$$
$$C_{D_0} = 0.038, \quad C_{D_0,L} = 0.0, \quad e = 0.74, \quad C_L = 0.40, \quad C_{L_{\max}} = 1.60,$$
$$T_A = (\rho/\rho_0)[10{,}000 \text{ lbf} - (12.0 \text{ lbf} \cdot \text{sec/ft}) V]$$

3.55. Consider the takeoff performance of the human-powered airplane described in problem 3.19. Determine the total ground roll required for takeoff at sea level with no wind and with a headwind of 5 mph. For this airplane in takeoff configuration,

$$S_w = 775 \text{ ft}^2, \quad b_w = 96.4 \text{ ft}, \quad h_w = 11 \text{ ft}, \quad W = 200 \text{ lbf}, \quad \mu_r = 0.05,$$
$$C_{D_0} = 0.010, \quad C_{D_0,L} = 0.0, \quad e = 0.80, \quad C_L = 0.40, \quad C_{L_{\max}} = 1.40,$$
$$T_A = (\rho/\rho_0)[31.0 \text{ lbf} - (1.0 \text{ lbf} \cdot \text{sec/ft}) V]$$

3.56. Consider the takeoff performance of a general aviation airplane with tail-dragger landing gear. Determine the total ground roll required for takeoff at sea level with no wind. Assume a lift coefficient equal to the maximum lift coefficient during the tail-down portion of the ground roll and a lift coefficient of 0.40 for the tail-up portion of the ground roll. The minimum ground control speed for this airplane is 30 mph. For this airplane in takeoff configuration,

$$S_w = 180 \text{ ft}^2, \quad b_w = 33 \text{ ft}, \quad h_w = 6.0 \text{ ft}, \quad W = 2{,}700 \text{ lbf}, \quad \mu_r = 0.04,$$
$$C_{D_0} = 0.036, \quad C_{D_0,L} = 0.0, \quad e = 0.82, \quad C_{L_{\max}} = 1.40,$$
$$T_A = (\rho/\rho_0)[1{,}200 \text{ lbf} - (4.0 \text{ lbf} \cdot \text{sec/ft}) V]$$

3.57. One advantage of the tail-dragger landing gear is that it allows the pilot to control the angle of attack during the high-speed phase of the takeoff ground roll. This gives better takeoff performance on a wider variety of ground surfaces. On rough, soft, or loose ground the coefficient of rolling friction is much higher than that for a paved surface and adjusting the angle of attack to maximize acceleration on any given surface can reduce takeoff distance. For the tail-dragger described in problem 3.56, compute the optimum lift coefficient for the high-speed phase of the takeoff ground roll for a coefficient of rolling friction of 0.04 and for a coefficient of rolling friction of 0.15.

3.58. Consider the landing performance of the jet transport described in problem 3.10. Determine the total no-wind ground roll required for landing at sea level and at 5,000 feet. For this airplane in landing configuration,

$$S_w = 5{,}500 \text{ ft}^2, \quad b_w = 196 \text{ ft}, \quad h_w = 16 \text{ ft}, \quad W = 636{,}600 \text{ lbf}, \quad \mu_r = 0.4,$$
$$C_{D_0} = 0.033, \quad C_{D_0,L} = 0.0, \quad e = 0.64, \quad C_L = 0.10, \quad C_{L_{\max}} = 2.30,$$
$$T_A = -(\rho/\rho_0)^{0.8} 70{,}000 \text{ lbf} \ (V > 100 \text{ ft/sec}), \quad T_A = 0 \ (V < 100 \text{ ft/sec})$$

3.59. Consider the landing performance of the propeller-driven transport in problem 3.17. Determine the total no-wind ground roll required for landing at sea level and at 5,000 feet. For this airplane in landing configuration,

$$S_w = 945 \text{ ft}^2,\ b_w = 96 \text{ ft},\ h_w = 12 \text{ ft},\ W = 40{,}000 \text{ lbf},\ \mu_r = 0.4,\ C_{D_0} = 0.038,$$
$$C_{D_0,L} = 0.0,\ e = 0.74,\ C_L = 0.10,\ C_{L_{\max}} = 2.10,\ T_A = 0.0$$

3.60. Consider the no-brake landing performance of the human-powered airplane described in problem 3.19. Determine the total ground roll required for landing at sea level with no wind and with a headwind of 5 mph. For this airplane in landing configuration,

$$S_w = 775 \text{ ft}^2,\ b_w = 96.4 \text{ ft},\ h_w = 11 \text{ ft},\ W = 200 \text{ lbf},\ \mu_r = 0.05,\ C_{D_0} = 0.010,$$
$$C_{D_0,L} = 0.0,\ e = 0.80,\ C_L = 0.40,\ C_{L_{\max}} = 1.40,\ T_A = 0$$

3.61. Assume that the small jet transport described in problem 3.7 has the following properties in cruise configuration:

$$S_w = 950 \text{ ft}^2,\quad b_w = 75 \text{ ft},\quad W = 73{,}000 \text{ lbf},$$
$$C_{D_0} = 0.020,\quad C_{D_0,L} = 0.0,\quad e = 0.67,$$
$$T_A = \frac{\rho}{\rho_0} 27{,}700 \text{ lbf}$$

Using the small-thrust-angle approximation, determine the service ceiling.

3.62. Assume that the large jet transport described in problem 3.10 has the following properties in cruise configuration:

$$S_w = 5{,}500 \text{ ft}^2,\quad b_w = 196 \text{ ft},\quad W = 636{,}600 \text{ lbf},$$
$$C_{D_0} = 0.020,\quad C_{D_0,L} = 0.0,\quad e = 0.72,$$
$$T_A = \left(\frac{\rho}{\rho_0}\right)^{0.8} 250{,}000 \text{ lbf}$$

Using the small-thrust-angle approximation, determine the service ceiling.

3.63. Assume that the propeller-driven transport described in problem 3.17 has the following properties in cruise configuration:

$$S_w = 945 \text{ ft}^2,\quad b_w = 96 \text{ ft},\quad W = 40{,}000 \text{ lbf},$$
$$C_{D_0} = 0.025,\quad C_{D_0,L} = 0.0,\quad e = 0.80,$$
$$T_A = (\rho/\rho_0)[10{,}000 \text{ lbf} - (12.0 \text{ lbf} \cdot \text{sec/ft})\, V]$$

Using the small-thrust-angle approximation, determine the service ceiling.

3.64. Assume that the human-powered airplane described in problem 3.19 has the following properties:

$$S_w = 775\ \text{ft}^2, \quad b_w = 96.4\ \text{ft}, \quad W = 200\ \text{lbf},$$
$$C_{D_0} = 0.010, \quad C_{D_0,L} = 0.0, \quad e = 0.80,$$
$$P_A = (\rho/\rho_0)0.42\ \text{hp}$$

Using the small-thrust-angle approximation, determine the absolute ceiling for this aircraft.

3.65. For the large jet transport described in problem 3.53, determine the FAR Part 25 takeoff distance at standard sea level with no wind. This airplane is fitted with four turbofan engines that produce a thrust that varies significantly with airspeed. Assume a 3-second rotation time and use the following properties for takeoff configuration:

$$S_w = 5{,}500\ \text{ft}^2, \quad b_w = 196\ \text{ft}, \quad h_w = 16\ \text{ft}, \quad W = 636{,}600\ \text{lbf}, \quad \mu_r = 0.04,$$
$$C_{D_0} = 0.033, \quad C_{D_0,L} = 0.0, \quad e = 0.64, \quad C_L = 0.30, \quad C_{L_{\max}} = 1.94,$$
$$T_A = (\rho/\rho_0)^{0.741}[199{,}000\ \text{lbf} - (177.6\ \text{lbf}\cdot\text{sec/ft})\,V + (0.1193\ \text{lbf}\cdot\text{sec}^2/\text{ft}^2)\,V^2]$$

3.66. Consider the jet transport described in problem 3.65. Assuming that one of the four engines fails during a no-wind takeoff at standard sea level, plot the total field length required to stop the aircraft after engine failure and the total field length required to continue the FAR Part 25 takeoff using the remaining three engines as a function of the engine failure recognition speed. Use an obstacle clearance altitude of 35 feet and assume 1 second for engine failure recognition and another second for the pilot to react and apply the brakes. What are the critical engine failure recognition speed and the balanced field length?

3.67. While the distance traveled from brake release to obstacle clearance altitude is the most important factor associated with airplane takeoff, it is sometimes necessary to estimate the takeoff time. For example, to estimate the fuel consumed during takeoff, it is necessary to know how long the engines must be operated at full throttle during the acceleration, rotation, and climb to obstacle clearance altitude. The acceleration time can be computed in much the same way that the acceleration distance was computed in Sec. 3.10. Starting with Newton's second law, as expressed in Eq. (3.10.1) and assuming a parabolic variation in thrust with airspeed, show that the time required to accelerate from airspeed V_i to airspeed V_{i+1} is

$$t_{i+1} - t_i = (K_W)_i/g$$

where $(K_W)_i$ is given by Eq. (3.10.14).

3.68. For the jet transport in problem 3.52, determine the total time required for the takeoff ground roll with no wind at sea level and at 5,000 feet.

3.69. For the large jet transport in problem 3.53, determine the total time required for the takeoff ground roll with no wind at sea level and at 5,000 feet.

3.70. For the propeller-driven transport in problem 3.54, determine the total time required for the takeoff ground roll with no wind at sea level and at 5,000 feet.

3.71. For the human-powered airplane in problem 3.55, determine the total time required for the takeoff ground roll at sea level with no wind and with a headwind of 5 mph.

3.72. For the tail-dragger in problem 3.56, determine the total time required for the takeoff ground roll with no wind at sea level.

3.73. Write a computer program to determine the total ground roll distance and time required for takeoff. Assume a thrust variation with airspeed and density of the form

$$T = (\rho/\rho_0)^a (T_0 - T'V + T''V^2)$$

where the air density ρ and the constants a, T_0, T', and T'' are specified by the user. The user should also be allowed to specify the following parameters,

$$S_w,\ b_w,\ h_w,\ W,\ \mu_r,\ C_{D_0},\ C_{D_{0,L}},\ e,\ C_L,\ C_{L_{\max}},\ V_{hw},\ t_r$$

Test your program by resolving problems 3.53, 3.55, 3.69, and 3.71.

3.74. Write a computer program to determine the critical engine failure recognition speed and the balanced field length for an aircraft as a function of the parameters specified in problems 3.65 and 3.66. Use a secant method to numerically find the engine failure speed that gives the same total field length required to either continue or abort the takeoff. Test your program by resolving Example 3.11.2 and problem 3.66.

Chapter 4
Longitudinal Static Stability and Trim

4.1. Fundamentals of Static Equilibrium and Stability

Much of the performance analysis in Chapter 3 was based on the concept of static equilibrium, which for an aircraft is often called *trimmed flight*. Static equilibrium occurs whenever there is no acceleration of the aircraft. Unaccelerated flight requires that the summations of forces and moments acting on the aircraft are zero. For example, in steady level flight with the thrust vector aligned with the direction of flight, the lift must equal the weight, $L = W$, and the thrust must equal the drag, $T = D$. These two relations were used to determine the thrust required for steady level flight as a function of aircraft weight and airspeed. Static equilibrium also requires that the side force acting on the aircraft is zero. This condition is often assumed to be satisfied as a result of aircraft symmetry. Additionally, the summation of moments about the center of gravity (CG) in roll, pitch, and yaw must all be zero for trimmed flight. Aircraft symmetry will often result in zero rolling and yawing moments, but the pitching moment is usually zeroed with control input. **When the controls are set so that the resultant forces and the moments about the center of gravity are all zero, the aircraft is said to be in *trim*, which simply means static equilibrium.**

As shown in Fig. 4.1.1, the control surfaces on a conventional airplane usually consist of ailerons, elevator, and rudder. The ailerons are used to control the rolling moment, the elevator is used to control the pitching moment, and the rudder is used to control the yawing moment. These aircraft control surfaces provide two functions. First, the control surfaces must be able to maintain static trim over the entire range of airspeed and altitude for which the aircraft is able to fly. This includes being able to trim the aircraft against any asymmetric thrust force, which may occur when one or more of the engines has failed on a multiengine aircraft. Additionally, the control surfaces must provide the moments necessary to adequately maneuver the aircraft over this same range of airspeed and altitude. Since trim is closely coupled with static stability, trim is covered in this and the following chapter. Maneuverability is covered in Chapter 6.

The ease with which a pilot is able to maintain trim is one important aspect of the aircraft characteristics known as *handling qualities*. If the pilot cannot maintain trim with relative ease, the aircraft will be difficult or even dangerous to fly. Any airplane that is difficult to fly will not be popular with pilots, no matter how well it performs in other regards. This point is very important for the designer to understand and remember. The student should commit it to memory now and never forget it.

The ease of maintaining static trim is related to a property of the equilibrium state, which is known as *static stability*. The static stability of any equilibrium state is related to the response of the system to a small disturbance from that equilibrium state. **If a system in an equilibrium state returns to equilibrium following a small disturbance, the state is said to be a *stable equilibrium*.** On the other hand, **if the system diverges from equilibrium when slightly disturbed, the state is said to be an *unstable equilibrium*.**

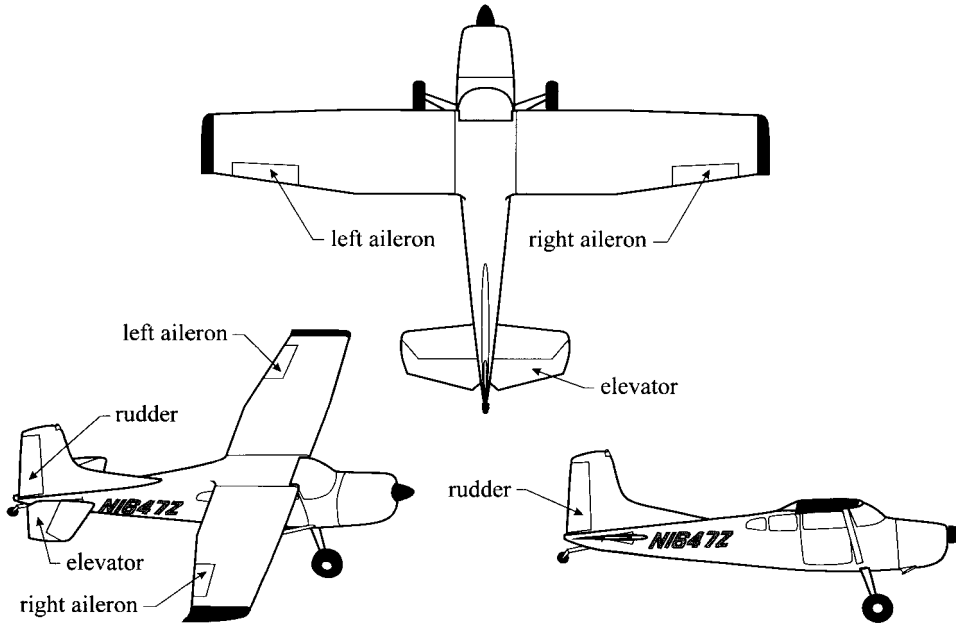
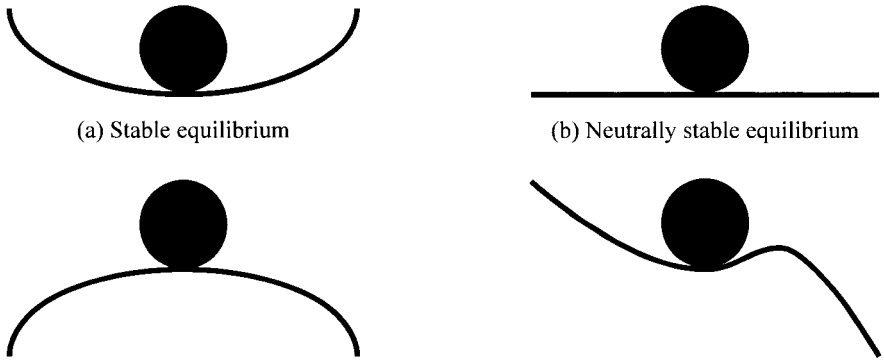


Figure 4.1.1. Typical control surfaces of a conventional airplane.

The most commonly used example of a stable equilibrium state is a ball in a bowl, as shown in Fig. 4.1.2a. When the ball is at rest in the bottom of the bowl, it is in an equilibrium state, since the force between the ball and the bowl exactly balances the force of gravity and there is no moment about the ball's center of gravity. If the ball were to be displaced from the bottom of the bowl, it would roll back to the bottom as a consequence of the resulting force and moment imbalance. For this reason, when the ball is at rest in the bottom of the bowl, it is said to be in a stable equilibrium state. Conversely, the situation shown in Fig. 4.1.2c is not a stable equilibrium. When the ball is at rest at the exact apex of the convex surface, it is in static equilibrium, because there is no force or moment imbalance at that exact position. However, any disturbance of the ball from the exact apex, no matter how small, would produce a force and moment imbalance, which would in turn cause the ball to roll away from the apex. Thus, the situation where a ball is resting exactly at the apex of a convex surface is classified as an unstable equilibrium state.

An equilibrium situation can also exist that is neither stable nor unstable. For example, consider a ball resting on a perfectly flat and horizontal surface, as shown in Fig. 4.1.2b. This situation is clearly an equilibrium state, since the summation of forces and moments acting on the ball are zero. When this ball is displaced from the equilibrium position, there is no force or moment imbalance produced. Thus, there is no tendency for the ball to either return to its original equilibrium point or to diverge from it. This condition is classified as a neutrally stable equilibrium state. Neutral stability is the dividing line between stable equilibrium and unstable equilibrium.



(a) Stable equilibrium

(b) Neutrally stable equilibrium

(c) Unstable equilibrium

(d) Stable equilibrium

Figure 4.1.2. Several different types of static equilibrium.

The situation shown in Fig. 4.1.2d is also worth some discussion at this point. Strictly speaking, this is a stable equilibrium, because a very small disturbance from the position shown would result in a force and moment imbalance that would return the ball to its original equilibrium state. However, a larger disturbance to the right could cause the ball to move past the apex, which would then produce a force and moment imbalance that would cause the ball to move away from its original equilibrium state. This type of stable equilibrium can sometimes occur with an aircraft in trimmed flight. This is a particularly dangerous situation and will be discussed in greater detail at a later point.

As shown in Fig. 4.1.3, a rigid airplane in free flight has six degrees of freedom, three translational degrees of freedom and three rotational degrees of freedom. For the airplane to be in fully stable trim, there can be no instability in any of the six degrees of freedom. Small translational disturbances in axial, normal, or sideslip velocity must all result in a return to the original trimmed equilibrium condition. Similarly, rotational disturbances in roll, pitch, and yaw must all result in a return to the original equilibrium attitude. With few exceptions, if the rotational degrees of freedom for an airplane are stable, translational stability will not be a problem.

Any object moving through the air will experience drag that opposes the motion. If the angle of attack remains fixed, this drag increases with increasing airspeed. Except for the case of a ramjet, which is not normally used for aircraft propulsion, the thrust developed by an aircraft engine is either constant with airspeed or decreases with increasing airspeed. When an airplane is in static equilibrium with regard to translation in the direction of motion, the forward component of thrust must balance the drag. At constant angle of attack, a small increase in airspeed will result in an increase in drag and either a decrease in thrust or no change in thrust. In either case, the increase in airspeed results in a drag that is greater than the thrust. This force imbalance in the axial direction will result in a deceleration, which will restore the airspeed to the original static equilibrium value. Conversely, if the airspeed is decreased by a small disturbance with no change in angle of attack, the drag will become less than the thrust and the aircraft will accelerate back to the equilibrium airspeed.

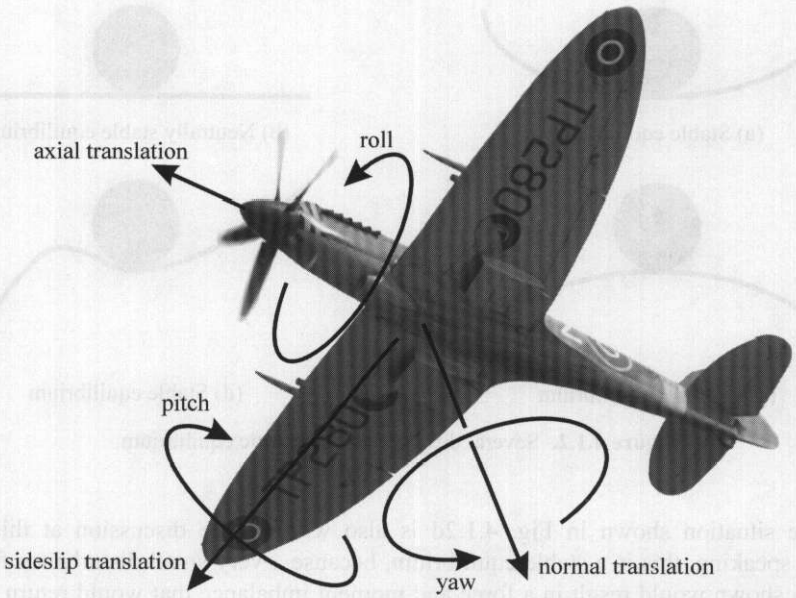


Figure 4.1.3. The six degrees of freedom for a rigid airplane in free flight.

In a similar manner, any disturbance in velocity in a direction normal to the equilibrium flight path will result in an aerodynamic force that opposes the disturbance, provided that the flow remains attached. Thus, when the attitude of an airplane is held constant, the aerodynamic forces quite naturally maintain translational static stability, in the absence of stall. It should be reemphasized that this translational stability is contingent on being able to maintain the equilibrium attitude of the aircraft. Since induced drag depends on angle of attack, if the angle of attack were to change along with the airspeed, it is possible that the total drag could decrease as the airspeed increases. In addition, this natural translational stability depends on maintaining attached flow. At some angles of attack beyond stall, the airplane may be unstable for disturbances in normal velocity. However, since rotational stability is most critical to maintaining trimmed flight in the absence of stall, static aircraft stability in roll, pitch, and yaw will be the primary emphasis of this and the following chapter.

A thorough understanding of the fundamental principles of static stability is very important to the airplane designer. However, it is also important to understand the influence of the pilot on the human-machine system that constitutes a modern airplane. Most of the technical problems associated with manned powered flight were solved well before the Wright brothers' first successful flight on December 17, 1903. What was lacking was a sufficient understanding of the influence of the pilot on aircraft stability and control. From an analytical point of view, it is easier to design an unmanned aircraft with an autopilot than it is to design a good manned airplane. The human pilot is a very complex component of the modern airplane, and whenever human ability and behavior become part of an engineered system, the designer's job takes on a new dimension.

While static stability is usually desired for most systems under human control, it is not an absolute requirement in all cases. Most humans can easily learn to ride a bicycle, which is inherently unstable. With a greater level of training and concentration, a human can even ride a unicycle, which is very unstable. Furthermore, after some initial practice, riding a bicycle does not even require conscious control by the human rider. The rider is still providing unconscious control. This is evidenced by the fact that a riderless bicycle will not travel a long distance without tipping over. Once a riderless bicycle is moving, however, it will usually travel for some short distance before tipping over. This is because even though the upright moving bicycle is in an unstable equilibrium, the divergence from that equilibrium is very slow at first. It is this slow initial divergence, associated with the instability, which makes it possible for a human rider to maintain the bicycle's equilibrium with no conscious effort. Flying an airplane is similar to riding a bicycle. Many of the control inputs furnished by the pilot are provided without conscious thought. Whereas the ability of a human to provide such control inputs with little or no conscious effort makes the pilot's job easier, such human control is very difficult or impossible to model analytically. The effects of having a human in the control loop have always been investigated experimentally. In some ways this makes the designer's job more difficult.

In this and the following chapter we discuss how to design an airplane for static stability, how to determine airplane trim requirements, and how to assure some aspects of good handling qualities when the airplane is interfaced with its human pilot.

4.2. Pitch Stability of a Cambered Wing

As previously discussed, static stability in the rotational degrees of freedom is of primary importance for maintaining aircraft trim. For an airplane to be statically stable in rotation, any disturbances in roll, pitch, or yaw must all result in the production of a restoring moment that will return the aircraft to the original equilibrium attitude. To begin our study of static aircraft stability, we shall consider the pitch stability of a simple cambered wing, the cross-section of which is shown in Fig. 4.2.1. We will first explore the requirements for trim and then examine the pitch stability of the equilibrium state.

Assuming that the wing is symmetric in the spanwise direction and that the motion of the wing through the air is in a direction normal to the span, there will be no side force and no rolling or yawing moment. For this symmetric flight condition, the aerodynamic forces acting on the wing can be resolved into a lift force, L, a drag force, D, and a pitching moment about the aerodynamic center of the wing, m_{ac}. To simplify this initial stability analysis we shall assume that the aerodynamic center and the center of gravity are aligned with the thrust vector, which is aligned with the direction of flight. For the wing to be in trim (i.e., static equilibrium), the summation of forces in both the horizontal and vertical direction must be zero. This requires that

$$T = D \tag{4.2.1}$$

and

$$L = W \tag{4.2.2}$$

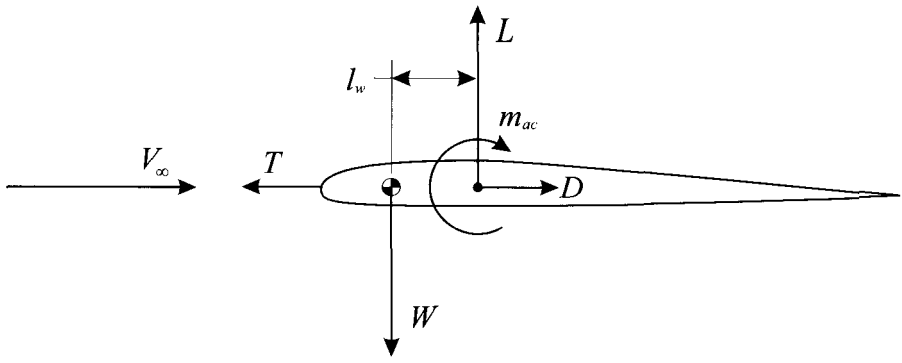


Figure 4.2.1. Forces and moments acting on a cambered wing in flight.

Additionally, trim requires that the summation of pitching moments about the center of gravity, m, must be zero. From Fig. 4.2.1, this yields

$$m = m_{ac} - l_w L = 0 \tag{4.2.3}$$

where l_w is the distance that the aerodynamic center of the wing is aft of the center of gravity. After applying the definitions of the lift and moment coefficients, Eq. (4.2.3) can be written as

$$\tfrac{1}{2}\rho V_\infty^2 S_w \bar{c} C_m = \tfrac{1}{2}\rho V_\infty^2 S_w (\bar{c} C_{m_{ac}} - l_w C_L) = 0 \tag{4.2.4}$$

or

$$C_m = C_{m_{ac}} - \frac{l_w}{\bar{c}} C_L = 0 \tag{4.2.5}$$

For a given weight and airspeed, the lift coefficient is fixed by the trim requirement in Eq. (4.2.2). The moment coefficient about the aerodynamic center is fixed by the wing geometry. Thus, for a given geometry, weight, and airspeed, Eq. (4.2.5) requires that

$$l_w = \frac{C_{m_{ac}}}{C_L} \bar{c} \tag{4.2.6}$$

Since the lift coefficient is positive and the moment coefficient about the aerodynamic center of a simple cambered wing is negative, we see that trim requires $l_w < 0$. Thus, for static equilibrium the aerodynamic center must be forward of the center of gravity.

If this static equilibrium state is stable in pitch, then a small increase in angle of attack must produce a negative pitching moment about the center of gravity, to decrease the angle of attack back toward trim. Conversely, a small decrease in angle of attack must produce a positive pitching moment, to increase the angle of attack and restore trim.

Thus, the pitching moment about the center of gravity must vary with angle of attack such that any change in angle of attack produces a change of opposite sign in the pitching moment about the center of gravity. The mathematical criterion for pitch stability is then

$$\frac{\partial m}{\partial \alpha} = \frac{1}{2}\rho V_\infty^2 S_w \bar{c} \frac{\partial C_m}{\partial \alpha} < 0 \tag{4.2.7}$$

Since the dynamic pressure, the wing area, and the mean chord length are always positive, pitch stability requires that

$$\frac{\partial C_m}{\partial \alpha} \equiv C_{m,\alpha} < 0 \tag{4.2.8}$$

which is **the general pitch stability criterion for any aircraft**. For this reason, the derivative in Eq. (4.2.8) is usually called the *pitch stability derivative* or *pitch stiffness*.

Using Eq. (4.2.5) in Eq. (4.2.8) gives

$$\frac{\partial C_{m_{ac}}}{\partial \alpha} - \frac{l_w}{\bar{c}} \frac{\partial C_L}{\partial \alpha} < 0 \tag{4.2.9}$$

By definition, the aerodynamic center is the point on the wing where the pitching moment coefficient does not vary with angle of attack,

$$\frac{\partial C_{m_{ac}}}{\partial \alpha} = 0 \tag{4.2.10}$$

and thus

$$-\frac{l_w}{\bar{c}} \frac{\partial C_L}{\partial \alpha} < 0 \tag{4.2.11}$$

Since the change in lift coefficient with angle of attack is positive for angles of attack less than stall, we see that stability requires $l_w > 0$. This means that for static stability, the aerodynamic center must be aft of the center of gravity. This condition is opposite to that required for static equilibrium. Thus, **a simple cambered wing is not statically stable in free flight.**

Using the trim requirement in Eq. (4.2.6) to eliminate l_w from the stability requirement in Eq. (4.2.11) gives

$$-\frac{C_{m_{ac}}}{C_L} \frac{\partial C_L}{\partial \alpha} < 0 \tag{4.2.12}$$

This is the requirement for stable trim in this tailless flying wing. The lift coefficient must be positive to support the weight of the aircraft and the lift slope is positive for any

wing at angles of attack below stall. Thus, **if stable trim is to be maintained, a single wing with no tail must always produce a positive pitching moment coefficient about its aerodynamic center**.

In our study of airfoil sections, we found that a symmetric airfoil produces no moment about the aerodynamic center, and an airfoil with simple positive camber produces a negative pitching moment about the aerodynamic center. Neither of these common airfoil sections meets the criterion required for stable trim in a flying wing.

To produce a positive pitching moment about the aerodynamic center, an airfoil section must have negative camber over at least some fraction of the chord. An airfoil with negative camber over the entire chord is inefficient when producing positive lift and has a low maximum lift coefficient. A better choice is an airfoil that has negative camber over only some portion of the chord near the trailing edge. Such an airfoil section is shown in Fig. 4.2.2. An airfoil of this type is said to have a *reflexed trailing edge*. It can be designed to produce a positive pitching moment about the aerodynamic center and can be used to satisfy the criterion for stable trim specified by Eq. (4.2.12).

It is possible to design an aircraft, consisting of only a single flying wing with no tail, so that stable trimmed flight can be achieved. However, such designs are difficult at best and usually do not provide good handling qualities without a significant reduction in performance or the implementation of some type of computer control. A better option usually is to combine a wing with a conventional aft tail. This is the design that is most often seen in nature and it is difficult to improve upon.

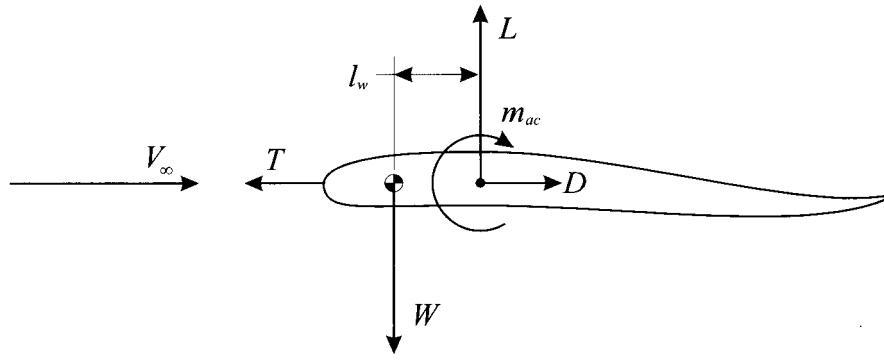


Figure 4.2.2. Forces and moments acting on a cambered wing with a reflexed trailing edge.

4.3. Simplified Pitch Stability Analysis for a Wing-Tail Combination

Trim and static stability in pitch are readily achieved in an airplane by combining a wing with a conventional aft tail, as shown in Fig. 4.3.1. The complete tail assembly, consisting of both the horizontal and vertical tail, is called the *empennage*. The purpose of the horizontal tail is to provide both stability and control in pitch. As can be seen in Fig. 4.3.2, the horizontal tail usually consists of a fixed forward section, called the

horizontal stabilizer or *tailplane*, and a rotating aft section, called the elevator. Both the horizontal stabilizer and the elevator contribute to pitch stability, but only the elevator provides pitch control. In some cases the entire horizontal tail rotates to provide pitch control. This is called an *all-flying tail*. On some airplanes both the front stabilizer section and the aft elevator section of the horizontal tail rotate separately to provide pitch control. This configuration is called a *stabilator*. The stabilator looks and responds very much like the conventional horizontal tail, but it differs somewhat in its mechanical operation.

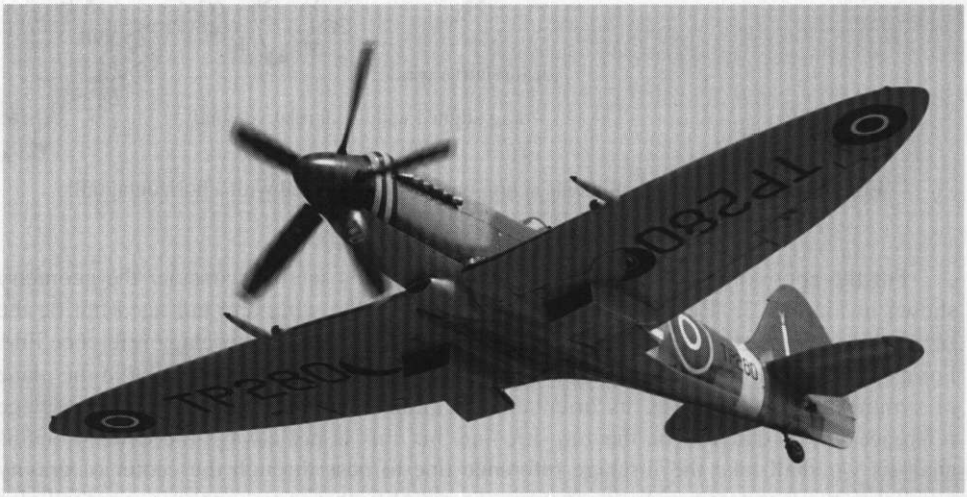


Figure 4.3.1. British Spitfire, showing the conventional aft tail. (Photograph by Barry Santana)

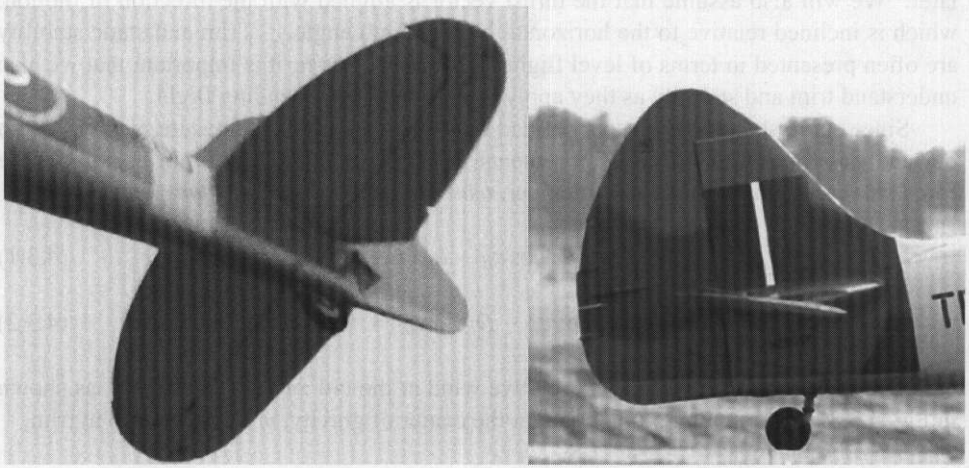


Figure 4.3.2. Empennage of the British Spitfire. (Photographs by Barry Santana)

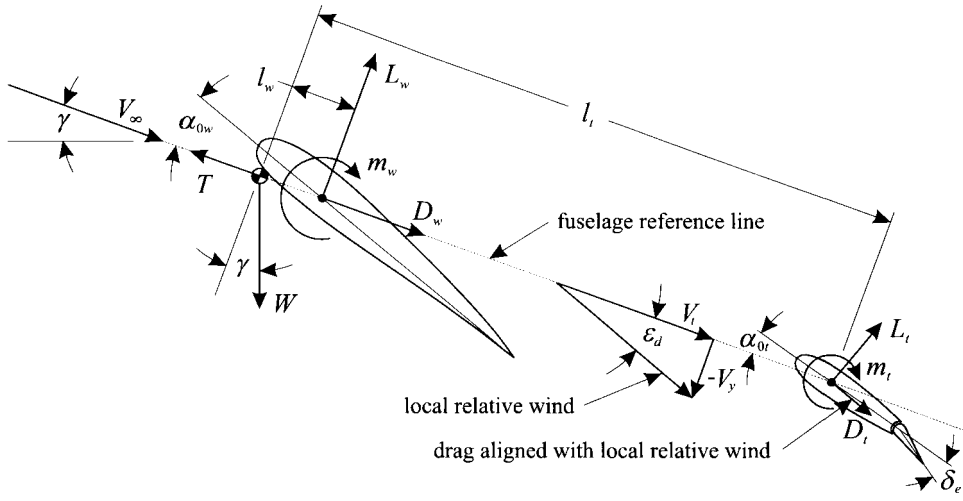


Figure 4.3.3. Forces and moments acting on a wing combined with a horizontal tail.

For the approximate analysis to be presented in this section, consider the geometry shown in Fig. 4.3.3. Because the angle of attack for the wing and tail need not be the same, the angle of attack for the airplane is specified relative to a fuselage reference line. For a spanwise symmetric aircraft, the fuselage reference line is chosen to be in the plane of symmetry, but otherwise, its orientation is quite arbitrary. Sometimes the fuselage reference line is taken to be the zero-lift line, but this is not always the case. For this analysis we shall take the fuselage reference line to pass through the center of gravity parallel to the freestream velocity at trim. To simplify this initial analysis, we shall also assume that the aerodynamic center of both the wing and the tail, as well as the center of thrust, all fall on this fuselage reference line. The more general case will be examined later. We will also assume that the thrust vector is aligned with the direction of motion, which is inclined relative to the horizontal by the climb angle γ. Trim and static stability are often presented in terms of level flight ($\gamma = 0$). However, it is important that we also understand trim and stability as they apply to climbing or descending flight.

Since static stability is always defined relative to an equilibrium state, we will begin our analysis by examining the requirements for static equilibrium. From Fig. 4.3.3, the force balance required for trim (remember, *trim* is read *static equilibrium*) gives

$$T = D_w + D_t \cos\varepsilon_d + L_t \sin\varepsilon_d + W \sin\gamma \tag{4.3.1}$$

$$L_w + L_t \cos\varepsilon_d - D_t \sin\varepsilon_d = W \cos\gamma \tag{4.3.2}$$

where ε_d is the angle between local relative wind at the tail and the freestream, as shown in Fig. 4.3.3. The pitching moment about the center of gravity, m, must be zero at trim,

$$m = m_w + m_t - l_w L_w - l_t L_t \cos\varepsilon_d + l_t D_t \sin\varepsilon_d = 0 \tag{4.3.3}$$

where m_w and m_t are, respectively, the pitching moments for the wing and the tail about their aerodynamic centers. The lengths l_w and l_t are the distances from the center of gravity to the aerodynamic center of the wing and the tail, respectively, both measured positive aft of the CG.

Equations (4.3.1) through (4.3.3) provide three of the six requirements for static equilibrium. The remaining three requirements are simply the trivial relations that the side force, rolling moment, and yawing moment must all be zero. From Eq. (4.3.1) we can determine the thrust required to maintain constant airspeed. From the requirements specified by Eqs. (4.3.2) and (4.3.3), we can relate the aerodynamic forces developed by the wing and tail to the weight of the aircraft and the position of the center of gravity. Equation (4.3.2) simply requires that at trim, the aerodynamic forces developed by the wing and tail combined must support the normal component of the aircraft weight. Equation (4.3.3) specifies how the aerodynamic force must be divided between the wing and tail, to maintain the attitude required for trim. Thus, if we are to be able to attain trim for a variety of flight conditions, we must have some means to control the lift developed by both the wing and the tail.

The downwash angle ε_d is typically small, so we can apply the usual small-angle approximations, $\cos\varepsilon_d \cong 1$ and $D_t \sin\varepsilon_d << L_t$. Using these approximations and dividing Eq. (4.3.2) by the freestream dynamic pressure and wing area gives

$$\frac{L_w}{\frac{1}{2}\rho V_\infty^2 S_w} + \frac{\frac{1}{2}\rho V_t^2 S_t}{\frac{1}{2}\rho V_\infty^2 S_w}\frac{L_t}{\frac{1}{2}\rho V_t^2 S_t} = \frac{W\cos\gamma}{\frac{1}{2}\rho V_\infty^2 S_w} \tag{4.3.4}$$

or

$$C_{L_w} + \frac{S_t}{S_w}\frac{\frac{1}{2}\rho V_t^2}{\frac{1}{2}\rho V_\infty^2} C_{L_t} = \frac{W\cos\gamma}{\frac{1}{2}\rho V_\infty^2 S_w} \tag{4.3.5}$$

where C_{L_w} and C_{L_t} are, respectively, the lift coefficients for the wing and isolated tail, each based on their own planform area. The dynamic pressure for the tail in Eq. (4.3.5) is distinguished from the freestream dynamic pressure because on average over the span of the tail, the dynamic pressure may be less than or greater than the freestream value. The average dynamic pressure for the tail depends on the location of the tail. If the tail is located in the wake of the wing or the fuselage, the dynamic pressure on the tail will be less than the freestream value. On the other hand, if the tail is located in the slipstream of a propeller or in the exhaust of a jet engine, the dynamic pressure on the tail will be greater than that for the freestream. Equation (4.3.5) is usually written as

$$C_{L_w} + \frac{S_t}{S_w}\eta_t C_{L_t} = \frac{W\cos\gamma}{\frac{1}{2}\rho V_\infty^2 S_w} \tag{4.3.6}$$

$$\eta_t \equiv \frac{\frac{1}{2}\rho V_t^2}{\frac{1}{2}\rho V_\infty^2} \tag{4.3.7}$$

This ratio of dynamic pressures is called the *tail efficiency*, and it can take values from about 0.8 to 1.2. However, the distribution of dynamic pressure over the span of the tail is very difficult to determine and is typically quite close to the freestream value. Thus, at least for the purpose of preliminary design, the tail efficiency is usually assumed to be unity.

In a manner similar to that used to obtain Eq. (4.3.6), we apply the small-angle approximations for ε_d to Eq. (4.3.3) and divide by the freestream dynamic pressure, the area of the main wing, and the mean chord length of the main wing:

$$\begin{aligned}\frac{m}{\frac{1}{2}\rho V_\infty^2 S_w \bar{c}_w} &= \frac{m_w}{\frac{1}{2}\rho V_\infty^2 S_w \bar{c}_w} + \frac{S_t \bar{c}_t}{S_w \bar{c}_w}\eta_t \frac{m_t}{\frac{1}{2}\rho V_t^2 S_t \bar{c}_t} \\ &\quad - \frac{l_w}{\bar{c}_w}\frac{L_w}{\frac{1}{2}\rho V_\infty^2 S_w} - \frac{S_t l_t}{S_w \bar{c}_w}\eta_t \frac{L_t}{\frac{1}{2}\rho V_t^2 S_t} = 0\end{aligned} \tag{4.3.8}$$

In terms of the definitions of the lift and moment coefficients, this gives

$$C_m = C_{m_w} + \frac{S_t \bar{c}_t}{S_w \bar{c}_w}\eta_t C_{m_t} - \frac{l_w}{\bar{c}_w} C_{L_w} - \frac{S_t l_t}{S_w \bar{c}_w}\eta_t C_{L_t} = 0 \tag{4.3.9}$$

Solving Eq. (4.3.6) for the wing lift coefficient at trim gives

$$C_{L_w} = \frac{W\cos\gamma}{\frac{1}{2}\rho V_\infty^2 S_w} - \frac{S_t}{S_w}\eta_t C_{L_t} \tag{4.3.10}$$

Using this result in Eq. (4.3.9), we can solve for the tail lift coefficient that is required to balance the airplane at trim. Thus, we obtain

$$C_{L_t} = \frac{S_w \bar{c}_w}{S_t (l_t - l_w)\eta_t} C_{m_w} + \frac{\bar{c}_t}{(l_t - l_w)} C_{m_t} - \frac{S_w l_w}{S_t (l_t - l_w)\eta_t}\frac{W\cos\gamma}{\frac{1}{2}\rho V_\infty^2 S_w} \tag{4.3.11}$$

Using Eq. (4.3.11) in Eq. (4.3.10), the lift coefficient required for the wing at trim can be written as

$$C_{L_w} = \frac{l_t}{l_t - l_w}\frac{W\cos\gamma}{\frac{1}{2}\rho V_\infty^2 S_w} - \frac{\bar{c}_w}{l_t - l_w} C_{m_w} - \frac{S_t \bar{c}_t}{S_w (l_t - l_w)}\eta_t C_{m_t} \tag{4.3.12}$$

To gain some additional insight into the trim requirements provided by Eqs. (4.3.11) and (4.3.12), consider the special case where both the wing and the tail have symmetric airfoil sections at every cross section along the span (remember, a symmetric airfoil section has no flap deflection). Since a symmetric airfoil produces no moment about its aerodynamic center, the moment coefficients in Eqs. (4.3.11) and (4.3.12) now go to zero. This gives

$$C_{L_t} = -\frac{S_w l_w}{S_t (l_t - l_w)\eta_t} \frac{W \cos\gamma}{\frac{1}{2}\rho V_\infty^2 S_w} \tag{4.3.13}$$

and

$$C_{L_w} = \frac{l_t}{(l_t - l_w)} \frac{W \cos\gamma}{\frac{1}{2}\rho V_\infty^2 S_w} \tag{4.3.14}$$

Since we are examining the particular case of an aft tail, the tail is aft of both the CG and the main wing. Thus, both l_t and $(l_t - l_w)$ are positive. The only parameter on the right-hand side of either Eq. (4.3.13) or Eq. (4.3.14) that could be negative is l_w. The center of gravity could be either forward or aft of the aerodynamic center of the main wing. Notice from Eq. (4.3.13) that the lift on the tail must be negative if the center of gravity is forward of the aerodynamic center of the main wing ($l_w > 0$). If l_w is positive, Eq. (4.3.14) requires that the lift produced by the main wing must be greater than the normal component of aircraft weight. This does not give the best performance in terms of aerodynamic efficiency. When the horizontal tail is carrying lift, positive or negative, induced drag is produced on the tail. If the lift on the tail is negative, the main wing must support this added load along with the normal component of aircraft weight. This increases the induced drag on the main wing as well. Thus, a double induced drag penalty is paid for negative lift carried on the tail. To avoid negative lift on the tail, Eq. (4.3.13) requires that the center of gravity be located at or behind the aerodynamic center of the main wing ($l_w \leq 0$). **It should be emphasized that the avoidance of negative lift on the tail is only for improved aerodynamic efficiency. It is not required for either trim or stability.** Most airplanes will carry some negative lift on the tail over some portion of the allowable range of operating conditions.

Even carrying positive lift on the tail will usually result in some reduction in aerodynamic efficiency. This is because the horizontal tail will usually have a lower aspect ratio and a lower aerodynamic efficiency than the main wing. If this is the case, any lift carried on the tail will result in more induced drag than if that same lift were carried on the more efficient wing. For this reason, a good preliminary design is often achieved by placing the center of gravity such that the lift on the tail is zero when the airplane is trimmed with no elevator deflection at the design cruise airspeed. From Eq. (4.3.13), this requires that $l_w = 0$, which means that the center of gravity is placed at the aerodynamic center of the main wing if both the wing and the tail have symmetric airfoil sections.

For the more general trim condition specified by Eq. (4.3.11), best aerodynamic efficiency is achieved when the position of the CG relative to the aerodynamic center of the main wing is specified by setting the lift on the tail to zero and solving for l_w. **For the case of level flight, zero lift on the aft tail requires that**

$$\frac{l_w}{\bar{c}_w} = \frac{\frac{1}{2}\rho V_\infty^2 S_w}{W}\left(C_{m_w} + \frac{S_t \bar{c}_t}{S_w \bar{c}_w}\eta_t C_{m_t}\right) \tag{4.3.15}$$

Since the pitching moment coefficient about the aerodynamic center is zero for a symmetric airfoil and negative for an airfoil with positive camber, this places the center of gravity at or slightly aft of the aerodynamic center of the main wing. For this reason, many conventional airplanes with cambered wings have the center of gravity located slightly aft of the wing quarter-chord.

Now that we have a better understanding of the requirements for static equilibrium in pitch, let us examine how the elevator of a conventional airplane is used to attain trim for a given flight condition. For small angles of attack, the lift coefficient for the main wing is a linear function of angle of attack,

$$C_{L_w} = C_{L_w,\alpha}(\alpha + \alpha_{0w} - \alpha_{L0w}) \tag{4.3.16}$$

where $C_{L_w,\alpha}$ is the lift slope for the main wing, α is the angle of attack for the airplane as measured relative to the fuselage reference line, α_{0w} is the angle that the wing chord makes with the fuselage reference line, and α_{L0w} is the zero-lift angle of attack for the wing (Sec. 1.8). For small angles of attack and elevator deflections, the lift coefficient for the tail varies linearly with both angle of attack and elevator deflection. However, the presence of the wing and other components of the aircraft also significantly affect the lift coefficient for the tail through the downwash angle, ε_d.

In our study of finite wings, we found that the vorticity trailing behind a lifting wing produces downwash in the region aft of the wing, as shown in Fig. 4.3.4. **This downwash has a significant effect on the lift developed by an aft tail and should never be ignored when designing the tail of an airplane.** The downwash induced on

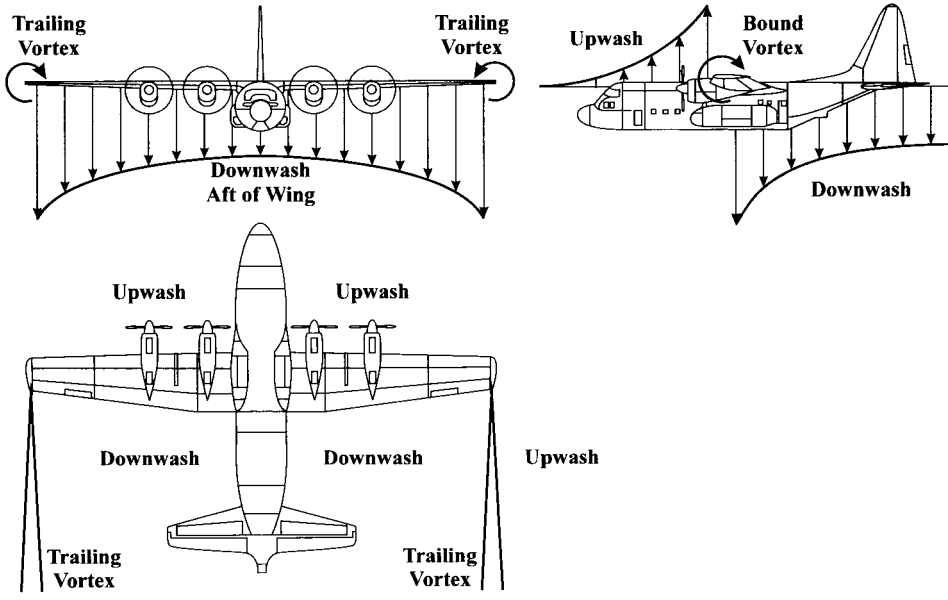


Figure 4.3.4. Downwash distribution created by the wing of a conventional airplane.

the tail by the main wing reduces the effective angle of attack for the horizontal tail and thus affects the trim. Additionally, since the downwash varies with wing angle of attack, it reduces the tail's effectiveness in stabilizing the airplane. This downwash varies along the span of the horizontal tail and is affected by the planform shape of the wing as well as the presence of the fuselage and nacelles. In reality, the performance of the wing is also affected by the presence of the tail but this effect is less significant. The only two ways to estimate accurately the interactions between the different surfaces of the airplane are by making use of computer simulations and/or wind tunnel tests. Such methods should always be employed in the later phases of the airplane design process. The effects of the interactions between the main wing and the horizontal tail can be adequately estimated using either the numerical lifting-line method or the vortex panel method.

For the purpose of preliminary design and to gain some useful insight into the basic principles involved, it is useful to have an approximate closed-form solution for estimating the downwash induced on the tail by the wing. Such an approximate method can be developed by assuming that the flow field in the vicinity of the airplane is affected only by the main wing. From Prandtl's lifting-line theory, it can be shown that the downwash at any point in the proximity of a finite lifting wing is proportional to the freestream velocity multiplied by the lift coefficient for the wing divided by the aspect ratio for the wing,

$$V_y = -K_d \frac{V_\infty C_{L_w}}{R_{A_w}} \tag{4.3.17}$$

where the proportionality constant, K_d, depends on the planform shape of the wing and the position of the tail relative to the wing. Because the downwash is small compared to the freestream velocity, the downwash angle, ε_d, can be closely approximated as the downwash velocity divided by the freestream velocity,

$$\varepsilon_d \cong \frac{-V_y}{V_\infty} = K_d \frac{C_{L_w}}{R_{A_w}} \tag{4.3.18}$$

Since the downwash angle at the tail is proportional to the lift coefficient for the wing, which is a linear function of angle of attack, the downwash angle can also be written as a linear function of the angle of attack,

$$\varepsilon_d = \varepsilon_{d0} + \varepsilon_{d,\alpha}\,\alpha \tag{4.3.19}$$

where ε_{d0} is the downwash angle when the fuselage reference line is at zero angle of attack and $\varepsilon_{d,\alpha}$ is the change in the downwash angle with respect to angle of attack.

For small angles of attack and elevator deflection and assuming that the tail has a symmetric airfoil section when the elevator is not deflected, the lift coefficient for the tail in the presence of the downwash that is specified by Eq. (4.3.19) can be written as

$$C_{L_t} = C_{L_t,\alpha}(\alpha + \alpha_{0t} - \varepsilon_d + \varepsilon_e \delta_e) = C_{L_t,\alpha}[(1-\varepsilon_{d,\alpha})\alpha + \alpha_{0t} - \varepsilon_{d0} + \varepsilon_e \delta_e] \tag{4.3.20}$$

Here $C_{L_t,\alpha}$ is the lift slope for the isolated tail, α_{0t} is the angle that the tail chord makes with the fuselage reference line, ε_e is the elevator effectiveness, and δ_e is the elevator deflection as shown in Fig. 4.3.3.

For small elevator deflection, the moment coefficient about the aerodynamic center of the horizontal tail is also a linear function of the elevator deflection. Since we are assuming the tail to have a symmetric airfoil section when the elevator is not deflected, we can write

$$C_{m_t} = C_{m_t,\delta_e}\,\delta_e \tag{4.3.21}$$

where C_{m_t,δ_e} is the change in the pitching moment coefficient for the isolated tail about the aerodynamic center with respect to elevator deflection. When the elevator is deflected downward, a negative pitching moment is produced about the aerodynamic center. Thus, the moment slope, C_{m_t,δ_e}, is always negative when δ_e is defined to be positive downward, as shown in Fig. 4.3.3.

Using Eqs. (4.3.16), (4.3.20), and (4.3.21) in Eqs. (4.3.6) and (4.3.9) results in

$$\begin{aligned}&\left[C_{L_w,\alpha}+\frac{S_t}{S_w}\eta_t C_{L_t,\alpha}(1-\varepsilon_{d,\alpha})\right]\alpha+\left[\frac{S_t}{S_w}\eta_t C_{L_t,\alpha}\varepsilon_e\right]\delta_e\\&\quad=\frac{W\cos\gamma}{\frac{1}{2}\rho V_\infty^2 S_w}-C_{L_w,\alpha}(\alpha_{0w}-\alpha_{L0w})-\frac{S_t}{S_w}\eta_t C_{L_t,\alpha}(\alpha_{0t}-\varepsilon_{d0})\end{aligned} \tag{4.3.22}$$

$$\begin{aligned}&\left[-\frac{l_w}{\bar{c}_w}C_{L_w,\alpha}-\frac{S_t l_t}{S_w\bar{c}_w}\eta_t C_{L_t,\alpha}(1-\varepsilon_{d,\alpha})\right]\alpha\\&+\left[\frac{S_t\bar{c}_t}{S_w\bar{c}_w}\eta_t C_{m_t,\delta_e}-\frac{S_t l_t}{S_w\bar{c}_w}\eta_t C_{L_t,\alpha}\varepsilon_e\right]\delta_e\\&\quad=-C_{m_w}+\frac{l_w}{\bar{c}_w}C_{L_w,\alpha}(\alpha_{0w}-\alpha_{L0w})+\frac{S_t l_t}{S_w\bar{c}_w}\eta_t C_{L_t,\alpha}(\alpha_{0t}-\varepsilon_{d0})\end{aligned} \tag{4.3.23}$$

These two equations provide the requirements necessary to solve for the angle of attack and the elevator deflection at trim. At any given airspeed, the elevator deflection controls the equilibrium angle of attack for the aircraft, and thus, controls the lift developed by both the wing and the tail. When the elevator is deflected downward, additional lift is generated on the tail. Since the tail is aft of the CG, this produces a negative pitching moment about the CG, which rotates the nose of the aircraft downward and reduces the angle of attack. As the angle of attack is reduced, the lift on both the wing and the tail are reduced, as is the magnitude of the negative pitching moment. The angle of attack will continue to decrease until the pitching moment about the CG is returned to zero. **A stable airplane in free flight will always seek the angle of attack that makes the pitching moment about the CG equal to zero.** At any given airspeed there is only one elevator deflection that will satisfy both Eqs. (4.3.22) and (4.3.23). This is the elevator deflection that results in trimmed flight at that particular airspeed and climb angle. For any other deflection of the elevator, the aircraft climb angle will either increase or

decrease if the airspeed remains fixed. Thus, at any airspeed above stall, the deflection of the elevator can be used to trim the airplane, provided that the elevator has sufficient size and effectiveness.

The angle of attack at trim, as computed from Eqs. (4.3.22) and (4.3.23), depends on the mounting angles for both the wing and the tail as well as the definition of the fuselage reference line. One convenient way to define the fuselage reference line is to define it as the minimum drag axis for the fuselage. With the fuselage reference line so defined, minimum drag on the fuselage and the tail are achieved when both the fuselage angle of attack and the elevator deflection are set to zero, with no lift on the horizontal tail. Using these three conditions at some design airspeed, say V_d, to fix the location of the center of gravity and the mounting angles for the wing and the tail will often result in a good preliminary design.

Since we are assuming the tail to have a symmetric airfoil section when there is no elevator deflection, the condition for **zero lift on the tail in level flight**, which is specified by Eq. (4.3.15), reduces to

$$l_w = \frac{\frac{1}{2}\rho V_d^2 S_w C_{m_w}}{W}\bar{c}_w \tag{4.3.24}$$

when the elevator is not deflected at the design airspeed. **With both the fuselage angle of attack and the elevator deflection set to zero for level flight at the design airspeed,** Eqs. (4.3.22) and (4.3.23) reduce to

$$S_w C_{L_w,\alpha}(\alpha_{0w} - \alpha_{L0w}) + S_t \eta_t C_{L_t,\alpha}(\alpha_{0t} - \varepsilon_{d0}) = \frac{W}{\frac{1}{2}\rho V_d^2} \tag{4.3.25}$$

and

$$S_w l_w C_{L_w,\alpha}(\alpha_{0w} - \alpha_{L0w}) + S_t l_t \eta_t C_{L_t,\alpha}(\alpha_{0t} - \varepsilon_{d0}) = S_w \bar{c}_w C_{m_w} \tag{4.3.26}$$

After applying Eq. (4.3.24), Eqs. (4.3.25) and (4.3.26) are readily solved for the mounting angles of the wing and the tail. This gives

$$\alpha_{0w} = \frac{W}{\frac{1}{2}\rho V_d^2 S_w C_{L_w,\alpha}} + \alpha_{L0w} \tag{4.3.27}$$

and

$$\alpha_{0t} = \varepsilon_{d0} \tag{4.3.28}$$

With the center of gravity located to satisfy Eq. (4.3.24) and the wing and the tail mounted to satisfy Eqs. (4.3.27) and (4.3.28), the drag will be minimized for level flight at the design airspeed, V_d. Under this condition, the wing supports the entire weight of the airplane and the tail provides only stability.

To see how the tail provides this stability, we return to the general pitch stability criterion that was specified in Eq. (4.2.8). For pitch stability, we require that the derivative of the pitching moment coefficient for the complete airplane with respect to angle of attack must be negative. For a symmetric tail with small angles of attack and elevator deflection, the total pitching moment coefficient can be expressed by applying Eqs. (4.3.16), (4.3.20), and (4.3.21) to Eq. (4.3.9). This gives

$$\begin{aligned} C_m &= C_{m_w} + \frac{S_t \bar{c}_t}{S_w \bar{c}_w} \eta_t C_{m_t,\delta_e} \delta_e - \frac{l_w}{\bar{c}_w} C_{L_w,\alpha} (\alpha + \alpha_{0w} - \alpha_{L0w}) \\ &\quad - \frac{S_t l_t}{S_w \bar{c}_w} \eta_t C_{L_t,\alpha} [(1 - \varepsilon_{d,\alpha})\alpha + \alpha_{0t} - \varepsilon_{d0} + \varepsilon_e \delta_e] \end{aligned} \tag{4.3.29}$$

For small angles of attack, the aerodynamic centers of the wing and tail are fixed points that do not vary with angle of attack. Thus, differentiating Eq. (4.3.29) with respect to angle of attack, we see that pitch stability for this wing-tail combination requires that

$$\frac{\partial C_m}{\partial \alpha} = -\frac{l_w}{\bar{c}_w} C_{L_w,\alpha} - \frac{S_t l_t}{S_w \bar{c}_w} \eta_t C_{L_t,\alpha} (1 - \varepsilon_{d,\alpha}) < 0 \tag{4.3.30}$$

The change in the downwash angle with respect to angle of attack is typically less than 1.0. Furthermore, the lift slope, the planform area, and the mean chord length are always positive for both the wing and the tail. Since we are by definition considering an aft tail, the aerodynamic center of the tail is aft of the center of gravity ($l_t > 0$). Thus, from Eq. (4.3.30), we see that this wing-tail combination will be unconditionally stable if the center of gravity is forward of the aerodynamic center of the main wing ($l_w > 0$). This is a good thing to remember when loading an airplane for the first test flight. Even if the airplane is designed to have the CG aft of the wing quarter-chord, it should probably be loaded to move the CG forward of the wing quarter-chord for the first test flight. For the geometry of the present case, this will assure stable flight but will require negative lift on the aft tail for all operating conditions. For the more general case, even this will not absolutely assure stability, because the fuselage, nacelles, and thrust deck can all have a significant destabilizing effect.

If the center of gravity is aft of the aerodynamic center of the main wing ($l_w < 0$), then the main wing is destabilizing and the product of the tail area and the tail length, $S_t l_t$, must be sufficiently large so that the total change in pitching moment with respect to angle of attack is still negative. Thus, we see that by varying the size and/or length of an aft tail we can control the pitch stability of a conventional subsonic airplane.

The second term in Eq. (4.3.30) is the contribution of the horizontal tail to the pitch stability of the airplane. It is this term that typically makes the major contribution to the overall pitch stability of the aircraft. Notice that this term is proportional to the product of the tail area and the tail length, $S_t l_t$, divided by the product of the wing area and the wing chord, $S_w \bar{c}_w$. Each of these products represents a characteristic *volume* associated with the airplane. The product, $S_t l_t$, is sometimes called the *tail volume*, and increasing this volume for an aft tail will always increase the stability of the airplane. The ratio, $S_t l_t / S_w \bar{c}_w$, is called the *horizontal tail volume ratio*,

$$\mathcal{V}_h \equiv \frac{S_t l_t}{S_w \bar{c}_w} \tag{4.3.31}$$

The designer can easily change this tail volume ratio by either changing the area of the horizontal tail or by changing its distance aft of the center of gravity. It is the magnitude of this tail volume ratio that can be used to most directly control the pitch stability of any airplane with an aft tail. Notice that the horizontal tail volume ratio, as well as the first term in Eq. (4.3.30), are affected by the location of the CG and are thus affected by the way in which the airplane is loaded. **Aircraft loading has a very dramatic effect on pitch stability.**

At this point it is worth reiterating some of the simplifying assumptions that were made in the development of Eq. (4.3.30). To simplify the analysis, we assumed that the aerodynamic center of both the wing and the tail, as well as the center of thrust, are all aligned with the direction of flight on the fuselage reference line. Additionally, we assumed that the thrust vector is always aligned with the center of gravity. With these assumptions, neither the thrust nor the drag contributes to the pitching moment. Such conditions are almost never exactly satisfied in a real airplane. However, in many cases these conditions are nearly satisfied and the two terms on the right-hand side of the equal sign in Eq. (4.3.30) are the dominant terms in determining pitch stability. The influence of thrust on trim and static stability can be important and very complex. The drag can also have a significant effect on trim and static stability, particularly if the wing is mounted either far above or below the center of gravity. Such effects will be discussed later in this chapter.

EXAMPLE 4.3.1. Consider a general aviation airplane with an aft tail. The airplane has a gross weight of 2,700 lbf. The wing and horizontal tail have the following properties:

$$S_w = 180\ \text{ft}^2, \quad b_w = 33\ \text{ft}, \quad C_{L_w,\alpha} = 4.44, \quad \alpha_{L0w} = -2.20°, \quad C_{m_w} = -0.053,$$
$$S_t = 36\ \text{ft}^2, \quad b_t = 12\ \text{ft}, \quad C_{L_t,\alpha} = 3.97, \quad \varepsilon_e = 0.60, \quad C_{m_t,\delta_e} = -0.55,$$
$$l_t - l_w = 15\ \text{ft}$$

The horizontal tail has a symmetric airfoil section when the elevator is not deflected. The aerodynamic centers of the wing and the tail both fall on the fuselage reference line, which is the minimum drag axis of the fuselage. The wing and the tail are mounted so that when the airplane is in level flight with an airspeed of 120 mph at standard sea level, trim is attained with no elevator deflection, no lift on the horizontal tail, and a zero angle of attack for the fuselage reference line. Neglecting any moments associated with the thrust deck and the fuselage, determine the location of the center of gravity, the mounting angles for the wing and the tail, and the pitch stability derivative for this wing-tail combination. Using the simplified analysis presented in this section, plot the elevator deflection and the angle of attack for trimmed level flight as a function of airspeed from 80 to 160 mph. Also plot the lift on the horizontal tail at level trim

for the same range of airspeed. Assume a tail efficiency of 1.0 and a downwash angle at the location of the tail given by the relation

$$\varepsilon_d = 0.6\frac{C_{L_w}}{R_{A_w}}$$

Solution. Since there is no lift on the tail at 120 mph, the lift on the wing must exactly support the weight of the airplane at this airspeed,

$$\tfrac{1}{2}\rho V_d^2 S_w C_{L_w 0} = W$$

where the notation $C_{L_w 0}$ is used to indicate that this is a lift coefficient evaluated at zero fuselage angle of attack and zero elevator deflection. Solving for this wing lift coefficient gives

$$C_{L_w 0} = \frac{W}{\tfrac{1}{2}\rho V_d^2 S_w} = \frac{2{,}700}{\tfrac{1}{2}0.0023769(120\times 5{,}280/3{,}600)^2 180} = 0.4075$$

The lift coefficient is related to angle of attack,

$$C_{L_w} = C_{L_w,\alpha}(\alpha + \alpha_{0w} - \alpha_{L0w})$$

Setting the fuselage reference line at zero angle of attack and solving for the mounting angle of the wing, we have

$$\alpha_{0w} = \frac{C_{L_w 0}}{C_{L_w,\alpha}} + \alpha_{L0w} = \frac{0.4075}{4.44} + \frac{(-2.20)\pi}{180} = 0.05338 \text{ rad} = \underline{3.1^\circ}$$

For this operating condition, the downwash angle at the tail is

$$\varepsilon_{d0} = 0.6\frac{C_{L_w 0}}{R_{A_w}} = 0.6\frac{0.4075}{33^2/180} = 0.04041 \text{ rad} = 2.315^\circ$$

There is to be no lift on the tail at this operating condition and

$$C_{L_t} = C_{L_t,\alpha}[(1-\varepsilon_{d,\alpha})\alpha + \alpha_{0t} - \varepsilon_{d0} + \varepsilon_e\delta_e]$$

Solving for the mounting angle of the horizontal tail that will give zero lift on the tail with the fuselage angle of attack and the elevator deflection set to zero, we obtain

$$\alpha_{0t} = \varepsilon_{d0} = \underline{2.3^\circ}$$

Since the pitching moment about the CG must be zero at trim,

$$C_m = C_{m_w} + \frac{S_t \bar{c}_t}{S_w \bar{c}_w} \eta_t C_{m_t} - \frac{l_w}{\bar{c}_w} C_{L_w} - \frac{S_t l_t}{S_w \bar{c}_w} \eta_t C_{L_t} = 0$$

At this operating condition, the lift and moment for the tail are both zero, so we have

$$C_{m0} = C_{m_w} - \frac{l_w}{\bar{c}_w} C_{L_w 0} = 0$$

or

$$l_w = \frac{C_{m_w}}{C_{L_w 0}} \bar{c}_w = \frac{-0.053}{0.4075} \frac{180 \text{ ft}^2}{33 \text{ ft}} = \underline{-0.71 \text{ ft}}$$

Thus, the CG is about 8.5 inches aft of the wing quarter-chord.

The downwash gradient at the tail is

$$\varepsilon_{d,\alpha} = \frac{\partial \varepsilon_d}{\partial \alpha} = 0.6 \frac{1}{R_{A_w}} \frac{\partial C_{L_w}}{\partial \alpha} = 0.6 \frac{C_{L_w,\alpha}}{R_{A_w}} = 0.6 \frac{4.44}{33^2/180} = 0.44$$

The pitch stability derivative for this simple wing-tail combination is given by Eq. (4.3.30),

$$\begin{aligned} \frac{\partial C_m}{\partial \alpha} &= -\frac{l_w}{\bar{c}_w} C_{L_w,\alpha} - \frac{S_t l_t}{S_w \bar{c}_w} \eta_t C_{L_t,\alpha} (1 - \varepsilon_{d,\alpha}) \\ &= -\frac{(-0.7094)}{180/33} 4.44 - \frac{36(15 - 0.7094)}{180(180/33)} (1.0)(3.97)(1 - 0.44) \\ &= \underline{-0.59 \text{ rad}^{-1}} \end{aligned}$$

Since the pitch stability derivative is negative, this wing-tail combination is stable.

For level trim at any other airspeed, the angle of attack and the elevator deflection must be such that the total lift is equal to the weight and the total pitching moment about the CG is zero,

$$C_{L_w,\alpha} (\alpha + \alpha_{0w} - \alpha_{L0w}) + \frac{S_t}{S_w} \eta_t C_{L_t,\alpha} [(1 - \varepsilon_{d,\alpha}) \alpha + \alpha_{0t} - \varepsilon_{d0} + \varepsilon_e \delta_e] = \frac{W}{\frac{1}{2} \rho V_\infty^2 S_w}$$

$$\begin{aligned} &C_{m_w} + \frac{S_t \bar{c}_t}{S_w \bar{c}_w} \eta_t C_{m_t,\delta_e} \delta_e - \frac{l_w}{\bar{c}_w} C_{L_w,\alpha} (\alpha + \alpha_{0w} - \alpha_{L0w}) \\ &\quad - \frac{S_t l_t}{S_w \bar{c}_w} \eta_t C_{L_t,\alpha} [(1 - \varepsilon_{d,\alpha}) \alpha + \alpha_{0t} - \varepsilon_{d0} + \varepsilon_e \delta_e] = 0 \end{aligned}$$

These two equations can be written as

$$\begin{bmatrix} C_{L,\alpha} & C_{L,\delta_e} \\ C_{m,\alpha} & C_{m,\delta_e} \end{bmatrix} \begin{Bmatrix} \alpha \\ \delta_e \end{Bmatrix} = \begin{Bmatrix} C_L - C_{L0} \\ -C_{m0} \end{Bmatrix}$$

where

$$C_{L,\alpha} = C_{L_w,\alpha} + \frac{S_t}{S_w}\eta_t C_{L_t,\alpha}(1-\varepsilon_{d,\alpha}) = 4.8844$$

$$C_{L,\delta_e} = \frac{S_t}{S_w}\eta_t C_{L_t,\alpha}\varepsilon_e = 0.4764$$

$$C_L = \frac{W}{\frac{1}{2}\rho V_\infty^2 S_w}$$

$$C_{L0} = C_{L_w,\alpha}(\alpha_{0w} - \alpha_{L0w}) + \frac{S_t}{S_w}\eta_t C_{L_t,\alpha}(\alpha_{0t} - \varepsilon_{d0}) = 0.4075$$

$$C_{m,\alpha} = -\frac{l_w}{\bar{c}_w}C_{L_w,\alpha} - \frac{S_t l_t}{S_w \bar{c}_w}\eta_t C_{L_t,\alpha}(1-\varepsilon_{d,\alpha}) = -0.5867$$

$$C_{m,\delta_e} = \frac{S_t \bar{c}_t}{S_w \bar{c}_w}\eta_t C_{m_t,\delta_e} - \frac{S_t l_t}{S_w \bar{c}_w}\eta_t C_{L_t,\alpha}\varepsilon_e = -1.3086$$

and

$$C_{m0} = C_{m_w} - \frac{l_w}{\bar{c}_w}C_{L_w,\alpha}(\alpha_{0w} - \alpha_{L0w}) - \frac{S_t l_t}{S_w \bar{c}_w}\eta_t C_{L_t,\alpha}(\alpha_{0t} - \varepsilon_{d0}) = 0.0$$

This 2×2 linear system of equations is easily solved for the angle of attack and elevator deflection:

$$\begin{Bmatrix} \alpha \\ \delta_e \end{Bmatrix} = \frac{1}{C_{L,\alpha}C_{m,\delta_e} - C_{L,\delta_e}C_{m,\alpha}} \begin{Bmatrix} (C_L - C_{L0})C_{m,\delta_e} + C_{L,\delta_e}C_{m0} \\ -(C_L - C_{L0})C_{m,\alpha} - C_{L,\alpha}C_{m0} \end{Bmatrix}$$

After substituting the values for this particular airplane, we have

$$\begin{Bmatrix} \alpha \\ \delta_e \end{Bmatrix} = \begin{Bmatrix} 0.214096C_L - 0.087236 \\ -0.095986C_L + 0.039111 \end{Bmatrix}$$

At 80 mph, the total lift coefficient is

$$C_L = \frac{W}{\frac{1}{2}\rho V_\infty^2 S_w} = \frac{2{,}700}{\frac{1}{2}0.0023769(80\times 5{,}280/3{,}600)^2 180} = 0.916785$$

and

$$\begin{Bmatrix} \alpha \\ \delta_e \end{Bmatrix} = \begin{Bmatrix} 0.214096(0.916785) - 0.087236 \\ -0.095986(0.916785) + 0.039111 \end{Bmatrix} = \begin{Bmatrix} 0.10904 \\ -0.04889 \end{Bmatrix} = \begin{Bmatrix} 6.2^\circ \\ -2.8^\circ \end{Bmatrix}$$

With these values of angle of attack and elevator deflection, the lift developed on the wing and the tail of this airplane are readily computed from the known properties of each lifting surface. This gives

$$L_w = \tfrac{1}{2}\rho V_\infty^2 S_w C_{L_w,\alpha}(\alpha + \alpha_{0w} - \alpha_{L0w}) = \underline{2{,}626 \text{ lbf}}$$

and

$$L_t = \tfrac{1}{2}\rho V_\infty^2 S_t \eta_t C_{L_t,\alpha}[(1-\varepsilon_{d,\alpha})\alpha + \alpha_{0t} - \varepsilon_{d0} + \varepsilon_e \delta_e] = \underline{74 \text{ lbf}}$$

Repeating these calculations at different airspeeds, the data plotted in Fig. 4.3.5 are obtained.

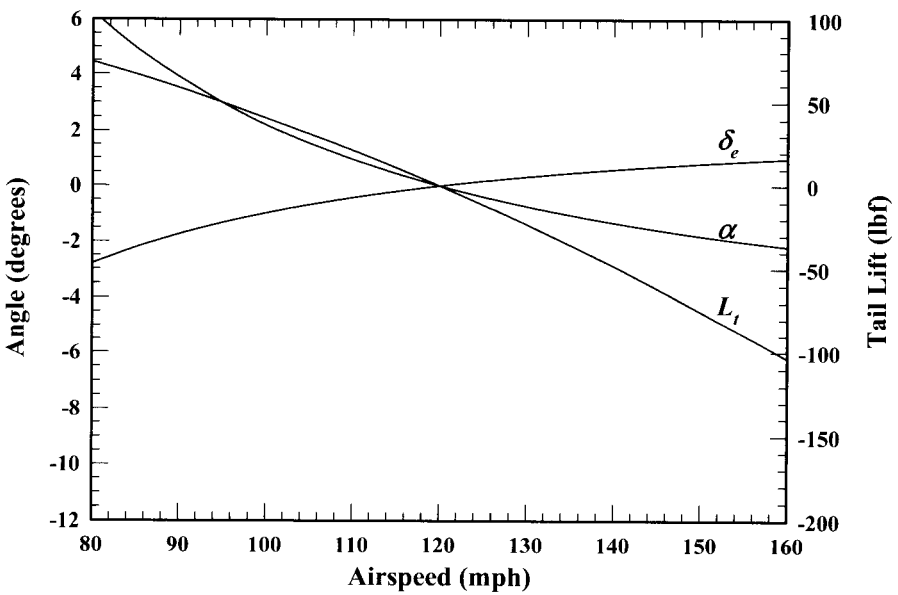


Figure 4.3.5. Conditions at level trim for the airplane in Example 4.3.1, with the center of gravity located 8.5 inches aft of the wing quarter-chord.

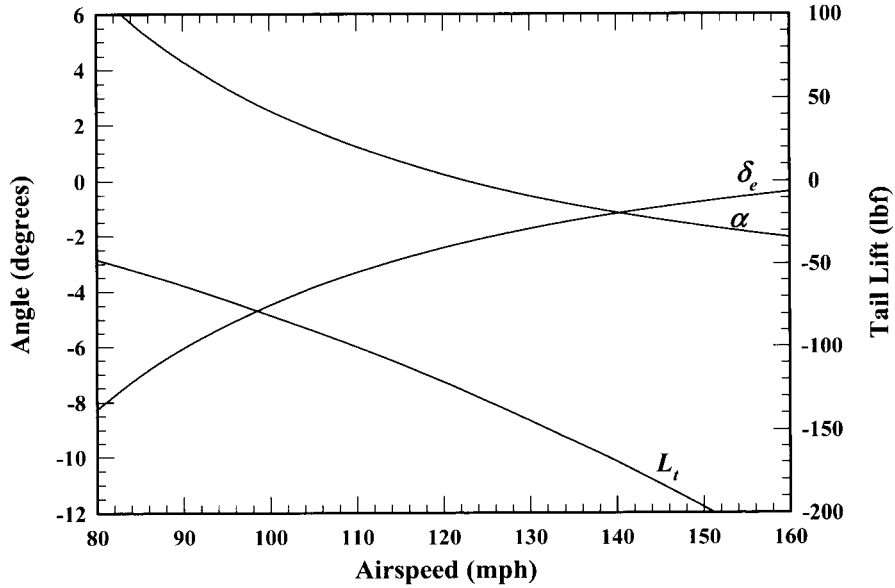


Figure 4.3.6. Conditions at level trim for the airplane in Example 4.3.1, with the center of gravity located exactly at the wing quarter-chord.

Notice from Example 4.3.1 that as the airspeed is decreased, a more negative elevator deflection is needed to trim the airplane. With the center of gravity located about 8.5 inches aft of the wing quarter-chord, at airspeeds above 120 mph the lift on the tail is negative, whereas for airspeeds below 120 mph the lift on the tail is positive. Figure 4.3.6 shows how these trim conditions change when the center of gravity is moved forward to the wing quarter-chord. Notice that moving the center of gravity forward requires more negative elevator deflection and results in more negative lift on the tail. As the center of gravity is moved even farther forward, still more negative elevator deflection is required for trim. Since the elevator deflection is limited, there is some forward limit to the CG location, beyond which the elevator is no longer able to trim the aircraft. The airplane would not be able to take off with the center of gravity located forward of this point.

4.4. Stick-Fixed Neutral Point and Static Margin

Some point on an airplane exists about which the total pitching moment is independent of angle of attack. This is similar to the aerodynamic center of an airfoil. In fact, this location is the aerodynamic center of the complete airplane. With the center of gravity located at this point, the airplane is neutrally stable in pitch. Thus, this point is usually referred to as the *stick-fixed neutral point* rather than the aerodynamic center.

To locate the stick-fixed neutral point for the simplified wing-tail combination discussed in Sec. 4.3, we replace the inequality in Eq. (4.3.30) with the equality

$$\frac{\partial C_{m_{np}}}{\partial \alpha} = -\frac{l_{wn}}{\bar{c}_w} C_{L_w,\alpha} - \frac{S_t l_{tn}}{S_w \bar{c}_w} \eta_t C_{L_t,\alpha}(1-\varepsilon_{d,\alpha}) = 0 \tag{4.4.1}$$

Here the variables l_w and l_t in Eq. (4.3.30) have been replaced with l_{wn} and l_{tn} to indicate a distance measured aft of the neutral point rather than a distance measured aft of the actual center of gravity. However, to be consistent with our previous notation, l should always indicate a distance measured aft of the actual center of gravity. Thus, a distance measured aft of the neutral point can be written as a distance measured aft of the CG less the distance that the neutral point is aft of the CG. Using this more consistent notation, Eq. (4.4.1) can be written in the form

$$\frac{\partial C_{m_{np}}}{\partial \alpha} = -\frac{l_w - l_{np}}{\bar{c}_w} C_{L_w,\alpha} - \frac{S_t (l_t - l_{np})}{S_w \bar{c}_w} \eta_t C_{L_t,\alpha}(1-\varepsilon_{d,\alpha}) = 0 \tag{4.4.2}$$

where l_{np} is the distance that the stick-fixed neutral point is aft of the CG, as shown in Fig 4.4.1. Equation (4.4.2) is readily solved for the location of the neutral point,

$$\frac{l_{np}}{\bar{c}_w} = \frac{\frac{l_w}{\bar{c}_w} C_{L_w,\alpha} + \frac{S_t l_t}{S_w \bar{c}_w} \eta_t C_{L_t,\alpha}(1-\varepsilon_{d,\alpha})}{C_{L_w,\alpha} + \frac{S_t}{S_w} \eta_t C_{L_t,\alpha}(1-\varepsilon_{d,\alpha})} \tag{4.4.3}$$

Using Eqs. (4.3.16) and (4.3.20) in Eq. (4.3.6), the lift coefficient for the wing-tail combination is

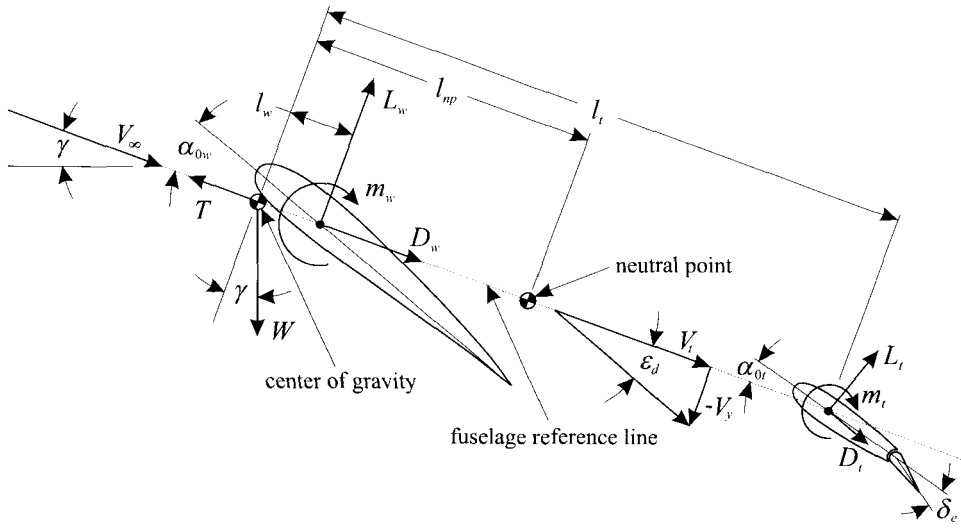


Figure 4.4.1. Location of the stick-fixed neutral point relative to the center of gravity.

$$C_L = \frac{W\cos\gamma}{\frac{1}{2}\rho V_\infty^2 S_w} = C_{L_w,\alpha}(\alpha + \alpha_{0w} - \alpha_{L0w}) + \frac{S_t}{S_w}\eta_t C_{L_t,\alpha}[(1-\varepsilon_{d,\alpha})\alpha + \alpha_{0t} - \varepsilon_{d0} + \varepsilon_e\delta_e] \tag{4.4.4}$$

and the lift slope for the wing-tail combination is

$$C_{L,\alpha} \equiv \frac{\partial C_L}{\partial\alpha} = C_{L_w,\alpha} + \frac{S_t}{S_w}\eta_t C_{L_t,\alpha}(1-\varepsilon_{d,\alpha}) \tag{4.4.5}$$

From Eq. (4.4.5), the denominator on the right-hand side of Eq. (4.4.3) is seen to be equal to the lift slope for the wing-tail combination. Thus,

$$\frac{l_{np}}{\bar{c}_w} = \frac{\frac{l_w}{\bar{c}_w}C_{L_w,\alpha} + \frac{S_t l_t}{S_w\bar{c}_w}\eta_t C_{L_t,\alpha}(1-\varepsilon_{d,\alpha})}{C_{L,\alpha}} \tag{4.4.6}$$

From Eq. (4.3.30), the stability derivative for this wing-tail combination is

$$C_{m,\alpha} \equiv \frac{\partial C_m}{\partial\alpha} = -\frac{l_w}{\bar{c}_w}C_{L_w,\alpha} - \frac{S_t l_t}{S_w\bar{c}_w}\eta_t C_{L_t,\alpha}(1-\varepsilon_{d,\alpha}) \tag{4.4.7}$$

Thus, the numerator on the right-hand side of Eq. (4.4.6) is equal to the negative of the stability derivative for the wing-tail combination,

$$\frac{l_{np}}{\bar{c}_w} = -\frac{C_{m,\alpha}}{C_{L,\alpha}} \tag{4.4.8}$$

In view of Eq. (4.4.8), the stability derivative can be rewritten as

$$C_{m,\alpha} = -\frac{l_{np}}{\bar{c}_w}C_{L,\alpha} \tag{4.4.9}$$

Since static stability requires a negative pitch stability derivative and the lift slope is positive for angles of attack below stall, it follows from Eq. (4.4.9) that **for an airplane to be statically stable, the center of gravity must be forward of the stick-fixed neutral point**. This is an important result that should be remembered.

The dimensionless ratio $l_{np}/\bar{c}_w$ is called the *stick-fixed static margin*. It is simply the distance that the CG is forward of the stick-fixed neutral point, expressed as a fraction of the mean chord length for the main wing. Extensive experience has shown that **to provide good handling qualities for a human pilot, a static margin of at least 5 percent should be maintained**. A higher static margin is not usually objectionable to pilots. However, there is a limit to how far the CG can be moved forward and still maintain trim.

While the relation given in Eq. (4.4.9) was obtained for the wing-tail combination shown in Fig. 4.4.1, the result is more general. The aerodynamic pressure and shear forces acting on any object moving through the air can always be resolved into a lift force, a drag force, and an aerodynamic moment, all acting at the center of gravity. For an airplane, the vertical offset between the neutral point and the center of gravity is typically small and the drag is much less than the lift, as is shown in Fig. 4.4.2. According to common notation, we have used m to represent the aerodynamic pitching moment about the center of gravity. If we now let m_{np} denote the aerodynamic pitching moment about the neutral point and assume that the neutral point is vertically aligned with the center of gravity, then from the free-body diagram in Fig. 4.4.2, a summation of moments about the neutral point gives

$$m_{np} = m + l_{np} L \tag{4.4.10}$$

Nondimensionalizing Eq. (4.4.10) in the usual way, we have

$$C_{m_{np}} = C_m + \frac{l_{np}}{\bar{c}_w} C_L \tag{4.4.11}$$

Differentiating Eq. (4.4.11) with respect to angle of attack results in

$$\frac{\partial C_{m_{np}}}{\partial \alpha} = \frac{\partial C_m}{\partial \alpha} + \frac{l_{np}}{\bar{c}_w} \frac{\partial C_L}{\partial \alpha} \tag{4.4.12}$$

By definition, the stick-fixed neutral point is the aerodynamic center of the airplane, so the moment about the stick-fixed neutral point does not change with α. Thus, the result in Eq. (4.4.12) reduces exactly to the more specific relation given in Eq. (4.4.9),

$$C_{m,\alpha} = -\frac{l_{np}}{\bar{c}_w} C_{L,\alpha} \tag{4.4.13}$$

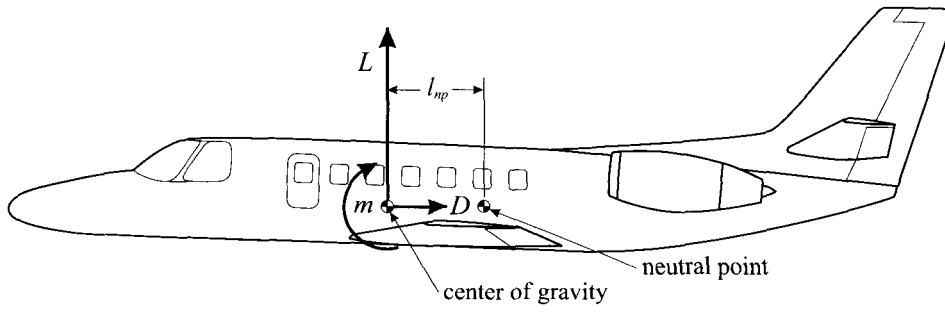


Figure 4.4.2. Stick-fixed neutral point for a complete airplane.

EXAMPLE 4.4.1. Determine the static margin in the range of linear lift for the wing-tail combination that is described in Example 4.3.1.

Solution. For this airplane we have

$$S_w = 180 \text{ ft}^2, \quad b_w = 33 \text{ ft}, \quad C_{L_w,\alpha} = 4.44, \quad l_w = -0.71 \text{ ft},$$
$$S_t = 36 \text{ ft}^2, \quad b_t = 12 \text{ ft}, \quad C_{L_t,\alpha} = 3.97, \quad l_t = 14.29 \text{ ft},$$
$$\eta_t = 1.0, \quad \varepsilon_{d,\alpha} = 0.44$$

By definition, the moment slope relative to the neutral point is zero. Thus,

$$\frac{\partial C_{m_{np}}}{\partial \alpha} = -\frac{l_{wn}}{\bar{c}_w} C_{L_w,\alpha} - \frac{S_t l_{tn}}{S_w \bar{c}_w} \eta_t C_{L_t,\alpha}(1-\varepsilon_{d,\alpha}) = 0$$

or in terms of the distances measured aft of the CG,

$$-\frac{l_w - l_{np}}{\bar{c}_w} C_{L_w,\alpha} - \frac{S_t(l_t - l_{np})}{S_w \bar{c}_w} \eta_t C_{L_t,\alpha}(1-\varepsilon_{d,\alpha}) = 0$$

Solving for the static margin gives

$$\frac{l_{np}}{\bar{c}_w} = \frac{l_w C_{L_w,\alpha} + \frac{S_t l_t}{S_w} \eta_t C_{L_t,\alpha}(1-\varepsilon_{d,\alpha})}{\bar{c}_w \left[C_{L_w,\alpha} + \frac{S_t}{S_w} \eta_t C_{L_t,\alpha}(1-\varepsilon_{d,\alpha}) \right]}$$

$$= \frac{(-0.71)4.44 + \frac{36(14.29)}{180} 1.0(3.97)(1-0.44)}{\frac{180}{33}\left[4.44 + \frac{36}{180} 1.0(3.97)(1-0.44) \right]} = 0.1202 = \underline{12\%}$$

It is important to recognize that static margin, and thus pitch stability, is not entirely under the control of the designer. The static margin of an airplane can be dramatically affected by the way in which the airplane is loaded. The difference between good handling qualities and poor handling qualities (or even static instability) can be a matter of a shift in the center of gravity of only a few inches. Such a shift in the CG can easily result from insufficient care in loading the airplane. The designer must correctly specify and communicate the allowable CG range for an airplane to the end user. However, from that point it is the responsibility of the pilot and crew to see that the airplane is properly loaded so as to keep the CG within design specifications.

Equation (4.4.13) specifies how the pitch stability of an airplane depends on the location of the center of gravity. The farther that the CG is moved forward, the more stable the airplane becomes. However, we have also seen from the results plotted for

Example 4.3.1 that as the center of gravity is moved forward, more negative elevator deflection is required for trim. Thus, there is a limit to how far the CG can be moved forward and still maintain trim. In Example 4.3.1, we found that the elevator deflection required for trim is given by

$$(\delta_e)_{\text{trim}} = -\frac{(C_L - C_{L0})C_{m,\alpha} + C_{L,\alpha}C_{m0}}{C_{L,\alpha}C_{m,\delta_e} - C_{L,\delta_e}C_{m,\alpha}} \tag{4.4.14}$$

Using Eq. (4.4.13) to express the pitch stability derivative in terms of the lift slope and static margin, Eq. (4.4.14) can be written as

$$(\delta_e)_{\text{trim}} = -\frac{C_{m0} - (C_L - C_{L0})(l_{np}/\bar{c}_w)}{C_{m,\delta_e} + C_{L,\delta_e}(l_{np}/\bar{c}_w)} \tag{4.4.15}$$

In addition to the static margin, both the pitching moment coefficient at zero angle of attack and the change in pitching moment coefficient with respect to elevator deflection depend on the position of the center of gravity. Thus, it is not obvious from Eq. (4.4.15) exactly how the elevator deflection required for trim will vary with the position of the center of gravity. This is examined in the following example.

EXAMPLE 4.4.2. For the wing-tail combination described in Examples 4.3.1 and 4.4.1, plot the elevator deflection required to trim the airplane at 80 mph as a function of the location of the center of gravity measured relative to the quarter-chord of the main wing.

Solution. Let x denote the distance measured aft of the quarter-chord of the main wing. For this airplane we have

$$S_w = 180\ \text{ft}^2, \quad b_w = 33\ \text{ft}, \quad C_{L_w,\alpha} = 4.44, \quad C_{m_w} = -0.053, \quad W = 2{,}700\ \text{lbf},$$
$$S_t = 36\ \text{ft}^2, \quad b_t = 12\ \text{ft}, \quad C_{L_t,\alpha} = 3.97, \quad C_{m_t,\delta_e} = -0.55,$$
$$\varepsilon_e = 0.60, \quad x_t = 15\ \text{ft}, \quad \eta_t = 1.0,$$
$$\alpha_{L0w} = -2.20°, \quad \alpha_{0w} = 3.1°, \quad \alpha_{L0t} = 0.0°, \quad \alpha_{0t} = \varepsilon_{d0} = 2.3°$$

From Example 4.3.1,

$$C_{L0} = C_{L_w,\alpha}(\alpha_{0w} - \alpha_{L0w}) + \frac{S_t}{S_w}\eta_t C_{L_t,\alpha}(\alpha_{0t} - \varepsilon_{d0}) = 0.4075$$

$$C_{L,\delta_e} = \frac{S_t}{S_w}\eta_t C_{L_t,\alpha}\varepsilon_e = 0.4764$$

and at 80 mph, the total lift coefficient was found to be

$$C_L = \frac{W}{\frac{1}{2}\rho V_\infty^2 S_w} = 0.9168$$

The pitching moment coefficient at zero angle of attack is

$$C_{m0} = C_{m_w} - \frac{l_w}{\bar{c}_w} C_{L_w,\alpha}(\alpha_{0w} - \alpha_{L0w}) - \frac{S_t l_t}{S_w \bar{c}_w} \eta_t C_{L_t,\alpha}(\alpha_{0t} - \varepsilon_{d0})$$

and the change in the pitching moment coefficient with respect to elevator deflection for this wing-tail combination is

$$C_{m,\delta_e} = \frac{S_t \bar{c}_t}{S_w \bar{c}_w} \eta_t C_{m_t,\delta_e} - \frac{S_t l_t}{S_w \bar{c}_w} \eta_t C_{L_t,\alpha} \varepsilon_e$$

Any distance, l, measured aft of the CG, is the distance measured aft of the wing quarter-chord, x, less the distance that the CG is aft of the wing quarter-chord, x_{CG}. So we can write

$$l_w = -x_{CG}$$

$$l_t = x_t - x_{CG}$$

$$l_{np} = x_{np} - x_{CG}$$

Thus we have

$$C_{m0} = C_{m_w} + \frac{x_{CG}}{\bar{c}_w} C_{L_w,\alpha}(\alpha_{0w} - \alpha_{L0w}) - \frac{S_t(x_t - x_{CG})}{S_w \bar{c}_w} \eta_t C_{L_t,\alpha}(\alpha_{0t} - \varepsilon_{d0})$$

$$C_{m,\delta_e} = \frac{S_t \bar{c}_t}{S_w \bar{c}_w} \eta_t C_{m_t,\delta_e} - \frac{S_t(x_t - x_{CG})}{S_w \bar{c}_w} \eta_t C_{L_t,\alpha} \varepsilon_e$$

or after substituting the values for this particular wing-tail combination,

$$C_{m0} = 0.4075 \frac{x_{CG}}{\bar{c}_w} - 0.053$$

$$C_{m,\delta_e} = 0.4764 \frac{x_{CG}}{\bar{c}_w} - 1.3706$$

From Example 4.4.1,

$$\frac{x_{np}}{\bar{c}_w} = \frac{l_{np}}{\bar{c}_w} - \frac{l_w}{\bar{c}_w} = 0.1202 - \frac{-0.71}{180/33} = 0.2504$$

Thus, for this wing-tail combination at 80 mph, Eq. (4.4.15) reduces to

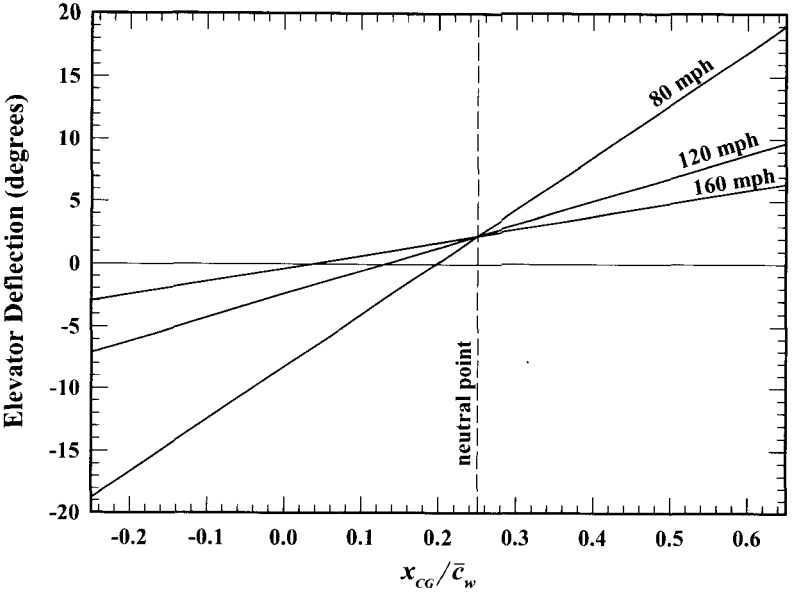


Figure 4.4.3. Elevator angle required for level trim as a function of CG location measured aft of the wing quarter-chord for the airplane in Example 4.4.2.

$$
\begin{aligned}
(\delta_e)_{\text{trim}} &= -\frac{C_{m0} - (C_L - C_{L0})[(x_{np} - x_{CG})/\bar{c}_w]}{C_{m,\delta_e} + C_{L,\delta_e}[(x_{np} - x_{CG})/\bar{c}_w]} \\
&= -\frac{0.4075(x_{CG}/\bar{c}_w) - 0.053 - (0.9168 - 0.4075)[0.2504 - (x_{CG}/\bar{c}_w)]}{0.4764(x_{CG}/\bar{c}_w) - 1.3706 + 0.4764[0.2504 - (x_{CG}/\bar{c}_w)]} \\
&= -\frac{0.9168(x_{CG}/\bar{c}_w) - 0.1805}{-1.2513} = \underline{0.7327(x_{CG}/\bar{c}_w) - 0.1442}
\end{aligned}
$$

Within the approximations used for this example, the elevator angle required to trim the airplane is a linear function of CG location. This is not obvious from Eq. (4.4.15). Results for the particular wing-tail combination used in the present example are shown in Fig. 4.4.3, for airspeeds of 80, 120, and 160 miles per hour.

From Example 4.4.2 we see that at low airspeed, large negative elevator deflections are required to trim the airplane if the CG is moved very far forward of the neutral point. When the elevator deflection becomes larger than about 10 degrees, the elevator effectiveness begins to decrease. Since there is a limit to how much elevator deflection can be used without stalling the tail, there is a limit to how far the CG can be moved forward of the neutral point. Thus, we have now seen that there are both forward and aft limits for the allowable position of the center of gravity. If the CG is moved too far aft, the airplane becomes unstable. If the CG is moved too far forward, the airplane cannot be trimmed at low airspeed. An absolute forward CG limit is that which requires

maximum up elevator (negative δ_e) to trim the airplane at the airspeed, which requires the maximum allowable lift coefficient. As we shall see later, there can be more restrictive constraints on the forward CG limit, based on control forces and maneuverability.

Another interesting point can be observed from Example 4.4.2. It can be seen from Fig. 4.4.3 that at any given airspeed, there is a CG location for which the airplane is in trim with no elevator deflection at all. This illustrates another possible method of trim control. An airplane with no elevator can be trimmed at any airspeed simply by moving the center of gravity. This is called *weight shift control*, and it was actually used for the very first controlled human flight in a craft heavier than air. This took place in 1891 with an unpowered aircraft, designed, built, and flown by Otto Lilienthal, one of the true giants in aviation history. A few of Lilienthal's many flights are shown in Fig. 4.4.4.

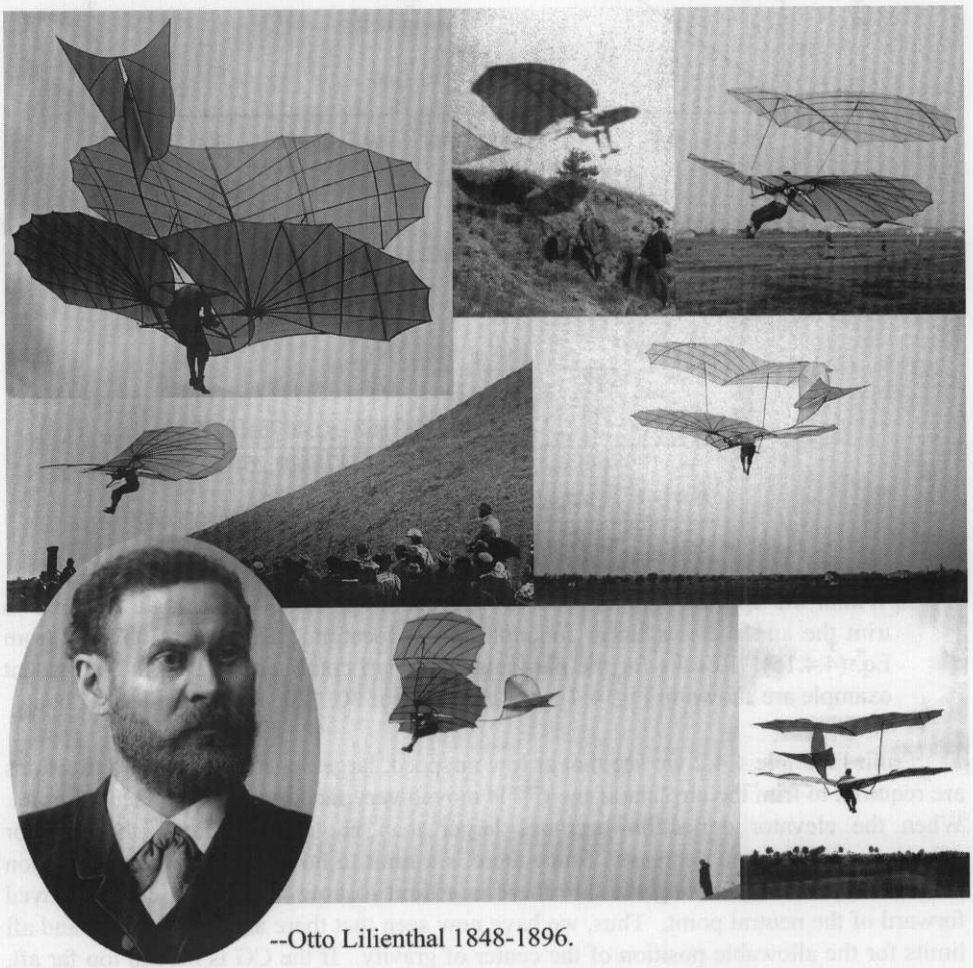


Figure 4.4.4. Otto Lilienthal, the true father of modern aviation, was the first human to pilot an aircraft in stable controlled flight. (Archives of the Otto-Lilienthal-Museum)

Otto Lilienthal was truly the first aviator and the father of modern aviation. His nineteenth-century predecessors felt that the key to flight was to *build an engine with sufficient power and attach it to an airframe of sufficient strength and man could propel himself into aviation history with brute force alone.* By contrast, Lilienthal was the first to recognize the need to get in the air and fly with gliders before an engine could be used successfully for powered flight. The Wright brothers carried on his philosophy, which ultimately led to the control solutions that made powered flight possible. During the period from 1891 to 1896, Lilienthal made more than 2,000 successful glider flights. He published papers on flight that were read throughout the world, and these papers inspired other aviation pioneers, including the Wright brothers. At the time of his death, Lilienthal was working on powered flight and it is more than likely that had he lived a few more years, he would have achieved powered flight before the Wright brothers.

On Sunday, August 9, 1896, Otto Lilienthal, the father of modern aviation, was seriously injured in a glider crash near Stollen, Germany. He died the next day in Berlin. According to a witness at the crash, Lilienthal did not know that he was fatally injured. The witness gave Lilienthal's last words as: "Ich muss etwas ausruhen, dann machen wir weiter" (I must rest a little, then we continue). During his life, Lilienthal used the phrase "Opfer müssen gebracht werden" (Sacrifices must be made). This is the epitaph now carved on his tombstone in Lichterfelde cemetery.

4.5. Estimating the Downwash Angle on an Aft Tail

We have seen that the downwash induced on an aft tail by the main wing has a significant effect on the trim and static stability of an airplane. This downwash reduces the effective angle of attack for the horizontal tail and also reduces its effectiveness in stabilizing the airplane. The downwash varies along the span of the horizontal tail and is affected by the planform shape of the wing as well as the presence of the fuselage and nacelles. To accurately estimate the interactions between the main wing and the tail, we must make use of computer simulations and/or wind tunnel tests. Such methods are always employed in the later phases of the airplane design process. However, for the purpose of preliminary design, it is useful to have an approximate closed-form solution for estimating the downwash induced on the tail by the main wing. Such an approximate solution can be developed by assuming that the flow field in the vicinity of the airplane is affected only by the main wing.

The downwash induced on an aft tail is a direct result of the vorticity generated by the main wing. At any given point in space, the downwash velocity, V_y, is directly proportional to the wingtip vortex strength, Γ_{wt}. From the vortex lifting law, for any given wing geometry, the strength of the wingtip vortex is proportional to the lift generated by the wing divided by the air density and the freestream velocity. Thus, we see that the downwash velocity induced by a lifting wing of some given geometry, at any given point in space, is directly proportional to the freestream velocity multiplied by the lift coefficient for the wing,

$$V_y \sim \Gamma_{wt} \sim \frac{L_w}{\rho V_\infty} \sim V_\infty C_{L_w} \tag{4.5.1}$$

The downwash velocity is independent of air density and the proportionality constant between the far right- and left-hand sides of Eq. (4.5.1) varies with position and the geometry of the wing.

More specifically, from Prandtl's lifting-line theory and the Biot-Savart law, the downwash induced a few chord lengths or more downstream from an unswept wing can be approximated as

$$V_y(\bar{x},\bar{y},\bar{z}) = -\frac{V_\infty C_{L_w}\kappa_v}{\pi^2 R_{A_w}}\left\{\frac{\kappa_b-\bar{z}}{\bar{y}^2+(\kappa_b-\bar{z})^2}\left[1+\frac{\bar{x}}{\sqrt{\bar{x}^2+\bar{y}^2+(\kappa_b-\bar{z})^2}}\right]\right.$$
$$+\frac{\bar{x}}{\bar{x}^2+\bar{y}^2}\left[\frac{\kappa_b-\bar{z}}{\sqrt{\bar{x}^2+\bar{y}^2+(\kappa_b-\bar{z})^2}}+\frac{\kappa_b+\bar{z}}{\sqrt{\bar{x}^2+\bar{y}^2+(\kappa_b+\bar{z})^2}}\right] \qquad (4.5.2)$$
$$\left.+\frac{\kappa_b+\bar{z}}{\bar{y}^2+(\kappa_b+\bar{z})^2}\left[1+\frac{\bar{x}}{\sqrt{\bar{x}^2+\bar{y}^2+(\kappa_b+\bar{z})^2}}\right]\right\}$$

where R_{A_w} is the aspect ratio of the wing,

$$\bar{x} = \frac{x}{b_w/2}, \quad \bar{y} = \frac{y}{b_w/2}, \quad \bar{z} = \frac{z}{b_w/2}$$

x is the axial coordinate in the direction of the freestream, y is the upward normal coordinate, and z is the spanwise coordinate, all measured relative to the wing quarter-chord at the aircraft plane of symmetry as shown in Fig 4.5.1.

The parameters κ_v and κ_b depend on the geometry of the wing. The vortex strength factor, κ_v, is a ratio of the wingtip vortex strength to that generated by an elliptic wing having the same lift coefficient and aspect ratio. The vortex span factor, κ_b, is defined as the spacing between the wingtip vortices divided by the wingspan. Both κ_v and κ_b can be determined analytically from the series solution to Prandtl's lifting-line equation. For the details of this solution, see Phillips, Anderson, Jenkins, and Sunouchi (2002). The results are

$$\kappa_v = 1+\sum_{n=2}^{\infty}\frac{A_n}{A_1}\sin(n\pi/2) \qquad (4.5.3)$$

$$\kappa_b = \frac{\frac{\pi}{4}+\sum_{n=2}^{\infty}\frac{nA_n}{(n^2-1)A_1}\cos(n\pi/2)}{1+\sum_{n=2}^{\infty}\frac{A_n}{A_1}\sin(n\pi/2)} \qquad (4.5.4)$$

where the coefficients, A_n, are the Fourier coefficients in the series solution to Prandtl's lifting-line equation, which was presented in Sec. 1.8.

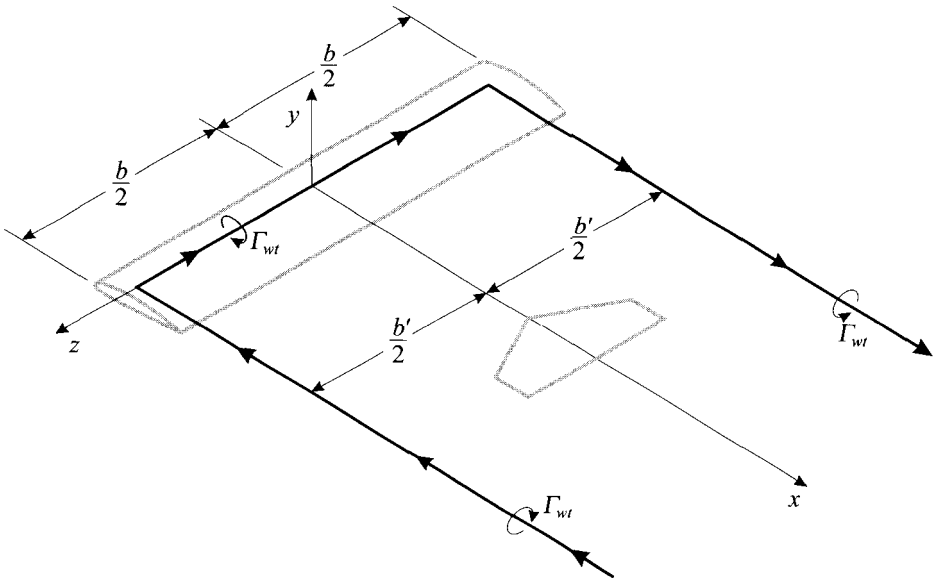


Figure 4.5.1. Vortex model for estimating the downwash on an aft tail behind an unswept wing.

For an elliptic wing with no sweep, dihedral, or twist, κ_v is 1.0 and κ_b is $\pi/4$. For an unswept tapered wing with no dihedral or twist, κ_v and κ_b are related to aspect ratio and taper ratio as shown in Figs. 4.5.2 and 4.5.3. The effects of washout are handled using Eqs. (4.5.3) and (4.5.4) with the Fourier coefficients evaluated as described in Sec. 1.8.

As a first approximation, the variation in downwash along the span of the horizontal tail is usually neglected. The downwash for the entire tail is typically taken to be that evaluated at the aerodynamic center. For a symmetric airplane, the aerodynamic center of the tail is in the plane of symmetry. The change in the downwash with respect to the spanwise coordinate is zero at the aircraft plane of symmetry. Furthermore, the span of the horizontal tail is usually small compared to that of the wing. Thus, the downwash is often fairly uniform over this span, and a reasonable first approximation for the downwash on an aft tail is found by setting the dimensionless spanwise coordinate, $\bar{z}$, equal to zero in Eq. (4.5.2).

Because the downwash is small compared to the freestream velocity, the downwash angle, ε_d, can be closely approximated as the downwash velocity divided by the freestream velocity. Thus, the downwash angle in the aircraft plane of symmetry a few chord lengths or more downstream from an unswept wing is approximated from Eq. (4.5.2) as

$$\varepsilon_d(\bar{x},\bar{y},0) = \frac{-V_y(\bar{x},\bar{y},0)}{V_\infty} = \frac{\kappa_v \kappa_p}{\kappa_b}\frac{C_{L_w}}{R_{A_w}} \tag{4.5.5}$$

where

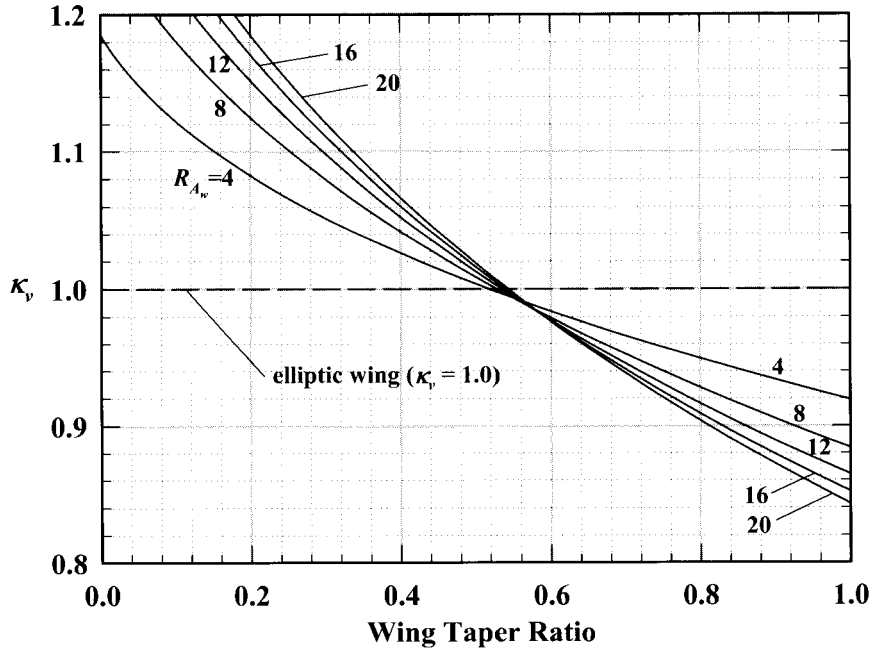


Figure 4.5.2. Wingtip vortex strength factor from Prandtl's lifting-line theory.

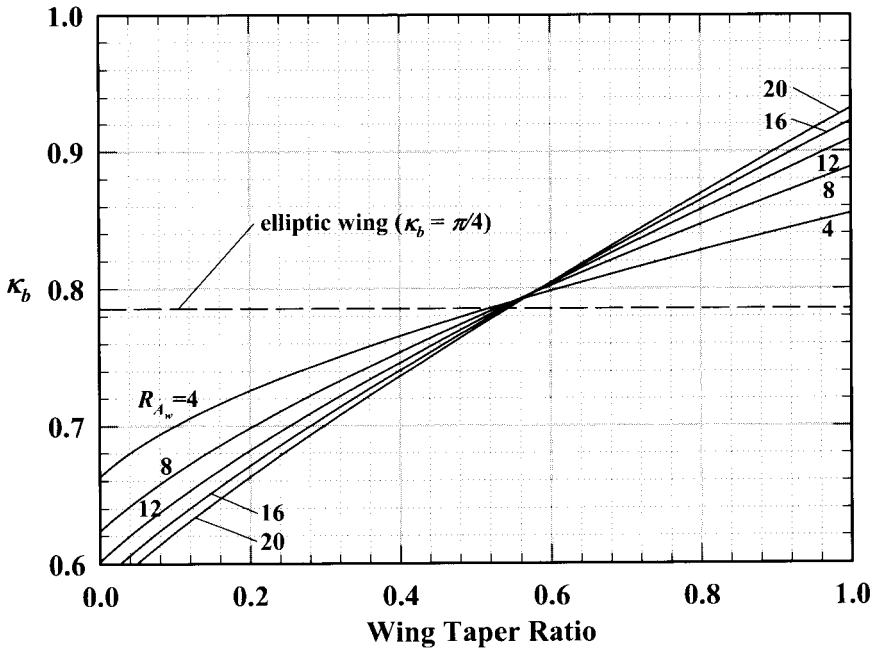


Figure 4.5.3. Wingtip vortex span factor from Prandtl's lifting-line theory.

$$\kappa_p = \frac{2\kappa_b^2}{\pi^2(\bar{y}^2+\kappa_b^2)}\left[1+\frac{\bar{x}(\bar{x}^2+2\bar{y}^2+\kappa_b^2)}{(\bar{x}^2+\bar{y}^2)\sqrt{\bar{x}^2+\bar{y}^2+\kappa_b^2}}\right] \tag{4.5.6}$$

The tail position factor, κ_p, depends on the planform shape of the wing and the position of the tail relative to the wing. However, for a wing with no twist, κ_v, κ_b, and κ_p are all independent of angle of attack. Thus, as a first approximation, the downwash angle at the tail is estimated as being linearly proportional to the lift coefficient for the wing. The variation in κ_p with tail position is shown in Fig. 4.5.4. The planform shape of the wing affects the value of κ_p only through its effect on κ_b. Thus, for a main wing with no sweep or dihedral, κ_p is a unique function of $\bar{x}/\kappa_b$ and $\bar{y}/\kappa_b$, as shown in Fig. 4.5.4.

Sweep in the main wing also has a significant effect on the downwash induced on an aft tail. Sweep affects this downwash in three ways. First, because sweep changes the spanwise distribution of vorticity on the wing, it changes the strength of the wingtip vortices for a given lift coefficient and aspect ratio. This same change in the vorticity distribution will also change the location of the center of vorticity in the vortex sheet trailing behind each semispan. Since each wingtip vortex rolls up around the center of vorticity from one side of the wing, wing sweep affects the spacing of the wingtip vortices. Because wing sweep affects both the strength and spacing of the wingtip

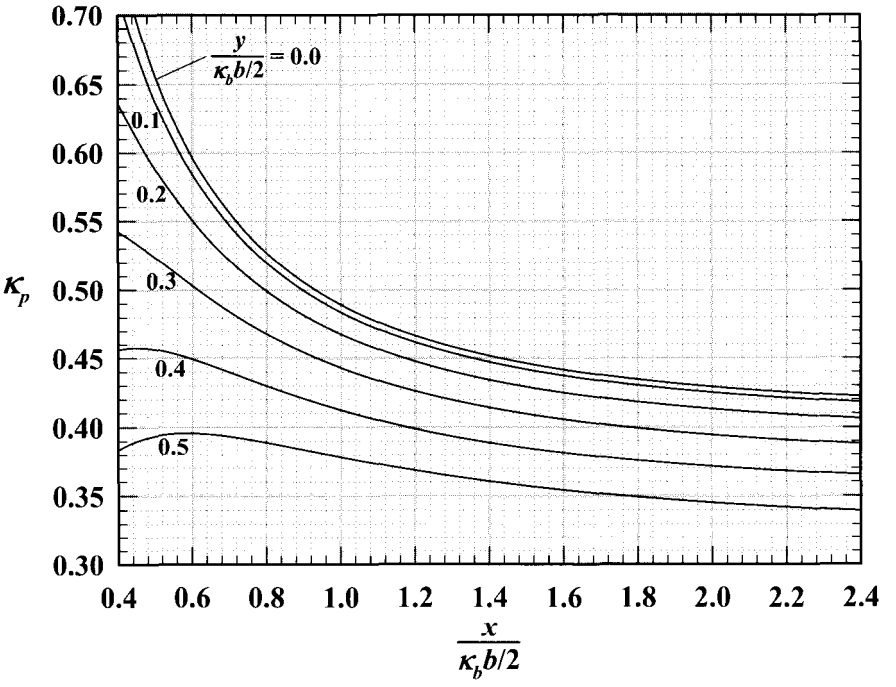


Figure 4.5.4. Effect of tail position on the downwash angle in the plane of symmetry aft of an unswept wing.

vortices, sweep in the main wing will affect both the vortex strength factor, κ_v, and the vortex span factor, κ_b. More significantly, sweep in the main wing affects the downwash on an aft tail through a simple change in proximity of the wing surface to the tail. As the wing is swept back, the outboard portions of the wing are brought closer to the tail as is shown in Fig. 4.5.5. This places the bound portion of the vortex system closer to the aft tail, and thus changes the downwash induced on the tail.

Unfortunately, the series solution to Prandtl's classical lifting-line equation does not apply to a swept wing. No closed-form solution for the spanwise vorticity distribution on a swept wing has ever been obtained. In the absence of such a solution for this vorticity distribution, it is not possible to obtain a closed-form solution for the variation of κ_v and κ_b with sweep. Neglecting the effects of sweep on κ_v and κ_b is quite restrictive and such results should be used with extreme caution for highly swept wings. Nevertheless, if we are willing to neglect the effect of sweep on κ_v and κ_b, it is possible to obtain a closed-form approximation for the proximity effect that results from moving the bound vortex closer to the aft tail when the wing is swept back.

This approximation is based on the vortex model suggested by McCormick (1995), which has been shown here in Fig. 4.5.5. With this model, the bound vorticity is approximated as two straight vortex line segments, one aligned with the quarter-chord of each semispan. Each wingtip vortex is modeled as a semi-infinite line vortex trailing from the wing at the center of shed vorticity. In reality, the direction of the trailing wingtip vortices is determined by the geometry of the airplane, the angle of attack, and the downward deflection of the vortex system, which is caused by the downwash that is induced on one vortex by the other. However, this level of sophistication is hardly

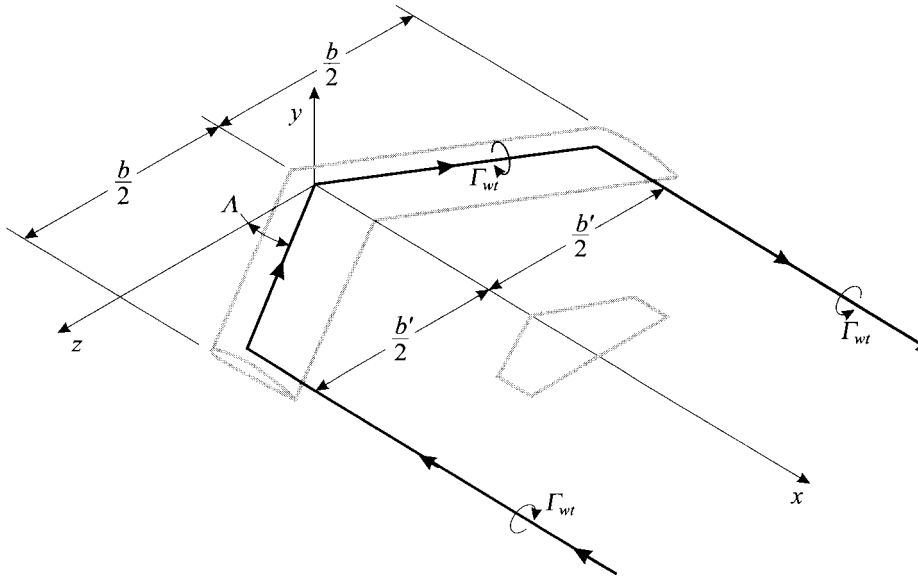


Figure 4.5.5. Vortex model for estimating the downwash on an aft tail behind a swept wing.

justified when one considers the approximate nature of the other aspects of this vortex model. Instead, we shall simply assume that wingtip vortices trail downstream from the wing quarter-chord at the center of shed vorticity in a direction parallel to the x-axis. This same approximation was made in the development of Prandtl's classical theory.

With these approximations, the vorticity generated by a lifting swept wing is modeled as four straight vortex line segments, all of which fall in the x-z plane as shown in Fig. 4.5.5. Applying the Biot-Savart law to this vortex system, the downwash in the aircraft plane of symmetry is found to be

$$V_y(x,y,0) = \frac{\Gamma_{wt}}{2\pi}\left\{\frac{-(b'/2)}{(x-s')^2+y^2+(b'/2)^2-(x-s')\sqrt{(x-s')^2+y^2+(b'/2)^2}}\right.$$
$$\left.+\frac{-(b'/2)x\left(\sqrt{x^2+y^2}+\sqrt{(x-s')^2+y^2+(b'/2)^2}\right)}{(x^2+y^2)[(x-s')^2+y^2+(b'/2)^2]+(x^2-xs'+y^2)\sqrt{x^2+y^2}\sqrt{(x-s')^2+y^2+(b'/2)^2}}\right\} \tag{4.5.7}$$

where

$$s' \equiv (b'/2)\tan\Lambda \tag{4.5.8}$$

and Λ is the quarter-chord sweep angle. The series solution to Prandtl's classical lifting-line equation predicts that the strength of each wingtip vortex is related to the lift coefficient developed by the wing according to the relation

$$\Gamma_{wt} = \kappa_v \frac{2bV_\infty C_{L_w}}{\pi R_{A_w}} \tag{4.5.9}$$

where κ_v is 1.0 for an elliptic wing and is expressed in terms of an infinite series for any other planform shape. For a tapered wing, the results shown Fig. 4.5.2 can be used. Also from Prandtl's lifting-line theory, the spacing between the wingtip vortices is related to the wingspan according to

$$b' = \kappa_b b \tag{4.5.10}$$

where κ_b takes a value of $\pi/4$ for an elliptic planform shape and is expressed as an infinite series for other planforms. For the tapered wing, Fig. 4.5.3 can be used.

Applying Eqs. (4.5.9) and (4.5.10) to Eq. (4.5.7), the downwash angle in the aircraft plane of symmetry, a few chord lengths or more downstream from a swept wing, can be approximated as

$$\varepsilon_d(\bar{x},\bar{y},0) = \frac{-V_y(\bar{x},\bar{y},0)}{V_\infty} = \frac{\kappa_v \kappa_p \kappa_s}{\kappa_b}\frac{C_{L_w}}{R_{A_w}} \tag{4.5.11}$$

where

$$\kappa_s = \frac{1 + \dfrac{\bar{x} - \bar{s}}{\bar{t}} + \dfrac{\bar{x}(\bar{r} + \bar{t})(\bar{t}_0^2 - \bar{x}^2)}{\bar{r}\bar{t}(\bar{r}\bar{t} + \bar{r}^2 - \bar{x}\bar{s})}}{1 + \dfrac{\bar{x}(\bar{r}^2 + \bar{t}_0^2 - \bar{x}^2)}{\bar{r}^2 \bar{t}_0}} \tag{4.5.12}$$

$$\bar{r} \equiv \sqrt{\bar{x}^2 + \bar{y}^2} \tag{4.5.13}$$

$$\bar{s} \equiv \kappa_b \tan \Lambda \tag{4.5.14}$$

$$\bar{t} \equiv \sqrt{(\bar{x} - \bar{s})^2 + \bar{y}^2 + \kappa_b^2} \tag{4.5.15}$$

$$\bar{t}_0 \equiv \sqrt{\bar{x}^2 + \bar{y}^2 + \kappa_b^2} \tag{4.5.16}$$

The wing sweep factor, κ_s, depends on the planform shape of the wing and the position of the tail in addition to the quarter-chord sweep angle, Λ. However, as was the case for κ_p, the planform shape of the wing affects the value of κ_s as predicted by Eq. (4.5.12), only through its effect on κ_b. Thus, κ_s is found to be a unique function of Λ, $\bar{x}/\kappa_b$, and $\bar{y}/\kappa_b$. The variation in κ_s with axial tail position is shown in Fig. 4.5.6 for several values of quarter-chord sweep and tail height. The results shown in Fig. 4.5.6 for the case $y = 0$ agree exactly with the results presented by McCormick (1995) for the special case of an elliptic planform shape (i.e., $\kappa_b = \pi/4$). However, McCormick states that the sweep correction "does not depend significantly on the tail height," and he suggests that the zero-height solution be used in general. Figure 4.5.6 does not support that statement.

The downwash computed using the analytical method presented in this section agrees very well with experimental data and the commonly used empirical correlation recommended in the U.S. Air Force Stability and Control DATCOM (Hoak, 1960). For a detailed comparison, see Phillips, Anderson, Jenkins, and Sunouchi (2002).

If the position of the tail and the planform shape of the main wing are known, Eq. (4.5.11) can be combined with Eq. (4.5.6), Eq. (4.5.12), and the results presented in Figs. 4.5.2 and 4.5.3 to estimate the downwash angle. However, at the beginning of the preliminary design process the position of the tail is not typically known. When the tail is mounted sufficiently aft of the main wing, the downwash angle is independent of axial position. As the dimensionless axial position of the tail approaches infinity, from Eq. (4.5.6), the tail position factor along the x-axis reduces to

$$\kappa_p(\bar{x},0,0) \underset{\bar{x}\to\infty}{=} \frac{4}{\pi^2} \tag{4.5.17}$$

and from Eq. (4.5.12), the wing sweep factor becomes

$$\kappa_s(\bar{x},0,0) \underset{\bar{x}\to\infty}{=} 1.0 \tag{4.5.18}$$

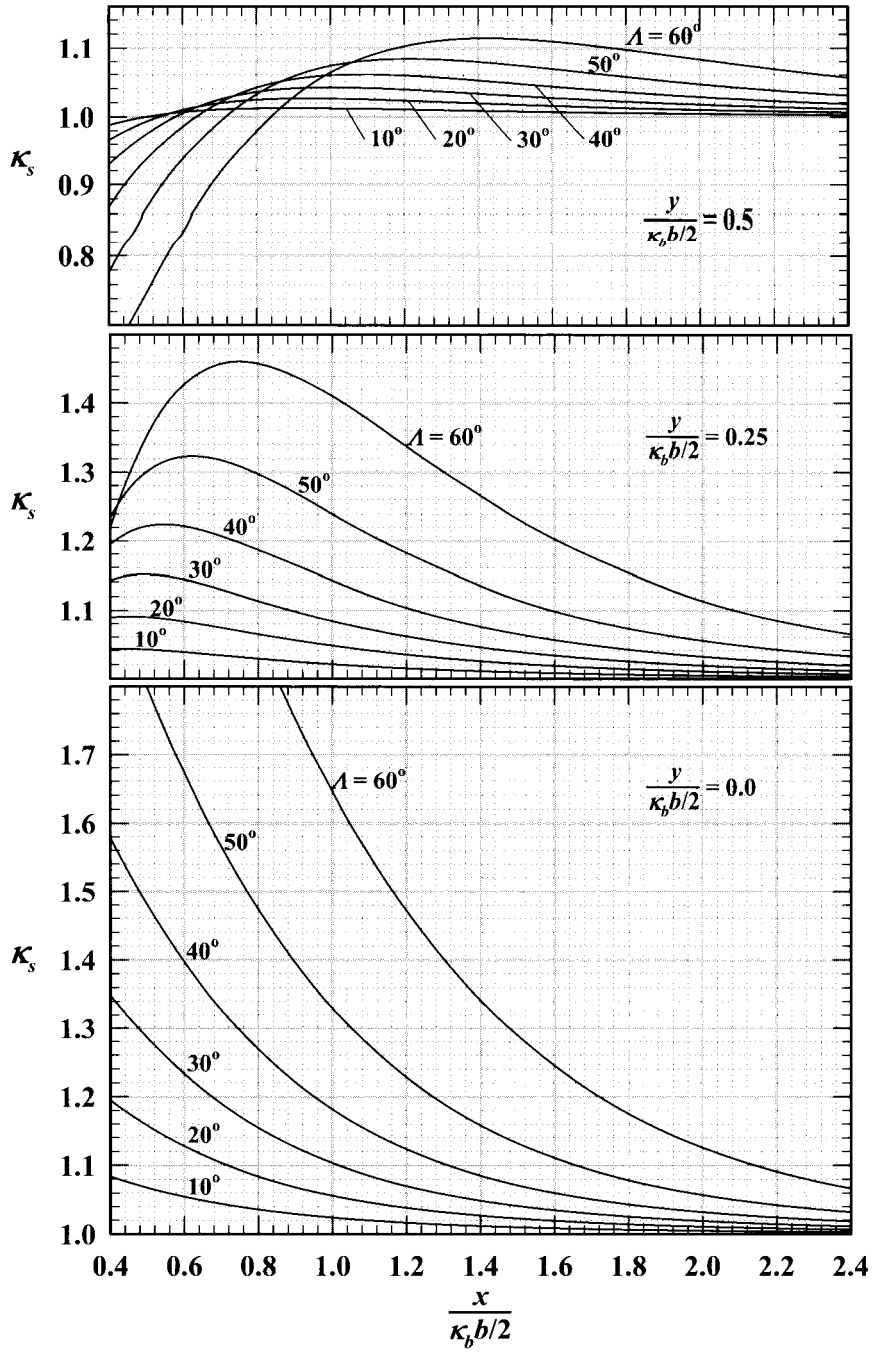


Figure 4.5.6. Effect of wing sweep on the downwash angle in the plane of symmetry aft of the main wing.

Using Eqs. (4.5.17) and (4.5.18) in Eq. (4.5.11), the downwash angle along the x-axis far behind the main wing can be approximated as

$$\varepsilon_d(\bar{x},0,0) \underset{\bar{x}\to\infty}{=} \frac{4\kappa_v}{\pi^2\kappa_b}\frac{C_{L_w}}{R_{A_w}} \tag{4.5.19}$$

For an elliptic wing ($\kappa_v = 1.0$ and $\kappa_b = \pi/4$), this gives

$$\varepsilon_d(\bar{x},0,0) \underset{\bar{x}\to\infty}{=} \frac{16}{\pi^3}\frac{C_{L_w}}{R_{A_w}} \tag{4.5.20}$$

Equation (4.5.20) can be used as a rough estimate for the downwash angle on an aft tail.

EXAMPLE 4.5.1. Consider the general aviation aircraft, which was described in Example 4.3.1. The wing has a taper ratio of 0.4 and a quarter-chord sweep of 10°. If the horizontal tail were mounted 3.4 ft above the aerodynamic center of the wing, estimate the downwash gradient using the approximation presented in this section.

Solution. For this wing-tail combination, we have

$$S_w = 180\ \text{ft}^2,\quad b_w = 33\ \text{ft},\quad R_{A_w} = 33^2/180 = 6.05,\quad C_{L_w,\alpha} = 4.44,\quad R_{T_w} = 0.40,$$
$$\Lambda = 10°,\quad l_t - l_w = 15\ \text{ft},\quad \bar{x} = 15/(33/2) = 0.909,\quad \bar{y} = 3.4/(33/2) = 0.206$$

From Figs. 4.5.2 and 4.5.3 (or using a computer program based on the series solution to Prandtl's lifting-line equation), for a wing aspect ratio of 6.05 and a wing taper ratio of 0.40, the following results are obtained:

$$\kappa_v = 1.035$$

$$\kappa_b = 0.759$$

From Eqs. (4.5.6) and (4.5.12), the position factor and the sweep factor are found to be

$$\kappa_p = 0.433$$

$$\kappa_s = 1.015$$

From Eq. (4.5.11), the downwash at the position of the horizontal tail is

$$\varepsilon_d = \frac{\kappa_v\kappa_p\kappa_s}{\kappa_b}\frac{C_{L_w}}{R_{A_w}} = \frac{1.035(0.433)1.015}{0.759}\frac{C_{L_w}}{R_{A_w}} = 0.599\frac{C_{L_w}}{R_{A_w}}$$

The downwash gradient is then

$$\varepsilon_{d,\alpha} = \frac{\partial \varepsilon_d}{\partial \alpha} = 0.599 \frac{1}{R_{A_w}} \frac{\partial C_{L_w}}{\partial \alpha} = 0.599 \frac{C_{L_w,\alpha}}{R_{A_w}} = 0.599 \frac{4.44}{6.05} = \underline{0.44}$$

This means that for each degree of increase in the angle of attack, the downwash on the tail is increased by 0.44 degree. Thus, only 56 percent of any change in angle of attack is actually felt by the tail. This reduces the effectiveness of the horizontal stabilizer by 44 percent. For comparison, as a rough estimate for this example, Eq. (4.5.20) gives $\varepsilon_{d,\alpha} = 0.38$.

To reiterate, **the downwash induced on an aft tail by the main wing has a critical effect and should never be ignored when designing the tail of an airplane.**

4.6. Simplified Pitch Stability Analysis for a Wing-Canard Combination

Trim and static pitch stability can also be achieved by combining a wing with a forward canard, as shown in Fig. 4.6.1. A canard is a horizontal lifting surface mounted ahead of the main wing rather than behind it. While the canard configuration is not nearly as common as the aft tail, the first successful powered airplane, the 1903 *Wright Flyer* shown in Fig. 4.6.2, was a canard design. Shortly after the Wright Brothers, most airplane designers abandoned the canard in favor of the aft tail. However, this probably had more to do with avoiding patent difficulties with the Wrights than with any intrinsic inferiority of the canard design. In fact, as we shall see, the canard design has some inherent advantages, and the student should understand the workings of this design.



Figure 4.6.1. Beech Starship with a forward canard design. (Photograph by Barry Santana)